

# LANDOLT-BÖRNSTEIN

Numerical Data and Functional Relationships  
in Science and Technology

*New Series*

Editor in Chief: K.-H. Hellwege

Group III: Crystal and Solid State Physics

Volume 4

Magnetic and Other Properties  
of Oxides and Related Compounds

Part a

J. B. Goodenough · W. Gräper · F. Holtzberg · D. L. Huber  
R. A. Lefever · J. M. Longo · T. R. McGuire · S. Methfessel

Editors: K.-H. Hellwege and A. M. Hellwege



Springer-Verlag Berlin · Heidelberg · New York 1970

BEST AVAILABLE COPY

N

IS

# LANDOLT-BÖRNSTEIN

Zahlenwerte und Funktionen  
aus Naturwissenschaften und Technik

*Neue Serie*

Gesamtherausgabe: K.-H. Hellwege

Gruppe III: Kristall- und Festkörperphysik

Band 4

Magnetische und andere Eigenschaften  
von Oxiden und verwandten Verbindungen

Teil a

J. B. Goodenough · W. Gräper · F. Holtzberg · D. L. Huber  
R. A. Lefever · J. M. Longo · T. R. McGuire · S. Methfessel

Herausgeber: K.-H. Hellwege und A. M. Hellwege



1970

Springer-Verlag Berlin · Heidelberg · New York 1970

### 3 Crystallographic and magnetic properties of perovskite and perovskite-related compounds \*)

#### 3.0 Introduction — Einleitung

##### 3.0.1 General remarks — Allgemeines

The perovskites form a family of compounds having a crystal structure similar to that of the mineral perovskite,  $\text{CaTiO}_3$ . There are two classes of materials crystallizing with this general structure type: primarily ionic materials having the ideal chemical formula  $\text{ABX}_3$ , (A = larger cation, B = smaller cation, X = anion), and alloys having the ideal formula  $\text{M}^e\text{XM}_f^i$ , (X = interstitial atom,  $\text{M}^e$  and  $\text{M}^i$  are metal atoms). Of these two classes, the former is much larger and the more important.

The stability of the  $\text{ABX}_3$  perovskite structure is primarily derived from the electrostatic (Madelung) energy achieved if cations occupy corner-shared octahedra. Thus the first prerequisite for a stable  $\text{ABX}_3$  perovskite is the existence of stable, polar octahedral-site building blocks. This, in turn, requires that the B cation have a preference for octahedral coordination and that there be an effective charge on the B cation. Since any A cation must occupy the relatively large anionic interstice created by corner-shared octahedra, a second prerequisite is an appropriate size for the A cation. Where it is too large, the B-X bond length cannot be optimized, and hexagonal stacking with face-shared octahedra becomes competitive. Where the A cation is too small, A-X bonding stabilizes structures having a smaller anionic coordination about the A cation. Thus  $\text{ABX}_3$  perovskites are commonly found in fluorides and oxides having B cations with a preference energy for octahedral coordination. By contrast, the chlorides and sulfides, having larger anions, not only require the largest A cations, but also form layer structures, where the A cations are missing, because they have anionic *d* orbitals energetically available for orbital hybridization.

There are many perovskite-related structures, and these have been included in these tables. For example, the structure can tolerate mixed systems such as  $\text{A}_{1-x}\text{A}'_x\text{BX}_3$  and  $\text{AB}_{1-x}\text{B}'_x\text{X}_3$ , A-cationic vacancies  $\square$  as in  $\square_{1-x}\text{A}_x\text{BX}_3$ , and cationic ordering as in  $\text{A}_2\text{BB}'\text{X}_6$ . Although anion-deficient perovskites have been reported many times, the anion vacancies  $\oplus$  are probably not distributed randomly. In compounds containing  $\text{Fe}^{3+}$  ions, for example, they appear to condense in pairs at individual B-site octahedra to convert the local anion interstice from an octahedron to a tetrahedron. In

Die Perowskite sind eine Gruppe von Verbindungen mit der gleichen Kristallstruktur wie das Mineral Perowskit,  $\text{CaTiO}_3$ . Man unterscheidet zwei Klassen von Substanzen, die in diesem allgemeinen Strukturtyp kristallisieren: in erster Linie Ionenverbindungen mit der idealen chemischen Formel  $\text{ABX}_3$  (A = größeres Kation, B = kleineres Kation, X = Anion) und Legierungen mit der idealen Formel  $\text{M}^e\text{XM}_f^i$  (X = Zwischengitteratom,  $\text{M}^e$  und  $\text{M}^i$  = Metallatome). Von diesen beiden Klassen ist die erstere wesentlich umfangreicher und wichtiger.

Die Stabilität der  $\text{ABX}_3$ -Perowskitstruktur beruht in erster Linie auf der elektrostatischen (Madelung-) Energie, die dann zustande kommt, wenn Kationen Oktaeder mit gemeinsamen Ecken besetzen. So ist die Existenz von stabilen, polaren Oktaeder-Bausteinen die erste Vorbedingung für ein stabiles  $\text{ABX}_3$ -Perowskit. Dies wiederum erfordert, daß das B-Kation die Oktaeder-Koordination bevorzugt und daß beim B-Kation eine effektive Ladung existiert. Da ein jedes A-Kation die relativ große Anionen-Lücke besetzen muß, die zwischen Oktaedern mit gemeinsamen Ecken entsteht, ist die passende Größe des A-Kations die zweite Vorbedingung. Wenn das A-Kation zu groß ist, läßt sich der optimale B-X-Bindungsabstand nicht erreichen, und eine hexagonale Packung von Oktaedern mit gemeinsamen Flächen kann ebenso auftreten. Wenn das A-Kation zu klein ist, ergibt die A-X-Bindung Strukturen mit einer kleineren Anionen-Koordination um das A-Kation. Daher sind  $\text{ABX}_3$ -Perowskite gewöhnlich unter den Fluoriden und Oxiden zu finden, in denen die B-Kationen Oktaeder-Koordination energetisch bevorzugen. Dagegen erfordern Chloride und Sulfide, die größere Anionen haben, nicht nur die größten A-Kationen, sondern sie bilden, weil sie anionische *d*-Elektronenbahnen mit der richtigen Energie für eine Bahn-Hybridisierung haben, auch Schichtstrukturen, bei denen die A-Kationen ganz fehlen.

Es gibt viele dem Perowskit verwandte Strukturen, die in diese Tabellen aufgenommen wurden. Zum Beispiel können gemischte Systeme wie  $\text{A}_{1-x}\text{A}'_x\text{BX}_3$  und  $\text{AB}_{1-x}\text{B}'_x\text{X}_3$  mit dieser Struktur auftreten, weiter A-Kationenlücken  $\square$  wie in  $\square_{1-x}\text{A}_x\text{BX}_3$  und geordnete Kationen wie in  $\text{A}_2\text{BB}'\text{X}_6$ . Über Perowskite mit Anionenlücken ist schon häufig berichtet worden, vermutlich sind die Anionenleerstellen  $\oplus$  nicht willkürlich verteilt. In Verbindungen, die  $\text{Fe}^{3+}$ -Ionen enthalten, scheinen sie z. B. paarweise im Oktaeder eines einzelnen B-Platzes zusammenzutreffen und die

\*) This work was sponsored by the U. S. Air Force.

compou  
it is mor  
anions f  
deficient  
cations,  
contain  
across w  
edges (l  
ciencies  
alloys.  
B-occup  
perovsk  
cation v  
an inter  
(Fig. 23  
stackin  
nal stae  
cies (F  
(AX)<sub>m</sub>  
rocksal  
stacked  
also oc  
an A c  
structu  
with i  
classifi  
and B  
rather  
for ex:  
18). S  
of the

Th  
ing pl  
BaTiO  
ferror  
condu  
ducti  
lator  
tor a  
patib  
trans  
ture  
ABX  
mult  
[Sm  
ferro  
ed f  
Ba,  
pero  
and  
mag  
of t  
mag  
app  
tura  
that

\*) 1  
c  
f

compounds containing  $Ti^{4+}$  ions, on the other hand, it is more probable that local rearrangements of the anions form trigonal bipyramidal sites. Anion-deficient, ionic materials in which there are no A-cations, such as  $\square WO_{3-x}$ , have been shown to contain  $\square BX_3$  blocks connected by "shear" planes across which the occupied octahedra share common edges (Fig. 22). On the other hand, anion deficiencies may occur randomly in the  $M^cX_{1-x}M_f^f$  alloys. B-cation defects cannot occur, because the B-occupied octahedra form the basis of the  $ABX_3$ -perovskite structure. Where there are apparent B-cation vacancies, as in  $A_mB_{m-1}X_{3m}$ , there is either an interleaving of perovskite layers with  $A_2X_2$  layers (Fig. 23) or an interleaving of cubic (perovskite) stacking of  $AO_3$  layers with regularly spaced hexagonal stackings at which are located the B-ion vacancies (Fig. 24). Similarly, the series of compounds  $(AX)_m(ABX_3)_n$  crystallize with an interleaving of rocksalt layers (Fig. 25). Interleaving of cubic-stacked  $AO_3$  layers and hexagonal-stacked layers also occurs in  $ABX_3$  compounds having too large an A cation to be accommodated by the perovskite structure (Fig. 3). Finally, there are a few alloys with interesting magnetic properties that can be classified as  $A_2BB'X_6$  compounds if the symbols B and B' are allowed to represent atomic clusters rather than single cations. These are illustrated, for example, by the alloy  $Al_2(AlCo_{12})(Co_9)B_6$  (Fig. 18). Sections 3.1 and 3.2 are devoted to descriptions of the perovskite and perovskite-related structures.

The  $ABX_3$  perovskites exhibit several interesting physical properties such as ferroelectricity (as in  $BaTiO_3$ ), ferromagnetism (as in  $SrRuO_3$ ), weak ferromagnetism (as in  $LaFeO_3$  or  $HoFeO_3$ ), superconductivity (as in  $SrTiO_{3-x}$ ), a large thermal conductivity due to exciton transport ( $LaCoO_3$ ), insulator-to-metallic transitions of interest for thermistor applications (as in  $LaCoO_3$ ), fluorescence compatible with laser action (as in  $LaAlO_3:Nd$ ), and transport properties of interest for high-temperature thermoelectric power (as in  $La_2CuO_4$ ). A few  $ABX_3$  perovskites have been found that are simultaneously antiferromagnetic and ferroelectric [*Sm16, Mi7, Sm9*]. The simultaneous occurrence of ferroelectricity and ferromagnetism has been reported for systems like  $Sr_{0.25}La_{0.75}MnO_3-ATiO_3$  ( $A = Ba, Pb, Bi_{0.5}K_{0.5}$ ) [*To3, To6*]. Many of the  $M^cXM_f^f$  perovskite alloys are ferromagnetic or ferrimagnetic, and a few exhibit first-order ferrimagnetic-to-ferromagnetic transitions. Nevertheless, the significance of the entire perovskite family for the field of magnetism\*) lies not yet in their technological applications, but in their provision of an isostructural series of compounds having outer  $d$  electrons that are localized and spontaneously magnetic in

\*) The technologically important dielectric properties are outside the scope of this summary. See Vol. III/3 of the New Series of Landolt-Börnstein.

dortige Anionenlücke von einem Oktaeder in einen Tetraeder umzuwandeln. Bei Verbindungen, die  $Ti^{4+}$ -Ionen enthalten, ist es dagegen wahrscheinlicher, daß die lokale Anordnung der Anionen trigonale Doppelpyramiden-Plätze bildet. Für Ionenverbindungen mit Anionenlücken, die keine A-Kationen haben, wie  $\square WO_{3-x}$ , ist gezeigt worden, daß sie  $\square BX_3$ -Blöcke enthalten, die durch „Gleit“-ebenen verbunden sind, in denen die besetzten Oktaeder gemeinsame Kanten innehaben (Fig. 22). In  $M^cX_{1-x}M_f^f$ -Legierungen können jedoch Anionenlücken auch beliebig auftreten. B-Kationenlücken können nicht vorkommen, weil die von B besetzten Oktaeder die Basis der  $ABX_3$ -Perowskitstruktur bilden. Wo scheinbare B-Kationenleerstellen auftreten, wie in  $A_mB_{m-1}X_{3m}$ , sind entweder  $A_2X_2$ -Schichten zwischen Perowskitschichten eingeschoben (Fig. 23), oder kubische (Perowskit-) Anordnungen von  $AO_3$ -Schichten wechseln mit regelmäßig verteilten hexagonalen Anordnungen, in denen die B-Ionenlücken auftreten, ab (Fig. 24). Ähnlich kristallisieren die Verbindungen der Reihe  $(AX)_m(ABX_3)_n$  mit einer Einschiebung von Steinsalzschichten (Fig. 25). Einschiebungen von kubisch gepackten  $AO_3$ -Schichten und hexagonal gepackten Schichten treten auch in solchen  $ABX_3$ -Verbindungen auf, deren A-Kation für die Perowskit-Struktur zu groß ist (Fig. 3). Schließlich gibt es einige wenige Legierungen mit interessanten magnetischen Eigenschaften, die als  $A_2BB'X_6$ -Verbindungen eingeordnet werden können, wenn man unter den Symbolen B und B' Atomgruppen statt einzelner Kationen versteht. Dies gilt z. B. für die Legierung  $Al_2(AlCo_{12})(Co_9)B_6$  (Fig. 18). Die Abschnitte 3.1 und 3.2 sind der Beschreibung der Perowskit- und verwandter Strukturen gewidmet.

Die  $ABX_3$ -Perowskite weisen einige interessante physikalische Eigenschaften auf, wie Ferroelektrizität (in  $BaTiO_3$ ), Ferromagnetismus (in  $SrRuO_3$ ), schwachen Ferromagnetismus (in  $LaFeO_3$  oder  $HoFeO_3$ ), Supraleitfähigkeit (in  $SrTiO_{3-x}$ ), große Wärmeleitfähigkeit durch Excitonentransport (in  $LaCoO_3$ ), für Thermistoren interessante Übergänge zwischen Nichtleiter und metallischem Leiter (in  $LaCoO_3$ ), für Laser-Anwendungen geeignete Fluoreszenz (in  $LaAlO_3:Nd$ ), und Transporteigenschaften, die für Thermospannungen bei hohen Temperaturen von Interesse sind (in  $La_2CuO_4$ ). Einige wenige  $ABX_3$ -Perowskite wurden gefunden, die sowohl ferromagnetisch als auch ferroelektrisch sind [*Sm16, Mi7, Sm9*]. Das gleichzeitige Auftreten von Ferroelektrizität und Ferromagnetismus wurde bei Systemen wie  $Sr_{0.25}La_{0.75}MnO_3-ATiO_3$  ( $A = Ba, Pb, Bi_{0.5}K_{0.5}$ ) [*To3, To6*] beschrieben. Viele  $M^cXM_f^f$ -Perowskitlegierungen sind ferromagnetisch oder ferrimagnetisch, und einige zeigen Übergänge erster Ordnung von Ferri- zu Ferromagnetismus. Trotzdem liegt die Bedeutung der gesamten Perowskit-Familie für den Magnetismus\*) noch nicht in der technologischen Anwendung, sondern im Vorhandensein einer isostrukturellen Reihe von Verbin-

\*) Die technologisch wichtigen dielektrischen Eigenschaften liegen nicht im Rahmen dieser Zusammenstellung. Siehe Band III/3 der Neuen Serie des Landolt-Börnstein.



one member, collective and spontaneously magnetic in another, and collective and Pauli paramagnetic in yet another. This permits a systematic experimental investigation of the properties of the  $d$  electrons on passing through the transition from a localized character, where crystal-field plus superexchange and/or double-exchange theories apply, to an uncorrelated (except below a superconducting transition temperature) collective-electron character, where the conventional band theory applies. In addition, the simplicity of the perovskite  $ABX_3$  structure minimizes competitive magnetic interactions between neighboring magnetic cations. Therefore from a study of magnetic order, as revealed by neutron diffraction, together with detailed structural information, as revealed by x-ray diffraction, it has been possible to test the semi-empirical rules for  $180^\circ$  cation-anion-cation isotropic superexchange interactions between localized electrons, the double-exchange hypothesis, antisymmetric exchange, and predictions of magnetic order and spontaneous atomic moments due to collective electrons.

Section 3.3 presents the general phenomenological exchange Hamiltonian for localized electrons and summarizes the microscopic models for isotropic superexchange, double exchange, and antisymmetric exchange. From these models, general rules for the interactions responsible for magnetic order are developed for comparison with the tabulated magnetic data.

Section 3.4 presents the fundamental physical concepts needed to construct a qualitative phase diagram for the outer  $d$  electrons as a function of the number  $n_l$  of electrons per relevant orbital, the magnitude of a nearest-neighbor transfer energy  $b$ , and the temperature  $T$ . It also summarizes the various characters of several physical properties imparted by outer electrons to show how they can be used to distinguish the electronic phases in different perovskites. Information from the tabulated data is used to show the influence of covalence and intra-atomic exchange, which help determine the parameter  $b$ , on the character of the electrons. Spontaneous collective-electron magnetism is seen to occur only in a narrow transitional interval of  $b$  between localized-electron magnetism and collective-electron Pauli paramagnetism.

Section 3.5 provides schematic energy diagrams for the alloys  $M^cXM_f^d$ . These are shown to be useful guides to predictions of the magnitudes of the atomic moments and the magnetic order.

dungen mit äußeren  $d$ -Elektronen, die lokalisiert und spontan magnetisch in der einen Verbindung, kollektiv und spontan magnetisch in einer anderen, und kollektiv und Pauli-paramagnetisch in noch einer weiteren sind. Dies erlaubt systematische experimentelle Untersuchungen der Eigenschaften der  $d$ -Elektronen, indem man von einem lokalisierten Zustand, in dem Kristallfeld plus Superaustausch- und/oder Doppelaustausch-Theorien gelten, zu einem Zustand unkorrelierter Kollektivelektronen (außer bei Temperaturen unterhalb des Übergangs zur Supraleitung) übergeht, in dem die konventionelle Bändertheorie anzuwenden ist. Weiterhin führt die Einfachheit der Perowskit- $ABX_3$ -Struktur zu minimalen konkurrierenden Wechselwirkungen zwischen benachbarten magnetischen Kationen. Aufgrund der Untersuchung der magnetischen Ordnung, die man durch die Neutronenbeugung kennt, und einer genauen Kenntnis der Struktur, wie man sie durch Röntgenbeugung gewonnen hat, war es deshalb möglich, die halbempirischen Gesetze über die isotrope  $180^\circ$ -Kation-Anion—Kation—Superaustausch—Wechselwirkung zwischen lokalisierten Elektronen, die Doppelaustausch-Hypothese, den antisymmetrischen Austausch und Voraussagen für magnetische Ordnung und spontane Atom-Momente, die von Kollektivelektronen herrühren, zu prüfen.

Der Abschnitt 3.3 enthält den allgemeinen phänomenologischen Hamilton-Austausch-Operator für lokalisierte Elektronen und faßt die mikroskopischen Modelle für den isotropen Superaustausch, den Doppelaustausch und den antisymmetrischen Austausch zusammen. Aus diesen Modellen werden allgemeine Regeln für die Wechselwirkungen, die für die magnetische Ordnung verantwortlich sind, zum Vergleich mit den tabellierten Daten entwickelt.

Der Abschnitt 3.4 enthält die grundlegenden physikalischen Ideen, die für die Herstellung eines qualitativen Phasendiagramms für die äußeren  $d$ -Elektronen als Funktion der Elektronenzahl  $n_l$  pro betreffenden Bahnzustand, der Größe einer Übertragungsenergie  $b$  zwischen nächsten Nachbarn und der Temperatur  $T$  notwendig sind. Außerdem werden hier verschiedene Charakteristika einiger durch die äußeren Elektronen gegebenen physikalischen Eigenschaften zusammengestellt, um zu zeigen, wie man mit ihrer Hilfe die elektronischen Phasen verschiedener Perowskite unterscheiden kann. Auf Grund der tabellierten Werte wird der Einfluß von Kovalenz und intra-atomarem Austausch, die den Parameter  $b$  mitbestimmen, auf den Charakter der Elektronen gezeigt. Spontane Magnetisierung der Kollektivelektronen tritt, wie man sieht, nur in einem schmalen Übergangsintervall von  $b$  zwischen dem Magnetismus lokalisierter Elektronen und dem Pauli-Paramagnetismus der Kollektivelektronen auf.

Der Abschnitt 3.5 enthält schematische Energie-diagramme für die Legierungen  $M^cXM_f^d$ . Es wird gezeigt, daß sie zu brauchbaren Voraussagen über die Größe der Atom-Momente und die magnetische Ordnung führen können.

In the introductions to the sections 3.2...3.5 we have referenced the principle theoretical contribution discussed, but no attempt was made to do this systematically for the experimental contributions, which are thoroughly referenced in the tables. — In the crystallographic tables, the crystal parameters quoted either represent the most complete analysis, in our judgment, or belong to the most complete set of parameters for a series of similar compounds. They do not necessarily represent the historical reference that established the unit-cell dimensions.

Literature was considered up to 1969.

Finally, we would like to thank DAVID MAHONEY for his willing assistance, the library and publications personnel of Lincoln Laboratory for their efficient support, and Mrs. G. E. BOYD for her help with all the foreign references.

In den Einleitungen zu den Abschnitten 3.2...3.5 haben wir die grundlegenden theoretischen Beiträge, die diskutiert werden, mit Literaturhinweisen versehen; für die experimentellen Beiträge haben wir dies nicht systematisch durchzuführen versucht, da die entsprechenden Tabellen vollständig mit Literaturhinweisen versehen sind. — In den kristallographischen Tabellen stellen die angeführten Kristallparameter entweder die nach unserer Beurteilung vollständigste Analyse dar, oder sie gehören zum vollständigsten Satz von Parametern für eine Reihe ähnlicher Verbindungen. Sie geben nicht notwendigerweise den historischen Literaturhinweis, der die Dimensionen der Einheitszelle festlegte.

Die Literatur wurde bis 1969 berücksichtigt.

Schließlich möchten wir DAVID MAHONEY für seine bereitwillige Hilfe, den Angestellten der Bibliothek und der Veröffentlichungsabteilung des Lincoln-Laboratoriums für ihre wirksame Unterstützung und Mrs. G. E. BOYD für ihre Hilfe bei der ausländischen Literatur danken.

### 3.0.2 Symbols and units used in tables and figures

#### Crystallographic structure

symmetry

$a, b, c$  [Å]

$\alpha, \beta, \gamma$  [deg]

$\Theta_{\text{trans}}, \Theta_{\text{ord}}$  [°K]

$\Theta_D$  [°K]

$T_{\text{melt}}$  [°K]

$c_{ij}$

$\epsilon_l$

$r_{A,B,B'}$  [Å]

symmetry classification for perovskite structures: C = cubic, H = hexagonal, R = rhombohedral, O = orthorhombic ( $a < c/\sqrt{2}$ ), O' = orthorhombic ( $c/\sqrt{2} < a$ ), T = tetragonal, M = monoclinic, Tr = triclinic

lattice parameters

angle between crystallographic axes

crystallographic transition and ordering temperatures

Debye temperature

melting temperature

elastic constants

crystalline strains

radius of A, B, B' cation

#### Magnetic properties (static measurements)

magnetic order

$n_A, n_B$

$\bar{n}_m$

$n_{\text{eff}}$

$\Theta_C$  [°K]

$\Theta_N$  [°K]

$\Theta_r$  [°K]

$\Theta_p$  [°K]

$\Theta'$  [°K]

$C_m$  [emu °K mole<sup>-1</sup>]

$\chi_g$  [emu/g], [cm<sup>3</sup>/g]

$\chi_m$  [emu/mole]

$p_A, p^A$  [ $\mu_B$ ]

$p_m, p^{(xy)}$

$p^*$

$J_{nn}/k$  [°K]

$d$

$\sigma_w$  [erg/cm<sup>2</sup>]

$W_{nn}$

see magnetic structure type from Fig. 26

atomic moment and component of atomic moment parallel to net ferromagnetic moment in numbers of Bohr magnetons:  $p_A = n_A \mu_B$

net magnetization per molecule in numbers of Bohr magneton:  $p_m = \bar{n}_m \mu_B$

$n_{\text{eff}} = \sqrt{8C_m}$  is the effective paramagnetic moment:  $p_{\text{eff}} = n_{\text{eff}} \mu_B$

Curie temperature

Néel temperature; extrapolated Néel temperature

temperature for spin reorientation

paramagnetic Curie temperature ( $\Theta_p < 0$  if antiferromagnetic coupling)

temperature below which parasitic  $n_0^A$  deviates appreciably from 0.05

molar Curie constant determined from Curie-Weiss law  $\chi_m = C_m/(T - \Theta_p)$

specific paramagnetic susceptibility

molar paramagnetic susceptibility

atomic moment, atomic moment of element A

molecular moment (of molecule  $xy$ )

effective paramagnetic moment:  $p^* = \sqrt{\chi_m T}$

isotropic exchange constant of Eq. (16) for near-neighbor interactions

Ln-Fe interaction parameter defined by

$M(t) = \sigma_0(0) B(t) [1 + (d/t)]$ , where  $t = T/\Theta_C$  and  $B(t)$  is the Brillouin function

domain wall energy density

net near-neighbor Weiss molecular field constant:  $H_{wi} = \sum_{j=1}^N W_{ij} M_j$

$\sigma$ { [Gauss cm <sup>3</sup> /g] [emu/g]	magnetic moment per gram = specific magnetization
$\sigma_0$ [emu/g]	specific parasitic (weak) magnetization as obtained from $\sigma = \sigma_0 + \chi_g H_a$
$\sigma_{sp}$	spontaneous specific magnetization
$H_a$ [Oe]	externally applied field
$H_{crit}$ [Oe]	critical applied field for antiferromagnetic-ferromagnetic transition or for spin-flop transition
$H_c$	coercivity
$\alpha$	cant angle
$b_1, b_2$ [dyn/cm <sup>2</sup> ]	magnetoelectric coefficients
$\lambda_{100}$	magnetostriction constant for [100] direction: $\lambda_{100} = -4b_1/3(c_{11} - c_{12})$
$C_{ijk}$	components of the tensor describing the quadratic dependence of magnetization on applied field: Eq. (36)
$\mu_B$	the Bohr magneton = 5585 emu/g
$T$ [erg/g]	torque: $T = \sigma \times H_a$
<b>Magnetic properties (resonance measurements)</b>	
$H_A$	effective crystalline-anisotropy field
$H_{ex}$	exchange field
$H_D$	spin-canting field (Dzialoshinskii field)
$H_{int}$	internal magnetic field at the nucleus
$H_n$	axial hyperfine field arising from nuclear polarization
$H_{hyp}$	hyperfine field $I \cdot A \cdot S$ , where $I$ = nuclear spin, $S$ = net atomic spin, and the components of the interaction tensor are $A_s, A_{ns}, A_\sigma, A_\pi, A_{2p}$ .
$f_s^A, f_n^A, f_\pi^A$	fraction of unpaired $s, p_\sigma$ or $p_\pi$ electron spins involved in covalent bonding: $f_s^A = 2SA_s/A_{ns} = \frac{1}{3} N_0^2 \lambda_s^2, f_n^A = 2SA_n/A_{2p} = \frac{1}{3} N_0^2 \lambda_n^2, f_\pi^A = 2SA_\pi/A_{2p} = \frac{1}{3} N_0^2 \lambda_\pi^2$ .
$\epsilon, \Delta E$	See Eq. (4) for $N_e, N_t, \lambda_s, \lambda_\sigma, \lambda_\pi$ .
$F_{ij}, G_{ij}$	nuclear quadrupole coupling constant and quadrupole splitting
$\nu_R$ [Hz]	dipolar and quadrupolar magnetoelastic coefficients: $\delta g_i = \sum_{j=1}^6 F_{ij} \epsilon_j$ and
$\Delta \nu$ [Hz]	$d_i = \sum_{j=1}^6 G_{ij} \epsilon_j$ , where $\mathcal{H}_{spin-lattice} = \mu_B H_a \cdot \delta g \cdot S + S \cdot d \cdot S$
$T_1$ [sec]	resonance frequency for NMR
$T_2$ [sec]	half-line width
$T_{1e}$ [sec]	nuclear spin-lattice relaxation time
	nuclear spin-spin relaxation time
	nuclear spin-lattice relaxation time during a locking pulse
<b>Optical measurements</b>	
$n$	index of refraction
$\epsilon_0$	low-frequency dielectric constant
$\rho$ [°/cm]	Faraday rotation
$\nu_{TO}, \nu_{LO}$ [Hz]	frequency of transverse and longitudinal optical modes
<b>Transport measurements</b>	
$\theta_{cs}$	superconducting critical temperature
$E_F$	Fermi energy
$E_a$	activation energy for a small-polaron hop
$\rho$ [ $\Omega$ cm]	electrical resistivity
$S$ [ $\mu$ V/°K]	Seebeck coefficient
$e$ [esu]	magnitude of the electronic charge
$c, n_i, n_\pm$ [cm <sup>-3</sup> ]	charge-carrier density
$\mu$ [cm <sup>2</sup> /Vsec]	charge-carrier mobility
$\tau$ [sec]	charge-carrier collision time
$m^*$ [g]	charge-carrier effective mass
$D_0$ [cm <sup>2</sup> /sec]	charge-carrier diffusion coefficient at $E_a = 0$
$N_\pm$	density of unoccupied states: $2(2\pi m_\pm^* k T / h^2)^{3/2}$
<b>General properties</b>	
$T$ [°K]	temperature
$p$	pressure
$c_p$	specific heat at constant pressure

## Abbreviations for text and indices

AFMR	antiferromagnetic resonance
APR	acoustic paramagnetic resonance
BPW	Bethe-Peierls-Weiss method
C, cub	cubic
DS	Danielson-Stevens method
DTA	differential thermal analysis
ESR	electron spin resonance = paramagnetic resonance
f.c.	face-centered permutation
FMR	ferromagnetic resonance
F <sub>R</sub>	ferromagnetic with reduced $n_A$
H, hex, hex (nL)	hexagonal, hexagonal n-layer structure
I.R.	infrared
Ln	Lanthanone = any of the rare-earth elements
MF	molecular field approximation
M, mon	monoclinic
NAR	nuclear acoustic resonance
NMR	nuclear magnetic resonance
ncub	noncubic
O, O', orth	orthorhombic (O: $a < c/\sqrt{2}$ ; O': $c/\sqrt{2} < a$ )
P&S	reference to preparation and structural information
Prep.	reference to material preparation
Prop.	reference to material properties
pscub	pseudocubic
psmon	pseudomonoclinic
R, rh	rhombohedral
RW	Rushbrooke-Wood method
S. G.	space group
S.S.	solid solution
T, tetr	tetragonal
Tr, tr	triclinic

3.1 Descriptions of stoichiometric ABX<sub>3</sub> and M<sup>e</sup>XM<sub>3</sub><sup>f</sup> structures

## 3.1.1 The ideal perovskite structure

The ideal perovskite structure has the cubic unit cell of Fig. 1 with space group Pm3m. Fig. 1(a) shows the corner-sharing octahedral units (BX<sub>3</sub> array in ABX<sub>3</sub> and XM<sub>3</sub><sup>f</sup> array in M<sup>e</sup>XM<sub>3</sub><sup>f</sup>), which form the stable skeleton of the structure. The A cation (or M<sup>e</sup> atom) occupies the body-center position. Fig. 1(b) shows the unit cell with the A cation (or M<sup>e</sup> atom) at the origin, or corner position. This shows the face-centered-cubic character (with Cu<sub>3</sub>Au-type order) of the AX<sub>3</sub> or M<sup>e</sup>M<sub>3</sub><sup>f</sup> subarrays. Fig. 1(c) shows the cubic perovskite on a hexagonal basis, with the *c* axis along the cubic [111] direction. The alternate AX<sub>3</sub> and B ionic layers each have cubic stacking. Also indicated is the ordering of B and B' layers in the ordered A(B<sub>2/3</sub>B'<sub>1/3</sub>)X<sub>3</sub> structures.

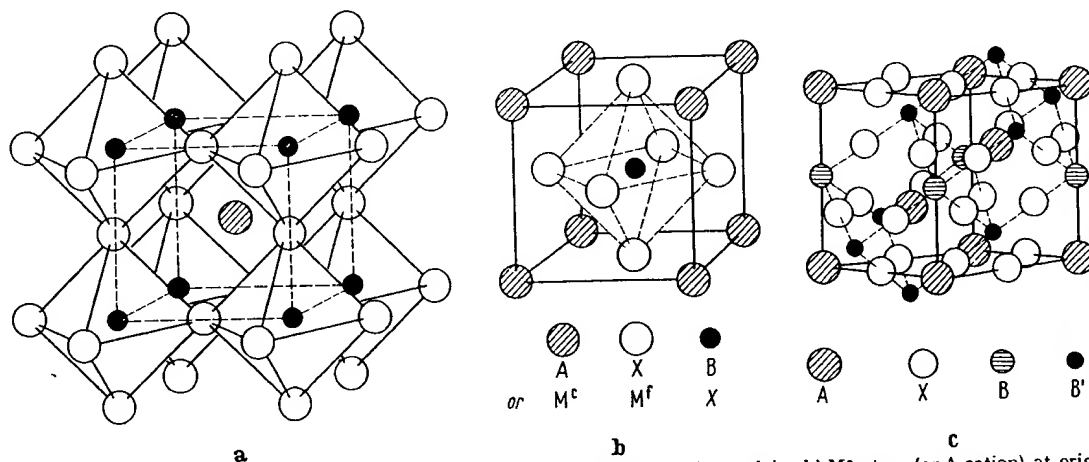


Fig. 1. ABX<sub>3</sub>, M<sup>e</sup>XM<sub>3</sub><sup>f</sup>. Ideal perovskite structure: a) B cation (or X atom) at origin. b) M<sup>e</sup> atom (or A cation) at origin. c) A cation at origin in hexagonal basis [Ga10].

The alloys M<sup>x</sup>XM<sub>1</sub><sup>1-x</sup> are stabilized by covalent M-X bonding and by metallic M-M bonding, so that they are generally cubic. Only in phases exhibiting complex magnetic order are there distortions to lower symmetry. On the other hand, the ABX<sub>3</sub> perovskites, which are primarily stabilized by the Madelung energy, are rarely cubic at normal temperatures. Madelung energy calculations are available [Ro15a, Sa2b, Mi1].

Although cubic at high temperatures, most ABX<sub>3</sub> compounds exhibit distortions to lower symmetry below some temperature  $\Theta_{\text{trans}}$  as a result of atomic displacements. Such displacive transitions can be described by a finite set of normal vibrational modes that become soft, their vibrational frequency increasing with  $T > \Theta_{\text{trans}}$ . From LANDAU's [La2] theory of phase transitions, it may be argued [Ha1, Co2] that at a second-order displacive transition, the frequency of one normal mode becomes zero. Thus the occurrence of ferroelectricity in perovskite-type crystals such as BaTiO<sub>3</sub> has been correlated both theoretically and experimentally [An2, Co1, Ba17, Co28, Ne8, Sh26] with the existence of a transverse optic mode of lattice vibration having wave number  $k \approx 0$  and a temperature-dependent frequency  $\omega \sim (T - \Theta_{\text{trans}})^{1/2}$ .

Similarly, in the case of LaAlO<sub>3</sub>, softening of a single normal mode can produce the R $\bar{3}c$ -to-cubic transition, and this transition is probably second-order. Investigation [Ha1] of the atomic displacements involved in other distortions from cubic symmetry, on the other hand, has shown that several normal modes are involved, and these displacive transitions are first-order.

SrTiO<sub>3</sub> exhibits a tetragonal (D<sub>4h</sub><sup>18</sup> with  $c/a = 1.00056$ ) to cubic transition at  $\Theta_{\text{trans}} = 110^\circ\text{K}$  [Ly2, Ri5] that appears to illustrate the softening of a triply degenerate phonon at the  $R$  point of the Brillouin zone in the cubic phase. For  $T < \Theta_{\text{trans}}$ , it splits into two zone-center phonons having a frequency dependence  $\omega \sim (\Theta_{\text{trans}} - T)^{0.31}$  [Fi2]. In the presence of an external electric field  $E_a$  the symmetry is further reduced to C<sub>4v</sub> if  $E_a \parallel c$ -axis, or C<sub>2v</sub> if  $E_a \perp c$ -axis, and the critical modes have the same symmetry as the ferroelectric TO modes. "Anticrossing" of the modes occurs for  $E_a = 1.5 \text{ kV/cm}$  and  $15 \text{ kV/cm}$  [Ne7, Wo19]. Thus the observed [He5] maximum in the electric susceptibility of SrTiO<sub>3</sub> at very low temperatures does not appear to be associated with a ferroelectric transition.

Theoretical interest in the analytic description of these phase transitions continues [Go1a, Mu4a, Ta14a, Th3].

The physical origins of the various crystallographic distortions may be separated into three parts: relative ionic sizes, electron ordering among localized electrons, and electron ordering among collective electrons.

### 3.1.2 The influence of relative ionic sizes

#### 3.1.2.1 Tolerance factor

The first prerequisite for a stable perovskite structure is the existence of a stable BX<sub>3</sub> skeletal subarray. If the B-cation radius is  $r_B < 0.51 \text{ \AA}$  in oxides, for example, the B cation does not achieve its optimum B-O separation in an octahedral site and therefore stabilizes a structure with a smaller anion coordination. The Al<sup>3+</sup> ion is borderline, being stable in four, five or six coordination. However, Ga<sup>3+</sup>, Ge<sup>4+</sup> and V<sup>5+</sup> ions are definitely more stable in tetrahedral sites at ambient pressures.

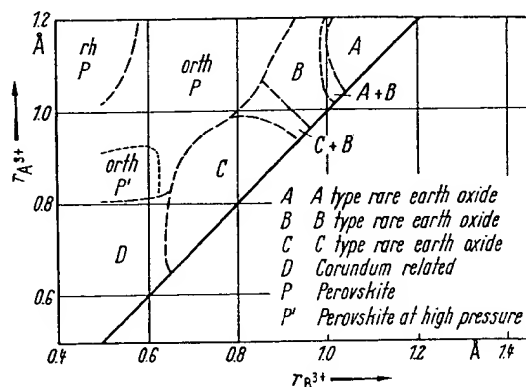
Given the BX<sub>3</sub> skeletal subarray, additional stabilization is achieved by accommodating a large A cation within this skeleton. Because there is an optimum A-X bond length, the presence of an A atom generally distorts the BX<sub>3</sub> array so as to optimize the A-X bonding. However, if this distortion is too large, then other space groups become competitive. GOLDSCHMIDT [Go2] defined the tolerable limits on the size of the A cation via a tolerance factor

$$t = (r_A + r_X) / \sqrt{2} (r_B + r_X) \quad (1)$$

where  $r_A$ ,  $r_B$ ,  $r_X$  are empirical radii of the respective ions. By geometry, the ideal cubic structure should have  $t = 1$ . The perovskite structure occurs only within the range  $0.75 < t < 1.00$ . However, this is not a sufficient condition, since the A and B cations must, in themselves, be stable in twelvefold (12 or 8 + 4 or 6 + 6) and sixfold coordinations. This sets lower bounds for the cationic radii. In oxides these bounds are  $r_A > 0.90 \text{ \AA}$  and  $r_B > 0.51 \text{ \AA}$ . In addition, MEGAW [Me5] noted that, if  $0.75 < t < 0.9$ , a cooperative buckling of the corner-shared octahedra to optimize the A-X bond lengths enlarges the unit cell; on the other hand, if  $0.9 < t < 1$ , such buckling may not be found, although small distortions to rhombohedral symmetry occur. These structures are to be distinguished from perovskites that exhibit additional distortions as a result of electron ordering. The cubic phase is found at high temperatures or where the A-X bond is more ionic (especially if  $t \approx 1$ ).

Where the A cation is too small ( $r_A < 0.9 \text{ \AA}$ ) to accommodate twelve nearest neighbors, a structure in which the A and B cations are both six-coordinated becomes competitive. From the phase diagram of Fig. 2 for the oxides A<sup>3+</sup>B<sup>3+</sup>O<sub>3</sub>, which has been adapted from SCHNEIDER, ROTH, and WARING [Sc13], the initial competition is the C-M<sub>2</sub>O<sub>3</sub> structure, which contains two unusual types of corner-shared, six-coordinated sites. The C-M<sub>2</sub>O<sub>3</sub> structure consists of a face-centered-cubic array of cations with anions occupying  $\frac{1}{2}$  of the tetrahedral interstices in an ordered manner. Thus each cation has six out of eight near-neighbor anions at the corners of a circumscribing cube:  $\frac{1}{4}$  of the cations have two anions missing at the ends of a body diagonal and  $\frac{1}{2}$  of the cations have two anions missing at the end of a face diagonal of the circumscribing cube. This arrangement minimizes the electrostatic repulsive forces between the cations.

Fig. 2. General  $r_A - r_B$  phase diagram for  $A^{2+}B^{3+}O_3$  compounds based on ionic-size considerations. Exceptions may occur where considerations other than ionic radii  $r_A, r_B$  become important, as in the case  $A = Bi$ . A similar plot for  $A^{2+}B^{4+}O_3$  perovskites is not useful because secondary considerations are amplified by ferroelectric distortions and the possibility of different layer sequences where larger A cations are present. [Adapted from *Sc13*].



Given smaller A cations, however, electrostatic screening between face-shared octahedra can be achieved by displacements of the cations away from the shared face, and the structure competitive with perovskite is generally built from an hexagonal-close-packed anion array, which has octahedral holes sharing common faces along the  $c$ -axis. With one octahedral hole per anion and a cation/anion ratio 2/3, the cations are ordered among these holes so as to minimize the electrostatic energy. If the A and B cations carry the same charge, as in  $A^{3+}B^{3+}O_3$ , only pairs of cations share common octahedral-site faces and there is no ordering of A and B within the cationic array. This allows the electrostatic force between two cations sharing a common octahedral face to be reduced by displacements of the cations away from each other, thus distorting the octahedra. The result is the corundum structure of  $Al_2O_3$ . If the cations A and B carry different charges, as in  $A^{2+}B^{4+}O_3$ , then the A and the B cations order into alternate puckered cationic (111) planes of the rhombohedral corundum structure to form the ilmenite structure. However, where there is a large difference in the cationic charges, as in  $Li^+Sb^{5+}O_3$  and  $Li^+Nb^{5+}O_3$ , two other alternatives become competitive: (1) The  $A^+$  ions order in strings of face-shared octahedra so as to permit the  $B^{5+}$ -ion octahedra to share only edges with near-neighbor occupied octahedra. This structure is illustrated by  $LiSbO_3$  [*Ed1*]. (2) After ordering  $B^{5+}$  and  $Li^+$  ions within each cationic (111) plane of the corundum structure in such a way that  $B^{5+}$  and  $Li^+$  ions share common octahedral-site faces, each  $A^+$  cation is then displaced into the far face of its octahedron, where it is equally spaced from  $B^{5+}$  cations above and below so long as the  $B^{5+}$  cations remain in the centers of their octahedra. This is the structure of paraelectric  $LiNbO_3$  and  $LiTaO_3$  [*Ab3*].

Where the A cation is too large ( $t > 1.0$ ), the close-packed  $AX_3$  layers of Fig. 1(c) tend to change their stacking sequence from cubic to hexagonal. However, the change from the all-cubic stacking of the rhombohedral perovskite structure to the all-hexagonal stacking of the hexagonal (hex. 2L)  $CsNiCl_3$  structure goes via the three intermediate steps shown in Fig. 3 [*Lo1*]. The first step is the hexagonal  $BaTiO_3$  structure of Fig. 3(c). It is a six-layer structure with stacking sequence  $a-b-c-a-c-b-a$ , corresponding to one hexagonal stacking out of three. In this structure (hex. 6L), two-out-of-three B cations form pairs sharing a common octahedral-site face, and one-out-of-three B cation shares only common octahedral-site corners as in the perovskite structure. Many ordered compounds  $A_3B_2B'O_3$  are known to have this structure. The second step, illustrated by the hexagonal  $BaMnO_3$  structure of Fig. 3(d), alternates hexagonal and cubic stackings with the sequence  $a-b-c-b-a$ . This four-layer structure (hex. 4L), contains only B-cation pairs sharing common octahedral-site faces. The electrostatic forces between paired B-cations in Figs. 3(c), (d) displace the paired cations from one another along the  $c$  axis, exactly as in the corundum

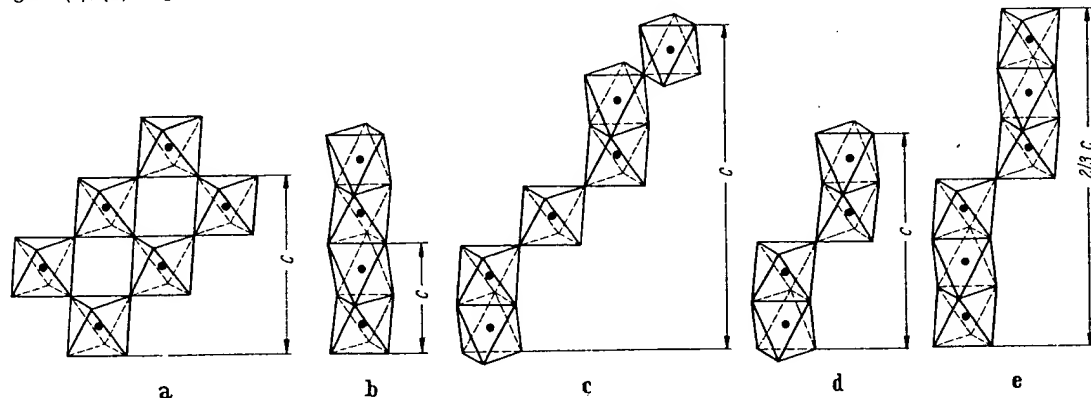


Fig. 3. Stable structures intermediate to a) cubic perovskite and b) the two-layer hexagonal  $CsNiCl_3$  structure, c) six-layer hexagonal  $BaTiO_3$  structure, d) four-layer hexagonal  $BaMnO_3$  structure, e) nine-layer hexagonal  $BaRuO_3$  structure. [Adapted from *Ca2*].

structure. The third step is the nine-layer (hex. 9L) structure of  $\text{BaRuO}_3$ , which has two hexagonal stackings out of three in the sequence  $a-b-c-b-c-a-b-a$ . Here the B cations form strings of three sharing common octahedral-site faces along the  $c$ -axis. Electrostatic forces displace the two end-member B cations away from the center B cation of each string, as shown in Fig. 3(e). Because cubic stacking is stabilized by hydrostatic pressure, it is possible to convert under pressure and high temperature the hexagonal structures to the perovskite structure through the successive sequence of steps. This is well illustrated by the  $\text{Ba}_{1-x}\text{Sr}_x\text{RuO}_3$  system as shown in Fig. 4(a). These particular intermediate structures appear to be stabilized by the cation displacements, but at the cost of alternating the stacking sequence. The (hex. 4L) structure, which has the maximum alternation of stacking, is not always found, and the intermediate structures tend to be stabilized by smaller B cations, as illustrated in Fig. 4(b).

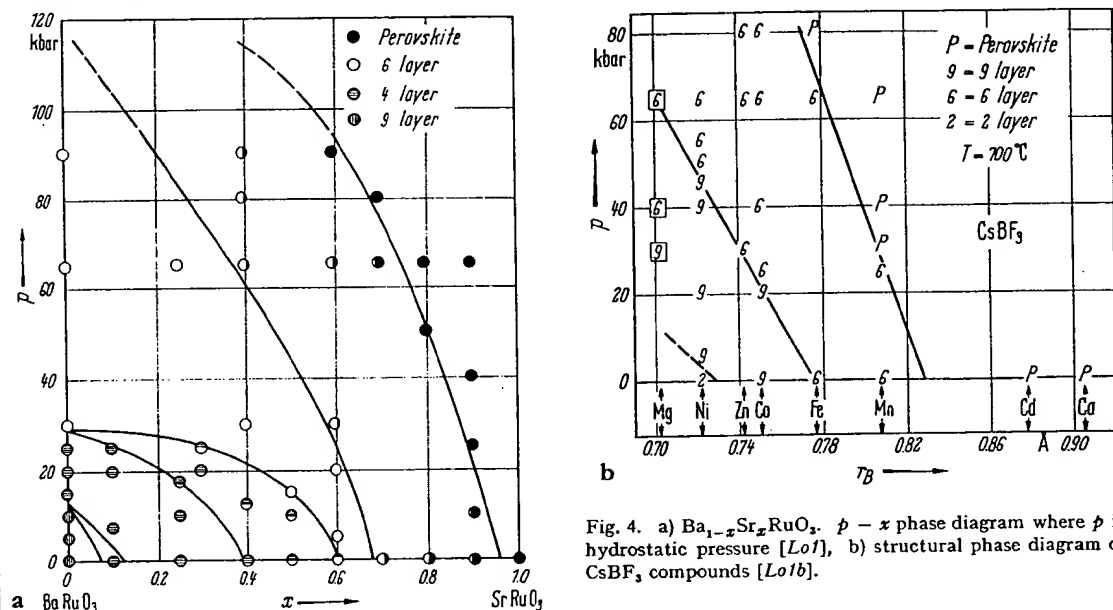


Fig. 4. a)  $\text{Ba}_{1-x}\text{Sr}_x\text{RuO}_3$ .  $p-x$  phase diagram where  $p$  is hydrostatic pressure [Lo1], b) structural phase diagram of  $\text{CsBF}_3$  compounds [Lo1b].

### 3.1.2.2 O-orthorhombic structure

Cooperative buckling of corner-shared octahedra, although indexed on a monoclinic pseudocell in earlier work, may produce the orthorhombic primitive cell of Fig. 5 containing four formula units. It was first identified in single crystals of  $\text{GdFeO}_3$  [Ge1] and later confirmed [Co21]. Powder photographs taken with  $\text{CrK}_\alpha$  radiation could be indexed on the monoclinic pseudocell containing a single  $\text{GdFeO}_3$  molecule, which is the origin of the earlier classification. The pseudocell dimensions of  $\text{GdFeO}_3$  are  $a = c = 3.87 \text{ \AA}$ ,  $b = 3.83 \text{ \AA}$ ,  $\beta = 92.8^\circ$ , where  $2b_{\text{pseudocell}} = c_{\text{true cell}}$ . The true orthorhombic cell is referred to in the tables as O-orthorhombic and is distinguished from the O'-orthorhombic structure by a lattice-parameter ratio

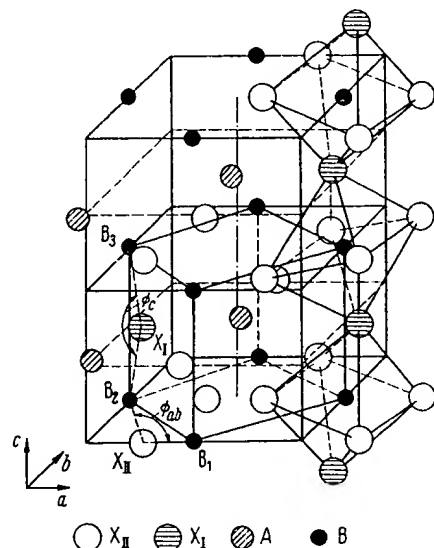


Fig. 5.  $\text{GdFeO}_3$ . O-orthorhombic structure.

$\phi_{ab} = \frac{1}{2} \text{B}_1\text{X}_{II}\text{B}_2$ ,  $\phi_c = \frac{1}{2} \text{B}_2\text{X}_I\text{B}_3$ .

Fig. from [Ve12], structure [Ge1], coordinates [Co21].

ion	position	coordinates		
		$x$	$y$	$z$
$\text{Gd}^{3+}$	4(c)	-0.018	0.060	$\frac{1}{2}$
$\text{Fe}^{3+}$	4(b)	$\frac{1}{2}$	0	0
$\text{O}_1^{2-}$	4(c)	0.05	0.470	$\frac{1}{2}$
$\text{O}_2^{2-}$	8(d)	-0.29	0.275	0.05

$c/a > \sqrt{2}$ , where  $a < b$ . The O'-orthorhombic structure, which has  $c/a < \sqrt{2}$ , is the result of a superposed Jahn-Teller (with or without spin-orbit coupling) distortion. It is also to be distinguished from ferroelectric O<sub>B</sub><sup>F</sup>-orthorhombic and O<sub>B</sub><sup>F</sup>-orthorhombic distortions in which each B cation is removed from the center of symmetry of its interstice. Other orthorhombic distortions have been reported for NdGaO<sub>3</sub> [Br26] and NaCoF<sub>3</sub> [Ok5].

The O-orthorhombic unit cell has the probable space group Pbnm with A cations in positions 4(c):  $\pm(x, y, \frac{1}{2}; \frac{1}{2} - x, \frac{1}{2} + y, \frac{1}{2})$ , the B cations in 4(b):  $(\frac{1}{2}, 0, 0; \frac{1}{2}, 0, \frac{1}{2}; 0, \frac{1}{2}, 0; 0, \frac{1}{2}, \frac{1}{2})$ , eight anions X<sub>II</sub> in 8(d):  $\pm(x, y, z; \frac{1}{2} - x, \frac{1}{2} + y, \frac{1}{2} - z; \bar{x}, \bar{y}, \frac{1}{2} + z; \frac{1}{2} + x, \frac{1}{2} - y, \bar{z})$ , and the remaining four anions X<sub>I</sub> in 4(c). Coordinates for the ions in GdFeO<sub>3</sub> are also given in Fig. 5.

The buckling of the corner-shared octahedra decreases the cation-anion-cation angle  $\Phi$  from 180°. If the B cations and the anions are distinguished as B<sub>1</sub>( $\frac{1}{2}, 0, 0$ ), B<sub>2</sub>( $0, \frac{1}{2}, 0$ ), B<sub>3</sub>( $\frac{1}{2}, 0, \frac{1}{2}$ ), X<sub>II</sub>( $\frac{1}{2} + x, \frac{1}{2} - y, \bar{z}$ ), and X<sub>I</sub>( $\frac{1}{2} - x, \frac{1}{2} + y, \frac{1}{2}$ ), then the two representative angles are  $\Phi_{ab} = (B_1 - X_{II} - B_2)$  and  $\Phi_c = (B_2 - X_I - B_3)$ . GILLES [Gi4] has estimated that in La(Co<sub>0.2</sub>Mn<sub>0.8</sub>)O<sub>3</sub> these angles are  $\Phi_{ab} = 150^\circ \pm 3^\circ$  and  $\Phi_c = 177^\circ \pm 3^\circ$  with B<sub>1</sub> - O<sub>II</sub> = 1.95 Å, B<sub>2</sub> - O<sub>II</sub> = 2.10 Å, B<sub>1</sub> - O<sub>I</sub> = B<sub>3</sub> - O<sub>I</sub> = 1.96 Å. The angles in GdFeO<sub>3</sub> are similar.

### 3.1.2.3 Rhombohedral structures

Where there is no buckling of the octahedra, the perovskites ABX<sub>3</sub> may have a small deformation from cubic to rhombohedral symmetry. Where this deformation does not enlarge the unit cell, it is possible to index it either on a unit cell containing two formula units, as shown in Fig. 6, or on a unit cell containing one formula unit. The corresponding rhombohedral angles are  $\alpha \approx 60^\circ$  or  $\alpha \approx 90^\circ$ . In the early literature, detailed anion positions were not known, and it was common to use the smaller cell with  $\alpha \approx 90^\circ$ . However, the anions are generally displaced so as to require the larger unit cell of Fig. 6, which has  $\alpha \approx 60^\circ$ .

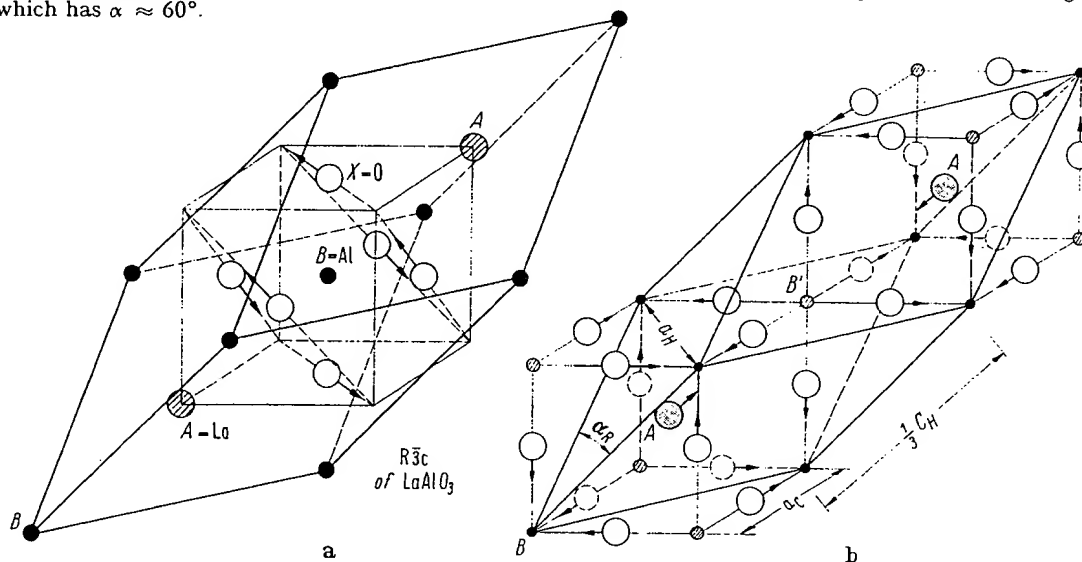


Fig. 6. Rhombohedral ABX<sub>3</sub> structures: a) anion shifts for symmetry R $\bar{3}c$ ; b) the simplest ionic displacements, corresponding to symmetry R $\bar{3}m$  for ordered A<sub>2</sub>B'B'<sub>2</sub>X<sub>6</sub> structures having  $r_{B'} > r_B$  [Ra3].

Anion displacements from their ideal positions may be of three different types: (1) AX<sub>3</sub>(111) planes remain equidistant from neighboring B-cation (111) planes, leaving all the B-cations equivalent. Within these planes, three A-X distances are reduced and three are enlarged via cooperative rotations of the B-cation octahedra, as shown in Fig. 6(a). (2) The anions may move within pseudocubic {110} planes including the B-B axes so as to create two distinguishable B positions: B positions having a shorter B-X separation and B' positions having a larger B'-X separation. This gives the symmetry R $\bar{3}m$ , which allows the A cations to be displaced along the [111] axis so as to make the separations B-A  $\neq$  B'-A. (3) In the most general case, the anion displacements may be decomposed into R $\bar{3}c$  and R $\bar{3}m$  components. The resulting symmetry R $\bar{3}$  also gives distinguishable B and B' positions via its R $\bar{3}m$  component.

Although the distinction between these possibilities has been determined in only a few cases, it appears that R $\bar{3}c$  can be anticipated unless there is a physical reason for creating two distinguishable positions B and B'. This conclusion is based on the fact that LaAlO<sub>3</sub> has been shown to have the symmetry R $\bar{3}c$  by neutron diffraction, [De14] nuclear quadrupole resonance [Mu5], electron-spin resonance, [Ki3] and x-ray techniques [Ge4b, De17]. It is strongly supported by the observation [Ra3] that LaCoO<sub>3</sub> has the symmetry R $\bar{3}c$  at low temperatures, where all of the trivalent cobalt are in their low-spin state, but has the symmetry R $\bar{3}$  at higher temperatures where thermal activation creates a nearly equal population of high-spin and low-spin cobalt ions. These are crystallographically distinguishable, via different ionic radii, as B and B'.



## 3.1.3 The influence of localized-electron ordering

## 3.1.3.1 Crystal-field theory

Crystal-field theory rests on the assumption that the outer electrons to be described are localized at discrete atomic positions. This assumption is valid for outer *f* electrons; it is valid for *d* electrons in fluorides and in many oxides. Given this assumption, the Schroedinger equation  $\mathcal{H}\psi = E\psi$  that describes the localized orbitals and their energies contains the Hamiltonian

$$\mathcal{H} = \mathcal{H}_0 + V_{el} + V_{cub} + (V_{LS} + V_{ncub} + V_{\lambda} + \sum_j V_{ij}) \quad (2)$$

where  $\mathcal{H}_0$  is the Hamiltonian for a hydrogen-like, spherical potential,  $V_{el}$  is the atomic correction for spherical symmetry that enters if there is more than one outer *d* electron, and  $V_{cub}$  is the energy correction due to the cubic component of the crystalline fields. For outer *d* electrons,  $V_{el}$  and  $V_{cub}$  are generally  $\approx 1$  eV, and the ion is in a high-spin or a low-spin state depending upon the relative magnitudes of these two terms. In the case of 3*d* electrons, the perturbations listed within the parentheses are all  $< 0.1$  eV, and they must be considered simultaneously.  $V_{LS} = \lambda \mathbf{L} \cdot \mathbf{S}$  is the spin-orbit coupling energy, and covalent mixing reduces slightly the parameter  $\lambda$  from its free-atom value.  $V_{ncub}$  is the noncubic component of the crystalline field,  $V_{\lambda}$  is the elastic coupling energy associated with cooperative local distortions, and  $V_{ij}$  is the magnetic exchange energy coupling localized atomic moments on neighboring cations.

Solution of the zero-order equation  $\mathcal{H}_0\psi = E\psi$  gives hydrogenic wave functions  $f_{l,m} = R_l(r) Y_l^m(\theta, \phi)$ . From the spherical harmonics  $Y_l^m(\theta, \phi)$ , the *d* electrons ( $l = 2$ ) have the following angular dependence and azimuthal-angular-momentum quantum number *m* derived from  $L_z f = -i\hbar \partial f / \partial \phi = m\hbar f$ :

$$\begin{aligned} f_A &\sim (3z^2 - r^2)/r^2 &= (3\cos^2\theta - 1); & m = 0 \\ (f_D \pm if_E) &\sim 2(zx \pm iyz)/r^2 &= \sin 2\theta \exp(\pm i\phi); & m = \pm 1 \\ (f_B \pm if_C) &\sim (x^2 - y^2 \pm i2xy)/r^2 &= \sin^2\theta \exp(\pm i2\phi); & m = \pm 2 \end{aligned} \quad (3)$$

where  $\theta, \phi$  are conventional spherical coordinates. The perturbation  $V_{el}$  reflects the fact that outer electrons of parallel spin are excluded from one another and therefore screen each other less from the positive atomic nucleus than do those of antiparallel spin. This correction is responsible for Hund's highest-multiplicity rule for the free atoms. It influences the radial part of the wave function, and hence the relative energies of states of different spin, but not the angular part.

Given the cartesian axes at a B cation formed by the principal axes of its octahedral interstice, the five *d* orbitals of Eq. (3) are separated into two symmetry groups;  $f_A$  and  $f_B$ , which are directed along the cartesian axes toward near-neighbor anions, have  $E_g$  symmetry and are referred to as  $e_g$  orbitals;  $f_C, f_D$ , and  $f_E$ , which are more stable because they are directed away from the near-neighbor anions, have  $T_{2g}$  symmetry and are referred to as  $t_{2g}$  orbitals. The principal contribution to the cubic-field splitting 10 Dq of  $T_{2g}$  and  $E_g$  energies is due to covalent mixing, not to electrostatic energies as calculated on a point-charge model. If covalent mixing with the near-neighbor anionic and A-cationic orbitals is introduced, then the crystalline localized orbitals of  $t_{2g}$  and  $e_g$  symmetry become

$$\begin{aligned} \psi_t &= N_t(f_t - \lambda_n \phi_n + \lambda_A \phi_A) \\ \psi_e &= N_e(f_e - \lambda_s \phi_s - \lambda_\sigma \phi_\sigma) \end{aligned} \quad (4)$$

where  $f_t$  and  $f_e$  are linear combinations of the atomic  $f_C, f_D, f_E$  and  $f_A, f_B$  orbitals. The symmetrized anionic  $p_n, s$  and  $p_\sigma$  orbitals are  $\phi_n, \phi_s$  and  $\phi_\sigma$ ; the symmetrized A-cationic *s, p* orbitals are  $\phi_A$ . The covalent-mixing parameters  $\lambda_\sigma, \lambda_n, \lambda_A, \lambda_s$  are roughly proportional to the overlap integral for atomic orbitals on neighboring ions and inversely proportional to their energy separation. Initially, the energy separations of cationic *d* and  $\phi_\sigma$  or  $\phi_n$  are given by  $E_M - E_I$ , the difference between the Madelung energy and ionization potentials for the "effective" ionic charges, so that by symmetry

$$10Dq = \Delta_M + (\lambda_\sigma^2 - \lambda_n^2)(E_M - E_I), \lambda_n < \lambda_\sigma \quad (5)$$

where  $\Delta_M$  is any electrostatic contribution to 10 Dq. The one-electron crystal-field splitting of the *d*-state manifold is shown in Fig. 7(a). The relationship  $\lambda_n < \lambda_\sigma$  has been confirmed by nuclear magnetic resonance studies of  $\text{KMnF}_3$ ,  $\text{KNiF}_3$ , and  $\text{K}_2\text{NiCrF}_6$  [Sh30, Hu4]. In these experiments the fractional occupancies by unpaired spins of the 2*s*, 2*p<sub>σ</sub>*, and 2*p<sub>n</sub>* orbitals are:

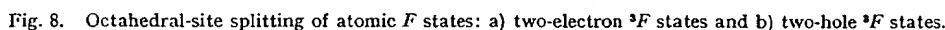
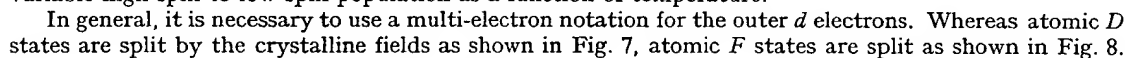
$$fx_s \equiv 2SA_s/A_{2s} \sim N_s^2\lambda_s^2, \quad fx_\sigma = 2SA_\sigma/A_{2p} \sim N_\sigma^2\lambda_\sigma^2, \quad fx_n = 2SA_n/A_{2p} \sim N_n^2\lambda_n^2$$

where  $A_s$  is the isotropic component and  $A_\sigma, A_n$  the anisotropic components of the hyperfine interaction tensor  $A_{ij}$  entering the nuclear spin-electron spin coupling energy  $\sum_j \mathbf{I}_j \cdot \mathbf{A}_{ij} \cdot \mathbf{S}_j$ . Interpretation of the phenomenological parameters  $\lambda_n, \lambda_\sigma$  and 10 Dq has been discussed extensively [Hu4].

With more than one outer *d* electron or *d* hole, it is necessary to introduce  $V_{el}$ , which is responsible for Hund's highest multiplicity rule (highest net *S* and *L*) for the free atoms. For four outer electrons, the atomic ground term is therefore  $^5D$ . In a crystal, this rule may break down as a result of the crystalline

field  
may  
with  
( $\Delta_{ex}$ )Fig  
a)  $\Delta$ Hu  
sio:  
Sir  
is:  
pa:  
pe:  
the  
va:  
stao  
 $t_2$   
t

3



137

parameter  $\lambda$  is reversed [Gr9]. Therefore ground states having an orbital degeneracy and  $m \neq 0$  are split by  $V_{LS}$  into  $(2J + 1)$  multiplet states corresponding to states of different  $J = L + S$ . However, the order of the levels is inverted (largest  $J$  lowest for less than five  $d$  electrons, smallest  $J$  lowest for more than five  $d$  electrons) because of the change in sign of  $\lambda$ . According to the Landé interval rule, the separation between states  $J$  and  $J + 1$  is  $|\lambda|(J + 1)$ . The first-order multiplet splittings, which do not include mixing of higher states of similar symmetry, are shown in Fig. 9 for  $\text{Fe}^{2+}$  and  $\text{Co}^{2+}$  ions. Note that the term is now identified by its symmetry character  $T_{2g}$  or  $T_{1g}$  rather than by its atomic orbital-momentum character  $D$  or  $F$ . Tab. 1 summarizes the various symmetry notations for different spin states.

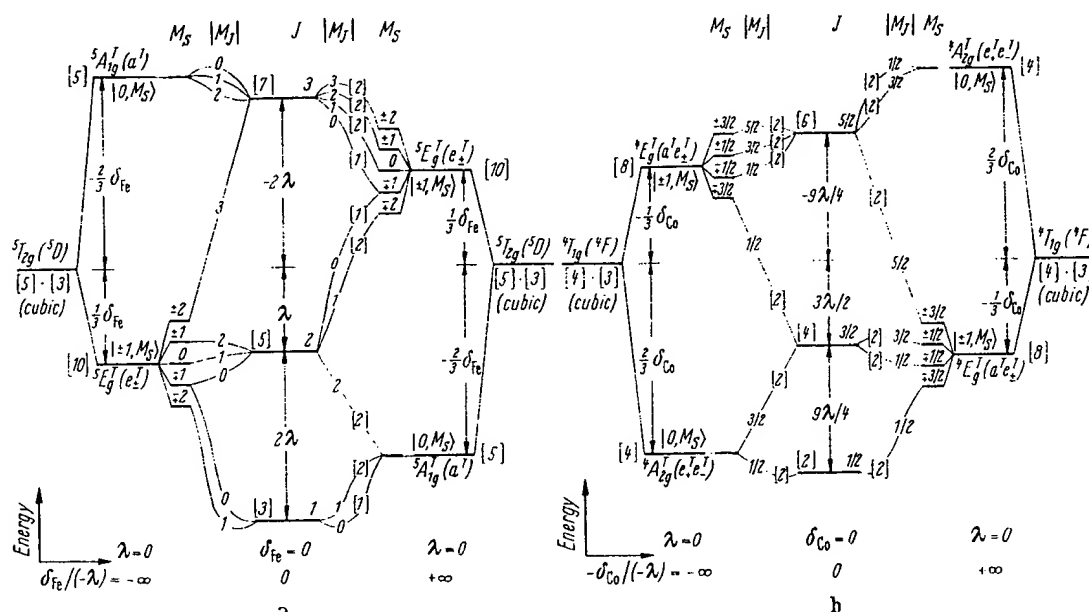


Fig. 9. Schematic spin-orbit plus trigonal-field, or tetragonal-field, splittings of cubic-field levels as a function of the ratio  $\delta/(-\lambda)$  for a)  ${}^5T_{2g}$  level of  $\text{Fe}^{2+}$  and b)  ${}^4T_{1g}$  level of  $\text{Co}^{2+}$ .

Spin-orbit coupling introduces an axial symmetry to the charge distribution, where the spin (or atomic-moment) defines the axis. Therefore, if there is a noncubic component to the crystalline field ( $V_{\text{ncub}} \neq 0$ ), then there is a spin-lattice interaction via the orbital-lattice interaction that introduces a magnetic anisotropy. For localized electrons, this is a local, one-ion anisotropy. Conversely, if the spins are ordered below some transition temperature, then the local interstices have time to relax about the noncubic charge distribution, thereby distorting the octahedral site. Therefore there is an intimate connection between the noncubic symmetry and the magnitude of the multiplet splitting. The noncubic component is usually parametrized as

$$V_{\text{ncub}} = \delta(L_z^2 - \frac{3}{2}), \quad (6)$$

and Fig. 9 includes the total perturbation  $V_{LS} + V_{\text{ncub}}$  of the one-electron and two-electron ground states.

With one or two holes in a half-shell, the one-electron and two-electron energy diagrams are inverted. In these cases  $M_L = \sum m_l = 0$ , so that  $V_{LS} = 0$ , and there is no multiplet splitting.

Tab. 1 also displays the general ground-state wave functions for a magnetically ordered phase having collinear spins. The coefficients  $a_1, a_2, a_3$  of the Kramers' doublets and  $b_1, b_2$  of the singlets all depend upon the relative magnitudes of the five perturbation terms  $V_{LS} + V_{\text{ncub}} + V_\lambda + \mathcal{H}_Z$  where  $\mathcal{H}_Z$  is the Zeeman energy due to the internal molecular field resulting from magnetic order. The molecular-field approximation is used for the first-order, isotropic magnetic-coupling energy  $\mathcal{H}_{\text{ex}}$ , which is the dominant term in  $\sum_j V_{ij}$  [see discussion of Eq. (13)]. This gives

$$\mathcal{H}_Z \approx 2J_p \langle S \rangle S_z \quad (7)$$

where  $J_p$ , the sum of all near-neighbor exchange parameters, can be determined from the temperature dependence of the magnetic susceptibility and  $z$  is along the axis of the average spin  $\langle S \rangle$  on the neighboring cations. This term contributes to the spectroscopic-splitting factor  $g$ , and hence to the net atomic moment, if  $V_{LS} \neq 0$ . In Tab. 1, the components of the wave functions are designated by the notation  $|M_L, M_S\rangle$ , where  $M_L, M_S$  are the azimuthal quantum numbers for the net orbital and spin momenta.

Tab. 1. Lowest terms and ground state wave function for octahedral-site cations having *n* localized outer *d* electrons

<i>n</i>	Ion	<i>t<sub>2g</sub><sup>n</sup></i>	<i>V<sub>el</sub></i>	<i>V<sub>cub</sub></i>	<i>V<sub>LS</sub></i>	<i>V<sub>LS</sub> + V<sub>ncub</sub> (δ &lt; 0) + ℳ<sub>Z</sub></i>	<i>V<sub>LS</sub> + V<sub>ncub</sub> (δ &gt; 0) + ℳ<sub>Z</sub></i>
1	Ti <sup>3+</sup> , V <sup>4+</sup> , W <sup>5+</sup> , Re <sup>6+</sup>	<i>t<sub>2g</sub><sup>1</sup></i>	<sup>2</sup> D	<sup>2</sup> T <sub>2g</sub>	$J = \frac{3}{2}$	$ +1, +\frac{1}{2}\rangle$	$a_1 0, +\frac{1}{2}\rangle + a_2 +1, -\frac{1}{2}\rangle$
2	V <sup>3+</sup> , Cr <sup>4+</sup> , Mo <sup>5+</sup>	<i>t<sub>2g</sub><sup>2</sup></i>	<sup>3</sup> F	<sup>3</sup> T <sub>1g</sub>	$J = 2$	$ +1, +1\rangle$	$b_1 +1, -1\rangle + b_2 0, 0\rangle + b_3 -1, +1\rangle$
3	V <sup>2+</sup> , Cr <sup>3+</sup> , Mn <sup>4+</sup> , Mo <sup>3+</sup>	<i>t<sub>2g</sub><sup>3</sup></i>	<sup>4</sup> F	<sup>4</sup> A <sub>1g</sub>	$J = \frac{3}{2}$	$ 0, +\frac{3}{2}\rangle$	$ 0, +\frac{3}{2}\rangle$
4	Cr <sup>2+</sup> , Mn <sup>3+</sup>	<i>t<sub>2g</sub><sup>4</sup></i>	<sup>5</sup> D	<sup>5</sup> E <sub>g</sub>	$J = 2$	${}^5B_{1g} 0, +2\rangle$	${}^5A_{1g} 0, +2\rangle$
5	Fe <sup>4+</sup> , Ru <sup>IV</sup> , Os <sup>IV</sup>	<i>t<sub>2g</sub><sup>5</sup></i>	<sup>6</sup> S	<sup>3</sup> T <sub>1g</sub>	$J = 0$	$b_1 +1, -1\rangle + b_2 0, 0\rangle + b_3 -1, +1\rangle$	$b_1 +1, -1\rangle + b_2 0, 0\rangle + b_3 -1, +1\rangle$
6	Mn <sup>2+</sup> , Fe <sup>3+</sup>	<i>t<sub>2g</sub><sup>6</sup></i>	<sup>6</sup> S	<sup>6</sup> A <sub>1g</sub>	$J = \frac{5}{2}$	$ 0, +\frac{5}{2}\rangle$	$ 0, +\frac{5}{2}\rangle$
7	Fe <sup>2+</sup> , Co <sup>3+</sup>	<i>t<sub>2g</sub><sup>7</sup></i>	<sup>5</sup> D	<sup>2</sup> T <sub>2g</sub>	$J = \frac{1}{2}$	$a_1 0, +\frac{1}{2}\rangle + a_2 +1, -\frac{1}{2}\rangle$	$a_1 0, +\frac{1}{2}\rangle + a_2 +1, -\frac{1}{2}\rangle$
8	Co <sup>2+</sup>	<i>t<sub>2g</sub><sup>8</sup></i>	<sup>5</sup> D	<sup>5</sup> T <sub>2g</sub>	$J = 1$	$a_1 -1, +2\rangle + a_2 0, +1\rangle + a_3 +1, 0\rangle$	$b_1 +1, -1\rangle + b_2 0, 0\rangle + b_3 -1, +1\rangle$
9	Co <sup>III</sup> , Rh <sup>III</sup> , Pt <sup>IV</sup>	<i>t<sub>2g</sub><sup>9</sup></i>	<sup>4</sup> F	<sup>1</sup> A <sub>1g</sub>	$J = 0$	$ 0, 0\rangle$	$ 0, 0\rangle$
10	Ni <sup>2+</sup> , Pd <sup>2+</sup>	<i>t<sub>2g</sub><sup>10</sup></i>	<sup>4</sup> F	<sup>4</sup> T <sub>1g</sub>	$J = \frac{1}{2}$	$a_1 -1, +\frac{3}{2}\rangle + a_2 0, +\frac{1}{2}\rangle + a_3 +1, -\frac{1}{2}\rangle$	$a_1 -1, +\frac{3}{2}\rangle + a_2 0, +\frac{1}{2}\rangle + a_3 +1, -\frac{1}{2}\rangle$
11	Ni <sup>III</sup>	<i>t<sub>2g</sub><sup>11</sup></i>	<sup>3</sup> F	<sup>2</sup> E <sub>g</sub>	$J = 1$	${}^2B_{1g} 0, +\frac{1}{2}\rangle$	${}^2A_{1g} 0, +\frac{1}{2}\rangle$
12	Cu <sup>2+</sup>	<i>t<sub>2g</sub><sup>12</sup></i>	<sup>2</sup> D	<sup>3</sup> A <sub>1g</sub>	$J = 1$	$ 0, +1\rangle$	$ 0, +1\rangle$
13		<i>t<sub>2g</sub><sup>13</sup></i>	<sup>2</sup> D	<sup>2</sup> E <sub>g</sub>	$J = \frac{1}{2}$	${}^2B_{1g} 0, +\frac{1}{2}\rangle$	${}^2A_{1g} 0, +\frac{1}{2}\rangle$

## 3.1.3.2 Jahn-Teller distortions

If the cubic-field ground state of the B cation is an orbitally two-fold-degenerate  $E_g$  state, then the  $t_{2g}$  orbitals are either full or half-filled, so that  $M_L = 0$ , and there is no spin-orbit coupling ( $V_{LS} = 0$ ). JAHN and TELLER [Ja6] have shown that, if there is no perturbation available to remove a ground-state orbital degeneracy, then there will be a spontaneous distortion to lower local symmetry below some transition temperature  $\Theta_{trans} < T_{melt}$  where  $T_{melt}$  is the melting point. Since the energy gained by a local distortion is reduced by the work done against the elastic restoring forces of the crystal, transition temperatures  $\Theta_{trans}$  are small for isolated ions. However, if all of the B cations are similar, then cooperative distortions are possible, and the net energy gained per ion is much greater because of the elastic-coupling energy  $V_\lambda$  of Eq. (2). Such a cooperative phenomenon is characterized by thermal hysteresis and a definite (usually first-order) transition temperature. Since they are due to electronic ordering, such transitions are martensitic.

VAN VLECK [Va15] pointed out that the normal vibrational modes that split an  $E_g$  electronic state are themselves twofold-degenerate with symmetry  $E_g$ . One mode gives the interstice a tetragonal distortion, the other an orthorhombic distortion. It follows that, from first-order theory, there is no static distortion of the interstice, only a dynamic coupling between the electronic charge density and the vibrational modes. Moreover, this dynamic coupling greatly enhances the two  $E_g$  vibrational modes and gives a dynamic splitting of the electronic  $E_g$  state. This mechanism has important consequences for the acoustic properties and, as discussed in 3.3, for the sign of the magnetic superexchange coupling.

Inclusion in the theory of higher-order coupling terms and anharmonic elastic terms shows that a static, tetragonal ( $c/a > 1$ ) distortion of the interstice is stable below some  $\Theta_{trans}$  [Ka10]. This sign for the static distortion was first established experimentally through the interpretation [Go15] and further study of cooperative tetragonal-to-cubic transitions in spinel systems. However, application to the perovskites requires a solution of the lowest-energy cooperative distortion via inclusion of the elastic-coupling energy  $V_\lambda$ . GOODENOUGH [Go6] proposed that individual tetragonal ( $c/a > 1$ ) octahedra order their long axes alternately along [100] and [010] axes of the pseudocubic cell. KANAMORI [Ka10] generalized this solution to include an orthorhombic component to the local-octahedron distortions. This gives B-B separations within (001) planes having a long (l) and a short (s) B-X separation and along the [001] axis two intermediate (m) B-X separations where  $s < m < (l + s)/2$ . This prediction was later verified by HEPWORTH and JACK [He9] for  $\square \text{MnF}_3$  and by OKAZAKI [Ok1] for  $\text{KCuF}_3$  (see Fig. 10). Superposition of this distortion on an O-orthorhombic cell stabilizes the unique axis along the orthorhombic c-axis, and

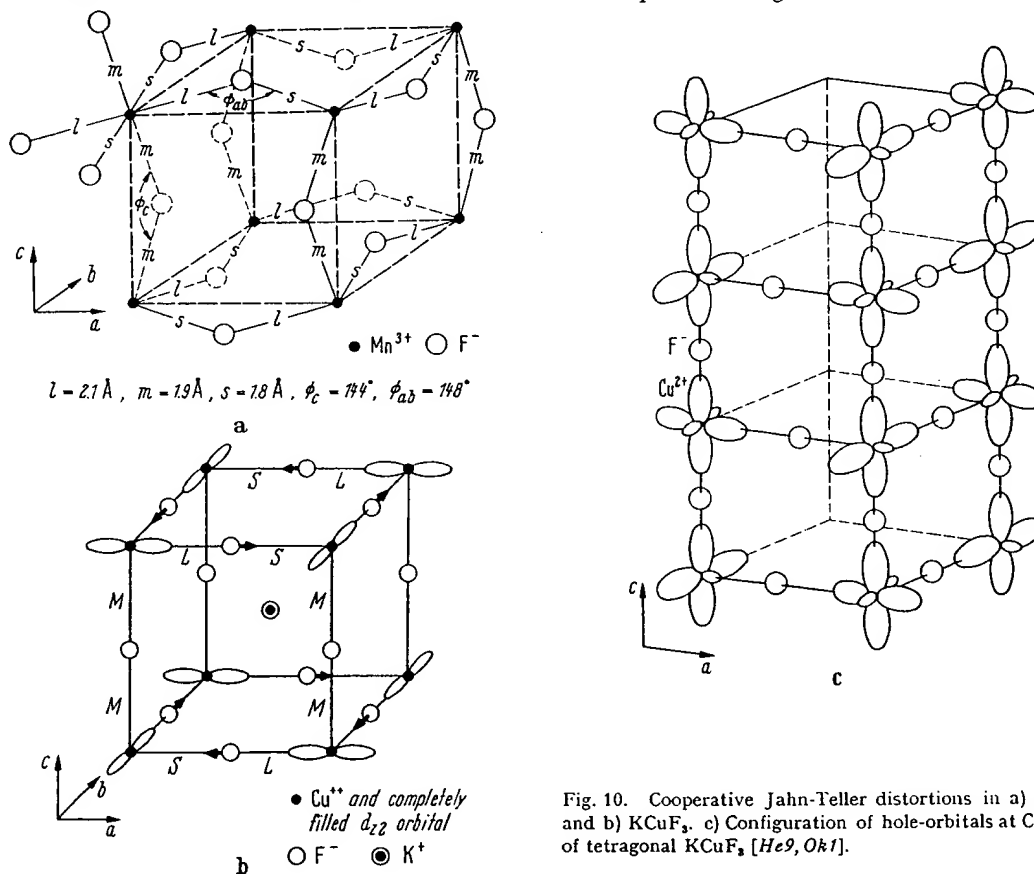


Fig. 10. Cooperative Jahn-Teller distortions in a)  $\square \text{MnF}_3$  and b)  $\text{KCuF}_3$ . c) Configuration of hole-orbitals at Cu<sup>2+</sup> ions of tetragonal  $\text{KCuF}_3$  [He9, Ok1].

the axial ratios of the O'-orthorhombic cell are transformed from  $a < c/\sqrt{2}$  to  $c/\sqrt{2} < a$ . To signal the fact that a Jahn-Teller distortion (with or without spin-orbit coupling) has been superposed on a distortion due to relative ionic sizes, the notation O'-orthorhombic is used in Tab. 2 wherever  $c/\sqrt{2} < a$ .

The important B cations that exhibit dynamic and static JAHN-TELLER stabilizations in the absence of spin-orbit coupling are:  $\text{Cu}^{2+} {}^2E_g(t_{2g}^6 e_g^2)$ ,  $\text{Cr}^{2+}$  and  $\text{Mn}^{3+} {}^5E_g(t_{2g}^3 e_g^2)$ ,  $\text{Ni}^{\text{III}} {}^2E_g(t_{2g}^6 e_g^1)$ , where Roman numerals are used for the valence state of a low-spin cation. Tab. 2 shows that O'-orthorhombic symmetry above a magnetic-ordering temperature is associated with these ions, provided the  $d$  electrons are localized, and only with these ions, with the exception of  $\text{LaVO}_3$  and  $\text{CeVO}_3$ , where sharply enhanced distortions appear abruptly below  $\Theta_N$  [Ro3; Go10]. The cubic  ${}^3T_{1g}$  state of  $\text{V}^{3+}$  is orbitally threefold-degenerate, so that it may induce small distortions above  $\Theta_N$ , larger distortions below  $\Theta_N$  (see discussion Go14).  $\text{LaNiO}_3$  remains  $R\bar{3}c$  because the  $e_g$  electrons are collective. In  $\text{La}_2\text{Li}_{0.5}\text{Ni}_{0.5}\text{O}_4$  crystals, on the other hand, the ordered  $\text{Ni}^{\text{III}}$  ions have localized  $e_g$  electrons, and there is a tetragonal ( $c/a > 1$ ) distortion. The sign of this distortion is manifest by the large  $c/a$  ratio. Strictly speaking, this is not a Jahn-Teller distortion, since the  $\text{K}_2\text{NiF}_4$  structure is tetragonal, but ordering of the localized electron of unpaired spin in the tetragonal field distorts the  $\text{Ni}^{\text{III}}$  octahedra to tetragonal symmetry with axes parallel to the unique axis. Pure Jahn-Teller distortions can be distinguished from distortions associated with spin-orbit coupling because they are independent of magnetic order and generally occur at a  $\Theta_{\text{trans}}$  above the magnetic-ordering temperature.

### 3.1.3.3 Spin-orbit coupling

B cations having cubic-field ground-state terms  $T_{2g}$  or  $T_{1g}$  are orbitally threefold-degenerate with  $M_L = 0, \pm 1$ , so that  $V_{LS} \neq 0$ . The combined perturbations  $V_{LS} + V_{\text{ncub}}$  separate into secular equations for different  $M_J$ , as shown in Fig. 9. With a single outer electron, the  ${}^2T_{2g}$  cubic-field term is split in two, the energies for different  $M_J$  shifting by

$$\begin{aligned} E_{3/2} &= \frac{1}{3}\delta - \frac{1}{2}\lambda \\ E_{1/2}^\pm &= -\frac{1}{6}\delta + \frac{1}{4}\lambda \pm \frac{1}{2}\{\delta^2 + \lambda\delta + (\frac{3}{2}\lambda)^2\}^{1/2} \end{aligned} \quad (8)$$

where  $\lambda > 0$ . In a cubic field

$$E_{3/2} = E_{1/2}^- = E_{1/2}^+ - \frac{3}{2}\lambda, \quad (9)$$

and spin-orbit coupling leaves an orbitally twofold-degenerate ground state. Therefore it is necessary to consider an additional Jahn-Teller stabilization via  $V_{\text{ncub}} + V_\lambda + \mathcal{H}_Z$ . GOODENOUGH [Go14] has shown that it is necessary to consider two temperature regions:  $T > \Theta_N$  and  $T < \Theta_N$ , where  $\Theta_N$  is the temperature below which the spins order collinearly. In the paramagnetic domain  $T > \Theta_N$ , the molecular fields vanish ( $\langle S \rangle = 0$ ) and, from Eq. (7),  $\mathcal{H}_Z = 0$ . In this case, the ground-state energy varies as  $(\delta^2/\lambda)$ . Since the work done against elastic restoring forces is  $q_s\delta^2$ , there is a spontaneous Jahn-Teller distortion, corresponding to  $\delta > 0$ , at a  $\Theta_{\text{trans}} > \Theta_N$  only if the product  $\lambda q_s$  is relatively small. In the magnetically ordered state ( $T < \Theta_N$ ), on the other hand, there is an internal molecular field  $H_{\text{int}}$  at each atom, which produces a Zeeman splitting of the orbitals of different spin. The magnitude of this splitting depends upon the spectroscopic splitting factor, which has the components

$$g_\parallel = 2 - 2g_1(\delta/\lambda) \text{ and } g_\perp = 2 + g_1(\delta/\lambda) \quad (10)$$

where  $g_1 > 0$ . Therefore the Zeeman splitting in the molecular fields is maximized by making  $\delta < 0$  and having the spins parallel to the unique axis defined by  $\delta$ . Further, this energy is linear in  $\delta$ , so that a spontaneous distortion should occur at some  $\Theta_{\text{trans}} < \Theta_N$ . A similar argument holds for the orbitally twofold-degenerate  $J = 1$  and  $J = \frac{1}{2}$  states of octahedral-site  $\text{Fe}^{2+} {}^5T_{2g}$  and  $\text{Co}^{2+} {}^4T_{1g}$ .

In summary, if multiplet splitting leaves a ground state with a twofold, accidental orbital degeneracy, then there is a spontaneous Jahn-Teller distortion at some  $\Theta_{\text{trans}}$  that removes this degeneracy. If  $\Theta_{\text{trans}} > \Theta_N$ , then  $\delta > 0$ . However, this alternative requires special crystallographic conditions that do not appear to be met in perovskites. On the other hand, a  $\Theta_{\text{trans}} \leq \Theta_N$  and  $\delta < 0$  can be generally anticipated wherever the spins order collinearly and the  $d$  electrons are localized. Further, from Eqs. (3) and (6), it follows that  $T_{2g}$  states (one outer  $t_{2g}$  electron) have  $\delta < 0$  if the site symmetry is tetragonal ( $c/a > 1$ ), whereas  $T_{1g}$  states (two outer  $t_{2g}$  electrons) have  $\delta < 0$  if it is tetragonal ( $c/a < 1$ ). Alternatively, distortions of the site symmetry may be to trigonal symmetry. A  $\delta < 0$  corresponds to  $\alpha < 60^\circ$  for  $T_{2g}$  states, to  $\alpha > 60^\circ$  for  $T_{1g}$  states. These relationships are also summarized in Tab. 1. Experimentally,  $\text{Fe}^{2+} {}^5T_{2g}$  octahedra become trigonal ( $\alpha < 60^\circ$ ) below  $\Theta_N$ , as exhibited by  $\text{KFeF}_3$ , whereas  $\text{Co}^{2+} {}^4T_{1g}$  octahedra become tetragonal ( $c/a < 1$ ) below  $\Theta_N$ , as exhibited by  $\text{KCoF}_3$ . Where  $\Theta_{\text{trans}} = \Theta_N$ , the magnetic-ordering temperature may be first-order. In addition, the spontaneous distortions introduce large magnetostriction and magnetic anisotropy.

The cubic-field ground state of  $\text{V}^{3+} {}^3T_{1g}$  is orbitally threefold-degenerate. As a result, any spontaneous distortion must correspond to  $\delta < 0$ , i.e., tetragonal ( $c/a < 1$ ) or trigonal ( $\alpha > 60^\circ$ ). However, as in the other cases a  $\Theta_{\text{trans}} \lesssim \Theta_N$  is to be expected in the perovskite structure. The  $\text{V}^{3+}$  ion generally occurs in an O-orthorhombic perovskite, and superposition of a tetragonal ( $c/a < 1$ ) distortion with coincident unique axes again results in O'-orthorhombic symmetry. The perovskite  $\text{LaVO}_3$  exhibits an abrupt contraction of the  $c$ -axis on cooling through  $\Theta_N$ .

## 3.1.4 The influence of collective-electron ordering

## 3.1.4.1 Band theory

Conventional band theory rests on three principal assumptions: (1) A description of the outer electrons may be built up from solutions of a single electron moving in a periodic potential. (2) Multiplet structure on individual atoms may be disregarded. (3) Electron-phonon interactions may be treated as a small perturbation. For an infinite crystal, the unperturbed solution of running waves in a periodic potential gives the Bloch functions and energies

$$\psi_{\mathbf{k}\mathbf{m}} = \exp(i\mathbf{k} \cdot \mathbf{r}) u_{\mathbf{k}\mathbf{m}}(\mathbf{r}); E_{\mathbf{k}} = E_0 + \hbar^2 k^2 / 2m^* \quad (11)$$

where  $\hbar\mathbf{k}$  is the momentum of an electron of effective mass  $m^*$  and  $u_{\mathbf{k}}(\mathbf{r})$  is a periodic function. In the tight-binding approximation appropriate for narrow bands, the Bloch functions are

$$\psi_{\mathbf{k}}(\mathbf{r}) = 1/\sqrt{N} \sum_{\mathbf{r}_n} \exp(i\mathbf{k} \cdot \mathbf{r}_n) w(\mathbf{r} - \mathbf{r}_n)$$

where  $w(\mathbf{r} - \mathbf{r}_n)$  is a localized wave function for the atom at  $\mathbf{r}_n$  defined by

$$w(\mathbf{r} - \mathbf{r}_n) = 1/\sqrt{N} \sum_{\mathbf{k}} \exp[i\mathbf{k} \cdot (\mathbf{r} - \mathbf{r}_n)] u_{\mathbf{k}}(\mathbf{r})$$

and  $u_{\mathbf{k}}(\mathbf{r})$  is a localized crystalline orbital. At the Brillouin-zone boundaries defined by

$$2\mathbf{k} \cdot \mathbf{K} + |\mathbf{K}|^2 = 0, \quad (12)$$

where  $\mathbf{K}$  is a reciprocal lattice vector, there are energy discontinuities in energy-momentum space. In polar insulators, this introduces an energy gap  $E_g$  between occupied, primarily anionic states and empty, primarily cationic states. Cooperative displacements  $\delta$  of the cationic sublattice relative to the anionic sublattice may increase this gap, thereby stabilizing the total energy of the occupied states by  $\epsilon_2 \delta^2$ . Since the resulting elastic-strain energy is  $q_2 \delta^2$ , there can be a spontaneous displacement only for the exceptional case  $q_2 < \epsilon_2$  and a ground state corresponding to a small distortion parameter  $\delta$ . In this case vibrational entropy may stabilize the higher symmetry at the higher temperatures. This differs from the usual criterion for spontaneous distortions, where a term linear in  $\delta$  is identified. There appear to be two situations occurring in perovskites where the requirement  $q_2 < \epsilon_2$  is met: (1) Where B-cations have empty  $d$  orbitals, there is a critical range of covalent-mixing parameters through which the site preference changes from octahedral to tetrahedral. In this range  $q_2$  is very small for B-cation displacements within an octahedron that reduce the coordination number from six towards four. The origin of the small  $q_2$  is a balance of the electrostatic energy lost and covalent-bond energy gained on going to smaller anion coordination. (2) The high polarizability of the outer core electrons of  $\text{Pb}^{2+}$  and  $\text{Bi}^{3+}$  ions makes  $q_2$  relatively small, so that displacements that permit a relatively large  $\epsilon_2$  can occur spontaneously.

What distinguishes these spontaneous distortions from those due to an ordering of localized electrons is the displacement of the cations from the centers of symmetry of their interstices. (The Jahn-Teller distortions, with or without spin-orbit coupling, leave the cations in the centers of symmetry of their interstices.) Unlike the structures, such as corundum, where pairs of octahedra share a common face, these cationic displacements from the centers of symmetry of their interstices do not follow from point-charge electrostatic arguments. In polar insulators, these displacements lead to ferroelectricity or antiferroelectricity, and they often induce displacements of neighboring cations. Further, where the requirement  $q_2 \approx \epsilon_2$  occurs just above  $\Theta_{\text{trans}}$ , there must be a strong interaction of the bonding (mostly anionic) electrons with those vibrational modes that anticipate the cooperative ionic displacements below  $\Theta_{\text{trans}}$ . These "soft" vibrational modes impart several anomalous physical properties, including a high electric susceptibility.

## 3.1.4.2 Distortions due to B-X bonding

Transition-metal cations having no outer  $d$  electrons have the following site preferences:

$\text{Sc}^{3+}$	<u><math>\text{Ti}^{4+}</math></u>	<u><math>\text{V}^{5+}</math></u>	$\text{Cr}^{6+}$	$\text{Mn}^{7+}$
$\text{Y}^{3+}$	<u><math>\text{Zr}^{4+}</math></u>	<u><math>\text{Nb}^{5+}</math></u>	<u><math>\text{Mo}^{6+}</math></u>	$\text{Tc}^{7+}$
	$\text{Hf}^{4+}$	<u><math>\text{Ta}^{5+}</math></u>	<u><math>\text{W}^{6+}</math></u>	<u><math>\text{Re}^{7+}</math></u>

where cations at the left of each row have definite octahedral-site (or larger anion coordination) preference and those to the right have definite tetrahedral-site preference. Those underlined by a solid line may be stabilized in the octahedral sites of a perovskite-type structure, but they tend to induce spontaneous ferroelectric or antiferroelectric distortions, the ions moving cooperatively out of the centers of symmetry of their interstices. The ions underlined by dashed lines only occur in ordered perovskites  $\text{A}_2\text{BB}'\text{O}_6$  and  $\text{A}_3\text{BB}'_2\text{O}_9$ . In general, they are found in tetrahedral sites or in strongly distorted octahedral sites. However, in the ordered perovskites they are able to strongly polarize the anion near neighbors so as to stabilize the octahedral symmetry.

tran  
site  
nun  
 $\text{Y}^{3+}$   
stat  
any  
at tl  
the  
nor

neon  
sym  
this  
cha:  
axis  
orbi  
alor  
pos:

tha  
bon  
nun  
strc  
que  
illu:  
pol:  
elec  
cati  
by  
the:  
a fe  
tur  
the  
dist  
or f

OC

Fig.  
oct:

O

It is significant that spontaneous ferroelectric distortions are only induced by B cations if these are transition-metal cations having empty  $d$  orbitals. It is also significant that the change from octahedral-site to tetrahedral-site preference is associated with a relative stabilization of the  $d$  orbitals (larger atomic number in any long period) as well as with a decrease in ionic size. (The ionic radii decrease in the order  $Y^{3+}$ ,  $Sc^{3+}$ ,  $Hf^{4+}$ ,  $Zr^{4+}$ ,  $Ta^{5+}$ ,  $Nb^{5+}$ ,  $Ti^{4+}$ ,  $W^{6+}$ ,  $Mo^{6+}$ ,  $Re^{7+}$ ,  $V^{5+}$ ,  $Tc^{7+}$ ,  $Cr^{6+}$ ,  $Mn^{7+}$ ). The greater the relative stability of the  $d$  orbitals, the larger are the parameters  $\lambda_\sigma$  and  $\lambda_\pi$  of Eq. (4), and these are enhanced by any displacement that decreases a B-X separation. Such an enhancement stabilizes the occupied states at the expense of the  $d$  states, and a net stabilization can occur if the  $d$  states are empty. Also the smaller the cationic size, the smaller the elastic resistance to displacements within an octahedral interstice. (Phenomenological ionic models for the ferroelectric distortions have also been given [Me7, Ha33].)

There are three B-cation displacements relative to their octahedral interstices that would simultaneously stabilize the occupied anionic  $p_\pi$  orbitals relative to the unoccupied  $t_{2g}$  orbitals: (1) *Tetragonal symmetry*. Displacements along an [001] axis that create alternate long and short B-X distances along this axis would stabilize  $s$ ,  $p_\sigma$  and the two  $p_\pi$  orbitals per anion on this axis and strongly polarize the charge density toward the short B-X separation. (2) *Orthorhombic symmetry*. Displacement along a [110] axis that created two shortest and two longest B-X distances would stabilize the  $s$ ,  $p_\sigma$  and the two  $p_\pi$  orbitals per anion on two out of the three cartesian axes. (3) *Rhombohedral symmetry*. Displacement along a [111] axis would stabilize the  $s$ ,  $p_\sigma$  and the two  $p_\pi$  orbitals per anion on all the anions. These three possibilities are illustrated in Fig. 11.

Such distortions also induce changes in the A-X separations, and the particular cooperative distortion that is stabilized depends upon the character of the A-X bonding. The covalency contribution to the A-X bond increases with formal A cationic charge; for a fixed charge it decreases with increasing atomic number of the A cation down any column of the periodic table. If A-X covalent bonding is relatively strong and the perovskite is distorted to O-orthorhombic symmetry, all ferroelectric distortions may be quenched because the  $p_\pi$  orbitals are stabilized by  $\sigma$ -bonding with the A cations. This appears to be illustrated by  $CaTiO_3$ , and almost so by  $SrTiO_3$ . On the other hand, if the A atom is stabilized by a polarization of its outer core electrons ( $Pb^{2+}$  and  $Bi^{3+}$  as discussed in 3.1.4.3), then a tetragonal, ferroelectric distortion is stabilized so as to allow a cooperative displacement of the A and B cations, the A cation moving along the [001] axis to stabilize two  $p_\pi$  orbitals per anion not on [001] axes. This is illustrated by the  $PbTiO_3$  structure of Fig. 12. If the covalency contribution to the A-X bonding is relatively weak, then the B-X covalency contribution should dominate. For large A cations ( $t > 0.9$ ), this would stabilize a ferroelectric, rhombohedral distortion at lowest temperatures, as illustrated by  $BaTiO_3$ . As the temperature increases, successive distorted structures ( $R_B^F \rightarrow O_B^F \rightarrow T_B^F \rightarrow C$ ) introduce incremental additions to the entropy. However, a small A cation and weak A-X covalency contribution may lead to a ferroelectric distortion superposed on the O-orthorhombic structure to give the  $O_B^F$ -orthorhombic structure of  $CdTiO_3$  or  $NaTaO_3$  shown in Fig. 13. Even more complex distortions are found in  $NaNbO_3$  [V06]. The room-tem-

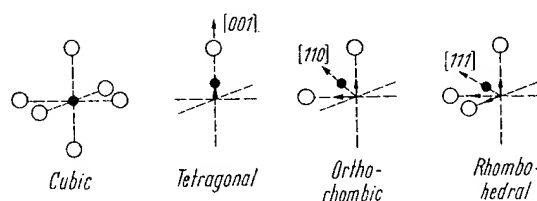


Fig. 11. Possible B-cationic displacements within their octahedra in ferroelectric or antiferroelectric distortions.

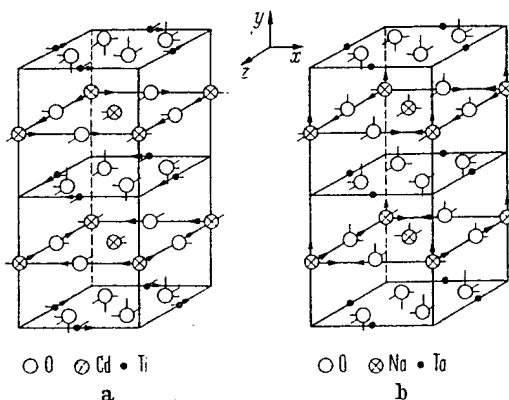


Fig. 13. Ionic displacements in a)  $CdTiO_3$  and b)  $NaTaO_3$  [Ka22].

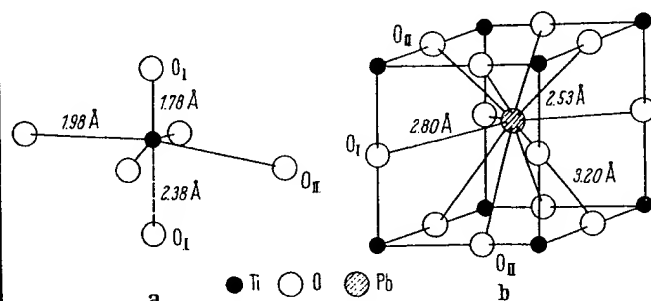


Fig. 12. Tetragonal  $PbTiO_3$ : a) environment of Ti and b) environment of Pb [Sh27].



perature form has parallel pairs of (001) NbO<sub>2</sub> planes coupled antiparallel to give an antiferroelectric phase, as shown in Fig. 14. The Na atoms are also displaced antiparallel to one another.

### 3.1.4.3 Distortions due to core polarization: Pb<sup>2+</sup> and Bi<sup>3+</sup>

Lead and bismuth are heavy ions, and the 6s orbitals are sufficiently more stable than the 6p orbitals that Pb<sup>2+</sup> and Bi<sup>3+</sup> ions are commonly stable. However, the outer 6s<sup>2</sup> core electrons have a relatively large radial extension, making the ionic radius large, and this reduces the overlap of the 6p orbitals with the orbitals on near-neighbor anions. This reduction in overlap reduces the strength of the A-X bond. However, hybridization of 6s and 6p orbitals, which costs the energy separation of 6s and 6p orbitals, produces a polarization of the outer-core electrons, so that the effective ionic radius is much smaller on one side of the cation than on the other. This permits the formation of a much more stable bond on one side of the cation, and the energy gained in this bonding may be greater than the hybridization energy required to polarize the core. It is for this reason that Pb<sup>2+</sup> and Bi<sup>3+</sup> ions are stabilized in many crystals with an asymmetric anion coordination.

There are three possible displacements of the A cations that would stabilize the anion *p<sub>π</sub>* orbitals (which σ-bond with the A cations): (1) *Tetragonal symmetry*. Displacement of the A cations along [001] axes to stabilize the two *p<sub>π</sub>* orbitals per anion not on [001] axes, as found for PbTiO<sub>3</sub> (see Fig. 12). (2) *Orthorhombic symmetry*. Displacement of the A cations along [110] axes to stabilize strongly one *p<sub>π</sub>* orbital per anion on [001] axes and less strongly one *p<sub>π</sub>* orbital per anion not on [001] axes. The smallest induced distortion of the B-cation octahedra occurs for an antiferroelectric displacement of the type illustrated by PbZrO<sub>3</sub>, Fig. 15. (3) *Rhombohedral symmetry*. Displacement of the A cations along [111] axes to stabilize strongly one *p<sub>π</sub>* orbital per anion. To be cooperative, such a distortion must be ferroelectric, as in BiFeO<sub>3</sub>, Fig. 16. Further, since the A cation is moved toward a B cation, there is an electrostatic repulsion between them that displaces the B cation from the center of symmetry of its interstice.

Given spontaneous distortions due to A-cation displacements, there remains the possibility that electron ordering among localized *d* electrons on B cations can superpose an additional distortion. Whether this is the origin of the triclinic symmetry reported for ferromagnetic BiMnO<sub>3</sub>, where Mn<sup>3+</sup> is a Jahn-Teller ion, is not known.

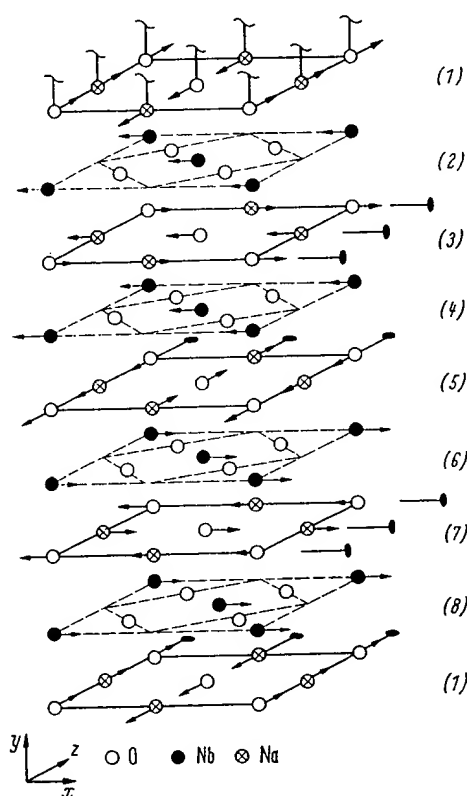


Fig. 14. Ionic displacements in orthorhombic NaNbO<sub>3</sub>. The shifts of the anions in NbO<sub>2</sub> planes and the small *x* shifts of the Nb ions have been omitted for clarity [Voe6].

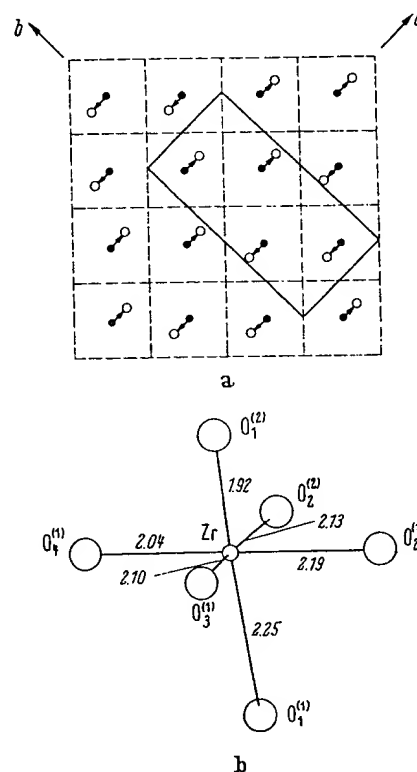


Fig. 15. a) Pb-ion shifts ( $\approx 0.26$  Å) in a (001) plane of antiferroelectric PbZrO<sub>3</sub>. b) Distorted Zr octahedra as a result of simultaneous anion displacements. Zr-O distances are given in [Å] [Sa8, Jo5].

## 3.1.4.4 Competitive phases

A few compounds have atomic radii compatible with the formation of a perovskite phase and yet are stabilized in other structures at ordinary temperature and pressure. Two important competitive structures of this type are represented by  $\text{YAlO}_3$  and  $\text{PbRuO}_3$ . Both of these compounds convert to the perovskite structure under hydrostatic pressure.

The hexagonal  $\text{YAlO}_3$  structure of Fig. 17(a) consists of close-packed layers having the sequence  $b-a-b'-a-b-c-b'-c-b$ , where  $b$  is an A-cation layer,  $b'$  is a B-X layer with anions stacked beneath A cations ( $b$  stacking) and B cations in the trigonal bipyramids formed by face-shared tetrahedra in the hexagonal  $a-b-a$  or  $c-b-c$  anion-stacking sequence. The structure apparently forms because both the A cations and the B cations simultaneously approach the lower limit for cationic size:  $r_B = 0.51 \text{ \AA}$ ,  $r_A = 0.90 \text{ \AA}$ . The small  $\text{Al}^{3+}$  ion is relatively stable in the five-fold coordination of the trigonal-bipyramid sites, and the small  $\text{Y}^{3+}$  ion is more stable in an eightfold (or  $6 + 2$ ) coordination instead of a twelvefold (or  $9 + 3$ ) coordination. These site preferences reflect an increased stabilization of the bonding, anionic orbitals as a result of closer cation-anion distances.

The antiferromagnetic, ferroelectric compound  $\text{YMnO}_3$  has a similar structure, but with an  $a$ -axis  $\sqrt{3}$  larger than that of  $\text{YAlO}_3$  to give six molecules per unit cell. The  $\text{Mn}^{3+}$  ion can be stabilized in a trigonal-bipyramid site because it has four outer  $d$  electrons with configuration  $e_g^2 e_\pi^2 a_1^0$ , where the empty  $a_1$  orbital is directed along the  $c$ -axis to bond covalently with the two collinear oxygen ions. The larger unit cell and the ferroelectricity are reflected in the complex magnetic order shown in Fig. 17(b). Below  $\Theta_N$ , exchange striction favors antiferromagnetic Mn-O-O-Mn interactions. The ferroelectric transition that occurs above  $600^\circ\text{C}$  is apparently due to the relatively large size of the  $\text{Mn}^{3+}$  ion, which creates a large enough interstice for the  $\text{Y}^{3+}$  ion that it is stabilized by a displacement from the center of symmetry of its interstice so as to lower its near-neighbor anion coordination from eight toward seven.

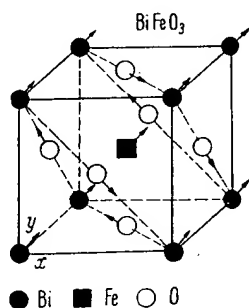


Fig. 16. Structure of  $\text{BiFeO}_3$  showing displacements in perovskite subcell [ $M\bar{1}0$ ].

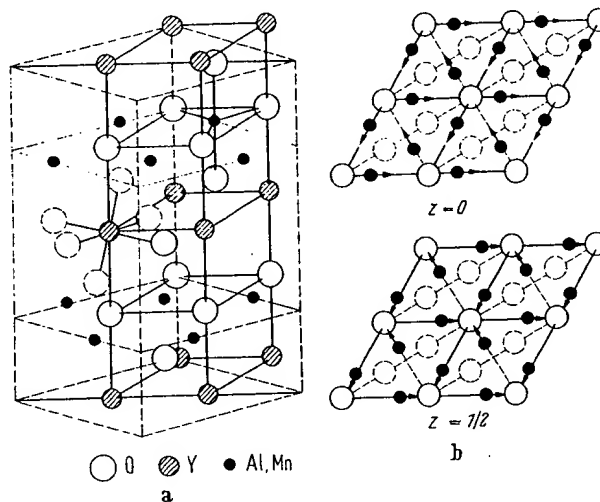


Fig. 17. a) Comparison of the unit cells of  $\text{YAlO}_3$  (solid lines) and  $\text{YMnO}_3$  (dashed lines). b) Magnetic structure of  $\text{YMnO}_3$  [Be36, Be39].

$a = 3.678 \text{ \AA}$ ,  $c = 10.52 \text{ \AA}$  for  $\text{YAlO}_3$ .

Cubic  $\text{PbRuO}_3$  gives an x-ray pattern of the pyrochlore structure, corresponding to chemical formula  $\text{A}_2\text{B}_2\text{O}_7$ , and therefore may be written as  $\text{Pb}_2\text{Ru}_2\text{O}_6\oplus$ . This structure is competitive with the perovskite structure in several  $\text{PbB}^{4+}\text{O}_3$  compounds. It has been shown [Lo4] that the anion vacancies  $\oplus$  are located at the centers of  $\text{Pb}^{2+}$ -ion tetrahedra sharing common corners and that the electrostatic repulsion between the Pb ions may be counteracted by a transfer of the two outer-core electrons per Pb ion to the  $\oplus$  sites, which act as traps for four electrons per vacancy. Thus, the outer core electrons at the  $\text{Pb}^{2+}$  ions induce a completely new structure rather than a ferroelectric-type displacement of the A-cations within the perovskite structure. This new structure contains B cations in corner-shared octahedra, as in perovskite, but the B-X-B angle is reduced to about  $135^\circ$ . This structure is also stabilized in  $\text{AgSbO}_3$  [Sc22] presumably because there is a small effective charge on the  $\text{Ag}^+$  ions. The pyrochlore  $\text{A}_2\text{B}_2\text{O}_7$  structure itself is competitive if attempts are made to force a low valence state on one of the cations.

## 3.1.5 Structures encountered with ordered B, B' cations

## 3.1.5.1 Same B atom

There are three ways of creating two different cations from the same atom:

(1) Two A cations of different valence can create two different valence states of the same B atom, and these may order at lower temperature as a result of different cationic charge. The ordering temperature may be quite low, since only electron transfers are required for cationic ordering. This is illustrated by (La<sub>0.5</sub>Ca<sub>0.5</sub>)(Mn<sub>0.5</sub><sup>3+</sup>Mn<sub>0.5</sub><sup>4+</sup>)O<sub>3</sub>, which has the Mn<sup>3+</sup>, Mn<sup>4+</sup> ordering in a rocksalt-type array. Because Mn<sup>3+</sup>(*t*<sub>2g</sub><sup>3</sup>*e*<sub>g</sub><sup>2</sup>) is a Jahn-Teller ion having localized outer *d* electrons, there is also a cooperative distortion to tetragonal (*c/a* > 1) symmetry of the Mn<sup>3+</sup>-occupied octahedra, and the ordering of these distortions gives a macroscopic distortion to tetragonal (*c/a* < 1) symmetry (see Fig. 26).

(2) Where the energy difference between the high-spin and low-spin states of the B cation are nearly equal, the populations of the two energy states approach each other at higher temperatures. In LaCoO<sub>3</sub>, high-spin Co<sup>3+</sup> and low-spin Co<sup>III</sup> are separated by only  $E_{3+} - E_{III} \approx 0.08$  eV, and the populations of the two spin states are nearly equal at 400 °K. This temperature is sufficiently low that ordering of the two different spin states occurs above this temperature, and the symmetry changes from R3c to R3̄ [Ra3]. In this case, it is the difference in ionic size and covalent bonding, which results in a difference in the effective ionic charge—not the formal ionic charge—that is the driving force for the ionic ordering.

(3) Disproportionation of B<sup>m+</sup> cations into B<sup>(m-1)+</sup> and B<sup>(m+1)+</sup> cations may create ions of different size and charge that become ordered. This is illustrated by □PdF<sub>3</sub>, which has been shown by magnetic susceptibility measurements to be Pd<sup>2+</sup>Pd<sup>IV</sup>F<sub>6</sub> [Ba19]. (The A cation is missing.) Such a disproportionation permits the formation of (PdF<sub>6</sub>)<sup>2-</sup> clusters in which the anionic orbitals are stabilized by strong covalent mixing with the σ-bonding 4*d* orbitals of *e*<sub>g</sub> symmetry. This is accomplished by a shifting of the F<sup>-</sup> ions toward the Pd<sup>4+</sup> ions and away from the Pd<sup>2+</sup> ions. Simultaneously, the anionic shift reduces covalent mixing in the occupied, antibonding 4*d* orbitals of *e*<sub>g</sub> symmetry at the Pd<sup>2+</sup> ions. These orbitals are therefore localized and further stabilized by intra-atomic exchange (Hund splitting), so that each Pd<sup>2+</sup> ion carries an atomic moment of 2μ<sub>B</sub>. Were there no disproportionation, the single electron per low-spin Pd<sup>III</sup> ion would occupy antibonding *e*<sub>g</sub> orbitals that were more unstable than the occupied, localized *e*<sub>g</sub> orbitals at the Pd<sup>2+</sup> ions. However, the transformation 2 Pd<sup>III</sup> → Pd<sup>2+</sup> + Pd<sup>IV</sup> costs ionization energy, and this is usually too large (as in LaNiO<sub>3</sub>) for disproportionation to occur.

## 3.1.5.2 Different B atoms

There are many examples of ordered B, B' structures in compounds having different B atoms: A<sub>2</sub>B<sup>2+</sup>B<sup>3+</sup>F<sub>6</sub>; A<sub>2</sub>B<sup>2+</sup>B<sup>3+</sup>B<sup>5+</sup>O<sub>6</sub>; A<sub>2</sub>B<sup>2+</sup>B<sup>3+</sup>B<sup>6+</sup>O<sub>6</sub>; A<sub>2</sub>B<sup>2+</sup>B<sup>3+</sup>B<sup>7+</sup>O<sub>6</sub>; A<sub>2</sub>B<sup>2+</sup>B<sup>3+</sup>B<sup>4+</sup>O<sub>6</sub>; A<sub>2</sub>B<sup>2+</sup>B<sup>3+</sup>B<sup>5+</sup>O<sub>6</sub>; and A<sub>2</sub>B<sup>2+</sup>B<sup>3+</sup>B<sup>6+</sup>O<sub>6</sub>. In the A<sub>2</sub>BB'X<sub>6</sub> group, ordering is on alternate (111) planes of B cations, in the A<sub>2</sub>B<sub>2</sub>B'X<sub>6</sub> group the B' cations occupy every third B-cation (111) layer, Fig. 1(c). The probability for an ordered arrangement of the B, B' cations is determined by the differences between their ionic charges and their ionic radii [Fe22, Fe23, Ga1, Ga10]. To first approximation, the order-disorder transition temperature Θ<sub>ord</sub> induced by the charge difference Δ*q* = (*q*' - *q*) at cations B' and B is Θ<sub>ord</sub> ~ (Δ*q*)<sup>2</sup>. Thus superstructure has been observed in all the known compounds having (Δ*q*)<sup>2</sup> = 36 and 16, whereas those having (Δ*q*)<sup>2</sup> = 4 are disordered unless there is a relatively large difference in ionic sizes. The minimum difference in ionic size that results in ordered A<sub>2</sub>B<sup>2+</sup>B<sup>3+</sup>B<sup>5+</sup>O<sub>6</sub> compounds is |*r*<sub>B</sub> - *r*<sub>B'</sub>|/*r*<sub>B</sub> ≈ 0.09, and this has been achieved where B' = Nb or Ta, having empty *d* orbitals for the formation of stable (B'O<sub>6</sub>)<sup>7-</sup> clusters, while the B cation has no relatively stable, empty *d* orbitals.

Given the formation of (B'X<sub>6</sub>) octahedra, a confusion arises as to where the structure corresponds to an ordered A<sub>2</sub>BB'O<sub>6</sub> perovskite built up of corner-shared octahedra plus A cations and where it corresponds to the isostructural (NH<sub>4</sub>)<sub>3</sub>FeF<sub>6</sub> structure, which consists of discrete (B'X<sub>6</sub>) octahedra separated by A and B cations. (The cubic K<sub>2</sub>NaAlF<sub>6</sub> structure with space group T<sub>h</sub><sup>h</sup>(Pa3) is similar to (NH<sub>4</sub>)<sub>3</sub>FeF<sub>6</sub>, but has a lower symmetry because there are very small rotations of the (B'X<sub>6</sub>) octahedra.) Some authors [Fe22] select as a criterion for the perovskite structure the cationic radius ratio *r*<sub>B</sub>/*r*<sub>A</sub> < 0.8 where *r*<sub>B</sub> > *r*<sub>B'</sub>. This decision is based on the observation that a plot of the cubic lattice parameter *a*<sub>0</sub> vs. B-cation radius *r*<sub>B</sub> is a straight line for *r*<sub>B</sub>/*r*<sub>A</sub> < 0.8, but bends over for *r*<sub>B</sub>/*r*<sub>A</sub> > 0.8. However, this probably reflects the ratio at which electrostatic forces inhibit (or reverse) any A-cation displacements rather than the ratio at which discrete (B'X<sub>6</sub>) octahedra are formed. For most physical properties this criterion is probably arbitrary.

Without electron-ordering distortions superposed on the size effects, ordered A<sub>2</sub>BB'X<sub>6</sub> perovskites can be described by either the O-orthorhombic cell of Fig. 5 or by the rhombohedral R3̄ (or R3m) cell of Fig. 6. Where α = 60°, a tetramolecular cubic cell may be chosen provided the A cations are not displaced from their ideal positions. Like cubic (NH<sub>4</sub>)<sub>3</sub>FeF<sub>6</sub>, the cubic cell has the space group O<sub>h</sub><sup>h</sup>(Fm3m) with B cations in 4(b) ( $\frac{1}{2}, \frac{1}{2}, \frac{1}{2}$ ); f.c., A cations in 8(c) ( $\frac{1}{4}, \frac{1}{4}, \frac{1}{4}$ ); f.c., B' cations in 4(a) (0, 0, 0); f.c., and X-anions in 24(e) ( $\frac{1}{2}, 0, 0$ ; 0,  $\frac{1}{2}, 0$ ; 0, 0,  $\frac{1}{2}$ ); f.c. with 0.2 < *u* < 0.25. However, even where α = 60°, motions of the A cations along the [111] axes may occur, thereby destroying the cubic symmetry.

If an electron-ordering transition superposes a distortion at every other octahedron of Fig. 5, either the B or the B' octahedra remaining cubic, cooperative elastic interactions between the distorted octahedra give a further reduction in symmetry. The resulting monoclinic cell [F19, B18], which is pseudotriclinic, is not to be confused with the pseudomonoclinic symmetry reported in early work for the O-orthorhombic structures. The origin of the superposed electron-ordering transition could be either a Jahn-Teller ordering of localized electrons or a ferroelectric-type displacement of the anions about a (B'X<sub>6</sub>) octahedron.

Several Ca<sub>2</sub>B<sup>3+</sup>Ta<sup>5+</sup>O<sub>6</sub> and Sr<sub>2</sub>B<sup>3+</sup>Nb<sup>5+</sup>O<sub>6</sub> perovskites having B = rare-earth atom exhibit the monoclinic symmetry of a distorted O-orthorhombic cell [F18]. Since the 4f electrons at the rare-earth ions are localized, it is tempting to attribute this to a Jahn-Teller distortion with spin-orbit coupling. Although Fig. 9 shows that the octahedral site splitting of one-electron 4f orbitals gives orbitally threefold-degenerate levels having an accidental degeneracy that is not removed by spin-orbit coupling, nevertheless there are two reasons why this explanation cannot be correct: (1) There is no magnetic ordering of the 4f electrons at room temperature and (2) Sr<sub>2</sub>GdNbO<sub>6</sub> shows the distortion even though Gd<sup>3+</sup> has a half-filled 4f<sup>7</sup> shell, which has no orbital degeneracy associated with the ground state. It is therefore concluded that the additional distortions are due to the potentially ferroelectric cations Nb<sup>5+</sup> and Ta<sup>5+</sup>.

### 3.1.5.3 Complex alloys A<sub>2</sub>BB'X<sub>6</sub>, where B = M<sub>13</sub>, B' = M<sub>8</sub>

Several complex interstitial alloys have a formal structural relationship to the ordered perovskite A<sub>2</sub>BB'X<sub>6</sub> as well as interesting magnetic properties. In this group, having space group Fm3m, the B position is occupied by a thirteen-atom cluster of a metal atom at position 4(a) at the center of a cubo-octahedral, twelve-atom cluster of M atoms at positions 48(h); the B' position is occupied by a simple cube of eight M' atoms at 32(f). The three principal axes of each cluster are along the cubic axes of the perovskite cell, as shown schematically in Fig. 18, so that each X atom at positions 24(e) has eight near neighbors. The eight A atoms of the tetra-molecular cell are at the 8(c) positions. The 4(b) position at the center of the M<sub>8</sub> clusters is empty. Alloys with this structure include the ferromagnetic borides Al<sub>2</sub>[(AlM<sub>12</sub>)(M'<sub>8</sub>)]B<sub>6</sub>, where M = Fe, Co, Ni, as well as Cr<sub>23</sub>C<sub>6</sub>.

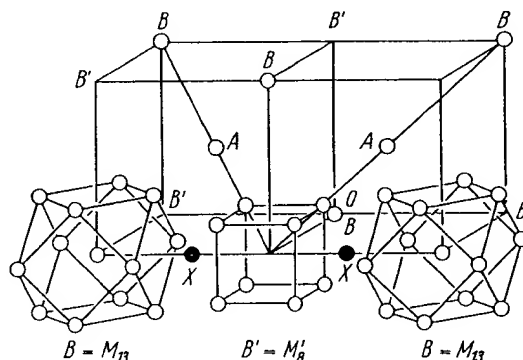


Fig. 18. One quadrant of the A<sub>2</sub>BB'X<sub>6</sub> structure showing the atomic positions of the B = M<sub>13</sub> and B' = M<sub>8</sub> clusters [We19].

### 3.1.6 First-order magnetic transition in M<sup>c</sup>XM<sub>3</sub><sup>f</sup> perovskites

Many perovskites M<sup>c</sup>XM<sub>3</sub><sup>f</sup> exhibit first-order phase changes at magnetic-ordering transitions. Most of these are reported to be cubic-to-cubic transitions, but in ZnCMn<sub>3</sub> it is a tetragonal (ferrimagnetic)-to-cubic (ferromagnetic) transition. These crystallographic changes are induced by a complex interplay of collective electrons in overlapping bands. Because of the intimate connection with the magnetic properties and because of the necessarily speculative character of any model at this time, discussion of these compounds is deferred to 3.5.

### 3.1.7 Data: Crystallographic properties of ABX<sub>3</sub>, A<sub>2</sub>BB'X<sub>6</sub>, A<sub>3</sub>B<sub>2</sub>BX<sub>9</sub> and A(B<sub>x</sub>B'<sub>y</sub>B''<sub>z</sub>)X<sub>3</sub> compounds with perovskite or perovskite-related structure (Tab. 2)

Tab. 2.

Within any section, the compounds are in general first ordered according to the atomic number of the B cation and then by the basicity of the A cation. For the ordered perovskites of Tab. 2b, c, d, the compounds are further ordered by the atomic number of the other B cation. The order of the sections is as follows:

#### Tab. 2a — ABX<sub>3</sub>

A<sup>2+</sup>LiH<sub>3</sub>  
 A(H<sub>2</sub>O) (Li<sub>1/3</sub>)<sub>3</sub>; A = I<sup>-1</sup>, Br<sup>-1</sup>  
 A<sup>+</sup>B<sup>2+</sup>X<sub>3</sub>; X = F<sup>-1</sup>, Cl<sup>-1</sup>, Br<sup>-1</sup>  
 A<sup>+</sup>B<sup>5+</sup>O<sub>3</sub>; B = V, Nb, Sb, Ta, I, Pa, U  
 A<sup>2+</sup>B<sup>4+</sup>O<sub>3</sub>; B = Ti, V, Cr, Mn, Fe, Co, Ni, Ge, Zr, Mo, Tc, Ru, Sn, Ce, Pr, Hf, Re, Ir, Pb, Th, U, Np, Pu  
 A<sup>2+</sup>B<sup>4+</sup>X<sub>3</sub> or A<sup>3+</sup>B<sup>3+</sup>X<sub>3</sub>; X = S or Se, B = Ti, Zr, Ta, In, Ga  
 A<sup>3+</sup>B<sup>3+</sup>O<sub>3</sub>; B = Al, Sc, Ti, V, Cr, Mn, Fe, Co, Ni, Ga, Y, Nb, Rh, In, Ho, Er, Tm, Yb, Lu

#### Tab. 2b — A<sub>2</sub>BB'X<sub>6</sub>

A<sub>2</sub>BB<sup>3+</sup>X<sub>6</sub>; X = F<sup>-1</sup>, Cl<sup>-1</sup>, B<sup>3+</sup> = Al, Sc, Ti, V, Cr, Mn, Fe, Co, Ni, Cu, Ga, Ag, In, Ce, Pr, Au, Tl  
 A<sup>2+</sup>A<sup>3+</sup>B<sup>3+</sup>B<sup>4+</sup>O<sub>6</sub>; B<sup>4+</sup> = Ti, Ir  
 A<sub>2</sub>BB<sup>n+</sup>O<sub>6</sub>; B<sup>4+</sup> = Ti, Mn, Ge, Zr, Ru, Ir  
     B<sup>5+</sup> = V, Nb, Sb, Ta, Bi, Pa, Pu  
     B<sup>6+</sup> = Mo, Te, W, Re<sup>6+,5+</sup>, Os<sup>6+,5+</sup>, U<sup>6+,5+</sup>, Np<sup>6+</sup>, Pu<sup>6+</sup>  
     B<sup>7+</sup> = Tc, Re, Os, I

#### Tab. 2c — A<sub>3</sub>BB<sub>2</sub>O<sub>9</sub>

A<sub>3</sub>BB<sub>2</sub><sup>5+</sup>O<sub>9</sub>; B<sup>5+</sup> = Nb, Ru, Sb, Ta  
 La<sub>3</sub>Co<sub>2</sub>B<sup>5+</sup>O<sub>9</sub>; B<sup>5+</sup> = Nb, Sb  
 A<sub>3</sub>B<sub>2</sub>B<sup>6+</sup>O<sub>9</sub>; B<sup>6+</sup> = Mo, W, Re, U

#### Tab. 2d — A<sup>2+</sup>(B<sub>x</sub>B'<sub>y</sub>B''<sub>z</sub>)O<sub>3</sub>

)X<sub>3</sub>the  
om-  
s as

, U,

, Ti

Abbreviations in Tab. 2:

Symmetry: C = cubic, H = hexagonal, M = monoclinic, O = orthorhombic ( $a < c/\sqrt{2}$ ), O' = orthorhombic ( $c/\sqrt{2} < a$ ), R = rhombohedral, T = tetragonal, Tr = triclinic.  
Remarks: for abbreviations, see p. 131.

Tab. 2a. ABX<sub>3</sub> compounds

Compound	Sym	a Å	b Å	c Å	angle	Ref.	Remarks	Magnetic Data
A <sup>3+</sup> Li <sup>+</sup> H <sub>3</sub> <sup>-1</sup>								
BaLiH <sub>3</sub>	C	4.023				Me25	P & S [Me26]; Neutron diffraction shows S.G.	
BaLiD <sub>3</sub>	C	4.02				Ma11a	Pm3m [Ma11a]	
SrLiH <sub>3</sub>	C	3.833				Me25	Neutron diffraction shows S.G. Pm3m [Ma11a]	
EuLiH <sub>3</sub>	C	3.796				Me24	P & S [Me26]	
BaLiF <sub>3</sub>	C	3.996				Lu1	P & S [Ro20, Be22a, Bu3a]	
A(H <sub>2</sub> O) (Li <sub>1/3</sub> ) <sub>3</sub> ; A = I <sup>-1</sup> , Br <sup>-1</sup>								
I(H <sub>2</sub> O) (Li <sub>1/3</sub> ) <sub>3</sub>	C	4.296				We6		
Br(H <sub>2</sub> O) (Li <sub>1/3</sub> ) <sub>3</sub>	C	3.99				Ke14		
A <sup>+</sup> B <sup>2+</sup> X <sub>3</sub> ; X = F <sup>-1</sup> , Cl <sup>-1</sup> , Br <sup>-1</sup>								
CsMgF <sub>3</sub>	H	6.04		14.45		Lo1b	Hex (6L), high pressure phase	
	H	6.16		22.13		Lo1b	Hex (9L), high pressure phase	
	T	9.39		8.72		Lu1	Prep. [Be22a, Bu3a]	
	M	8.19	8.19	8.19	$\beta = 98^\circ 30'$	Lu1	S.S. with Co, Hex (6L), $\theta_c = 15^\circ \text{K}$ (50% Co) [Sh1a]	
RbMgF <sub>3</sub>	C	3.973				Re6	P & S [De22, Lu1, Be53], I.R. spectra [Pe5, Yo2]	
KMgF <sub>3</sub>	O	5.363		7.676		Ch5	NMR, F <sup>19</sup> [Al1a], elastic properties [Re7a]	
	T	3.942	5.503	3.933		Ch5	P & S [Lu1, Be53, Ru8, Ba1], NMR, F <sup>19</sup> [Al1a]	
	C	3.955				Ch5	T = 760 °C, tetr. 760 < T < 900 °C	
	C	4.06				Ch8a	T = 900 °C, cubic T ≥ 900 °C	
NH <sub>4</sub> MgF <sub>3</sub>	H	7.278		6.19		Yd1	Pseudocubic	
CsMgCl <sub>3</sub>	O	6.954	6.971	9.922		Br28	Hex (2L)	
KMgCl <sub>3</sub>							Absorption spectra: Ni [Br28], ESR: Mn [Zd1]	
CsCaF <sub>3</sub>	C	4.523				Lu1		
RbCaF <sub>3</sub>	C	4.457				Lu1		
KCaF <sub>3</sub>	C	8.76				Br9	P & S [Lu1]	
CsCaCl <sub>3</sub>	C	5.396				Yd1		
CsTiCl <sub>3</sub>	H	7.297		6.048		Yd1	Hex (2L)	

Compound	Sym	a Å	b Å	c Å	angle	Ref.	Remarks	Magnetic Data
A <sup>+</sup> B <sup>3+</sup> X <sub>3</sub> ; X = F <sup>-1</sup> , Cl <sup>-1</sup> , Br <sup>-1</sup> (continued)								
CsVCl <sub>3</sub>	H	7.23		6.03		Se1b	Hex (2L), P & S [Yd1]	in 3.3.4, Tab.
RbVCl <sub>3</sub>	H	7.04		6.0		Gr8a	Hex (2L), optical and magnetic properties	
KVCl <sub>3</sub>	H	6.90		5.98		Se1b	Hex (2L), P & S [Yd1]	
RbCrF <sub>3</sub>	T	6.149		8.088		Vo1	P & S [Co27]	6
KCrF <sub>3</sub>	T	6.04		8.01		Co27		
	C	4.158				Co27	T = 500 °C, P & S [Ed2, Vo1, Kn3, Yo1, Pe2a]	
NaCrF <sub>3</sub>	T	8.544		7.968		Se1	Neutron diffraction	
(NH <sub>4</sub> )CrF <sub>3</sub>	M	5.695	5.885	7.639	$\beta = 87^\circ 48'$	Vo1	a and b axis said to double	
TiCrF <sub>3</sub>	T	6.232		7.954		Vo1		
	T	6.194		8.064		Vo1		
CsCrCl <sub>3</sub>	H	7.249		6.228		Yd1	Hex (2L), P & S [Se2]	
RbCrCl <sub>3</sub>	H	7.03		6.08		Se2	Hex (2L) pseudohexagonal	
CsMnF <sub>3</sub>	H	6.213		15.074		Za1	Hex (6L), $\Theta_N = 54^\circ \text{K}$ , P & S [Si14, Be19], neutron diffraction [Pi1], optical properties [Si28, Si30], NMR [Mi4, We11], AFMR [Wi14], magnetic properties [Le3, Le4, Se1], S.S. with K and Na [Be19a]	6
							High pressure phase, P & S [Sy1]	
							P & S [Si14, Be19, Co25, Ho17], cubic to T = 20 °K [Te4], dielectric properties [Ig1, Ch4a], compressibility [Si29], I.R. spectra [Ax2, Pe5], bibliography [Fr10a]	
RbMnF <sub>3</sub>	C	4.328				Lo1b	P & S [Be14, Si14, Cr4, Be2, Be4, Kn3, Ok2, Ok3, Ok4, Be53, Ok6, Ho17, Gu1a], S.S. with Co + Ni [Ha28], I.R. spectra [Ax2, Pe5, Yo2], bibliography [Fr10a]	6
	C	4.2396				Wa8		
KMnF <sub>3</sub>	C	4.186				Be3		6
	O	5.885	5.885	8.376		Be3	T = 95 °K, $(c/a > \sqrt{2})$ 184 > T > 84 °K [Be3, De3, Ok6]	6
	O	5.900	5.900	8.330		Be3	T = 65 °K, $(c/a < \sqrt{2})$ T < 84 °K [Be3, De3, Ok6]	
	O	5.568	5.760	8.000		Si14	Prep. [Ho17, Be19b], a and b axis doubled [Si14], P & S [Ma9]	
NaMnF <sub>3</sub>							P & S [Cr4, Ho17, Co25], neutron diffraction [Pi1]	6
(NH <sub>4</sub> )MnF <sub>3</sub>	C	4.238				Si14		
TiMnF <sub>3</sub>	C	4.250				Ki9		
CsMnCl <sub>3</sub>	H	7.288		27.44		Ke7	Hex (9L), $\Theta_N = 69^\circ \text{K}$ , AFMR [Ke1, Sh5]	6
RbMnCl <sub>3</sub>	H	7.164		17.798		Ke7	Hex (6L), $\Theta_N = 86^\circ \text{K}$ , AFMR & ESR [Ke1, Sh3, Sh5]	
KMnCl <sub>3</sub>	T	10.024		9.972		Cr6	Cubic T > 458 °C, AFMR & ESR [Ke1, Sh5]	6

Compound	Sym	a Å	b Å	c Å	angle	Ref.	Remarks	Magnetic Data
A+B <sup>2+</sup> X <sub>3</sub> ; X = F <sup>-1</sup> , Cl <sup>-1</sup> , Br <sup>-1</sup> (continued)								
CsFeF <sub>3</sub>	H	6.158		14.855		<i>Ke19</i>	Hex (6L), structure [Ba5], $\Theta_c = 60^\circ$ K [Po9a, Po9b]	in 3.3.4, Tab.
RbFeF <sub>3</sub>	C	4.283				<i>Lo1b</i>	High pressure phase	
	C	4.173				<i>Wa12</i>	P & S [Ke19], neutron diffraction [Wa14], cubic $T > 97^\circ$ K, tetra. $97 > T > 86^\circ$ K, orth. $86 > T > 45^\circ$ K, mon. $T < 45^\circ$ K [Te11]	
KFeF <sub>3</sub>	C	4.122				<i>Ok6</i>	P & S [Kn3, Ma29, Ok2, Ok3, Ok4], neutron diffraction [Sc1]	6
NaFeF <sub>3</sub>	R	4.108			$\alpha = 89^\circ 51'$	<i>Ok6</i>	$T = 78^\circ$ K, rhombohedral $T < 121^\circ$ K	6
NH <sub>4</sub> FeF <sub>3</sub>	O	5.495	5.672	7.890		<i>Tr2</i>	P & S [Vo1, Ma9, Po9a]	6
TiFeF <sub>3</sub>	C	4.177				<i>Po9a</i>	P & S [Po9a]	6
CsFeCl <sub>3</sub>	C	4.188		6.045		<i>Yd1</i>	Hex (2L), P & S [Se2a]	6
RbFeCl <sub>3</sub>	H	7.237		6.020		<i>Se2a</i>	Hex (2L)	6
CsCoF <sub>3</sub>	H	7.060		22.61		<i>Ba5</i>	Hex (9L), magnetic properties [Ru6], P & S [Ba4]	6
	H	6.194		14.67		<i>Lo1b</i>	Hex (6L), high pressure phase	6
RbCoF <sub>3</sub>	C	6.09				<i>Ru6</i>	P & S [Ru8, Cr4], S.S. with Mg [Sh1a]	6
KCoF <sub>3</sub>	C	4.116				<i>Ok6</i>	P & S [Kn3, Ma29, Ok2, Ok3, Ok4, Ru8, Cr4]	6
	C	4.069					I.R. spectra [Ax1, Ax2, Pe5, Yo2, Pe2a]	
							$T = 78^\circ$ K	
NaCoF <sub>3</sub>	T	4.057		4.049		<i>Ok6</i>	P & S [Ru8, Og2, Tu5, Ma10]	6
NH <sub>4</sub> CoF <sub>3</sub>	O	5.420	5.603	7.792		<i>Ru6</i>	P & S [Cr4, Ru8]	6
TiCoF <sub>3</sub>	C	4.127				<i>Ru6</i>	P & S [Ru8]	6
CsCoCl <sub>3</sub>	H	4.138		6.032		<i>Yd1</i>	Hex (2L), complete structure and magnetic properties [So1]	6
		7.202						
RbCoCl <sub>3</sub>	H	6.996		5.996		<i>En1</i>	Hex (2L)	
CsNiF <sub>3</sub>	H	6.236		5.225		<i>Ba2</i>	Hex (2L)	
	H	6.15		22.32		<i>Lo1b</i>	Hex (9L), high pressure phase	
	H	6.05		14.54		<i>Lo1b</i>	Hex (6L) high pressure form: $\Theta_c = 111^\circ$ K	
RbNiF <sub>3</sub>	H	5.843		14.31		<i>Ru5</i>	Hex (6L), P & S [Si14], $\Theta_c = 139^\circ$ K, magnetic properties [Si19b, Mc1a, Sm32, Sm31, Sh1, Go3, Ku2, Go3a], S.S. with Co [Bo13, Su11, Pi16], optical properties [Sm32, Sm31, Sm21, Sm22, Sh1, Ty1, Pi8, Pi14, Pi15, Za1a, Be19c, Pi16], Raman scattering [Ch14a], NMR [Sm32a]	
							High pressure phase, P & S [Sy1]	
KNiF <sub>3</sub>	C	4.074				<i>Ka4</i>	P & S [Ok3, Ok4, Kn3, Ma10, Ru5, Ok2], I.R. spectra [Pe5, Ba17a]	6
	C	4.015				<i>Ok6</i>		6
	C	4.002				<i>Ok6</i>	$T = 78^\circ$ K	



Compound	Sym	a Å	b Å	c Å	angle	Ref.	Remarks	Magnetic Data
A <sup>+</sup> B <sup>2+</sup> X <sub>3</sub> ; X = F <sup>-</sup> , Cl <sup>-</sup> , Br <sup>-</sup> (continued)								
NaNiF <sub>3</sub>	O	5.360	5.524	7.688		Ru8	P & S [Og2, Ru5, Ok5]	in 3.3.4,
NH <sub>4</sub> NiF <sub>3</sub>	C	8.145				Ru5	P & S [Ru8]	Tab.
TiNiF <sub>3</sub>	H	5.87		14.37		Ko4	Hex (6L)	6
	C	4.10				Ko4	High pressure phase, P & S [Sy1]	6
CsNiCl <sub>3</sub>	H	7.169		5.940		Yd1	Hex (2L), P & S [As4], structure determination [Ti4]	
	H	9.019		6.109		Sl44	Hex (2L)	
(CH <sub>3</sub> ) <sub>4</sub> NNiCl <sub>3</sub>	H	7.488		12.480		As4	Related to Hex (2L)	
CsCuF <sub>3</sub>	H	12.55		11.56		Ba2	Related to Hex (2L), optical properties [Sc10a]	6
RbCuF <sub>3</sub>	T	6.001		7.894		Ru6	Optical properties [Sc10a]	6
KCuF <sub>3</sub>	T	5.855		7.846		Ru6	P & S [Ed2, Kn3, Ok1, Ok2, Ok6], neutron diffraction [Sc1], optical properties [Pe2a, Oef1, Sc10a]	
	T	4.121		3.913		Ok6	T = 78 °K	
NaCuF <sub>3</sub>	M	11.01	11.37	7.521	β = 86° 54'	Ru6	P & S [Ru3]	6
NH <sub>4</sub> CuF <sub>3</sub>	T	6.09		7.78		Cr4		
TiCuF <sub>3</sub>	T	6.083		7.866		Ru6	P & S [Ru3]	6
CsCuCl <sub>3</sub>	H	7.20		18.00		Yd1	Related to Hex (2L), P & S [Sc7, We9] magnetic properties Θ <sub>p</sub> = -3.5 °K, μ <sub>eff</sub> (300 °K) = 1.95 μB [Ri8c, Fi2]	
	M	4.029	13.785	8.736	β = 97° 20'	Ki10	Not perovskite, magnetic properties Θ <sub>N</sub> = 17.5 °K [Ma1, Sh5]	
KCuCl <sub>3</sub>	M	4.066	14.189	9.003	β = 97° 30'	Ki10	Not perovskite	
NH <sub>4</sub> CuCl <sub>3</sub>	M	4.05	14.43	9.30	β = 96° 5'	Ki10	Not perovskite, magnetic properties [In3]	
CsZnF <sub>3</sub>	T	9.90		9.05		Lu1		
	H	6.09		14.67		Lo1b	Hex (6L), high pressure phase	
RbZnF <sub>3</sub>	C	4.110				Ba1	P & S [Cr4, Lu1]	
	H	5.896		14.44		Ba1	Hex (6L) high temperature form	
KZnF <sub>3</sub>	C	4.055				Kn3	P & S [Lu1, Ma29], thermal conductivity [Su8], optical properties: Ni, Mn [Fe11, Fe15], I.R. spectra [Yo2, Pe2a]	
	O	5.404		7.743		Tu5	P & S [Lu1, Ru8, Ba1, Ma9, Ma10, Sc10]	
NaZnF <sub>3</sub>	C	4.115	5.569			Cr4		
AgZnF <sub>3</sub>	C	3.98				De22		
TiZnF <sub>3</sub>	H	5.934		14.52		Vo1	Hex (6L)	
	R	5.444			α = 89° 38'	Ch15	Nuclear quadrupole resonance [Vo0]	
CsGeCl <sub>3</sub>	C	5.475				Ch15	Cubic T > 155 °C, ferroelectric transition at 155 °C	

Compound	Sym	a Å	b Å	c Å	angle	Ref.	Remarks	Magnetic Data
A+B <sup>2+</sup> X <sub>3</sub> ; X = F <sup>-</sup> , Cl <sup>-</sup> , Br <sup>-</sup> (continued)								
CsSrF <sub>3</sub>	C	5.589				Yd1	[Ba22a, Ba3a] no cell dimensions	in 3, 3, 4, Tab.
CsSrCl <sub>3</sub>								
CsPdF <sub>3</sub>							Prep. + Prop. [Ba20, Fi3]	
CsCdF <sub>3</sub>	C	4.47				Kl1	P & S [Co27a]	
RbCdF <sub>3</sub>	C	4.395				Vo1	Mn emission [Kl1], P & S [Co27a]	
KCdF <sub>3</sub>	T	6.101		8.652		Ba5b	P & S [Ma29, Br9, Kl1, Co27a, Co26, Vo1], Mn emission [Kl1]	
(NH <sub>4</sub> )CdF <sub>3</sub>	T	4.368		4.447		Co27a		
TiCdF <sub>3</sub>	C	4.400				Co27a	T <sub>melt</sub> = 765 °C	
CsCdCl <sub>3</sub>	C	5.20				Fe20	Slight distortion [Na15], P & S [Si3]	
	H	7.418		18.39		Si3	Hex (6L)	
CsCdBr <sub>3</sub>	C	10.70				Na15	P & S [Na19]	
CsSnCl <sub>3</sub>	C	5.58				Do5		
CsSnBr <sub>3</sub>	C	5.94				Do5		
CsEuF <sub>3</sub>	C	4.77				Bo31		
CsHgCl <sub>3</sub>	C	10.88				Na15	P & S [Na19, Na18]	
CsHgBr <sub>3</sub>	C	5.77				Na15	P & S [Na19]	
CsPbF <sub>3</sub>	C	4.81				Sc9		
CsPbCl <sub>3</sub>	T	5.590		5.630		Mo2	Phase transition at 40 °C [Sa2a]	
CsPbBr <sub>3</sub>	C	5.599				Mo2	Cubic T > 47 °C [Mo3]	
A+B <sup>2+</sup> O <sub>3</sub>		5.874						
AVO <sub>3</sub>	O	5.720	5.739	3.984		Fe7	Not perovskite, A = Na, K, Rb, Cs and Ag	6
RbNbO <sub>3</sub>						Wo15	Not perovskite	
KNbO <sub>3</sub>	T	4.00		4.07		Wo15	Structure [Ka19, Vo4, Vo5], crystal growth [Bu2, Sh25], optical properties [Ka8, Ch13]; S.S. with: BaTiO <sub>3</sub> [Br2], NaNbO <sub>3</sub> [Du3, Te8c], Li [Ni2a]	
	C	4.024				Wo15	T = 260 °C, Tetr. 435 > T > 225 °C, S.S. with KTaO <sub>3</sub> (see KTaO <sub>3</sub> )	
	R	4.016				Wo15	T = 500 °C, cubic T > 435 °C	
	C	4.2				Sh23	T = -140 °C, neutron diffraction	
						Ad1	2Na + Nb <sub>2</sub> O <sub>6</sub>	
NaNbO <sub>2.5</sub>					α = 89° 50'			

Compound	Sym	a Å	b Å	c Å	angle	Ref.	Remarks	Magnetic Data
A+B <sup>3+</sup> O <sub>3</sub> (continued)								in 3.3.4, Tab.
NaNbO <sub>3</sub>	O	5.505	5.568	15.518		Vo6	Structure determined, P & S [Vo4, Vo5, We10, Ba18, Fe7, Wo15]; S.S. with: KNbO <sub>3</sub> [Du3, Te8c], NaTaO <sub>3</sub> [Iw4, Is7, Is14], SrNb <sub>2</sub> O <sub>6</sub> [Is16, Te7], CdTiO <sub>3</sub> [Le2], AgNbO <sub>3</sub> [Br24], Cd and Sr [Te8b]	
NaNbO <sub>3</sub>	O	5.51	5.57	7.77		Wo17	50 kV/cm applied to crystal; other phase transformations [Te6, So1b, Le5, Fr1, Sh20a, Cr6a, So1a, Is5a]; heat of transformations [Te8a]	
Na <sub>0.975</sub> K <sub>0.025</sub> NbO <sub>3</sub>	O	5.528	5.582	7.782		We10	Structure determined	
LiNbO <sub>3</sub>	H	5.1483		13.8631		Ab4	Not perovskite, see text	
AgNbO <sub>3</sub>	M	7.888	7.888	15.660	β = 90° 34'	Fr2	S.S. with KNbO <sub>3</sub> [We5]	
	C	3.595				Fr2	T = 550 °C, cubic T > 550 °C	
AgSbO <sub>3</sub>	C	10.32				Sc22	Defect pyrochlore	
RbTaO <sub>3</sub>	T	3.92		4.51		Sm11	[Fe7] says not perovskite	
KTaO <sub>3</sub>	C	3.9885				Vo4	P & S [Vo5], crystal growth [Sh25, Wi14, We13], optical properties [Fr20, Pr2, Di7, Di8, Be27, Ax1, Pe4, Jo15, Sh20, Ka7, Sc5, St20, La7a], Faraday rotation [Ba7], electrooptic properties [Fr20, Fa7, Fa8, Fr21, Fr22, Ge13, Zo3], S.S. with: KNbO <sub>3</sub> [Fu3, Ha2, Ch13, Ge9, We12, We14, Di6, Hi2a, La7a], Ca [Se4]; Raman spectrum [Fl1a, Pe6, Fl1b]; ESR: Eu, Gd [Un1], Fe, Ni [Ha9a, We18b]; ultrasonic attenuation [Ba17b]; Nuclear spin resonance [Gr7a]	
NaTaO <sub>3</sub>	O	5.494	5.513	7.751		Ka22	Crystal structure, P & S [Vo4, Vo5], S.S. with: NaNbO <sub>3</sub> [Is14, Is7]	
NaTaO <sub>3</sub>	C	3.929				Is5	630 °C, cubic T ≥ 630 °C, tetr. 630 > T > 550 °C	
LiTaO <sub>3</sub>	H	5.154		13.783		Ab2	Not perovskite, neutron diffraction [Ab3] (see text)	
CuTaO <sub>3</sub>	M	7.862	7.862	3.914	β = 90° 21'	Sh12	Actually Cu <sub>0.5</sub> TaO <sub>3</sub> , see "Bronze" section	
AgTaO <sub>3</sub>	C	3.949				Fr2	P & S [Br27]	
	C	4.674				Fr2	485 °C; cubic T > 485°	
CsIO <sub>3</sub>	C	4.541				Bo30	P & S [Na15]	
RbIO <sub>3</sub>	R	8.94	8.94	8.94	α = 89° 44'	Bo30	P & S [Na15]	
KIO <sub>3</sub>	M	4.410			β = 89° 12'	Na16	Perovskite (?), P & S [Na15]	
	R	4.510			α = 89° 25'	Sm3	P & S [Ri9]	
TiIO <sub>3</sub>	R	9.18				Sm3		
NH <sub>4</sub> IO <sub>3</sub>	C	4.368			α = 89° 20'	Na15		
CsPaO <sub>3</sub>	C					Ke5		

Compound	Sym	a Å	b Å	c Å	angle	Ref.	Remarks	Magnetic Data
A <sup>2+</sup> B <sup>4+</sup> O <sub>3</sub> (continued)								
KPaO <sub>3</sub>	C	4.341				Ke5		
NaPaO <sub>3</sub>	O	5.82	5.97	8.36		Ke5	P & S [Ru3a, Ip1], Prop. [Ke13]	6
RbUO <sub>3</sub>	C	4.323				Ke12	P & S [Ru3a, Ch1b], Prop. [Ke13]	6
KUO <sub>3</sub>	C	4.290				Ke12	P & S [Ru3a], Prop. [Ke13]	6
NaUO <sub>3</sub>	O	5.775	5.905	8.25		Ke12		
A <sup>3+</sup> B <sup>4+</sup> O <sub>3</sub>								
BaTiO <sub>3</sub>	C	4.012				Me1	T = 200 °C, cubic 120 < T < 1372 °C [Ed5], cubic T > 133 °C [We11a], high temperature phase [Me4, Me6, Me2, Ka23]	
	T	3.994		4.034		Me1	T = 20 °C, tetragonal 5 < T < 120 °C; structure determination: by x-rays [Ev2, Ev3, Ev4, Ch2], by neutrons [Sh18, Fr4], by electron microscope [Pl2]; P & S [De1, Sa5], further remarks:*)	
	O	5.682	5.669	3.990		Vo5	T = -10 °C, orthorhombic -90 < T < 5 °C [Ka24]	
	R	3.998			α = 89° 52'	Ka24	T = -100 °C, rhombohedral T < -90 °C	
	H	5.735		14.05		Bu4	Hex (6L); structure determination [Bu4, Ev1]. Further remarks:**)	
SrTiO <sub>3</sub>	C	3.905				Me4	T = 293 °K; cubic T > 110 °K, thermal expansion α = 9.4 · 10 <sup>-6</sup> Å/deg., may be tetr. with c/a = 1.00008 [Ly2]	
	T	3.8972		3.8991		Ly2	T = 100 °K, Tetr. 65 < T < 110 °K, c/a = 1.00056, on single crystal [Ly2]. Further remarks:***) See page 156	
	O					Ly2	a:b:c 0.9998:1:1.0002, orthorhombic 35 < T < 65 °K [Ly2]	
	R					Ly2	Possibly rhombohedral at 10°K	

\*) Complete bibliography to 1961 [Ha7]; Raman scattering [Di8, Du2, Pa6, Pi3, Ri3, Di8a, Ro19a]; study of structural changes [Ca4, Co15a, Fo6, Me6, Sc8, Ka24, We11a]; pressure dependence of dielectric properties [Co27, Ka1, Le9, Me23, Mo7, Mo8, Po3, Po4, Po5, Po6, Sa3]; radiation damage [Sc6, We3]; refractive index [Sh31, Ho3, Ho3a]; thermal conductivity [Di9, Ma23, Su7, In26]; surface layers [Or1, Le12, Ho10, Du1, Cr2, Ca1, Br3]. Optical properties [Mu11, Mu12, Mu13, Ve8, Ve6, Ha15, Jo1, Co30, Sh24, Re4, Po7, Na8, Kh3, Ba9, We11a]; ultrasonic propagation [Gr10]; ESR: Ti [Da4, Ta4, Ta6], Mn [Ik1, Ik2, Ik3, Ve10], Pt [Si3], Eu [Ta7, Ta8], Gd [Bu7, Ta3, Ta5, Ta8, Ri5]; dielectric properties [De9, Hu11, Si17, Fr17, We11a]. Transport properties [Ucl, Ue2, Ta9, Sc15, Ry1, Mu10, Ma32, Ma3, Ko9, Ka21, Ik5, Be28, An4], electromicroscopic observation [Mo12]. Lattice vibration [Ax1, Ha14, Ka3, Dr3], shock-wave compression [Do4], elastic properties [Fu5], grain size influence on  $\theta_0$  [Ri2], relaxation time [W15, Bo4]. Properties with additives: Mg [Is13], Mn [Bh1, As2], Fe [Sc25], Co, Ni [Ku1, Co23a], Zn [Si16], Nb + Ta [Gu1, Ku1], Ln [Go4, As2, Bo4, Jo11], Sr [He14, Al1, He6], Bi [Bo3, Jo11], Sb [He13, Jo11], Halogens [Jo10], PbNb<sub>2</sub>O<sub>6</sub> [Sr1], Ca, Zr, Si, Fe, Mg [Br22a]; defect study [Co24, Mu9, No8], neutron scattering [Ya2a].

\*\*) P & S [Wo16, Ma4, Ma36, Si19c, Ra5, Bi14a, Di4]; effect of additives on occurrence [Ra5, Ro20a, Di4], hex. form due to oxygen vacancies or metal substitution for Ti [Di4], magnetic properties with Ti, Cr, V, Mn, Re, Fe, Co, Ru, Ir, Pt substitution [Di4].

Compound	Sym	a Å	b Å	c Å	angle	Ref.	Remarks	Magnetic Data
A <sup>2+</sup> B <sup>4+</sup> O <sub>3</sub> (continued)								
CaTiO <sub>3</sub>	O	5.381	5.443	7.645		Pe3	P & S [Ba18, Ze1, Ze2, Le10, Na13, Na15, Me4, Ku2], optical properties [St21, Pe8, Mu13], de-tailed structure [Ka21a]	in 3.3.4, Tab.
CdTiO <sub>3</sub>	C					Gr3a	Cubic <i>T</i> > 1260 °C	
	O	5.348	5.417	7.615		Ka22	Structure determined Pbn2 <sub>1</sub> [Ka22], structure questioned [Ge3a], P & S [Me4], S.S. with NaNbO <sub>3</sub> [Le2], electrical properties [Sh24a], perovskite-ilmenite transformation [Li0]	
PbTiO <sub>3</sub>	T	3.904		4.152		Sh21	Complete structure [Sh21], P & S [Me4, Sh19, Co13, Sh15, Sh24b], optical properties [Pe8, Fu5], piezoelectric properties [Ue3, Fe2, Fe1, Is14a], slow neutron scattering [So2], S.S. with (Ba, Sr, Ca, Pb) (Ti, Zr, Sn)O <sub>3</sub> [Sh19, Ta14, Ha20, Ba12, No7, Ou1, Ou2, Th2, Ok7, Ta6, Kl7, Ou1a, Pe9, Is1, Ue2, Si34, Fe1, Bu10, Fe3, Fe9, Fu5, He14, Iw3, Si35, Di1a], radiation damage [Ha30], S.S. with PbGeO <sub>3</sub> [Di5b]	
	C	3.960				Sh21	<i>T</i> = 535 °C, cubic <i>T</i> > 490 °C	
(CuA)TiO <sub>3</sub>	C	≈ 7.4				De18	A = Ca (25%) <i>a</i> = 7.393 Å; Cd (25%) <i>a</i> = 7.399 Å; Sr (20%) <i>a</i> = 7.420 Å	6
EuTiO <sub>3</sub>	C	7.810				Ho12	P & S [Br20, Mc1b], Prop. [Mc2, Mc3, Mc4, Si4]	
La <sub>0.5</sub> K <sub>0.5</sub> TiO <sub>3</sub>	C	3.914				Ro20	Dielectric properties [Sm8, Ag1]	
La <sub>0.5</sub> Na <sub>0.5</sub> TiO <sub>3</sub>	C	3.86				Ag1	Dielectric properties [Sm8]	
Ce <sub>0.5</sub> K <sub>0.5</sub> TiO <sub>3</sub>	C	3.90				Ro20	S.S. with La	
Nd <sub>0.5</sub> K <sub>0.5</sub> TiO <sub>3</sub>	C	3.874				Ro20		
Y <sub>0.5</sub> Na <sub>0.5</sub> TiO <sub>3</sub>	O	5.326	5.443	7.614		Re2	Dielectric properties [Ag1, Bu3, Sm8, Sm26]	
Bi <sub>0.5</sub> K <sub>0.5</sub> TiO <sub>3</sub>	T	3.913		3.993		Iv2	Dielectric properties [Ag1, Bu3, Sm8, Sm26]	
Bi <sub>0.5</sub> Na <sub>0.5</sub> TiO <sub>3</sub>	R	3.891			α = 89° 36'	Iv2	S.S. with SrTiO <sub>3</sub> [Ta1, Ve9, We16]	
La <sub>2/3</sub> TiO <sub>3</sub>	C	3.887				Ke18		
SrVO <sub>3.5</sub>	C	3.848				Wo14	P & S [Re8]	6
SrVO <sub>3.0</sub>	C	3.838						

\*\*\* Superconductivity [Am2, Ap2, Ea2, Fr10, Ko7, Sc19, Sc20, Sc21]; Raman scattering [Sc4, Sc3, Ri6, Os1, Ni1a, Fl1b]; Mössbauer: Co<sup>57</sup> [Bh3]. Optical properties [Ba6, Ba15, Ba16, Ca6, Co9, Du1, Ea1, Gr1, Ka9, Mu11, Mu12, Mu13, Si12, Va6, Zo2, Am3, Fa4a, Fe10a]; Hall mobility [Fr6, Fr9, Pa5, Tu1]; ESR: Cr<sup>3+</sup> [Ri7], Fe<sup>3+</sup> [K12, Ba8, Ri7, Un2], Ni<sup>3+</sup> [Ho1]. Gd<sup>3+</sup> [Ri7, Ri5, Sa2, Si11]; magnetoresistance [Fr7, Tu3, Ya3b], piezoelectric properties [Tu2]; Shubnikov-deHaas effect [Fr6]; thermal conductivity (33 < *T* < 110 °K) [Sw2]; diffusion and formation of oxygen defects [Pa3, Pa4, Wa9, Wa10]; radiation damage [Sc6, Ro4]; band structure [Ka6]; dielectric properties: doped with Fe and Cr [Ma33] with Nb [Ti2]; elastic constants from sound wave attenuation [He6, Jo5a]; electromechanical behavior [Ru12]; pressure dependence of dielectric properties [He6a, Sa3]; photoconduction [Ya4, Ya5, Ya3a, Ya3b]; magnetic properties [Fr5]; vibrational modes [Ja8, Jo14]; thermal expansion [De19b], inelastic neutron scattering [Sh16a], electrooptic effect [So3].

Compound	Sym	a Å	b Å	c Å	angle	Ref.	Remarks	Magnetic Data
A <sup>2+</sup> B <sup>4+</sup> O <sub>3</sub> (continued)								
CaVO <sub>3.0</sub>	C	3.767	5.352	7.547		Wo14	P & S [Ru7, De2, Re8, Re9]	in 3.3.4, Tab. 6
	O	5.326				Wo16		
CaVO <sub>3.85</sub>	C	3.780		22.95		Ch1a	Hex (9L), high pressure phase, semiconducting, ΔE = 0.09 eV	
BaCrO <sub>3</sub>	H	5.62				Ch1a	Hex (4L), high pressure phase, semiconducting, ΔE = 0.11 eV	
	H	5.659		9.359		Ch1a	Hex (6L), high pressure phase	
	H	5.627		13.690		Ch1a	Hex (12L), high pressure phase	
	H	5.662		27.752		Ch1a	Hex (14L), high pressure phase	6
	H	5.652		32.515		Ch1a	Hex (27L), high pressure phase	
	H	5.649		62.706		Ch1		
SrCrO <sub>3</sub>	C	3.818		7.486		Go17	P & S [De21]	
CaCrO <sub>3</sub>	O	5.287	5.316			Ro19	Hex (2L), P & S [Ha16, Sy1]	
PbCrO <sub>3</sub>	C	4.00		4.71		Ha7	Hex (9L), high pressure phase	
BaMnO <sub>3</sub>	H	5.672		20.948		Sy1	Hex (4L), high pressure phase, P & S [Ha16]	6
	H	5.667		9.375		Ha7	Hex (4L), high temperature phase	
	H	5.669		9.264		Sy1	Hex (4L), S.S. with (Bi, Ba, La)MnO <sub>3</sub> [Iv1]	
	H	5.645		9.085		Sy1	Hex (6L), high pressure phase	
SrMnO <sub>3</sub>	H	5.449		13.396		Sy1	96% Mn <sup>4+</sup> , P & S [Vo12, To13, Yu1, Yu8], S. S.	
	H	5.431		7.464		Ma6	with Bi [Bo6, Bo12, Si19]	
CaMnO <sub>3</sub>	O	5.270	5.275			Ma6		6
	O	5.302	5.304	7.488		Mo10	α = 0.36 P & S [De15, Er1, Mo11, Ma22, Va8]	
Ca <sub>0.75</sub> Sr <sub>0.25</sub> MnO <sub>3</sub>	R	4.099			α = 88° 47'	Mo10	α = 0.25; K <sub>β</sub> X-ray spectra [Ko6a]	
BaFeO <sub>3-x</sub>	C	3.997				Mo10	α = 0.19	
	T	7.956		8.006		Mo10	Hex (6L); x = 0.08	
	H	5.672		13.90		Gal8	Brownmillerite structure, see Fig. 21	
BaFeO <sub>2.5</sub>	O	5.83	16.98	5.54		Mo11	T = 1000 °C, T = 20 °C (triclinic)	6
	C	4.15				Ma4	P & S [Wa17, Ya1 Ga17, Sh17], S.S. with La [Ga16, Wa17, Wa20], Bi [Ma8], Ti [Cl2, Br18]	
SrFeO <sub>3.0</sub>	C	3.850				Ma4		
	T	3.851		3.867		Ma4	P & S [Ba23], S.S. with Al [Ba24, Ba25], Brown-	
SrFeO <sub>2.84</sub>	O	5.671	15.59	5.528		Ma4	millerite structure, see Fig. 21	
SrFeO <sub>2.60</sub>	O					Be40	P & S [Be39, Sm4], neutron diffraction [Ta10, Fr16, Co22], Mössbauer [Go4, Gr6, Ge7, Ge8, Wi15, Wi16, Ta10, Gr4]	
CaFeO <sub>2.60</sub>	O	5.64	14.68	5.39		Be40	Prop. [Gr5, Pol, Wh4, Be40, Sm4]	6
	T					Be26	P & S [Mo15]	
CaFe <sub>0.6</sub> Al <sub>0.5</sub> O <sub>2.5</sub>	O	5.58	14.50	5.34		Ha10		6
PbFeO <sub>2.5</sub>	T	7.79		15.85		Be26		

Compound	Sym	a Å	b Å	c Å	angle	Ref.	Remarks	Magnetic Data in 3.3.4, Tab.
<b>A<sup>2+</sup>B<sup>4+</sup>O<sub>3</sub> (continued)</b>								
BaCoO <sub>2.72</sub>	H	5.59		4.83		Gu7	Hex (2L), P & S [Si41]	
SrCoO <sub>3-x</sub>	C	7.725				Yal	1.4% Co <sup>4+</sup> , S.S. with La [Wal17]	
BaNiO <sub>2.8</sub>	H	5.58		4.832		La4	Hex (2L) [La3, Gu7]	
CaGeO <sub>3</sub>	C	3.723				Ri8a	High pressure phase; doubled cell [Si3a]	
CdGeO <sub>3</sub>	C	3.70				Ri8a	High pressure phase, pseudocubic	
BaZrO <sub>3</sub>	C	4.20				Ha20	P & S [Ho2, Me4, Be24]; S.S. with BaTiO <sub>3</sub> [Ve7], PbTiO <sub>3</sub> [Ha20]; optical properties [Pe7, Du5]	
	C	4.26				Fo4	T = 2000 °C	
SrZrO <sub>3</sub>	O	5.792	5.818	8.189		Pe3	P & S [Ho2, Me4, Sm3, Sc18a], D.T.A., T < 1000 °C [Ca5], optical properties [Pe7, Du5], S.S. with Hf [Be24a]	
	C	4.18				Fo4	T = 2000 °C, cubic T > 1300 °C	
CaZrO <sub>3</sub>	O	5.587	5.758	8.008		Ti3	P & S [Si15, Me4, Ru9, Ru14], S.S. with Cr [Ni2]	
	C	4.10				Fo4	T = 2000 °C, cubic T > 1600 °C	
PbZrO <sub>3</sub>	O	5.872	11.744	8.202		Sa8	P & S [Is1, Me4, Sa7], phase transitions [Go28, Go29, Go30, Sa8, Te5, Te8, Ue1, Sh15a, Te8d], radiation damage [Ha30], optical properties [Pe7], neutron diffraction [Jo5], dielectric properties [Kh4, Kh6, Kh8, Go29], piezo-electric effect [Ro1, Th2, Is14a], S.S. with Ca [Kh4, Si15], (BiNa) and (BiK) [Bu3], Pb(Ni <sub>1/3</sub> Nb <sub>2/3</sub> )O <sub>3</sub> [Bu10], BiFeO <sub>3</sub> [Ge10], Hf [Go31]	
	C	4.149				Sa8	T = 230 °C, cubic T > 230 °C	6
	C	4.099				Ho12	P & S [Mc4]	
EuZrO <sub>3</sub>							Prep. + Prop. [Sm33, Bu3]	
Bi <sub>0.5</sub> K <sub>0.5</sub> ZrO <sub>3</sub>							Prep. + Prop. [Sm33, Bu3]	
Bi <sub>0.5</sub> Na <sub>0.5</sub> ZrO <sub>3</sub>						Sc17	P & S [Bo19, Sc16, Ro2a], S.S. with Sr [Br15]	6
BaMoO <sub>3</sub>	C	4.04				Sc17	P & S [Bo19, Sc16, Ro2a], S.S. with Ti [Ro2a, Br17], S.S. with Zr [Br17]	6
SrMoO <sub>3</sub>	C	3.98						
CaMoO <sub>3</sub>	O	5.45	5.58	7.77		Mc1	P & S [Sc16, Go17, Ro2a]	6
BaTcO <sub>3</sub>	H	5.758		14.046		Mu7	Hex (6L)	
	C	8.140				Ke9		
	C	3.95				Mu7	Slight distortion, P & S [Ke9]	
SrTcO <sub>3</sub>	C	3.87	3.96	3.76		Ke9		
CaTcO <sub>3</sub>	O	10.360				Mu7	Defect pyrochlore structure	
PbTcO <sub>3</sub>	C	5.75		21.60		Ra6	Hex (9L), structure determination [Do2], Prop. [Ca2], S.S. with Sr [Do3, Lo1], S.S. with Zr, Mn, Ir, Ni [Do3a]	
BaRuO <sub>3</sub>	H	5.73		9.50		Lo1	Hex (4L), high pressure phase	

Ref.	Magnetic	Remarks	Ref.	angle	c	b	a	c	angle	Ref.	Magnetic
------	----------	---------	------	-------	---	---	---	---	-------	------	----------

Compound	Sym	a Å	b Å	c Å	angle	Ref.	Remarks	Magnetic Data
A <sup>2+</sup> B <sup>4+</sup> O <sub>3</sub> (continued)								
BaRuO <sub>3</sub>	H	5.71	5.57	14.00		Lo1	Hex (6L), high pressure phase	in 3.3.4, Tab. 6
SrRuO <sub>3</sub>	O	5.53	5.53	7.85		Ra6	P & S [Kh1], Prop. [Ca2, Lo3]	
CaRuO <sub>3</sub>	O	5.36	5.53	7.67		Ra6	Prop. [Ca2, Lo3]	6
SrRu <sub>0.5</sub> Ir <sub>0.5</sub> O <sub>3</sub>	O	5.55	5.58	7.84		Ra6		
PbRuO <sub>3</sub>	C	10.25				Lo4	P & S [Ra6], Defect pyrochlore structure	
BaSnO <sub>3</sub>	O	5.56	5.61	7.86		Lo1a	High pressure phase	
	C	4.117				Me4	P & S [Wa2, Co8, Sm3], S.S. with Sr [Sm3], (Ba, Sr, Pb)TiO <sub>3</sub> [Na9, Du4, My2], optical properties [Du5, Ya3], Mössbauer in S.S. with Ti [Be7, Bo9, Kr6]; S.S. with Ti, tetragonal at 91% Ti [Do1]	
SrSnO <sub>3</sub>	C	8.070				Sm3	P & S [Ho2, Me4, Co8], optical properties [Du5]	
CaSnO <sub>3</sub>	O	5.519	5.668	7.885		Sm2	P & S [Ro12, Co8, Me4]; optical properties [Du5]; S.S. with BaTiO <sub>3</sub> cubic at 13% CaSnO <sub>3</sub> [Do1]	
CdSnO <sub>3</sub>	O	5.457	5.577	7.867		Sm2	P & S [Na13, Co8]	
PbSnO <sub>3</sub>	M	4.076	4.076	4.043	$\beta = 89^\circ 45'$	Su9	High pressure preparation	
BaCeO <sub>3</sub>	C	4.07				Su9	T = 125 °C, cubic T > 125 °C	
	C	4.397				Sm3	P & S [Ho2], optical properties [Du5], S.S. with Sr [Sm3], dielectric properties [Sm7a]	
SrCeO <sub>3</sub>	O	6.011	6.156	8.588		Sm3	P & S [Ho2], optical properties [Du5], dielectric properties [Sm7a]	
CaCeO <sub>3</sub>	C	7.70				Na14	Pseudocubic	
CdCeO <sub>3</sub>	C	7.65				Na14	Pseudocubic	
PbCeO <sub>3</sub>	C	7.62				Na14	Pseudocubic	
BaPrO <sub>3</sub>	C	8.708				Na15	P & S [Ho2]	
BaHfO <sub>3</sub>	C	4.172				Sh16	S.S. with CaZrO <sub>3</sub> [Be24], P & S [Sc18a]	
SrHfO <sub>3</sub>	C	4.069				Ho2	P & S [Na15], S.S. with SrZrO <sub>3</sub> [Be24a]	
CaHfO <sub>3</sub>	C	5.568				De7	Prep. [Ru14]	
CdHfO <sub>3</sub>	O	3.942	5.732	7.984	$\beta = 91^\circ 36'$	Av1	Cubic T > 215 °C, S.S. with PbZrO <sub>3</sub> [Go31]	
PbHfO <sub>3</sub>	T	4.136	3.982	3.942		Sh16	T = 250 °C, cubic T > 215 °C	
PbReO <sub>3</sub>	C	4.134				Lo4	Defect pyrochlore type	
	C	10.425				Do3	S.S. with Sr [Do3], distorted Hex. (9L); structure [Ro2b]	
BaIrO <sub>3</sub>	H	5.76	44.4					
SrIrO <sub>3</sub>	M	5.60	9.62	14.17	$\beta = 93^\circ 16'$	Lo1a	Prep. [Ro2a], distorted Hex (6L)	
PbIrO <sub>3</sub>	O	5.58	5.60	7.89		Lo1a	High pressure phase (Perovskite)	
	C	10.271				Lo4	P & S [Ra6], defect pyrochlore type	
CaIrO <sub>3</sub>	O	3.145	9.855	7.293		Ro2b	Not perovskite	
BaPbO <sub>3</sub>	C	4.265				Wa2	P & S [We7, Ni3], electrical properties [Ik4]	
SrPbO <sub>3</sub>	O	5.864	5.949	8.336		We7		



Compound	Sym	a Å	b Å	c Å	angle	Ref.	Remarks	Magnetic Data
A <sup>2+</sup> B <sup>4+</sup> O <sub>3</sub> (continued)								
BaThO <sub>3</sub>	C	8.985				Sm30	P & S [Ho2, Na15, Me4, Be24]	in 3.3.4, Tab.
SrThO <sub>3</sub>	C	8.84				Na15	Pseudocubic, S.S. with Ba [Be24]	
CaThO <sub>3</sub>	C	8.74				Na15	Pseudocubic	
CdThO <sub>3</sub>	C	8.74				Na15	Pseudocubic	
PbThO <sub>3</sub>	C	8.960				Na15	Pseudocubic	
BaUO <sub>3</sub>	C	4.387				La5	P & S [Sc16, Ru4, Tr9], S.S. with BaTiO <sub>3</sub> [Va9]	
BaNpO <sub>3</sub>	C	4.384				Ke4		
BaPuO <sub>3</sub>	C	4.357				Ke3	Pseudocubic	
SrPuO <sub>3</sub>	C	4.28				Ke3	Pseudocubic	
A <sup>2+</sup> B <sup>4+</sup> X <sub>3</sub> or A <sup>3+</sup> B <sup>3+</sup> X <sub>3</sub> ; X = S, Se								
BaTiS <sub>3</sub>	H	6.77		5.74		Cl1	Hex (2L), P & S [No9, As3b], orthorhombic and tetragonal modifications [Ha6]	
BaTiSe <sub>3</sub>	H	7.054		6.033		As3a	Hex (2L), P & S [No9]	
SrTiS <sub>3</sub>	H	6.730		5.829		Ha6	Hex (2L), P & S [No9], orthorhombic and tetragonal modifications [Ha6]	
PbTiS <sub>3</sub>	T	4.16		11.752		St27	"Layer structure" P & S [No9]	
BaZrS <sub>3</sub>	O	7.037	9.983	7.050		Cl3	Distorted perovskite, P & S [No9]	
BaZrSe <sub>3</sub>	H	7.188		6.025		As3a	Hex (2L), P & S [No9]	
SrZrS <sub>3</sub>	O	13.49	9.79	14.23		Cl1	Distorted perovskite, P & S [No9]	
CaZrS <sub>3</sub>	O	13.07	9.58	14.05		Cl1	Distorted perovskite	
BaLaS <sub>3</sub>	H	6.847		5.742		As3b	Hex (2L) P & S [No9]	
BaTaSe <sub>3</sub>	H	7.134		5.987		As3a	Hex (2L) P & S [No9]	
ATaSe <sub>3</sub>	O	11.0	6.8	11.9		No9	A = Sr and Pb—not perovskite	
LnInS <sub>3</sub>	O	≈ 3.95	≈ 11.78	20.98		Ka13	Ln = La, Ce, Pr, Nd and Sm; T <sub>melt</sub> ≈ 1100 °C	
LnGaSe <sub>3</sub>	H	≈ 10.3		≈ 6.2		Ka12a	Ln = La, Ce, Pr, Nd, Sm; T <sub>melt</sub> = 1100 °C	
A <sup>3+</sup> B <sup>3+</sup> O <sub>3</sub>								
LaAlO <sub>3</sub>	R	5.357			α = 60° 6'	Ge5	P & S [Be34, Da1, Re5, De14], ESR: Gd, Cr [Ki3, Si16a]. Luminescence: Eu [Ya3, Bl13, Bl14], Pr [Ma30, De8], Cr [Bl15, Bo14]; twinning + detwinning [Fa9, Fa10]; nuclear quadrupole resonance [De17]; S.S. with BaTiO <sub>3</sub> [Sm15, Is2b]; space group, R3c [Ra3, Ge4b], Review [Ge4b] T = 650 °C; cubic T > 522 °C [Wo15a, Ge4b, Ax3], inelastic neutron scattering [Ax3]	6
CeAlO <sub>3</sub>	C	3.818				Ge5		
PrAlO <sub>3</sub>	R	5.327 5.307			α = 60° 15' α = 60° 22'	Ki1 Ge5	P & S [Be34, Ro16, Sc13, Ke2] P & S [Be34, Ma27, Yu4, Zo1, Re5, Li2, Ru10, Sc13]	

Compound	Sym	a Å	b Å	c Å	angle	Ref.	Remarks	Magnetic Data
A <sup>3+</sup> B <sup>3+</sup> O <sub>3</sub> (continued)								in 3.3.4, Tab. 6
PrAlO <sub>3</sub>	T	3.74		3.76		Ma27	Discussion of disagreement between [Ge5] and [Ma27] given in [Ge4a] and [To12a]	6
NdAlO <sub>3</sub>	R	5.286			α = 60° 25'	Ge5	P & S [Be34, Da2, Zo1, Ke2, Ge5, Re5, Li2, Ru10, Sc13, Da1]	6
SmAlO <sub>3</sub>	O	5.285	5.290	7.473		Ge5	P & S [Be34, Ke2, Re5, Li2, Sc13, Zo1]	6
	O	7.46	7.46	7.43		Ma27	Discussion of disagreement between [Ge5] and [Ma27] given in [Ge4a] and [To12a]	
EuAlO <sub>3</sub>	R	5.316		7.458	α = 60° 19'	Ge2	T = 850 °C, rhombohedral T > 800 °C	
	O	5.271	5.292	10.52		Ge5	P & S [Bo14, Re5, Li2]	6
GdAlO <sub>3</sub>	H	3.760		10.52		Be36	Prep. T < 900 °C, see Fig. 17a	6
	O	5.247	5.304	7.447		Ge5	P & S [Be34, Da1, Ga28, Sc13, Li2, Ma39]; optical properties [Bi13, Bi14, Bi16, Ca8, Oh1]; NMR, Al <sup>27</sup> [Bo2a]	
TbAlO <sub>3</sub>	H	3.73		10.51		Be36	Prep. < 900 °C, see Fig. 17a	6
	O	5.229	5.308	7.415		Bi2	Neutron diffraction [Bi2], P & S [Ga28, Sc13], optical properties [Hu6, Hu6a]	
DyAlO <sub>3</sub>	H	3.730		10.51		Be36	Prop. < 900 °C, see Fig. 17a	6
	O	5.23	5.31	7.40		Gi3	P & S [Be34, Ga28, Da1, Da2, Sc13], neutron diffraction [Bi1, He12], optical properties [Hu5, Sc24, Fa5]	
HoAlO <sub>3</sub>	H	3.700		10.50		Be36	Prep. < 900 °C, see Fig. 17a	6
	O	5.18	5.33	7.36		Sc13	P & S [Ga28]	
ErAlO <sub>3</sub>	H	3.670		10.51		Be36	Prep. < 900 °C, see Fig. 17a	6
	O	5.16	5.32	7.33		Sc13	P & S [Ga28]	
TmAlO <sub>3</sub>	H	3.660		10.50		Be36	Prep. < 900 °C, see Fig. 17a	6
YbAlO <sub>3</sub>	O	5.15	5.33	7.29		Sc13	P & S [Ga28]	
LuAlO <sub>3</sub>	O	5.128	5.332	7.317		Ga28		
YAlO <sub>3</sub>	O	5.179	5.329	7.370		Ge6	No perovskite [Ga28, Sc13]	
						Be36	P & S [Mi8, Be34], ESR: Fe <sup>3+</sup> and Gd <sup>3+</sup> [Wh3]; decomposition of YAG [Ma26]	
BiAlO <sub>3</sub>	H	3.68		10.52		Na15	Prep. < 900 °C, see Fig. 17a	
PuAlO <sub>3</sub>	T	7.61		7.94	α = 90° 24'	Ru13	Not able to be reproduced [Bu3]	
AmAlO <sub>3</sub>	R	3.78			α = 90° 28'	Ke8		
LaScO <sub>3</sub>	R	3.75				Ge2	P & S [Sc13, Ke2]	
CeScO <sub>3</sub>	O	5.678	5.787	8.098		Ke2	No dimensions	
PrScO <sub>3</sub>	O	5.615	5.776	8.027		Ge2	P & S [Sc13]	
NdScO <sub>3</sub>	O	5.574	5.771	7.998		Ge2	P & S [Sc13, Ke2]	
SmScO <sub>3</sub>	O	5.53	5.76	7.95		Sc13		

Goodenough/Longo

161

Compound	Sym	a Å	b Å	c Å	angle	Ref.	Remarks	Magnetic Data
A <sup>3+</sup> B <sup>3+</sup> O <sub>3</sub> (continued)								
EuScO <sub>3</sub>	O	5.51	5.76	7.94		Sc13	P & S [Sc13], Prop. [Bo36]	6
GdScO <sub>3</sub>	O	5.487	5.756	7.925		Ge2		
DyScO <sub>3</sub>	O	5.43	5.71	7.89		Sc13		
HoScO <sub>3</sub>	O	5.42	5.71	7.87		Sc13		
YScO <sub>3</sub>	O	5.431	5.712	7.894		Ge2	P & S [Sc13, Ke2]	
BiScO <sub>3</sub>	Tr	4.042	4.127	4.042	$\alpha = \gamma = 90^\circ 41'$ $\beta = 91^\circ 52'$	To11b	High pressure preparation [To11a]	
LaTiO <sub>3-x</sub>	C	3.934				We16	P & S [Si4, Be33, Ho12, Ke15, Ke16, Jo4]	6
La <sub>0.87</sub> TiO <sub>3</sub>	C	3.887				Ke18	Ti <sup>4+</sup> , S.S. with SrTiO <sub>3</sub> [Ti1, Ke18, Ve9, We16], BaTiO <sub>3</sub> [Jo4]	6
CeTiO <sub>3</sub>	T	5.513		7.760		We16	P & S [Be33, Ho12, Si4]	6
PrTiO <sub>3</sub>	T	5.508		7.742		We16	P & S [Be33, Ho12, Si4]	6
NdTiO <sub>3</sub>	O	5.482	5.521	7.728		We16	P & S [Be33, Ho12, Si4]	6
SmTiO <sub>3</sub>	O	5.398	5.568	7.651		We16	P & S [Be33, Si4, Mc1c]	6
GdTiO <sub>3</sub>	O	5.353	5.655	7.616		We16	P & S [Bo36, Ho12, Si4, Mc1c]	6
EuTiO <sub>3</sub>	C	7.810				Ho12	Ti <sup>4+</sup> , P & S [Br20, Mc1b], Prop. [Mc3, Mc4, Si4], neutron diffraction [Mc2]	6
TbTiO <sub>3</sub>	O	5.388	5.648	7.676		Mc1c		
DyTiO <sub>3</sub>	O	5.361	5.659	7.647		Mc1c		
HoTiO <sub>3</sub>	O	5.339	5.665	7.626		Mc1c		
ErTiO <sub>3</sub>	O	5.318	5.657	7.613		Mc1c		
TmTiO <sub>3</sub>	O	5.306	5.647	7.607		Mc1c		
YbTiO <sub>3</sub>	O	5.293	5.633	7.598		Mc1c		
LuTiO <sub>3</sub>	O	5.274	5.633	7.580		Mc1c		
YTiO <sub>3</sub>	O	5.340	5.665	7.624		Mc1c		
LaVO <sub>3</sub>	O'	5.540	5.540	7.83		Wo14	P & S [Si5, Be33, Ke16, Re8, Wo4, Ke18, Ke15, Ya1, Ro3], S.S. with: SrVO <sub>3</sub> [Ke18, Wo14], S.S. with CaVO <sub>3</sub> [Wo14]	6
CeVO <sub>3</sub>	O'	5.486	5.486	7.74		Wo14	P & S [Be33, Re8, Wo4]	6
PrVO <sub>3</sub>	O'	5.487	5.562	7.751		Wo14	P & S [Be33, Re8, Wo4, Vi2, Ge2]	6
NdVO <sub>3</sub>	O	5.451	5.579	7.734		Wo14	P & S [Be33, Re8, Wo4, Vi2, Ge2]	6
SmVO <sub>3</sub>	O	5.393	5.588	7.672		Wo14	P & S [Be33, Re8, Wo4]	6
GdVO <sub>3</sub>	O	5.343	5.614	7.637		Wo14	P & S [Be33, Bo36, Re8, Ge2]	6
DyVO <sub>3</sub>	O	5.302	5.602	7.601		Wo14	P & S [Re8]	6
ErVO <sub>3</sub>	O	5.262	5.604	7.578		Wo14	P & S [Re8]	6
YVO <sub>3</sub>	O	5.284	5.605	7.587		Wo14	P & S [Re8]	6
PuVO <sub>3</sub>	O	5.45	5.58	7.76		Ru13	P & S [Ro3, Re8]	6
AmVO <sub>3</sub>	O	5.48	5.61	7.78		Ke8		6

Compound	Sym	a Å	b Å	c Å	angle	Ref.	Remarks	Magnetic Data in 3.3.4, Tab. 6
A <sup>3+</sup> B <sup>3+</sup> O <sub>3</sub> (continued)								
LaCrO <sub>3</sub>	O	5.479	5.515	7.753		Qu1	Semiconducting 0.6 eV [Ru11], neutron diffraction [Ko1], optical properties [Ru11], dielectric properties [Ra8], P & S [Ge2, Ru11, Wo4, Ke2, Na14], S.S. with Ni, Mn [Be33, Be21]; T <sub>melt</sub> = 2500 °C [Fo2], EPR [Wo4] T = 280 °C, rhombohedral 280 < T < 1030 °C T = 1230 °C	
	R	5.47			α = 60° 32'	Ru11		6
	C	3.92				Ru11		
La <sub>0.8</sub> Bi <sub>0.1</sub> CrO <sub>3</sub>	O	5.47	5.50	7.75		Iw1		6
La <sub>0.5</sub> Sr <sub>0.5</sub> CrO <sub>3-z</sub>	O	7.754				Ya1		6
CeCrO <sub>3</sub>	O	5.475	5.475	7.740		Qu1	P & S [Ru10, Be33, Wo4, Ke2] T <sub>melt</sub> = 2420 °C	6
PrCrO <sub>3</sub>	O	5.448	5.479	7.718		Qu1	[Fo2], dielectric properties [Ra8]	6
NdCrO <sub>3</sub>	O	5.425	5.478	7.694		Qu1	P & S [Ru10, Ge2, Be33, Wo4, Ke2], T <sub>melt</sub> = 2405 °C [Fo2]	6
SmCrO <sub>3</sub>	O	5.367	5.508	7.643		Qu1	P & S [Ru10, Ge2, Be33, Wo4, Ke2], T <sub>melt</sub> = 2385 °C [Fo2]	6
EuCrO <sub>3</sub>	O	5.340	5.515	7.622		Qu1	P & S [Ru10]	6
GdCrO <sub>3</sub>	O	5.312	5.525	7.606		Qu1	P & S [Ru10, Ge2, Be33], T <sub>melt</sub> = 2370 °C [Fo2]	6
TbCrO <sub>3</sub>	O	5.291	5.518	7.576		Qu1	Neutron diffraction [Be42, Ma24], specific heat [De1a]	6
DyCrO <sub>3</sub>	O	5.265	5.520	7.552		Qu1	Neutron diffraction [Be38], T <sub>melt</sub> = 2345 °C [Fo2]; dielectric hysteresis disappears at ≈ 540 °C indicating no center of symmetry [Ra8]	6
HoCrO <sub>3</sub>	O	5.243	5.519	7.538		Qu1	Neutron diffraction [Be32, Be47, Be50], dielectric properties [Co6], T <sub>melt</sub> = 2330 °C [Fo2], dielectric hysteresis disappears at ≈ 460 °C indicating no center of symmetry [Ra8], S.S. with HoMnO <sub>3</sub> [Ap1b]	6
ErCrO <sub>3</sub>	O	5.223	5.516	7.519		Qu1	Dielectric properties [Co6], T <sub>melt</sub> = 2325 °C [Fo2]	6
TmCrO <sub>3</sub>	O	5.209	5.508	7.500		Qu1	T <sub>melt</sub> = 2320 °C [Fo2], dielectric hysteresis disappears at ≈ 520 °C indicating no center of symmetry [Ra8]	6
YbCrO <sub>3</sub>	O	5.195	5.510	7.490		Qu1	Dielectric hysteresis disappears at ≈ 480 °C indicating no center of symmetry [Ra8]	6
LuCrO <sub>3</sub>	O	5.176	5.497	7.475		Qu1	P & S [Ge6, Ge2, Lo5, Ka18, Pa14, Yu5], dielectric properties [Ra8], T <sub>melt</sub> = 2340 °C [Fo2] High pressure preparation	6
YCrO <sub>3</sub>	O	5.241	5.521	7.532		Qu1		
InCrO <sub>3</sub>	O	5.170	5.355	7.543		Sh9		

Compound	Sym	a Å	b Å	c Å	angle	Ref.	Remarks	Magnetic Data in 3.3.4, Tab.
A <sup>3+</sup> B <sup>3+</sup> O <sub>3</sub> (continued)								
TiCrO <sub>3</sub>	O	5.302	5.405	7.647	$\alpha = \gamma = 90^\circ 35'$ $\beta = 89^\circ 10'$	Sh9	High pressure preparation	6
BiCrO <sub>3</sub>	Tr	3.90	3.87	3.90		Su10	High pressure preparation; S.S. with BiMnO <sub>3</sub> [To11a]	
PuCrO <sub>3</sub>	O	5.46	5.51	7.76	$\alpha = 90^\circ 36'$	Ru13	P & S [Na14], neutron diffraction [Ko1, Wo12], S.S. with Ba, Sr, Ca [Wo12, Ja4, Ja5, Jo8, Jo12, Ha22, Jo7, Jo9, Ya1, Ro11], S.S. with Cr, Fe, Co, Ni [Be33, Be21, Gi4, Jo7, Jo8, Jo9, Wo2, Wo6, Fu2, Bl7], S.S. with (Ba, Sr, Ca, Pb)TiO <sub>3</sub> [Ha31, Ha32, To3, To6, To12], S.S. with GdCoO <sub>3</sub> [De23] 24% Mn <sup>4+</sup>	6
LaMnO <sub>3</sub>	O'	5.533	5.722	7.694		Wo2		
CeMnO <sub>3</sub>	R	3.892				Wo2		
PrMnO <sub>3</sub>	O'	5.537	5.557	7.818		Ve12		
NdMnO <sub>3</sub>	O'	5.445	5.787	7.575		Ve12	P & S [Be33, Vi1], complete structure [Qu2]	
SmMnO <sub>3</sub>	O'	5.380	5.854	7.557		Ve12	P & S [Be33]	
EuMnO <sub>3</sub>	O'	5.359	5.843	7.482		Ve12	P & S [Sz1]	
GdMnO <sub>3</sub>	O'	5.338	5.842	7.453		Ve12	P & S [Be33, Sz1], S.S. with LaCoO <sub>3</sub> [De23]	
TbMnO <sub>3</sub>	O'	5.313	5.853	7.432		Ve12	Complete structure determination [Qu2]	
DyMnO <sub>3</sub>	O'	5.297	5.831	7.403		Ve12	P & S [Sz1]	
HoMnO <sub>3</sub>	H	5.275	5.828	7.375		Sz1	Preparation temperature 1600 °C, see Fig. 17a	6
ErMnO <sub>3</sub>	H	6.177		11.43		Ya2	Magnetic properties [Ve12, Be32], dielectric properties [Be35, Co7], P & S [Sz1], see Fig. 17a	
		6.136		11.42			High pressure phase, P & S [Wa5, Vi1, Sz1]	
		5.26	5.84	7.35		Wa4	Magnetic properties [Ve12, Be32], dielectric properties [Be35, Co7], see Fig. 17a	
		6.115		11.41		Ya2	Magnetic properties [Ve12, Be32], dielectric properties [Be35, Co7], see Fig. 17a	
		5.24	5.82	7.335		Wa4	High pressure phase	
		6.062		11.40		Ya2	Magnetic properties [Ve12, Be32], dielectric properties [Be35, Co7], see Fig. 17a	
		5.23	5.81	7.32		Wa4	High pressure phase	
		6.062		11.40		Ya2	Magnetic properties [Ve12, Be32, Ro8, Bo11], dielectric properties [Be35, Ro8, Bo11, Co7, Is11], P & S [Sz1], see Fig. 17a	
		5.22	5.80	7.30		Wa4	High pressure phase	
		6.042		11.37		Ya2	Magnetic properties [Ve12, Be32], dielectric properties [Be35, Co7], see Fig. 17a	6
		5.205	5.79	7.31		Wa4	High pressure phase	
		6.125		11.41		Ya2	Dielectric or magnetic properties [Ta13, Ro8, Be35, Co5, Co7, Co3, Bo11, Is11, Pe17, Pe16, Be32, Be39, Be43, Be44, Be49, Ko3, Ki8], see Fig. 17a	

**Berichtigungen zu Band III/4a**

- S. 177, letzte Zeile: statt  $\text{Ba}_2\text{TdPaO}_6$  lies  $\text{Ba}_2\text{TbPaO}_6$   
S. 219, Zeile 16 von unten: statt  $\text{KMg}_{1-x}\text{Ni}_x\text{Fe}_3$  lies  $\text{KMg}_{1-x}\text{Ni}_x\text{F}_3$   
S. 252, Zeile 26 von oben (Überschrift): statt  $\text{Sr}_3\text{Fe}_3\text{UO}_9$  lies  $\text{Sr}_3\text{Fe}_2\text{UO}_9$

**Errata in Vol. III/4a**

- p. 177, bottom line: instead of  $\text{Ba}_2\text{TdPaO}_6$  read  $\text{Ba}_2\text{TbPaO}_6$   
p. 219, line 16 from the bottom: instead of  $\text{KMg}_{1-x}\text{Ni}_x\text{Fe}_3$  read  $\text{KMg}_{1-x}\text{Ni}_x\text{F}_3$   
p. 252, line 26 from above (headline): instead of  $\text{Sr}_3\text{Fe}_3\text{UO}_9$  read  $\text{Sr}_3\text{Fe}_2\text{UO}_9$

Compound	Sym	a Å	b Å	c Å	angle	Ref.	Remarks	Magnetic Data
A <sup>3+</sup> B <sup>3+</sup> O <sub>3</sub> (continued)								in 3.3.4, Tab.
YMnO <sub>3</sub>	O'	5.26	5.84	7.35		Wa3	High pressure phase; S.S. with: Fe, perovskite at 15% Fe [Ch6]	
BiMnO <sub>3</sub>	M	10.93	11.31	7.98	$\beta = 92^\circ 24'$	Bo12	P & S [Su10]; S.S. with Ca [Bo6, Bo12, Su19], PbTiO <sub>3</sub> [Bo6, Bo7], Sr [Ju1], La [Ju1], BiCrO <sub>3</sub> [To11a]; crystallographic transformation T = 210 °C [To11a]	6
PuMnO <sub>3</sub> LaFeO <sub>3</sub>	C O	3.86 5.556	5.565	7.862		Ru13 Ge6	Pseudocubic P & S [Be33, Fo5, Re5, Wo3, Ke2, Da2, Na14, Ya1], S.S. with Ni, Mn [Be33], S.S. with Al, Co, Cr, Sc [Ka17, Wo3], rhombohedral T > 980 °C [Da1], S.S. with: PbNb <sub>2</sub> O <sub>6</sub> [Fr11], Pb [Re5a], Bi [Re5b]	6
CeFeO <sub>3</sub> PrFeO <sub>3</sub>	O O	5.541 5.495	5.577 5.578	7.809 7.810		Ro1a Ge6	P & S [Ke2, Be33]	6
NdFeO <sub>3</sub>	O	5.441	5.573	7.753		Ge6	P & S [Be33, Fo5, Re5, Wo3], S.S. with Pb [Re5a], Bi [Re5b]	6
SmFeO <sub>3</sub>	O	5.394	5.592	7.711		Ge6	P & S [Be33, Fo5, Re5, Wo3], S.S. with Pb [Re5a], Bi [Re5b]	6
EuFeO <sub>3</sub> GdFeO <sub>3</sub>	O O	5.371 5.346	5.611 5.616	7.686 7.668		Ge6 Ge6	P & S [Re5], S.S. with Pb [Re5a], Bi [Re5b] P & S [Be33, Re5], crystal structure [Co21], S.S. with Pb [Re5a], Bi [Re5b]	6 6
TbFeO <sub>3</sub> DyFeO <sub>3</sub> HoFeO <sub>3</sub>	O O O	5.326 5.302 5.278	5.602 5.598 5.591	7.635 7.623 7.602		Ei1 Ei1 Ei1	P & S [Ko6], S.S. with: Pb [Re5a], Bi [Re5b] P & S [Da2], S.S. with: Pb [Re5a], Bi [Re5b] P & S [Ko6], S.S. with: Pb [Re5a], Bi [Re5b], HoMnO <sub>3</sub> [Ap1a]	6 6 6
ErFeO <sub>3</sub>	O	5.263	5.582	7.591		Ei1	P & S [Fo5], crystal structure [Wi7], S.S. with: Pb [Re5a], Bi [Re5b]	6
TmFeO <sub>3</sub>	O	5.251	5.576	7.584		Ei1	Crystal structure [Wi8], S.S. with: Pb [Re5a], Bi [Re5b]	6
YbFeO <sub>3</sub>	O	5.233	5.557	7.570		Ei1	P & S [Ko6, Be1, Ha21], S.S. with: Pb [Re5a], Bi [Re5b]	6
LuFeO <sub>3</sub> YFeO <sub>3</sub>	O O	5.213 5.283	5.547 5.592	7.565 7.603		Ei1 Ei1	P & S [Sa6], S.S. with: Pb [Re5a], Bi [Re5b] P & S [Fo5, Ru11, Ko6, Wo3, Ge4, Ma26, Ya7, Sh12a], crystal structure [Co21], S.S. with: Pb [Re5a], Bi [Re5b]	6 6
TlFeO <sub>3</sub>	O	5.319	5.448	7.796		Sh9		

Compound	Sym	a Å	b Å	c Å	angle	Ref.	Remarks	Magnetic Data
A <sup>3+</sup> B <sup>5+</sup> O <sub>3</sub> (continued)								
BiFeO <sub>3</sub>	R	5.62			α = 59° 41'	Mi0	P & S [Fi12, Is10, Ko5, Kr4, To7, To9, To12, Yu3, Yu1, Za2, Sm34, To10, Ge10a, Ro22], neutron diffraction [Pl1, Ki4, Ki5, Kh5, Ro7, Ro9, LaAlO <sub>3</sub> [Fe5], LnFeO <sub>3</sub> [Kr5, Kh5, Ro7, Ro9, Is10b, Ro10, Ki6], Pb(Ti, Zr)O <sub>3</sub> [La6, Fe8, Ge10, Fe2, Sm7], BaTiO <sub>3</sub> [Ve5, Ka15], SrTiO <sub>3</sub> [Fe6], LaCrO <sub>3</sub> [Ro5], SrSnO <sub>3</sub> [Hi1], Bi <sub>4</sub> Ti <sub>3</sub> O <sub>12</sub> [Is12], SrFeO <sub>3</sub> [Ma8], Pb <sub>2</sub> FeNbO <sub>6</sub> [Ro10, Yu1, Yu2, Sm12, Sm13, Is10a, Zh1, Is8, Kr3, Kr5], Sr(Sn <sub>1/3</sub> Mn <sub>2/3</sub> )O <sub>3</sub> [Mi6, Vi4], Sr <sub>0.7</sub> La <sub>0.3</sub> MnO <sub>3</sub> [Ro10], PbNb <sub>2</sub> O <sub>6</sub> [Fr11]; BiMnO <sub>3</sub> [Ma31], Pb(Fe <sub>2/3</sub> W <sub>1/3</sub> )O <sub>3</sub> [Sm26], PrFeO <sub>3</sub> [Vi4a], complete structure S.G. R3c [Mi0] R3c, T < 375 °C; R3, T > 375 °C [Ra3]; P & S [As3, Wo4, He7, Sc23], Prop. [Me17, Ko1, Ra3, Ge12, Ra3, Jo9, Go16, Na1, Bl6, He7, Mu4, Me18], S.S. with Sr [Me18, Ra4, Jo13], S.S. with Sr and Th [Sc23] T = 937 °C: atomic positions demand R3 symmetry	in 3.3.4, Tab. 6
LaCoO <sub>3</sub>	R	5.436			α = 60° 48'	Wo9		6
PrCoO <sub>3</sub>	O	5.331	5.373	7.587		Ra3		
NdCoO <sub>3</sub>	O	5.336	5.336	7.547		Be33		
SmCoO <sub>3</sub>	O	5.289	5.354	7.541		Be33		6
GdCoO <sub>3</sub>	O	5.228	5.404	7.436		Be33		6
TbCoO <sub>3</sub>	O					Be33		6
BiCoO <sub>3</sub>	C	4.228				To11b	No cell dimension	
LaNiO <sub>3</sub>	R	5.461				Wo8	High pressure preparation [To11a]	6
BiNiO <sub>3</sub>	C	4.173			α = 60° 49'	To11b	P & S [Wo6], neutron diffraction [Ko1]	6
LaGaO <sub>3</sub>	O	5.496	5.524	7.787		Ge2	High pressure preparation [To11a]	6
CeGaO <sub>3</sub>	R	5.544				Ge2	P & S [Ke2, Da2, Be34, Br25, Da1, Ma25a]	
PrGaO <sub>3</sub>	C	3.87			α = 60° 25'	Ke2	T = 900 °C, rhombohedral T > 875 °C (by DTA)	
NdGaO <sub>3</sub>	O	5.465	5.495	7.729		Ge2	Distorted	
	O	5.426	5.502	7.706		Ge2	P & S [Be34, Br25, Ma25a]	
SmGaO <sub>3</sub>	O	5.369	5.520	7.650		Ma25a	P & S [Da1, Be34, Br25, Ke2, Ma25a], complete structure [Br26], S.S. with LaGaO <sub>3</sub> [Br25]	6
EuGaO <sub>3</sub>	O	5.351	5.528	7.628		Ma25a	High pressure preparation	
GdGaO <sub>3</sub>	O	5.322	5.537	7.606		Ma25a	High pressure preparation [Ma25]	
TbGaO <sub>3</sub>	O	5.307	5.531	7.578		Ma25a	High pressure preparation	

Compound	Sym	a Å	b Å	c Å	angle	Ref.	Remarks	Magnetic Data
----------	-----	--------	--------	--------	-------	------	---------	------------------



Compound	Sym	a Å	b Å	c Å	angle	Ref.	Remarks	Magnetic Data in 3.3.4, Tab.
A <sup>3+</sup> B <sup>3+</sup> O <sub>3</sub> (continued)								
DyGaO <sub>3</sub>	O	5.282	5.534	7.556		Ma25a	High pressure preparation	
HoGaO <sub>3</sub>	O	5.251	5.531	7.536		Ma25a	High pressure preparation	
ErGaO <sub>3</sub>	O	5.239	5.527	7.522		Ma25a	High pressure preparation	
TmGaO <sub>3</sub>	O	5.224	5.515	7.505		Ma25a	High pressure preparation [Ma25]	
YbGaO <sub>3</sub>	O	5.208	5.510	7.490		Ma25a	High pressure preparation [Ma25]	
LuGaO <sub>3</sub>	O	5.188	5.505	7.484		Ma25a	High pressure preparation [Ma25]	
YGaO <sub>3</sub>	O	5.257	5.536	7.533		Ma25	High pressure preparation [Ma26]	
LaYO <sub>3</sub>	O	5.868	6.071	8.438		Ge3	P & S [Pa2, Mo6], optical properties (Eu <sup>3+</sup> ) [Bl13]	
BiYO <sub>3</sub>	C	4.2				To11b	High pressure preparation [To11a]	
LaNbO <sub>3</sub>	C	4.02				Si5	Pseudocubic	
LaRhO <sub>3</sub>	O	5.524	5.679	7.900		Wo5	P & S [Ch11, Wo9, Kh1]	
PrRhO <sub>3</sub>	O	5.4143	5.7473	7.8026		Sh8a	P & S [Ch11]	
NdRhO <sub>3</sub>	O	5.3778	5.7551	7.7745		Sh8a	P & S [Wo5]	
SmRhO <sub>3</sub>	O	5.3211	5.7613	7.7083		Sh8a	P & S [Ch11]	
EuRhO <sub>3</sub>	O	5.2985	5.7607	7.6802		Sh8a		
GdRhO <sub>3</sub>	O	5.2774	5.7605	7.6584		Sh8a	P & S [Ch11]	
TbRhO <sub>3</sub>	O	5.2541	5.7492	7.6226		Sh8a		
DyRhO <sub>3</sub>	O	5.2449	5.7314	7.6002		Sh8a		
HoRhO <sub>3</sub>	O	5.2299	5.7257	7.5823		Sh8a	P & S [Ch11]	
ErRhO <sub>3</sub>	O	5.2160	5.7117	7.5610		Sh8a	P & S [Ch11]	
TmRhO <sub>3</sub>	O	5.2028	5.6974	7.5428		Sh8a		
LuRhO <sub>3</sub>	O	5.1861	5.6700	7.5125		Sh8a		
InRhO <sub>3</sub>	O	5.301	5.435	7.586		Sh9	P & S [Ge3, Pa2]	
LaInO <sub>3</sub>	O	5.723	5.914	8.207		Ro16		
NdInO <sub>3</sub>	O	5.627	5.891	8.121		Ro16		
SmInO <sub>3</sub>	O	5.589	5.886	8.082		Ro16	High pressure preparation	
EuInO <sub>3</sub>	O	5.567	5.835	8.078		Sh9	High pressure preparation	
GdInO <sub>3</sub>	O	5.548	5.842	8.071		Sh9	High pressure preparation	
DyInO <sub>3</sub>	O	5.519	5.751	8.041		Sh9	High pressure preparation	
YInO <sub>3</sub>	O	5.500	5.787	8.053		Sh9		
LaHoO <sub>3</sub>	O	5.888	6.092	8.480		Mo6	P & S [Sc13, Mo6]	6
LaErO <sub>3</sub>	O	5.85	6.07	8.43		Sc12	P & S [Sc13, Mo6]	6
LaTmO <sub>3</sub>	O	5.85	6.06	8.42		Sc12	P & S [Sc13, Mo6], complete structure determined, S.G. Pbn2 <sub>1</sub> , [Mu8], T <sub>melt</sub> = 2120 °C [Tr0]	6
LaYbO <sub>3</sub>	O	5.85	6.02	8.41		Sc12	T = 2080 °C	6
LaLuO <sub>3</sub>	C	4.325	6.02	8.37		Tr0		
PrLuO <sub>3</sub>	O	5.82	5.977	8.320		Sc12	P & S [Sc13, Mo6]	

Tab. 2b. A<sub>2</sub>B'BX<sub>6</sub> compounds

Compound	Sym	a Å	b Å	c Å	angle	Ref.	Remarks	Magnetic Data
A <sub>2</sub> B'B <sup>+</sup> X <sub>6</sub> ; X = F <sup>-1</sup> , Cl <sup>-1</sup>								
Cs <sub>2</sub> NaAlF <sub>6</sub>	H	6.168		29.76		Ba5a	Hex (12 L)	in 3.3.4, Tab.
Rb <sub>2</sub> NaAlF <sub>6</sub>	C	8.29				Ba5a	Hex (12L)	
Rb <sub>2</sub> LiAlF <sub>6</sub>	H	5.802		28.02		Ba5a	R perovskite	
K <sub>2</sub> LiAlF <sub>6</sub>	H	5.574		13.648		Wi11b	Hex (6L), Prep. T > 470 °C	
K <sub>2</sub> NaAlF <sub>6</sub>	C	5.614		13.754		Wi11b		
K <sub>2</sub> KAIF <sub>6</sub>	C	8.105				Me21		
Na <sub>2</sub> NaAlF <sub>6</sub>	C	8.65	5.61	7.80	β = 90° 11'	Si33		
(NH <sub>4</sub> ) <sub>2</sub> (NH <sub>4</sub> )AlF <sub>6</sub>	M	5.46				Na17	P & S [Si33, Me19, Cr5a], S.S. with Fe [Cr5a]	
Cs <sub>2</sub> CsScF <sub>6</sub>	C	8.90				Pa9	P & S [Pa10, Me20]	
Cs <sub>2</sub> KScF <sub>6</sub>	C	9.32				Ho16a	Prep. [Ba0]	
Rb <sub>2</sub> RbScF <sub>6</sub>	C	17.46				Bo2	Prep. [Ba0]	High temperature form
K <sub>2</sub> KScF <sub>6</sub>	C	5.60	5.81	8.12	β = 90° 45'	Th1	Prep. [Ba0]	
Na <sub>2</sub> NaScF <sub>6</sub>	M	6.49		9.45		Bo2	Prep. [Ba0]	
(NH <sub>4</sub> ) <sub>2</sub> (NH <sub>4</sub> )ScF <sub>6</sub>	T	9.26				Bo2	T < 680 °C	
K <sub>2</sub> KTiF <sub>6</sub>	T	8.56		8.75		Br7		
K <sub>2</sub> NaTiF <sub>6</sub>	C	8.367				Br7		
Na <sub>2</sub> NaTiF <sub>6</sub>	M	5.53	5.83	7.99	β ≅ 90°	Br7		
Cs <sub>2</sub> KVF <sub>6</sub>	C	9.04				Ba5a	Structure determined [Bu4a]	
Cs <sub>2</sub> NaVF <sub>6</sub>	H	6.267		30.40		Ba5a	P & S [Ba5]	
Rb <sub>2</sub> KVF <sub>6</sub>	C	8.88				Ba5a	Hex (12L)	
Rb <sub>2</sub> NaVF <sub>6</sub>	C	8.47				Ba5a		Magnetic properties, 80 < T < 300 °K, n <sub>eff</sub> = 2.79, Θ <sub>p</sub> = -14 °K [Fi4]
Rb <sub>2</sub> LiVF <sub>6</sub>	H	5.891		28.77		Ba5a	Hex (12L)	
K <sub>2</sub> KVF <sub>6</sub>	C					Ba5		
K <sub>2</sub> NaVF <sub>6</sub>	C	8.315				Pa6a		
(NH <sub>4</sub> ) <sub>2</sub> (NH <sub>4</sub> )VF <sub>6</sub>	C	9.04				Ba5a		
Cs <sub>2</sub> RbCrF <sub>6</sub>	C	9.15				Ba5a		
Cs <sub>2</sub> KCrF <sub>6</sub>	C	8.99				Ba5a		
Cs <sub>2</sub> NaCrF <sub>6</sub>	H	6.231		30.24		Ba5a	Hex (12L)	
Rb <sub>2</sub> KCrF <sub>6</sub>	C	8.81				Ba5a		
Rb <sub>2</sub> NaCrF <sub>6</sub>	C	8.42				Ba5a		
Rb <sub>2</sub> LiCrF <sub>6</sub>	H	5.865		28.61		Ba5a	Hex (12L)	High temperature form
K <sub>2</sub> KCrF <sub>6</sub>	T	8.56		8.62		Kl6	P & S [Pe2]	
K <sub>2</sub> KCrF <sub>6</sub>	C	8.54				Bo2		

Compound	Sym	a Å	b Å	c Å	angle	Ref.	Remarks	Magnetic Data
A <sub>2</sub> B <sup>+</sup> B <sup>3+</sup> X <sub>6</sub> ; X = F <sup>-1</sup> , Cl <sup>-1</sup> (continued)								
K <sub>2</sub> NaCrF <sub>6</sub>	C	8.266		7.878	β ≈ 90°	<i>Kn5</i>	Prop. [Sh28]	in 3.3.4, Tab.
Na <sub>2</sub> NaCrF <sub>6</sub>	M	5.468	5.679			<i>Vo1</i>		
(NH <sub>4</sub> ) <sub>2</sub> (NH <sub>4</sub> )CrF <sub>6</sub>	C	9.01				<i>Pa6a</i>		
K <sub>2</sub> KMnF <sub>6</sub>	T	17.50		16.60		<i>Pe2</i>	Magnetic properties, $p^* = 4.95 \mu_B$ [Pe2]	
K <sub>2</sub> NaMnF <sub>6</sub>	T	8.171		8.577		<i>Kn4</i>		
Cs <sub>2</sub> CsFeF <sub>6</sub>	C	10.46				<i>Mi2</i>		
Cs <sub>2</sub> KFeF <sub>6</sub>	C	9.05				<i>Ba5a</i>	P & S [Ho16a]	
Cs <sub>2</sub> NaFeF <sub>6</sub>	H	6.260		30.40		<i>Ba5a</i>	Hex (12L)	
Rb <sub>2</sub> RbFeF <sub>6</sub>	C	8.88				<i>Bo2</i>		
Rb <sub>2</sub> KFeF <sub>6</sub>	C	8.87				<i>Ba5a</i>		
Rb <sub>2</sub> NaFeF <sub>6</sub>	C	8.47				<i>Ba5a</i>		
Rb <sub>2</sub> LiFeF <sub>6</sub>	H	5.891		28.77		<i>Ba5a</i>	Hex (12L)	
K <sub>2</sub> KFeF <sub>6</sub>	C	8.58				<i>Bo2</i>		
K <sub>2</sub> NaFeF <sub>6</sub>	C	8.323				<i>Kn5</i>		
Na <sub>2</sub> NaFeF <sub>6</sub>	M	5.506	5.719	7.925	β = 90° 28'	<i>Cr5a</i>	P & S [Mi5], magnetic properties, 92 < T < 296 °K, $n_{\text{eff}} = 5.85$ , $\Theta_p = -2$ °K [Fi1]	
Li <sub>2</sub> LiFeF <sub>6</sub>	C	8.88				<i>Mi2</i>	Magnetic properties, 93 < T < 293 °K, $n_{\text{eff}} = 6.00$ , $\Theta_p = 0$ °K [Fi1]	
(NH <sub>4</sub> ) <sub>2</sub> (NH <sub>4</sub> )FeF <sub>6</sub>	T	6.39		9.30		<i>Si33</i>	Low temperature form	
	C	9.10				<i>Pa9</i>	P & S [Si33, Kl6]; magnetic properties, 92 < T < 294 °K, $n_{\text{eff}} = 5.86$ , $\Theta_p = -2$ °K [Fi1]	
Cs <sub>2</sub> CsCoF <sub>6</sub>	C	9.23				<i>Kl6</i>	Magnetic properties, 90 < T < 290 °K, $n_{\text{eff}} = 5.28$ , $\Theta_p = +2$ °K [Kl6]	
Rb <sub>2</sub> RbCoF <sub>6</sub>	C	8.90				<i>Kl6</i>	P & S [Ho13], magnetic properties, 90 < T < 290 °K, $n_{\text{eff}} = 5.48$ , $\Theta_p = -2$ °K [Kl6]	
K <sub>2</sub> KCoF <sub>6</sub>	C	8.57				<i>Kl6</i>	P & S [Me27, Ho13], magnetic properties, 73 < T < 300 °K, $n_{\text{eff}} = 5.53$ , $\Theta_p = -10$ °K [Co23, Kl6]	
K <sub>2</sub> NaCoF <sub>6</sub>	C	8.22				<i>Me27</i>	Pseudocubic, P & S [Ho13], magnetic properties, 90 < T < 290 °K, $n_{\text{eff}} = 5.39$ , $\Theta_p = -5$ °K [Kl6]	
Na <sub>2</sub> NaCoF <sub>6</sub>	C	7.91				<i>Kl6</i>		
K <sub>2</sub> KNiF <sub>6</sub>	C	8.44				<i>Bo2</i>	P & S [Kl6], magnetic properties, 90 < T < 295 °K, does not obey Curie-Weiss law [Kl2, Kl3, We20]	
K <sub>2</sub> KCuF <sub>6</sub>	C	8.50				<i>Kl6</i>	Magnetic properties, $n_{\text{eff}} = 2.8$ [Kl2]	
Cs <sub>2</sub> KGaF <sub>6</sub>	C	8.975				<i>Ho16a</i>		
K <sub>2</sub> NaGaF <sub>6</sub>	C	8.246				<i>Kn5</i>		
(NH <sub>4</sub> ) <sub>2</sub> (NH <sub>4</sub> )GaF <sub>6</sub>	C	9.041				<i>Sc26</i>		
Cs <sub>2</sub> KAgF <sub>6</sub>	C	9.175				<i>Ho16</i>		

Compound	Sym	a Å	b Å	c Å	angle	Ref.	Remarks	Magnetic Data in 3.3.4, Tab.
$A_2^+B^+B^+X_6^-$ ; X = F <sup>-1</sup> , Cl <sup>-1</sup> (continued)								
Cs <sub>2</sub> CsInF <sub>6</sub>	C	9.50				Bo2		
Cs <sub>2</sub> KInF <sub>6</sub>	C	9.219				Ho16a		
Rb <sub>2</sub> RbInF <sub>6</sub>	C	9.20				Bo2		
K <sub>2</sub> KInF <sub>6</sub>	C	17.71				Bo2		
(NH <sub>4</sub> ) <sub>2</sub> (NH <sub>4</sub> )MoO <sub>3</sub> F <sub>3</sub>	C	9.10				Pa9		
Cs <sub>2</sub> NaCeF <sub>6</sub>	C	9.26				Be52a		
Cs <sub>2</sub> KCeF <sub>6</sub>	C	9.61				Be52a		
Cs <sub>2</sub> RbCeF <sub>6</sub>	C	9.75				Be52a		
Cs <sub>2</sub> CsCeF <sub>6</sub>	C	9.84				Be52a		
Cs <sub>2</sub> KKCeF <sub>6</sub>	C	9.36				Be52a		
CsRbRbCeF <sub>6</sub>	C	9.60				Be52a		
Rb <sub>2</sub> KCeF <sub>6</sub>	C	9.40				Be52a		
Rb <sub>2</sub> RbCeF <sub>6</sub>	C	9.49				Be52a		
RbKKCeF <sub>6</sub>	C	9.20				Be52a		
K <sub>2</sub> KCeF <sub>6</sub>	C	9.07				Be52a		
Rb <sub>2</sub> RbPrF <sub>6</sub>	C	9.48				Bo2		
Cs <sub>2</sub> NaSmF <sub>6</sub>	C	9.163				Al4		
Rb <sub>2</sub> NaSmF <sub>6</sub>	C	8.988				Al4		
Cs <sub>2</sub> NaTbF <sub>6</sub>	C	9.107				Al4		
Rb <sub>2</sub> NaTbF <sub>6</sub>	C	9.9208				Al4		
Rb <sub>2</sub> NaHoF <sub>6</sub>	C	8.881				Al4		
Cs <sub>2</sub> NaErF <sub>6</sub>	C	9.061				Al4		
Rb <sub>2</sub> NaErF <sub>6</sub>	C	8.867				Al4		
Cs <sub>2</sub> NaYbF <sub>6</sub>	C	9.022				Al4		
Rb <sub>2</sub> NaYbF <sub>6</sub>	C	8.824				Al4		
Cs <sub>2</sub> NaYF <sub>6</sub>	C	9.056				Al4		
Rb <sub>2</sub> NaYF <sub>6</sub>	C	8.8693				Al4		
Cs <sub>2</sub> AgAuCl <sub>6</sub>	T	7.38				El3		
Cs <sub>2</sub> AgAuCl <sub>6</sub>	T	5.28				El3		
Cs <sub>2</sub> AgAuCl <sub>6</sub>	T	7.49				El3		
Cs <sub>2</sub> KTiF <sub>6</sub>	C	9.36				Ho16a		
K <sub>2</sub> KTiF <sub>6</sub>	C	11.86				Bo2		
$(A^{2+}A^{3+})(B^{3+}B^{4+})O_6$								
BaLaMnTiO <sub>6</sub>	C	3.960				Ha32		
SrLaMnTiO <sub>6</sub>	R	3.912				Ha32		
CaLaMnTiO <sub>6</sub>	R	3.872				Ha32		
CaYMnTiO <sub>6</sub>	O	5.32				Ha32		
PbLaMnTiO <sub>6</sub>	R	3.933				Ha32		
			5.53	7.54	$\alpha = 90^\circ 12'$ $\alpha = 90^\circ 6'$ $\alpha = 90^\circ 12'$		S.S. with Sr, rhombohedral > 30% Sr Cubic > 700 °C S.S. with La S.S. with x = Pb <sub>2</sub> NbMnO <sub>6</sub> ; cubic ≥ 50%	

Compound	Sym	a Å	b Å	c Å	angle	Ref.	Remarks	Magnetic Data
PbLaMnTiO <sub>6</sub>	R	3.933			$\alpha = 90^\circ 12'$	Ha32	S.S. with $x = \text{Pb}_2\text{NbMnO}_6$ ; cubic $\geq 50\%$	
(A <sup>2+</sup> A <sup>3+</sup> ) (B <sup>3+</sup> B <sup>4+</sup> )O <sub>6</sub> (continued)								in 3.3.4, Tab.
SrLaFeTiO <sub>6</sub>	C	3.92				Bl8		
SrLaMnIrO <sub>6</sub>	C	3.93				Bl8		
SrLaFeIrO <sub>6</sub>	C	3.94				Bl8		
A <sub>2</sub> <sup>+</sup> BB'O <sub>6</sub>								
La <sub>2</sub> MgTiO <sub>6</sub>	C	3.96				Ag1	P & S [Ro20], Eu <sup>3+</sup> fluorescence [Bl14], S.S. with: Ni and optical properties [Re4a]	
Nd <sub>2</sub> MgTiO <sub>6</sub>	C	3.90				Ro20	Slight distortion	
LaCeMgTiO <sub>6</sub>	C	3.929				Ro20	Slight distortion	
Bi <sub>2</sub> MgTiO <sub>6</sub>	C	3.98				Su5	Some question on atom positions	
Y <sub>2</sub> Ni <sub>0.4</sub> Mg <sub>0.6</sub> TiO <sub>6</sub>	C	3.83				Re4a	Optical properties	
La <sub>2</sub> MgMnO <sub>6</sub>						Bl7		
La <sub>2</sub> CoMnO <sub>6</sub>						Bl7	See LaMnO <sub>3</sub> systems for magnetic properties	
La <sub>2</sub> NiMnO <sub>6</sub>						Bl7	See LaMnO <sub>3</sub> systems for magnetic properties, P & S [Fu2]	
La <sub>2</sub> CuMnO <sub>6</sub>						Bl7	See LaMnO <sub>3</sub> systems for magnetic properties	
La <sub>2</sub> MgGeO <sub>6</sub>	C	3.90				Ro20		
Y <sub>2</sub> MgGeO <sub>6</sub>	C	3.88				Re4a		
La <sub>2</sub> MgZrO <sub>6</sub>	C	4.06				Ra1	S.S. with Ni and optical properties [Re4a]	
La <sub>2</sub> CaZrO <sub>6</sub>	C	4.174				Ra1		
La <sub>2</sub> LiNbO <sub>6</sub>	O	5.59	5.76	7.92		Bl1a		
La <sub>2</sub> MgRuO <sub>6</sub>	C	7.91				Ga5	Eu <sup>3+</sup> fluorescence [Bl14]	
La <sub>2</sub> MnRuO <sub>6</sub>	C	7.84				Ga5	Semiconducting, $\Delta E = 0.046$ eV	
La <sub>2</sub> NiRuO <sub>6</sub>	C	7.90				Ga5	Semiconducting, $\Delta E = 0.12$ eV	
La <sub>2</sub> ZnRuO <sub>6</sub>	C	7.97				Ga5	Optical properties	
La <sub>2</sub> Ni <sub>0.4</sub> Mg <sub>0.6</sub> SnO <sub>6</sub>	C	4.02				Re4a		
La <sub>2</sub> MgReO <sub>6</sub>	C	7.926				Ba25a		
La <sub>2</sub> NiReO <sub>6</sub>	C	7.908				Ba25a		
La <sub>2</sub> CoReO <sub>6</sub>	T	5.611		7.968		Ba25a	Disproportionates [Ba25a] "Complex magnetic properties" [Bl7], P & S [Bl8]	
La <sub>2</sub> FeReO <sub>6</sub>	C	7.92				Ga5		
La <sub>2</sub> MgIrO <sub>6</sub>	C	7.86				Ga5	"Complex magnetic properties" [Bl7]	
La <sub>2</sub> MnIrO <sub>6</sub>	O	5.60	5.60	7.92		Bl8	"Complex magnetic properties" [Bl7], P & S [Bl8]	
La <sub>2</sub> CoIrO <sub>6</sub>	C	7.90				Ga5	"Complex magnetic properties" [Bl7], P & S [Bl8]	
La <sub>2</sub> NiIrO <sub>6</sub>	C	5.80	5.60	7.72	$\gamma = 86^\circ 56'$	Bl8	"Complex magnetic properties" [Bl7]	
La <sub>2</sub> CuIrO <sub>6</sub>	M							
A <sub>2</sub> <sup>+</sup> BV <sup>5+</sup> O <sub>6</sub>								
Ba <sub>2</sub> BiVO <sub>6</sub>	O	6.123	6.180	8.622		Ve2	P & S [Vi3, Ve3], dielectric properties [Vi2b]	
	C	4.372				Ve2	Cubic $> 320^\circ\text{C}$	

Compound	Sym	a Å	b Å	c Å	angle	Ref.	Remarks	Magnetic Data
A <sub>2</sub> <sup>+</sup> BNb <sup>5+</sup> O <sub>6</sub>								in 3.3.4, Tab.
Ba <sub>2</sub> ScNbO <sub>6</sub>	C	8.220				Fi10	P & S [Ag1, Br16]	
Ba <sub>2</sub> YNbO <sub>6</sub>	C	4.051				Ch10		
Ba <sub>2</sub> MnNbO <sub>6</sub>	C	4.090				Ha32	P & S [Ag1]	6
Ba <sub>2</sub> FeNbO <sub>6</sub>	C	4.057				Gal	P & S [Ga13, Fi10, Ag1]	
Ba <sub>2</sub> CoNbO <sub>6</sub>	C	4.06				Bl8		
Ba <sub>2</sub> NiNbO <sub>6</sub>	C	4.1				Bl8		
Ba <sub>2</sub> SrNbO <sub>6</sub> <sup>5.5</sup>	C	8.54				Gal	P & S [Fi10]	
Ba <sub>2</sub> YNbO <sub>6</sub>	C	4.180				Br16		
Ba <sub>2</sub> RhNbO <sub>6</sub>	C	8.17				Bl8		
Ba <sub>2</sub> InNbO <sub>6</sub>	C	8.279				Br16	P & S [Ga1]	
Ba <sub>2</sub> BaNbO <sub>6</sub>	C	8.68				Gal		
Ba <sub>2</sub> LaNbO <sub>6</sub> <sup>5.5</sup>	C	8.607				Gal	P & S [Br16], cubic T > 300 °C [Fi10]	
Ba <sub>2</sub> CeNbO <sub>6</sub>	T	4.293		8.690		Br16	Probably ordered	
Ba <sub>2</sub> PrNbO <sub>6</sub>	C	4.285				Br16	Probably ordered, cubic T > 300 °C [Fi10]	
Ba <sub>2</sub> NdNbO <sub>6</sub>	C	8.540				Gal	P & S [Br16], cubic T > 300 °C [Fi10]	
Ba <sub>2</sub> SmNbO <sub>6</sub>	C	8.518				Gal	P & S [Br16], cubic T > 300 °C [Fi10]	
Ba <sub>2</sub> EuNbO <sub>6</sub>	C	8.507				Gal	P & S [Br16]	
Ba <sub>2</sub> GdNbO <sub>6</sub>	C	8.496				Gal	P & S [Br16], fluorescences [Bl11, Ni1, Bl14]	6
Ba <sub>2</sub> TbNbO <sub>6</sub>	C	4.229				Br16	Probably ordered	
Ba <sub>2</sub> DyNbO <sub>6</sub>	C	8.437				Gal	P & S [Br16]	
Ba <sub>2</sub> HoNbO <sub>6</sub>	C	8.434				Gal	P & S [Br16]	
Ba <sub>2</sub> ErNbO <sub>6</sub>	C	8.427				Gal	P & S [Br16]	
Ba <sub>2</sub> TmNbO <sub>6</sub>	C	8.408				Gal	P & S [Br16], dielectric properties [Ag1]	
Ba <sub>2</sub> YbNbO <sub>6</sub>	C	8.374				Gal	P & S [Br16]	
Ba <sub>2</sub> LuNbO <sub>6</sub>	C	8.364				Gal		
Ba <sub>2</sub> TiNbO <sub>6</sub>	C	8.42				Sl6		
Ba <sub>2</sub> AlNbO <sub>6</sub>	R	6.086			α = 60° 21'	Ve2	P & S [Vi3, Ve3], dielectric properties [Vi2b]	
Sr <sub>2</sub> AlNbO <sub>6</sub>	C	7.784				Fi10	P & S [Sl1]	
Sr <sub>2</sub> CaNbO <sub>6</sub> <sup>5.5</sup>	C	8.20				Gal3		
Sr <sub>2</sub> YNbO <sub>6</sub>	C	3.965				Ch10		
Sr <sub>2</sub> CrNbO <sub>6</sub>	C	7.87				Bl8	P & S [Br14]	
Sr <sub>2</sub> MnNbO <sub>6</sub>	C	3.97			α ≈ 90°	Ha32	P & S [Ku12], cubic T > 200 °C [Ku12]	6
Sr <sub>2</sub> FeNbO <sub>6</sub>	T	3.960				Ku6	P & S [Ga13, Ku12]	
	C	3.968		3.980		Ku6	T = 250 °C, cubic T ≥ 250 °C	
Sr <sub>2</sub> CoNbO <sub>6</sub>	C	3.93				Bl8		
Sr <sub>2</sub> GaNbO <sub>6</sub>	C	3.9477				Br14		
Sr <sub>2</sub> SrNbO <sub>6</sub> <sup>5.5</sup>	C	8.34				Gal3		
Sr <sub>2</sub> YNbO <sub>6</sub>	R	5.184			α = 59° 51'	Ku12	Cubic T > 630 °C	
Sr <sub>2</sub> InNbO <sub>6</sub>	C	8.106				Fi10	P & S [Br14]	

Compound	Sym	a Å	b Å	c Å	angle	Ref.	Remarks	Magnetic Data
A <sub>2</sub> <sup>2+</sup> BNb <sup>5+</sup> O <sub>6</sub> (continued)								
Sr <sub>2</sub> PrNbO <sub>6</sub>	T	5.822		8.431		Ku12		in 3.3.4, Tab.
Sr <sub>2</sub> NdNbO <sub>6</sub>	T	5.780		8.367		Ku12		
Sr <sub>2</sub> SmNbO <sub>6</sub>	M	5.85	5.94	8.30	β = 90° 12'	Fi10	P & S [Ku12]	
Sr <sub>2</sub> EuNbO <sub>6</sub>	M	5.84	5.91	8.30	β = 90° 15'	Fi10		
Sr <sub>2</sub> GdNbO <sub>6</sub>	M	5.83	5.90	8.28	β = 90° 8'	Fi10		
Sr <sub>2</sub> TbNbO <sub>6</sub>	M	5.82	5.88	8.27	β = 90° 9'	Fi10		
Sr <sub>2</sub> DyNbO <sub>6</sub>	M	5.81	5.87	8.26	β = 90° 6'	Fi10		
Sr <sub>2</sub> HoNbO <sub>6</sub>	M	5.81	5.86	8.23	β = 90° 4'	Fi10		
Sr <sub>2</sub> ErNbO <sub>6</sub>	M	5.80	5.84	8.23		Fi10	Slight distortion Cubic T > 540 °C Cubic T > 540 °C	
Sr <sub>2</sub> TmNbO <sub>6</sub>	C	8.20				Fi10		
Sr <sub>2</sub> YbNbO <sub>6</sub>	C	8.196				Ku12		
Sr <sub>2</sub> LuNbO <sub>6</sub>	C	8.19				Ku12		6
SrLaCoNbO <sub>6</sub>	C	7.99				Bi8		6
SrLaNiNbO <sub>6</sub>	C	7.95				Bi8		
SrLaCuNbO <sub>6</sub>	T	7.80		8.28		Bi8	Ordered perovskite (Eu <sup>3+</sup> fluorescence) [Bi14]	
La <sub>2</sub> LiNbO <sub>6</sub>						Fi8		
Ca <sub>2</sub> AlNbO <sub>6</sub>	O	5.382	5.408	7.614		Ch9		
Ca <sub>2</sub> VNbO <sub>6</sub>	O	5.44	5.51	7.77		Fi8		
Ca <sub>2</sub> CrNbO <sub>6</sub>	O	5.418	5.494	3.858		Ch9		
Ca <sub>2</sub> MnNbO <sub>6</sub>	O	5.44	5.55	7.74		Ha32		
Ca <sub>2</sub> FeNbO <sub>6</sub>	O	5.451	5.551	3.881		Fi8		
Ca <sub>2</sub> YNbO <sub>6</sub>	O	5.580	5.819	8.046		Fi8		
Ca <sub>2</sub> InNbO <sub>6</sub>	O	5.532	5.715	7.913		Fi8		
Ca <sub>2</sub> LaNbO <sub>6</sub>	O	5.652	5.866	8.140		Fi8	Possibly lower symmetry	
Ca <sub>2</sub> PrNbO <sub>6</sub>	O	5.623	5.866	8.116		Fi8	Possibly lower symmetry	
Ca <sub>2</sub> NdNbO <sub>6</sub>	O	5.612	5.858	8.104		Fi8		
Ca <sub>2</sub> SmNbO <sub>6</sub>	M	5.590	5.860	8.090		Fi8		
Ca <sub>2</sub> GdNbO <sub>6</sub>	M	5.572	5.841	8.080		Fi8		
Ca <sub>2</sub> TbNbO <sub>6</sub>	O	5.571	5.830	8.072	β = 90° 10'	Fi8		
Ca <sub>2</sub> DyNbO <sub>6</sub>	O	5.580	5.819	8.062	β = 90° 12'	Fi8		
Ca <sub>2</sub> HoNbO <sub>6</sub>	O	5.580	5.812	8.050		Fi8		
Ca <sub>2</sub> ErNbO <sub>6</sub>	O	5.575	5.794	8.020		Fi8		
Ca <sub>2</sub> YbNbO <sub>6</sub>	O	5.571	5.769	8.000		Fi8		
Pb <sub>2</sub> AlNbO <sub>6</sub>	C	10.53				Fi11	Defect pyrochlore type P & S [Ag1, Ve4]	
Pb <sub>2</sub> ScNbO <sub>6</sub>	T	4.074		4.083		Is2	Dielectric properties [Jo3, Sm18, Te8e], S.S. with Pb(Ti, Zr, Hf)O <sub>3</sub> [Jo3], crystal growth [Ga5]	
Pb <sub>2</sub> Sc <sub>0.8</sub> Cr <sub>0.2</sub> NbO <sub>6</sub>	C	4.060				To1	Possible rhombohedral distortion	
Pb <sub>2</sub> CrNbO <sub>6</sub>	C	10.54				Fi11	Defect pyrochlore type	
Pb <sub>2</sub> MnNbO <sub>6</sub>	C	4.023				Fi11	P & S [Ha32], S.S. with Fe and PbTiO <sub>3</sub> [Ha31]	6

Compound	Sym	a Å	b Å	c Å	angle	Ref.	Remarks	Magnetic Data
A <sub>2</sub> <sup>+</sup> BNb <sup>5+</sup> O <sub>6</sub> (continued)								in 3.3.4, Tab. 6
Pb <sub>2</sub> FeNbO <sub>6</sub>	R	4.014			α = 89° 55'	Ku10	P & S [Ro8], S.S. with BiFeO <sub>3</sub> [Sm12, Is8, Yu2], complete structure [Pi3], crystal growth [Ga5], dielectric properties [Kh8, Sm25, Sm16, Bo8, Sh32, Sk1, Sh33], optical spectra [Pi5], B site ordering [Yu9], S.S. with Ta [Sh33]	6
Pb <sub>2</sub> CoNbO <sub>6</sub>	C	8.084				Ro8	Dielectric properties [Ku10, Ag1, Ve4]	6
Pb <sub>2</sub> NiNbO <sub>6</sub>	C	4.030				Ku10	Dielectric properties [Ku10] with 5% Ba [Sh32]	6
Pb <sub>2</sub> GaNbO <sub>6</sub>	C					Fi11	High pressure preparation, no dimension [To11a]	
Pb <sub>2</sub> YNbO <sub>6</sub>	C	10.65				Ku9	Pyrochlore type	
Pb <sub>2</sub> InNbO <sub>6</sub>	C	4.110				Ku9	Dielectric properties [Ku10]	
Pb <sub>2</sub> HoNbO <sub>6</sub>	O	5.86	5.91	8.21		Ku10	Dielectric properties [Ku10]	
Pb <sub>2</sub> TmNbO <sub>6</sub>	O	5.858	5.936	8.178		Fi11	Cubic T > 280 °C, dielectric properties [Sm25, Ku9, Ku10, Ag1, Is17], S.S. with PbFe <sub>2/3</sub> W <sub>1/3</sub> O <sub>3</sub> [To5, To11, Ro17]	
Pb <sub>2</sub> YbNbO <sub>6</sub>	O	5.848	5.918	8.186		Ku9	Cubic T > 280 °C, dielectric properties [Ku9, Ku10, Is17]	
Pb <sub>2</sub> LuNbO <sub>6</sub>	O	5.850	5.902	8.176		Vi3	Defect pyrochlore type	
Pb <sub>2</sub> BiNbO <sub>6</sub>	M	10.777	10.643	10.777	β = 90° 29'	Vi5	Dielectric properties [Ve4, Vi5]	6
Pb <sub>2</sub> Mg <sub>0.5</sub> Mn <sub>0.5</sub> NbO <sub>6</sub>	C	4.018				Vi5	Dielectric properties [Ve4, Vi5]	6
Pb <sub>2</sub> Co <sub>0.5</sub> Mn <sub>0.5</sub> NbO <sub>6</sub>	C	4.020				Vi5	Dielectric properties [Ve4, Vi5]	6
Pb <sub>2</sub> Ni <sub>0.5</sub> Mn <sub>0.5</sub> NbO <sub>6</sub>	C	4.018				Vi5	Dielectric properties [Ve4, Vi5]	6
Pb <sub>2</sub> Zn <sub>0.5</sub> Mn <sub>0.5</sub> NbO <sub>6</sub>	C	4.028				Ro8	Dielectric properties [Ve4, Vi5]	6
Pb <sub>2</sub> Cd <sub>0.5</sub> Mn <sub>0.5</sub> NbO <sub>6</sub>	C	4.060						
A <sub>2</sub> <sup>+</sup> BSb <sup>5+</sup> O <sub>6</sub>								
Ba <sub>2</sub> ScSbO <sub>6</sub>	C	8.197				Si6	Not perovskite [Bl8]	6
Ba <sub>2</sub> CrSbO <sub>6</sub>						Bl8	Not perovskite [Bl8]	
Ba <sub>2</sub> MnSbO <sub>6</sub>	H	5.79		14.22		Bl8	Hex (6L), P & S [Si6, Bl3]	
Ba <sub>2</sub> FeSbO <sub>6</sub>	H	5.72		14.00		Bl8	Hex (6L)	
Ba <sub>2</sub> CoSbO <sub>6</sub>						Bl8	Not perovskite [Bl8]	
Ba <sub>2</sub> NiSbO <sub>6</sub>	H	5.78		14.20		Si6	Hex (6L)	
Ba <sub>2</sub> RhSbO <sub>6</sub>	C	8.269				Bl8	P & S [Bl3, Bl8]	
Ba <sub>2</sub> InSbO <sub>6</sub>	C	8.44				Bl8	P & S [Si6, Bl3]	6
Ba <sub>2</sub> GdSbO <sub>6</sub>	C	7.87				Bl8	P & S [Si6, Bl3]	6
Sr <sub>2</sub> CrSbO <sub>6</sub>	C	7.86		8.08		Bl8	P & S [Si6, Bl3]	6
Sr <sub>2</sub> MnSbO <sub>6</sub>	T	7.86				Bl8	Not single phase (no dimensions)	6
Sr <sub>2</sub> FeSbO <sub>6</sub>	C	7.90				Bl8		
Sr <sub>2</sub> CoSbO <sub>6</sub>	C	7.88				Bl8		
Sr <sub>2</sub> NiSbO <sub>6</sub>	T							



Compound	Sym	a Å	b Å	c Å	angle	Ref.	Remarks	Magnetic Data
A <sub>2</sub> <sup>3+</sup> BSb <sup>5+</sup> O <sub>6</sub> (continued)								
Sr <sub>2</sub> GaSbO <sub>6</sub>	T	7.84		7.91		Sl6		
Sr <sub>2</sub> RhSbO <sub>6</sub>	O	5.55	5.77	7.99		Bl8		6
Ca <sub>2</sub> FeSbO <sub>6</sub>	O	5.47	5.54	7.74		Bl8	Eu <sup>3+</sup> fluorescence, no dimensions	
SrLaMgSbO <sub>6</sub>	C	7.99				Bl14		
SrLaCoSbO <sub>6</sub>	C	7.93				Bl8		6
SrLaNiSbO <sub>6</sub>	C	7.80				Bl8		6
SrLaCuSbO <sub>6</sub>	T			8.35		Bl8		
A <sub>2</sub> <sup>3+</sup> BTa <sup>5+</sup> O <sub>6</sub>								
Ba <sub>2</sub> AlTaO <sub>6</sub>	C	8.220				Fi10	No compound [Ag1, Sm8] Dielectric properties [Ag1, Br13, Br14], P & S [Ga15]	
Ba <sub>2</sub> ScTaO <sub>6</sub>	C	8.104				Sl1	P & S [Ch10]	
Ba <sub>2</sub> VTaO <sub>6</sub>	H	4.076				Sl1	Hex (6L), no dimensions	
Ba <sub>2</sub> CrTaO <sub>6</sub>	C	4.048				Fi5	P & S [Sl1]	
Ba <sub>2</sub> MnTaO <sub>6</sub>	C					Fi5	P & S [Ca13], dielectric properties [Ag1], S.S. with BaTiO <sub>3</sub> [Na9]	
Ba <sub>2</sub> FeTaO <sub>6</sub>	C	8.152				Sl1		
Ba <sub>2</sub> NiTaO <sub>6</sub>	C	8.424				Fi10	P & S [Ag1, Br13, Br14, Fi5, La9], doped with Nd, Sm, Yb [Ga15]	
Ba <sub>2</sub> YTaO <sub>6</sub>	C	8.282				Fi10	P & S [Ag1, Ga15] doped with Nd, Sm, Yb [Ga15]	
Ba <sub>2</sub> InTaO <sub>6</sub>	C	8.70				Ga13	P & S [Br13]	
Ba <sub>2</sub> BaTaO <sub>6</sub> .s	R	6.07			α = 60° 25'	Ga15	P & S [Br13], doped with Nd [Ga15], cubic > 300 °C [Fi5]	
Ba <sub>2</sub> LaTaO <sub>6</sub>	R				α = 60° 10'	Fi10	P & S [Br13, Fi5] cubic T > 300 °C [Fi5]	
Ba <sub>2</sub> PrTaO <sub>6</sub>	R	6.05			α = 60° 4'	Fi10	P & S [Br13, Fi5] cubic T > 300 °C [Fi5]	
Ba <sub>2</sub> NdTaO <sub>6</sub>	R	6.04			α = 60° 4'	Fi10	P & S [Br13, Fi5] cubic T > 300 °C [Fi5]	
Ba <sub>2</sub> SmTaO <sub>6</sub>	R	6.01			α = 60° 4'	Fi10	P & S [Br13, Fi5] cubic T > 300 °C [Fi5]	
Ba <sub>2</sub> EuTaO <sub>6</sub>	C	8.486				Fi10	P & S [Ga15]	
Ba <sub>2</sub> GdTaO <sub>6</sub>	C	8.470				Fi10	Doped with Nd [Ga15]	
Ba <sub>2</sub> TbTaO <sub>6</sub>	C	8.440				Fi10		
Ba <sub>2</sub> DyTaO <sub>6</sub>	C	8.420				Fi10	P & S [Ca15]	
Ba <sub>2</sub> HoTaO <sub>6</sub>	C	8.416				Fi10	P & S [Ga15]	
Ba <sub>2</sub> ErTaO <sub>6</sub>	C	8.398				Fi10	P & S [Ca15]	
Ba <sub>2</sub> TmTaO <sub>6</sub>	C	8.388				Fi10	P & S [Ca15], dielectric properties [Ag1]	
Ba <sub>2</sub> YbTaO <sub>6</sub>	C	8.378				Fi10	P & S [Ga15], doped with Nd [Ga15]	
Ba <sub>2</sub> LuTaO <sub>6</sub>	C	8.354				Fi10		
Ba <sub>2</sub> TiTaO <sub>6</sub>	C	8.42			α = 60° 15'	Sl1	Dielectric properties [Vi3, Ve3]	
Ba <sub>2</sub> BiTaO <sub>6</sub>	R	6.047				Ve2	P & S [Sl1], B-B' ordering [Sl1]	
Sr <sub>2</sub> AlTaO <sub>6</sub>	C	7.786				Fi10		

Compound	Sym	a Å	b Å	c Å	angle	Ref.	Remarks	Magnetic Data
A <sub>2</sub> <sup>2+</sup> BTa <sup>5+</sup> O <sub>6</sub> (continued)								
Sr <sub>2</sub> VTaO <sub>6</sub>	C	3.967				Ch10	P & S [Ro20], S.S. with Fe [Na7]	in 3.3.4, Tab.  6
Sr <sub>2</sub> CrTaO <sub>6</sub>	C	3.94				Na7		
Sr <sub>2</sub> MnTaO <sub>6</sub>	C	3.994				Ku12	P & S [Ku12, Sl1, Na5, Na6, Na7], B-B' ordering [Sl1, Be5], S.S. with SrTiO <sub>3</sub> and Ba <sub>2</sub> FeTaO <sub>6</sub> [Na5, Be5], S.S. with BaTiO <sub>3</sub> [Na6]	
Sr <sub>2</sub> FeTaO <sub>6</sub>	T	3.960		3.981		Ku7	Cubic at 250 °C [Ku7, Na5, Na6]	
Sr <sub>2</sub> CaTaO <sub>6</sub>	C	3.973				Ku7		
Sr <sub>2</sub> SrTaO <sub>6</sub>	C	7.892				Sl1	P & S [Br13]	
Sr <sub>2</sub> YTaO <sub>6</sub>	C	8.34				Ga13		Possibly lower symmetry Possibly lower symmetry
Sr <sub>2</sub> RhTaO <sub>6</sub>	R	5.837			α = 59° 46'	Ku12		
Sr <sub>2</sub> InTaO <sub>6</sub>	C	7.936				Sl1		
Sr <sub>2</sub> LaTaO <sub>6</sub>	C	8.110				Ku12		
Sr <sub>2</sub> PrTaO <sub>6</sub>	T	5.853				Sl1		
Sr <sub>2</sub> PrTaO <sub>6</sub>	M	5.87				Ku12	P & S [Sl1]	
Sr <sub>2</sub> NdTaO <sub>6</sub>	M	5.86				Ku12	P & S [Br13]	
Sr <sub>2</sub> SmTaO <sub>6</sub>	M	5.85				Fi10	P & S [Ku12]	
Sr <sub>2</sub> EuTaO <sub>6</sub>	M	5.84				Fi10	P & S [Ku12]	
Sr <sub>2</sub> GdTaO <sub>6</sub>	M	5.83				Fi10	P & S [Ku12]	
Sr <sub>2</sub> TbTaO <sub>6</sub>	M	5.82				Fi10	P & S [Ku12]	
Sr <sub>2</sub> DyTaO <sub>6</sub>	M	5.82				Fi10		
Sr <sub>2</sub> HoTaO <sub>6</sub>	M	5.81				Fi10		
Sr <sub>2</sub> ErTaO <sub>6</sub>	M	5.80				Fi10	Slight distortion	
Sr <sub>2</sub> TmTaO <sub>6</sub>	C	8.20				Fi10	Slight distortion	6 6
Sr <sub>2</sub> YbTaO <sub>6</sub>	C	8.196				Ku12		
Sr <sub>2</sub> LuTaO <sub>6</sub>	C	8.18				Fi10		
Sr <sub>2</sub> LaCoTaO <sub>6</sub>	C	7.99				Bl8		
Sr <sub>2</sub> LaNiTaO <sub>6</sub>	C	7.95				Bl8		
Sr <sub>2</sub> LaCuTaO <sub>6</sub>	C	7.80				Fi8		
Ca <sub>2</sub> AlTaO <sub>6</sub>	T	5.381				Ch9		
Ca <sub>2</sub> VTaO <sub>6</sub>	O	5.45				Fi8		
Ca <sub>2</sub> CrTaO <sub>6</sub>	O	5.418				Fi8		
Ca <sub>2</sub> MnTaO <sub>6</sub>	O	5.462				Fi8		
Ca <sub>2</sub> FeTaO <sub>6</sub>	O	5.451				Fi8		
Ca <sub>2</sub> YTaO <sub>6</sub>	O	5.580				Fi8		
Ca <sub>2</sub> InTaO <sub>6</sub>	O	5.531				Fi8		
Ca <sub>2</sub> LaTaO <sub>6</sub>	O	5.654				Fi8		
Ca <sub>2</sub> PrTaO <sub>6</sub>	O	5.629				Fi8		
Ca <sub>2</sub> NdTaO <sub>6</sub>	O	5.616				Fi8		
Ca <sub>2</sub> SmTaO <sub>6</sub>	O	5.606				Fi8		

Compound	Sym	a Å	b Å	c Å	angle	Ref.	Remarks	Magnetic Data
A <sub>2</sub> <sup>2+</sup> BTa <sub>5</sub> O <sub>6</sub> (continued)								
Ca <sub>2</sub> GdTlTaO <sub>6</sub>	M	5.572	5.841	8.080	β = 90° 12'	Fi8	Defect pyrochlore type, P & S [Ag1]	in 3.3.4, Tab.
Ca <sub>2</sub> TbTaO <sub>6</sub>	M	5.574	5.833	8.076	β = 90° 12'	Fi8	P & S [Is2, Ag1], crystal growth [Ga5], dielectric properties [Sm18]	
Ca <sub>2</sub> DyTaO <sub>6</sub>	O	5.582	5.820	8.064		Fi8	Defect pyrochlore type, 5% Sr for Pb gives perovskite [Sh32]	
Ca <sub>2</sub> HoTaO <sub>6</sub>	O	5.586	5.811	8.054		Fi8	P & S [Ag1], crystal growth [Ga5], Prop. [Sh32]	
Ca <sub>2</sub> ErTaO <sub>6</sub>	O	5.582	5.796	8.033		Fi8	Dielectric properties [Ku11, Sh32]	
Ca <sub>2</sub> YbTaO <sub>6</sub>	O	5.570	5.772	8.002		Fi8	Defect pyrochlore type	
Pb <sub>2</sub> AlTaO <sub>6</sub>	C	10.51				Fi11	Defect pyrochlore type	
Pb <sub>2</sub> ScTaO <sub>6</sub>	C	4.080				Ga5	Defect pyrochlore type	
Pb <sub>2</sub> MnTaO <sub>6</sub>	C	10.73				Fi11	perovskite [Sh32]	
Pb <sub>2</sub> FeTaO <sub>6</sub>	C	4.011				Ga5	P & S [Ag1], crystal growth [Ga5], Prop. [Sh32]	
Pb <sub>2</sub> CoTaO <sub>6.5</sub>	C	4.038				Ku11	Dielectric properties [Ku11, Sh32]	6
Pb <sub>2</sub> YTaO <sub>6</sub>	C	10.70				Fi11	Defect pyrochlore type	6
Pb <sub>2</sub> PbTaO <sub>6</sub>	C	10.75				Fi11	Defect pyrochlore type	6
Pb <sub>2</sub> NdTaO <sub>6</sub>	C	10.68				Fi11	Defect pyrochlore type	
Pb <sub>2</sub> SmTaO <sub>6</sub>	C	10.70				Fi11	Defect pyrochlore type	
Pb <sub>2</sub> YbTaO <sub>6</sub>	O	5.85	5.90	8.22		Ku9	Dielectric properties [Ag1, Is17, Fi11]	
Pb <sub>2</sub> LuTaO <sub>6</sub>	O	5.848	5.899	8.214		Ku9	Cubic T > 280 °C; dielectric properties [Is17]	
Pb <sub>2</sub> BiTaO <sub>6</sub>	T	10.686		10.816		Vi3	Distorted defect pyrochlore type	
Pb <sub>2</sub> Mg <sub>0.5</sub> Mn <sub>0.5</sub> TaO <sub>6</sub>	C	4.015				Vi5	Dielectric properties [Vi5, Ve4]	6
Pb <sub>2</sub> Ni <sub>0.5</sub> Mn <sub>0.5</sub> TaO <sub>6</sub>	C	4.009				Vi5	Dielectric properties [Vi5, Ve4]	6
A <sub>2</sub> <sup>2+</sup> BB'O <sub>6</sub> : B' = Bi <sup>3+</sup> , Pb <sup>2+</sup> , Pu <sup>3+</sup>								
Ba <sub>2</sub> LaBiO <sub>6</sub>	C	8.759				Sc18b	No dimensions, Bi <sup>3+</sup> -Bi <sup>3+</sup>	
Ba <sub>2</sub> BiBiO <sub>6</sub>	C					Sc18b		
Ba <sub>2</sub> ScPaO <sub>6</sub>	C	8.549				Ke5		
Ba <sub>2</sub> SrPaO <sub>6.5</sub>	C	8.860				Ke5		
Ba <sub>2</sub> YPaO <sub>6</sub>	C	8.718				Ke5		
Ba <sub>2</sub> InPaO <sub>6</sub>	C	8.596				Ke5		
Ba <sub>2</sub> BaPaO <sub>6.5</sub>	C	8.932				Ke5		
Ba <sub>2</sub> LaPaO <sub>6</sub>	C	8.885				Ke5		
Ba <sub>2</sub> CePaO <sub>6</sub>	C	8.800				Ke5		
Ba <sub>2</sub> PrPaO <sub>6</sub>	C	8.862				Ke5		
Ba <sub>2</sub> NdPaO <sub>6</sub>	C	8.840				Ke5		
Ba <sub>2</sub> SmPaO <sub>6</sub>	C	8.792				Ke5		
Ba <sub>2</sub> EuPaO <sub>6</sub>	C	8.783				Ke5		
Ba <sub>2</sub> GdPaO <sub>6</sub>	C	8.770				Ke5		
Ba <sub>2</sub> TdPaO <sub>6</sub>	C	8.753				Ke5		

Compound	Sym	a Å	b Å	c Å	angle	Ref.	Remarks	Magnetic Data in 3.3.4, Tab.
$A_2^+BB'O_6$ ; $B' = Bi^{3+}, Pa^{5+}, Pu^{5+}$ (continued)								
Ba <sub>2</sub> DyPaO <sub>6</sub>	C	8.740				Ke5		
Ba <sub>2</sub> HoPaO <sub>6</sub>	C	8.730				Ke5		
Ba <sub>2</sub> ErPaO <sub>6</sub>	C	8.716				Ke5		
Ba <sub>2</sub> TmPaO <sub>6</sub>	C	8.692				Ke5		
Ba <sub>2</sub> YbPaO <sub>6</sub>	C	8.678				Ke5		
Ba <sub>2</sub> LuPaO <sub>6</sub>	C	8.666				Ke5		
Ba <sub>2</sub> PuPaO <sub>6</sub>	C	8.748				Ke5		
Ba <sub>2</sub> AmPaO <sub>6</sub>	C	8.793				Ke5		
Sr <sub>2</sub> LuPaO <sub>6</sub>	C	8.462				Ke5		
BaSrSrPaO <sub>6.5</sub>	C	8.784				Aw2		
Ba <sub>2</sub> MnPuO <sub>6</sub>	C	8.32				Aw2	Pseudocubic	
Ba <sub>2</sub> InPuO <sub>6</sub>	C	8.50				Aw2		
Ba <sub>2</sub> LaPuO <sub>6</sub>	C	8.63				Aw2		
Ba <sub>2</sub> CePuO <sub>6</sub>	C	8.72				Aw2		
Ba <sub>2</sub> NdPuO <sub>6</sub>	C	8.66				Aw2		
Ba <sub>2</sub> TiPuO <sub>6</sub>	C	8.06				Aw2	Pu <sup>4+</sup>	
Ba <sub>2</sub> ZnPuO <sub>6</sub>	C	8.38				Aw2	Pseudocubic	
Ba <sub>2</sub> PbPuO <sub>6</sub>	C	8.58				Aw2		
$A_2^+BMo^{6+}O_6$								
Ba <sub>2</sub> CaMoO <sub>6</sub>	C	8.355				Si32	No compound [Pa7]	6
Ba <sub>2</sub> CrMoO <sub>6</sub>	C	8.08				Pa7	S.S. with Sr [Ga12]	
Ba <sub>2</sub> FeMoO <sub>6</sub>	C	4.043				Br14	Probably ordered	6
Ba <sub>2</sub> CoMoO <sub>6</sub>	C	4.022				Br14	Probably ordered	6
Ba <sub>2</sub> NiMoO <sub>6</sub>	C	3.91				Br14		6
Sr <sub>2</sub> CrMoO <sub>6</sub>	C	7.98		7.909		Br14		6
Sr <sub>2</sub> MnMoO <sub>6</sub>	T	7.888				Gal2	P & S [Pa7], Prop. [Ga12, Na4], S.S. with Ba and Ca [Ga12], neutron diffraction [Na11]	6
Sr <sub>2</sub> FeMoO <sub>6</sub>	T	5.581		7.940		Ku8	P & S [Br14]	
	C	7.918				Ku8	Cubic at 320 °C; no dielectric anomaly	
	T	5.560		7.886		Ku8	P & S [Br14], semiconducting, $\Delta E = 0.78$ eV $\leq 181$ °C $\leq 1.30$ eV [No1], S.S. with Ba, cubic at 22% Ba [No1, No3]	6
	C	7.878				Ku8	Cubic at 230 °C [Ku8, No3], no dielectric anomaly [Ku8]	
Sr <sub>2</sub> CoMoO <sub>6</sub>								
Sr <sub>2</sub> NiMoO <sub>6</sub>								
Sr <sub>2</sub> ZnMoO <sub>6</sub>	T	5.561		7.966		Ku8	Cubic at 420 °C; no dielectric anomaly	
	C	7.954				Ku8		

Compound	Sym	a Å	b Å	c Å	angle	Ref.	Remarks	Magnetic Data
A <sub>3</sub> BMo <sup>6+</sup> O <sub>6</sub> (continued)								in 3.3.4, Tab.
Ca <sub>2</sub> CrMoO <sub>6</sub>	O	5.36	5.49	7.70		Pa7		6
Ca <sub>2</sub> FeMoO <sub>6</sub>	O	5.42	5.53	7.73		Pa7		6
A <sub>3</sub> BTe <sup>6+</sup> O <sub>6</sub>								
Ba <sub>2</sub> MgTeO <sub>6</sub>	C	8.13				Sl6	P & S [Ba26, Re4a]	
Ba <sub>2</sub> CaTeO <sub>6</sub>	C	8.393				Sl6	P & S [Ba26], S.S. with Ni [Re4a]	
BaPbMgTeO <sub>6</sub>	C	8.08				Ba26		
Sr <sub>2</sub> MgTeO <sub>6</sub>	C	7.94				Ba26		
SrPbMgTeO <sub>6</sub>	C	7.955				Ba26		
Sr <sub>2</sub> NiTeO <sub>6</sub>	C	3.95				Re4a	Optical properties and S. S. with Ba	
Sr <sub>2</sub> CuTeO <sub>6</sub>	T	7.680		8.465		Re4b	Optical properties	
Ca <sub>2</sub> CaTeO <sub>6</sub>	O	5.55	5.77	7.98		Bl1a		
Pb <sub>2</sub> MgTeO <sub>6</sub>	C	7.99				Ba26		
A <sub>3</sub> BW <sup>6+</sup> O <sub>6</sub>								
Ba <sub>2</sub> MgWO <sub>6</sub>	C	8.099				Sl32	P & S [Be18], dielectric properties [Ag1]	
Ba <sub>2</sub> CaWO <sub>6</sub>	C	8.390				Be18	P & S [Sl32], S.S. with Ni [Re4a]	
Ba <sub>2</sub> CrWO <sub>6</sub>	C	8.133				Pa7	No perovskite	
Ba <sub>2</sub> FeWO <sub>6</sub>	C	8.098				Fr14		
Ba <sub>2</sub> CoWO <sub>6</sub>	C	8.066				Fr14	P & S [Br14], Prop., semiconducting, ΔE = 0.81 eV [Bo1], neutron diffraction [Co31]	6
Ba <sub>2</sub> NiWO <sub>6</sub>	C	8.066				Fr14	P & S [Br14, Ag1], S.S. with Sr [No2], neutron diffraction [Co31], optical properties [Re4a]	6
Ba <sub>2</sub> CuWO <sub>6</sub>	T	7.88		8.61		Bl8	P & S [Ka12, Ve2, Ve3], complete structure [Pl3]	6
Ba <sub>2</sub> ZnWO <sub>6</sub>	C	8.116				Fr14		
Ba <sub>2</sub> SrWO <sub>6</sub>	C	8.53				Be18		
Ba <sub>2</sub> CdWO <sub>6</sub>	C	8.383				Be18		
Ba <sub>2</sub> BaWO <sub>6</sub>	C	8.62				Be18	P & S [Fr10, Sl32], S.S. with Sr <sub>3</sub> WO <sub>6</sub> [Be18]	
BaSrMgWO <sub>6</sub>	C	8.02				Sl32	Slightly distorted; cubic T > 805 °C [Ch4]	
Ba <sub>1.9</sub> Ca <sub>0.1</sub> CaWO <sub>6</sub>	C	8.387				Be18	P & S [Sl32]	
BaSrCaWO <sub>6</sub>	C	8.29				Sl32	P & S [Be18]	
BaCaCaWO <sub>6</sub>	C	8.363				Sl32	Distorted	
BaSrZnWO <sub>6</sub>	C	8.07				Be18	Composition questionable	
BaCaZnWO <sub>6</sub>	C	8.38				Be18	Distorted	
Sr <sub>2</sub> MgWO <sub>6</sub>	C	7.8				Be18	Composition questionable	
Sr <sub>2</sub> CaWO <sub>6</sub>	C	8.2				Be18	P & S [Sl32], distorted	
Sr <sub>2</sub> CrWO <sub>6</sub>	C	7.82				Be18	Distorted	
Sr <sub>2</sub> MnWO <sub>6</sub>	C	8.01				Pa7	Prop. [Bl4]	6
Sr <sub>2</sub> FeWO <sub>6</sub>	C	7.96				Bl8	Prop. [Bl4]	6

Compound	Sym	a Å	b Å	c Å	angle	Ref.	Remarks	Magnetic Data
A <sub>2</sub> <sup>+</sup> BW <sup>6+</sup> O <sub>6</sub> (continued)								in 3.3.4, Tab.
Sr <sub>2</sub> CoWO <sub>6</sub>	T	7.89		7.98		Fr14	P & S [Br14], Prop. [No1, Ku8, Bl2, Bl4]	6
	C	7.904				Ku8	T ≈ 400 °C, cubic T > 400 °C; no dielectric anomaly	
Sr <sub>2</sub> NiWO <sub>6</sub>	T	7.86		7.91		Fr14	P & S [Br14], Prop. [No1, Bl2, Bl4, No2, Ve1, No2, Re4a], S.S. with LaFeO <sub>3</sub> [Sm23], S.S. with Ba [No2], ESR [No4], S.S. with Ca [Re4a]	6
	C	7.908				Ku8	T ≈ 300 °C, cubic T > 300 °C [Ku8, No4]	
Sr <sub>2</sub> CuWO <sub>6</sub>	T	7.66		8.40		Bl8	P & S [Ka12], dielectric properties [Ve2]	6
Sr <sub>2</sub> ZnWO <sub>6</sub>	T	7.92		8.01		Fr14	P & S [Ku8, Be18], S.S. with Ba, cubic > 40% Ba [Fr14]	
	C	7.956				Ku8	T ≈ 430 °C, cubic T > 430 °C [Ku8, Fr14], no dielectric anomaly [Ku8]	
Sr <sub>2</sub> SrWO <sub>6</sub>	C	8.3				Be18	Distorted, P & S [Si32]; cubic T > 1100 °C, S.S. with Ca [Ch3]	
SrCaMgWO <sub>6</sub>	C	7.87				Be18	Distorted, P & S [Si32]	
SrCaCaWO <sub>6</sub>	C	8.1				Be18	Distorted, P & S [Si32]	
Ca <sub>2</sub> MgWO <sub>6</sub>	C	7.75				Si32	Distorted, P & S [Be18]	
Ca <sub>2</sub> CaWO <sub>6</sub>	C	8.02				Si32	Distorted, P & S [Be18]; not cubic T < 1500 °K, S.S. with Sr [Ch3, Ch4]	
Ca <sub>2</sub> CrWO <sub>6</sub>	O	5.35	5.47	7.70		Pa7	Prop. [Bl2, Ki7]	6
Ca <sub>2</sub> CoWO <sub>6</sub>	O	5.43	5.60	7.73		Bl8	Optical properties [Re4a]	6
Ca <sub>2</sub> NiWO <sub>6</sub>	O	5.40	5.55	7.70		Bl8	Not perovskite [Bl8]	
Ca <sub>2</sub> CuWO <sub>6</sub>	C	8.0				Be8	Dielectric properties [Sm8, Ag1, Sm13, Kl5, Mi1a, Kh6, Si42], piezoelectric properties, S.S. with Ti, Zr [Si34], S.S. with Cd [Is15], S.S. with PbFe <sub>2</sub> /3W <sub>1</sub> /3O <sub>6</sub> [Sm10], S.S. with PbTiO <sub>3</sub> , Ca <sub>2</sub> MgWO <sub>6</sub> , Pb <sub>2</sub> MgNb <sub>2</sub> O <sub>6</sub> [Sm20, Si35]	
Pb <sub>2</sub> MgWO <sub>6</sub>	C					Be8	Distorted, dielectric properties [Ag1]	6
Pb <sub>2</sub> CaWO <sub>6</sub>	C	4.2				Be8	Prop. [Ve2, Ve4, Ro8]	6
Pb <sub>2</sub> MnWO <sub>6</sub>	O	5.736	5.756	8.066		Ve3	Prop., no cell dimensions [Ve4]	6
Pb <sub>2</sub> FeWO <sub>6</sub>	O	5.661	5.676	9.976		Bo10	P & S [Fi11, Be18], Prop. [Te13, Bo10, Ki7, Fi6], B site ordering [Yu9], S.S. with BaTiO <sub>3</sub> [To2]	6
Pb <sub>2</sub> CoWO <sub>6</sub>	O					Fi6	T ≈ 20 °C, cubic T > 20 °C	6
Pb <sub>2</sub> NiWO <sub>6</sub>	C	8.017				Fi6	Dielectric properties, P & S [To11a, To11b]	
Pb <sub>2</sub> NiWO <sub>6</sub>	C	7.997				No6	T = 173 °K - tetragonal below 290 °K	
Pb <sub>2</sub> CdWO <sub>6</sub>	T	8.006		7.920		No6	Distorted, dielectric properties [Ro6], S.S. with Mg [Is15]	
	C	4.1				Be18	Cubic at 400 °C, transformations [Po8], S.S. with Pb (Li <sub>1/3</sub> Nb <sub>1/3</sub> W <sub>1/3</sub> O <sub>3</sub> [Di5])	6
Pb <sub>2</sub> CdWO <sub>6</sub>	C	4.15				Fi7		

Compound	Sym	a Å	b Å	c Å	angle	Ref.	Remarks	Magnetic Data
A <sub>2</sub> <sup>+</sup> BW <sup>6+</sup> O <sub>6</sub> (continued)								
Pb <sub>2</sub> Na <sub>0.5</sub> Sc <sub>0.5</sub> WO <sub>6</sub>						Ve4	Dielectric properties, no cell dimensions	in 3.3.4, Tab.
Pb <sub>2</sub> Na <sub>0.5</sub> Fe <sub>0.5</sub> WO <sub>6</sub>						Ve4	Dielectric properties, no cell dimensions	
Pb <sub>2</sub> Na <sub>0.5</sub> Yb <sub>0.5</sub> WO <sub>6</sub>						Ve4	Dielectric properties, no cell dimensions	
Pb <sub>2</sub> Mg <sub>0.5</sub> Mn <sub>0.5</sub> WO <sub>6</sub>	T	8.202		8.104		Vi5	Dielectric properties [Vi5, Ve4]	6
Pb <sub>2</sub> Co <sub>0.5</sub> Mn <sub>0.5</sub> WO <sub>6</sub>	T	8.082		8.018		Vi5	Dielectric properties [Vi5, Ve4]	6
Pb <sub>2</sub> Ni <sub>0.5</sub> Mn <sub>0.5</sub> WO <sub>6</sub>	C	8.008				Ve3	No cell dimensions, Prop. [Vi5]	6
Pb <sub>2</sub> Li <sub>0.5</sub> Fe <sub>0.5</sub> WO <sub>6</sub>	C	4.013				Ve3	Dielectric properties [Vi5, Ve2, Ve3, Ve4]	
Pb <sub>2</sub> Li <sub>0.5</sub> Co <sub>0.5</sub> WO <sub>6</sub>	C	8.04				Vi5	Dielectric properties [Ve3]	
Pb <sub>2</sub> Li <sub>0.5</sub> La <sub>0.5</sub> WO <sub>6</sub>	C	4.100				Ve3	Dielectric properties [Vi5]	
Pb <sub>2</sub> Li <sub>0.5</sub> Yb <sub>0.5</sub> WO <sub>6</sub>	C					Ve3	Dielectric properties [Ve2, Ve3, Ve4]	
Pb <sub>2</sub> Li <sub>0.55</sub> Mn <sub>0.45</sub> WO <sub>6</sub>						Ve4	Dielectric properties, no cell dimensions	
Pb <sub>2</sub> Li <sub>0.55</sub> Zr <sub>0.45</sub> WO <sub>6</sub>						Ve4	Dielectric properties, no cell dimensions	
Pb <sub>2</sub> Li <sub>0.55</sub> Hf <sub>0.45</sub> WO <sub>6</sub>						Ve4	Dielectric properties, no cell dimensions	
Pb <sub>2</sub> YTi <sub>0.5</sub> W <sub>0.5</sub> O <sub>6</sub>	C	4.124				Ve3	Dielectric properties [Ve2, Ve3, Ve4]	
Pb <sub>2</sub> FeMn <sub>0.5</sub> W <sub>0.5</sub> O <sub>6</sub>	C	4.037				Ro8	Dielectric properties [Ve4]	6
A <sub>3</sub> <sup>+</sup> BReO <sub>6</sub> , Re <sup>5+</sup> and Re <sup>6+</sup>								
Ba <sub>2</sub> MgReO <sub>6</sub>	C	8.082				Si8	P & S [Lo2, Sc18], single crystal [Si7]	
Ba <sub>2</sub> CaReO <sub>6</sub>	C	8.356				Si8	P & S [Lo2, Sc18]	
Ba <sub>2</sub> ScReO <sub>6</sub>	C	8.163				Si8	P & S [Sc18]	
Ba <sub>2</sub> MnReO <sub>6</sub>	C	8.18				Si8	P & S [Lo2, Wa15], single crystal + Prop. [Si7]	6
Ba <sub>2</sub> FeReO <sub>6</sub>	C	8.05				Si8	P & S [Lo2, Wa15], single crystal + Prop. [Si7], [Ba25a] suggests Ba <sub>2</sub> Fe <sub>1+x</sub> Re <sub>1-x</sub> O <sub>6</sub>	6
Ba <sub>2</sub> CoReO <sub>6</sub>	C	8.086				Si8	P & S [Lo2, Wa15], single crystal + Prop. [Si7]	6
Ba <sub>2</sub> NiReO <sub>6</sub>	C	8.04				Si8	P & S [Lo2], single crystal + Prop. [Si7]	6
Ba <sub>2</sub> ZnReO <sub>6</sub>	C	8.106				Si8	P & S [Lo2]	
Ba <sub>2</sub> SrReO <sub>6</sub>	T	8.60		8.43		Si8	P & S [Sc18]	
Ba <sub>2</sub> YReO <sub>6</sub>	C	8.372				Si8	P & S [Lo2]	
Ba <sub>2</sub> CdReO <sub>6</sub>	C	8.322				Si8	P & S [Sc18]	
Ba <sub>2</sub> InReO <sub>6</sub>	C	8.258		8.33		Si8	P & S [Sc18]	
Ba <sub>2</sub> BaReO <sub>6</sub>	T	8.65				Ba25a	Prep. 900 °C, a <sub>0</sub> increases with prep. temperature suggesting Ba <sub>2</sub> Re <sup>3+</sup> Re <sup>5+</sup> La <sub>1-x</sub> Ba <sub>x</sub> O <sub>6</sub> ; P & S [Si8]	
Ba <sub>2</sub> LaReO <sub>6</sub>	C	8.547						
Ba <sub>2</sub> NdReO <sub>6</sub>	C	8.51				Si8	Prop. [Lo2], P & S [Sc18]	
Ba <sub>2</sub> SmReO <sub>6</sub>	C	8.458				Ba25a		
Ba <sub>2</sub> EuReO <sub>6</sub>	C	8.438				Ba25a		
Ba <sub>2</sub> GdReO <sub>6</sub>	C	8.431				Si8		
Ba <sub>2</sub> TbReO <sub>6</sub>	C	8.399				Ba25a		

Compound	Sym	a Å	b Å	c Å	angle	Ref.	Remarks	Magnetic Data
A <sub>2</sub> BR <sub>2</sub> O <sub>6</sub> , Re <sup>3+</sup> and Re <sup>4+</sup> (continued)								
Ba <sub>2</sub> DyReO <sub>6</sub>	C	8.391				Ba25a		
Ba <sub>2</sub> HoReO <sub>6</sub>	C	8.375				Ba25a		
Ba <sub>2</sub> ErReO <sub>6</sub>	C	8.354				Sl8	Prop. [Lo2], P & S [Sc18]	
Ba <sub>2</sub> TmReO <sub>6</sub>	C	8.342				Ba25a		
Ba <sub>2</sub> YbReO <sub>6</sub>	C	8.329				Ba25a	$x = 1.2$ , small positive deviation from Vegard's law	
Ba <sub>2-x</sub> Sr <sub>x</sub> YbReO <sub>6</sub>	C	8.230				Ba25a	Prop. [Sl8, Lo2] Single crystal [Sl7], Prep. [Sc18] P & S [Sc18]	
BaSrFeReO <sub>6</sub>						Sl8	distorted	6
Ba <sub>2</sub> YReO <sub>6</sub>	O	7.88	5.85	7.94		Sl8		
Sr <sub>2</sub> MgReO <sub>6</sub>	C	5.76		8.21		Sl8		
Sr <sub>2</sub> CaReO <sub>6</sub>	C	8.02				Sl8		
Sr <sub>2</sub> ScReO <sub>6</sub>	C	7.82				Sl8		
Sr <sub>2</sub> CrReO <sub>6</sub>	C	8.01				Sl8	distorted	6
Sr <sub>2</sub> MnReO <sub>6</sub>	C	7.86				Sl8	P & S [Lo2, Wa15]	
Sr <sub>2</sub> FeReO <sub>6</sub>	T	7.88		7.89		Sl8		
Sr <sub>2</sub> CoReO <sub>6</sub>	T	7.88		7.98		Sl8		
Sr <sub>2</sub> NiReO <sub>6</sub>	T	7.85		7.92		Sl8		
Sr <sub>2</sub> ZnReO <sub>6</sub>	T	7.89		8.01		Sl8		
Sr <sub>2</sub> GaReO <sub>6</sub>	T	7.843				Sl8		
Sr <sub>2</sub> SrReO <sub>6</sub>	T	8.41		8.13		Sl8	P & S [Sc18]	
Sr <sub>2</sub> YReO <sub>6</sub>	C	8.197				Ba25b		
Sr <sub>2</sub> CdReO <sub>6</sub>	C	5.73	5.81	8.16		Sl8		
Sr <sub>2</sub> InReO <sub>6</sub>	C	8.071				Sl8		
Sr <sub>2</sub> GdReO <sub>6</sub>	C	8.239				Ba25b		6
Sr <sub>2</sub> TbReO <sub>6</sub>	C	8.223				Ba25b		6
Sr <sub>2</sub> DyReO <sub>6</sub>	C	8.210				Ba25b		
Sr <sub>2</sub> HoReO <sub>6</sub>	C	8.200				Ba25b		6
Sr <sub>2</sub> ErReO <sub>6</sub>	C	8.181				Ba25b		
Sr <sub>2</sub> TmReO <sub>6</sub>	C	8.167				Ba25b		6
Sr <sub>2</sub> YbReO <sub>6</sub>	C	8.155				Ba25b		
Ca <sub>2</sub> MgReO <sub>6</sub>	O	5.48	5.56	7.77		Sl8	P & S [Sc18]	
Ca <sub>2</sub> CaReO <sub>6</sub>	O	5.67	5.78	8.05		Sl8	P & S [Sc18]	6
Ca <sub>2</sub> ScReO <sub>6</sub>	O	5.49	5.63	7.86		Sl8		
Ca <sub>2</sub> CrReO <sub>6</sub>	O	5.38	5.47	7.67		Sl8		
Ca <sub>2</sub> MnReO <sub>6</sub>	O	5.52	5.55	7.82		Sl8		
Ca <sub>2</sub> FeReO <sub>6</sub>	O	5.41	5.53	7.69		Sl8	P & S [Lo2]	6
Ca <sub>2</sub> CoReO <sub>6</sub>	O	5.46	5.58	7.71		Sl8		



Compound	Sym	a Å	b Å	c Å	angle	Ref.	Remarks	Magnetic Data
A <sub>2</sub> <sup>2+</sup> BReO <sub>6</sub> , Re <sup>6+</sup> and Re <sup>5+</sup> (continued)								
Ca <sub>2</sub> NiReO <sub>6</sub>	O	5.45	5.55	7.67		Sl8		in 3.3.4, Tab.
Ca <sub>2</sub> CdReO <sub>6</sub>	O	5.64	5.77	7.99		Sl8		
Pb <sub>2</sub> MnReO <sub>6</sub>	O	5.69	5.74	8.024		Ro8	Claim Mn <sup>3+</sup> — Re <sup>6+</sup> , Prop. [Ro8, Ro11]	
Pb <sub>2</sub> MnReO <sub>6</sub>	O	5.67	5.75	8.008		Ro8	Claim Mn <sup>3+</sup> — Re <sup>6+</sup> , Prop. [Ro8, Ve4]	
A <sub>2</sub> <sup>2+</sup> BOsO <sub>6</sub>								
Ba <sub>2</sub> MgOsO <sub>6</sub>	C	8.08				Sl8		6
Ba <sub>2</sub> CaOsO <sub>6</sub>	C	8.362				Sl8		
Ba <sub>2</sub> ScOsO <sub>6</sub>	C	8.152				Sl8		
Ba <sub>2</sub> MnOsO <sub>6</sub>	H	5.82		14.2		Sl8	Hex (6L)	
Ba <sub>2</sub> FeOsO <sub>6</sub>	H	5.76		14.1		Sl8	Hex (6L)	
Ba <sub>2</sub> ZnOsO <sub>6</sub>	C	8.095				Sl8		
Ba <sub>2</sub> SrOsO <sub>6</sub>	T	8.43		8.72		Sl8		
Ba <sub>2</sub> CdOsO <sub>6</sub>	C	8.325				Sl8		
Ba <sub>2</sub> InOsO <sub>6</sub>	C	8.224				Sl8		
Ba <sub>2</sub> BaOsO <sub>6</sub>	T	8.66		8.34		Sl8		
Sr <sub>2</sub> MgOsO <sub>6</sub>	T	7.86		7.92		Sl8		
Sr <sub>2</sub> CaOsO <sub>6</sub>	C	8.21				Sl8	Distorted	
Sr <sub>2</sub> ScOsO <sub>6</sub>	C	8.02				Sl8	Distorted	
Sr <sub>2</sub> CrOsO <sub>6</sub>	C	7.84				Sl8		
Sr <sub>2</sub> FeOsO <sub>6</sub>	C	7.85				Sl8		
Sr <sub>2</sub> CoOsO <sub>6</sub>	T	7.86		7.92		Sl8	Distorted	
Sr <sub>2</sub> GaOsO <sub>6</sub>	C	7.82				Sl8		
Sr <sub>2</sub> SrOsO <sub>6</sub>	T	8.32		8.12		Sl8		
Sr <sub>2</sub> InOsO <sub>6</sub>	C	8.06				Sl8		
Ca <sub>2</sub> CaOsO <sub>6</sub>	O	5.73	5.80	7.87		Sl8		
Ca <sub>2</sub> CrOsO <sub>6</sub>	O	5.38	5.47	7.66		Sl8		
Ca <sub>2</sub> CoOsO <sub>6</sub>	O	5.47	5.59	7.70		Sl8		
A <sub>2</sub> <sup>3+</sup> BUO <sub>6</sub>								
Ba <sub>2</sub> BeUO <sub>6</sub>	C	8.82				Aw1	Doubtful	6
Ba <sub>2</sub> MgUO <sub>6</sub>	C	8.381				Sl5		
Ba <sub>2</sub> CaUO <sub>6</sub>	C	8.67				Sl5	Distorted, P & S [Ru4]	
Ba <sub>2</sub> ScUO <sub>6</sub>	C	8.49				Sl5		
Ba <sub>2</sub> TiUO <sub>6</sub>	C	8.05				Aw1	Ti <sup>4+</sup>	
Ba <sub>2</sub> CrUO <sub>6</sub>	C	8.297				Sl5	Also prepared as Hex (6L)	
Ba <sub>2</sub> MnUO <sub>6</sub>	C	8.52				Sl5	P & S [Aw1]	
Ba <sub>2</sub> FeUO <sub>6</sub>	C	8.312				Sl5	Prop. [Dis]	
Ba <sub>2</sub> CoUO <sub>6</sub>	C	8.372				Sl5		

Compound	Sym	a Å	b Å	c Å	angle	Ref.	Remarks	Magnetic Data in 3.3.4, Tab.
A <sub>2</sub> <sup>2+</sup> BUO <sub>6</sub> (continued)								
Ba <sub>2</sub> NiUO <sub>6</sub>	C	8.336				Sl5	Optical properties [Re4a]	
Ba <sub>2</sub> CuUO <sub>6</sub>	T	8.18		8.84		Sl5		
Ba <sub>2</sub> ZnUO <sub>6</sub>	C	8.397				Sl5		
Ba <sub>2</sub> GeUO <sub>6</sub>	C	8.56				Aw1	Doubtful	
Ba <sub>2</sub> SrUO <sub>6</sub>	C	8.84				Sl5	Distorted, P & S [Ru4]	
Ba <sub>2</sub> YUO <sub>6</sub>	C	8.69				Sl5	Distorted	
Ba <sub>2</sub> ZrUO <sub>6</sub>	C	8.35				Aw1	Hex (6L)	
Ba <sub>2</sub> RhUO <sub>6</sub>	H	5.84		14.9		Sl5		
Ba <sub>2</sub> CdUO <sub>6</sub>	O	6.07	6.13	8.64		Sl5		
Ba <sub>2</sub> InUO <sub>6</sub>	C	8.521				Sl5		
Ba <sub>2</sub> InUO <sub>6.5</sub>	C	8.551				Sl5		
Ba <sub>2</sub> BaUO <sub>6</sub>	T	6.285		8.943		Ri4	Complete structure determined, P & S [Sl5, Ru4]	
Ba <sub>2</sub> LaUO <sub>6</sub>	C	8.73				Aw1	Distorted	
Ba <sub>2</sub> CeUO <sub>6</sub>	C	8.87				Aw1	Ce <sup>4+</sup>	
Ba <sub>2</sub> NdUO <sub>6</sub>	C	8.76				Aw1		
Ba <sub>2</sub> SmUO <sub>6</sub>	C	8.76				Aw1		
Ba <sub>2</sub> EuUO <sub>6</sub>	C	8.68				Aw1		
Ba <sub>2</sub> GdUO <sub>6</sub>	C	8.66				Aw1		
Ba <sub>2</sub> DyUO <sub>6</sub>	C	8.65				Aw1		
Ba <sub>2</sub> HoUO <sub>6</sub>	C	8.65				Aw1		
Ba <sub>2</sub> ErUO <sub>6</sub>	C	8.67				Aw1	Distorted	
Ba <sub>2</sub> YbUO <sub>6</sub>	C	8.60				Aw1		
Ba <sub>2</sub> LuUO <sub>6</sub>	C	8.57				Aw1		
Ba <sub>2</sub> HfUO <sub>6</sub>	C	8.31				Aw1	Doubtful	
Ba <sub>2</sub> HgUO <sub>6</sub>	C	8.83				Aw1	Doubtful	
Ba <sub>2</sub> PbUO <sub>6</sub>	C	8.85				Aw1		
Ba <sub>2</sub> SrUO <sub>6</sub>	C	8.66				Ru4		
Sr <sub>2</sub> MgUO <sub>6</sub>	C	8.19				Sl5	Distorted	
Sr <sub>2</sub> CaUO <sub>6</sub>	O	5.93	6.06	8.46		Sl5		
Sr <sub>2</sub> CrUO <sub>6</sub>	C	8.09				Sl5	Distorted	
Sr <sub>2</sub> MnUO <sub>6</sub>	C	8.28				Sl5	Distorted	
Sr <sub>2</sub> FeUO <sub>6</sub>	C	8.11				Sl5	Distorted	
Sr <sub>2</sub> CoUO <sub>6</sub>	C	8.19				Sl5	Distorted	
Sr <sub>2</sub> NiUO <sub>6</sub>	C	8.15				Sl5	Distorted, optical properties [Re4a]	6
Sr <sub>2</sub> SrUO <sub>6</sub>	M	5.959	6.179	8.553	$\beta = 90^\circ 11'$	Ri4	Complete structure; P & S [Sl5, Ru4, Be25, Ip1]	
Sr <sub>2</sub> CdUO <sub>6</sub>	O	5.91	6.03	8.42		Sl5		
Sr <sub>2</sub> InUO <sub>6</sub>	C	8.33	6.01	8.36		Sl5	Distorted; Prop. [Ke13]	6
SrCaCaUO <sub>6</sub>	O	5.83				Sl5		

Compound	Sym	a Å	b Å	c Å	angle	Ref.	Remarks	Magnetic Data
----------	-----	--------	--------	--------	-------	------	---------	------------------

Compound	Sym	a Å	b Å	c Å	angle	Ref.	Remarks	Magnetic Data
A <sub>2</sub> <sup>+</sup> B <sup>+</sup> UO <sub>6</sub> (continued)								
Ca <sub>2</sub> CaUO <sub>6</sub>	M	5.728	5.958	8.301	$\beta = 90^\circ 33'$	Ri4	Complete structure determined, P & S [Sl5, Ru4, Be25, Ip1]	in 3.3.4, Tab.
Pb <sub>2</sub> PbUO <sub>6</sub>	O	13.71	12.36	8.21		Sl26	Not perovskite	
A <sub>2</sub> <sup>+</sup> B <sup>+</sup> B'O <sub>6</sub> ; B' = Np <sup>4+</sup> , Pu <sup>4+</sup>								
Ba <sub>2</sub> SrNpO <sub>6</sub>	C	8.799				Ke4		
Ba <sub>2</sub> BaNpO <sub>6</sub>	C	8.860				Ke4		
Ba <sub>2</sub> SrNpO <sub>6</sub>	C	8.735				Ke4		
Ba <sub>2</sub> SrPuO <sub>6</sub>	C	8.780				Ke3		
Ba <sub>2</sub> BaPuO <sub>6</sub>	C	8.840				Ke3		
Ba <sub>2</sub> SrPuO <sub>6</sub>	C	8.717				Ke3		
Sr <sub>2</sub> SrPuO <sub>6</sub>						Ke3	Not perovskite	
A <sub>2</sub> <sup>+</sup> B <sup>+</sup> B'O <sub>6</sub> ; B' = Tc <sup>4+</sup> , Re <sup>4+</sup> , Os <sup>4+</sup> , Ir <sup>4+</sup>								
Ba <sub>2</sub> LiTcO <sub>6</sub>	C	8.092				Wa16	P & S [Ke9]	
Ba <sub>2</sub> NaTcO <sub>6</sub>	C	8.292				Wa16	P & S [Ke9]	
Sr <sub>2</sub> LiTcO <sub>6</sub>	C	7.84		8.14		Wa16	Distorted, P & S [Ke9]	
Sr <sub>2</sub> NaTcO <sub>6</sub>	T	8.09				Wa16	P & S [Ke9]	
Ca <sub>2</sub> LiTcO <sub>6</sub>							Not able to be made [Wa16]	
Ba <sub>2</sub> LiReO <sub>6</sub>	C	8.118				Sl4	S.S. with Na [Sl4]	
Ba <sub>2</sub> NaReO <sub>6</sub>	C	8.296				Sl4		
Sr <sub>2</sub> LiReO <sub>6</sub>	C	7.87				Sl8		
Sr <sub>2</sub> NaReO <sub>6</sub>	C	8.13				Sl8		
Ca <sub>2</sub> LiReO <sub>6</sub>	C	7.83				Sl8	Distorted	
Ba <sub>2</sub> LiOsO <sub>6</sub>	C	8.100				Sl8	S.S. with Re [Sl8]	
Ba <sub>2</sub> NaOsO <sub>6</sub>	C	8.282				Sl8		
Sr <sub>2</sub> LiOsO <sub>6</sub>	C	7.86				Sl8		
Sr <sub>2</sub> NaOsO <sub>6</sub>	C	8.13				Sl8		
Ca <sub>2</sub> LiOsO <sub>6</sub>	C	7.83				Sl8	Distorted	
Ba <sub>2</sub> NaIO <sub>6</sub>	C	8.33				Sl6		
Ba <sub>2</sub> AgIO <sub>6</sub>	C	8.46				Sl6		

6

Tab. 2c. A <sub>3</sub> BB' <sub>2</sub> O <sub>9</sub> (for H symmetry see Fig. 1c)						
Compound	Sym	a Å	b Å	c Å	angle	Ref.
A <sub>3</sub> BB' <sub>2</sub> O <sub>9</sub>						
Ba <sub>3</sub> MgNb <sub>2</sub> O <sub>9</sub>	H	5.77		7.08		Ga9
Ba <sub>3</sub> CaNb <sub>2</sub> O <sub>9</sub>	H	5.92		7.25		Ga9
Ba <sub>3</sub> FeNb <sub>2</sub> O <sub>9</sub>	C	4.085				Ga9
Ba <sub>3</sub> CoNb <sub>2</sub> O <sub>9</sub>	C	4.09				Ga13
Ba <sub>3</sub> NiNb <sub>2</sub> O <sub>9</sub>	C	4.074				Ga9
Ba <sub>3</sub> CuNb <sub>2</sub> O <sub>9</sub>	T	8.04		8.40		Bl8
Ba <sub>3</sub> ZnNb <sub>2</sub> O <sub>9</sub>	C	8.166				Ve2
Ba <sub>3</sub> CdNb <sub>2</sub> O <sub>9</sub>	C	4.094				Ga9
Ba <sub>3</sub> BaNb <sub>2</sub> O <sub>9</sub>	C	4.168				Ga9
Ba <sub>3</sub> PbNb <sub>2</sub> O <sub>9</sub>	H	6.01		8.0		Ga9
Sr <sub>3</sub> MgNb <sub>2</sub> O <sub>9</sub>	C	4.26				Ga9
Sr <sub>3</sub> CaNb <sub>2</sub> O <sub>9</sub>	H	5.66		6.98		Ga9
Sr <sub>3</sub> FeNb <sub>2</sub> O <sub>9</sub>	H	5.76		7.16		Ga9
Sr <sub>3</sub> CoNb <sub>2</sub> O <sub>9</sub>	T	3.997		4.018		Ga9
Sr <sub>3</sub> NiNb <sub>2</sub> O <sub>9</sub>	C	8.01				Bl8
Sr <sub>3</sub> NbNb <sub>2</sub> O <sub>9</sub>	H	5.64		6.90		Ga9
Sr <sub>3</sub> CuNb <sub>2</sub> O <sub>9</sub>	T	7.888		8.148		Ka12
Sr <sub>3</sub> ZnNb <sub>2</sub> O <sub>9</sub>	H	5.66		6.95		Ga9
Sr <sub>3</sub> CdNb <sub>2</sub> O <sub>9</sub>	C	4.089				Ga9
Ca <sub>3</sub> CaNb <sub>2</sub> O <sub>9</sub>	C					Bl8
Ca <sub>3</sub> NiNb <sub>2</sub> O <sub>9</sub>	C	3.88				Ag1
Pb <sub>3</sub> MgNb <sub>2</sub> O <sub>9</sub>	C	4.04				Ag1
Pb <sub>3</sub> MnNb <sub>2</sub> O <sub>9</sub>						
Pb <sub>3</sub> CoNb <sub>2</sub> O <sub>9</sub>	C	4.05				Ag1
Pb <sub>3</sub> NiNb <sub>2</sub> O <sub>9</sub>	C	4.02				Bo5
Pb <sub>3</sub> ZnNb <sub>2</sub> O <sub>9</sub>	C					Ag1
Pb <sub>3</sub> Sc <sub>1/3</sub> W <sub>2/3</sub> NbO <sub>9</sub>	C	4.05				Bo5
Pb <sub>3</sub> CdNb <sub>2</sub> O <sub>9</sub>	C	4.074				To1
	C	8.246				To1

Tab. 2c. A<sub>3</sub>BB'<sub>2</sub>O<sub>9</sub> (for H symmetry see Fig. 1c)

Compound	Sym	a Å	b Å	c Å	angle	Ref.	Remarks	Magnetic Data
A <sub>3</sub> BB' <sub>2</sub> O <sub>9</sub>								
Ba <sub>3</sub> MgNb <sub>2</sub> O <sub>9</sub>	H	5.77		7.08		Ga9	P & S [Ga13, Bl8], see Fig. 1(c)	
Ba <sub>3</sub> CaNb <sub>2</sub> O <sub>9</sub>	H	5.92		7.25		Ga9	See Fig. 1(c)	
Ba <sub>3</sub> FeNb <sub>2</sub> O <sub>9</sub>	C	4.085				Ga9		
Ba <sub>3</sub> CoNb <sub>2</sub> O <sub>9</sub>	C	4.09				Ga13	P & S [Ro20, Ag1], dielectric properties [Sm8], optical properties [Re4a]	
Ba <sub>3</sub> NiNb <sub>2</sub> O <sub>9</sub>	C	4.074				Ga9	Dielectric properties [Re4a]	
Ba <sub>3</sub> CuNb <sub>2</sub> O <sub>9</sub>	T	8.04		8.40		Bl8	Cubic > 653 °K	
Ba <sub>3</sub> ZnNb <sub>2</sub> O <sub>9</sub>	C	8.166				Ve2	P & S [Ga13, Ag1]	
Ba <sub>3</sub> CdNb <sub>2</sub> O <sub>9</sub>	C	4.094				Ga9		
Ba <sub>3</sub> BaNb <sub>2</sub> O <sub>9</sub>	C	4.168				Ga9	P & S [Bl8], see Fig. 1(c)	
Ba <sub>3</sub> PbNb <sub>2</sub> O <sub>9</sub>	H	6.01		8.0		Ga9		
Sr <sub>3</sub> MgNb <sub>2</sub> O <sub>9</sub>	C	4.26				Ga9	See Fig. 1(c)	
Sr <sub>3</sub> CaNb <sub>2</sub> O <sub>9</sub>	H	5.66		6.98		Ga9	See Fig. 1(c)	
Sr <sub>3</sub> FeNb <sub>2</sub> O <sub>9</sub>	H	5.76		7.16		Ga9	See Fig. 1(c)	
Sr <sub>3</sub> CoNb <sub>2</sub> O <sub>9</sub>	T	3.997		4.018		Ga9		
Sr <sub>3</sub> NiNb <sub>2</sub> O <sub>9</sub>	C	8.01				Bl8	P & S [Ag1], optical properties of S.S. with Ba and Ca [Re4a], see Fig. 1(c)	
Sr <sub>3</sub> NbNb <sub>2</sub> O <sub>9</sub>	H	5.64		6.90		Ga9	Prop. [Ve2]	
Sr <sub>3</sub> CuNb <sub>2</sub> O <sub>9</sub>	T	7.888		8.148		Ka12	P & S [Ga13], see Fig. 1(c)	
Sr <sub>3</sub> ZnNb <sub>2</sub> O <sub>9</sub>	H	5.66		6.95		Ga9	Distorted perovskite	
Sr <sub>3</sub> CdNb <sub>2</sub> O <sub>9</sub>	C	4.089				Ga9	Dielectric properties [Sm27, Ag1, Ou1, Ou1a, Ou2, Bo5, Is4, Bo16, Be23, Kh5, Kh4, Kh8, Sm14, Sm20, Sm29, Sm8, Cr66], crystal growth [Ba5, My3], electrooptic effect [Sm29]	
Ca <sub>3</sub> CaNb <sub>2</sub> O <sub>9</sub>	C					Bl8	No cell dimensions	
Ca <sub>3</sub> NiNb <sub>2</sub> O <sub>9</sub>	C	3.88				Ag1	Dielectric properties [Bo5, Ag1]	
Pb <sub>3</sub> MgNb <sub>2</sub> O <sub>9</sub>	C	4.04				Ag1	Dielectric properties [Ag1, Sm8, Bo5, Is4], crystal growth [Bo5, My3], S.S. with Mg [Sm20, Sm27, Sm14, Is4, Cr66], S.S. with Pb(Ti, Zr)O <sub>3</sub> [Bu10], electrooptic effect [Sm29a]	
Pb <sub>3</sub> MnNb <sub>2</sub> O <sub>9</sub>							Dielectric properties [Bo5, Ag1]	
Pb <sub>3</sub> CoNb <sub>2</sub> O <sub>9</sub>	C	4.05				Bo5	Dielectric properties [Bo5, Kh7, Be23a]	
Pb <sub>3</sub> NiNb <sub>2</sub> O <sub>9</sub>	C	4.02				Ag1	Dielectric properties [Ve4]	
Pb <sub>3</sub> ZnNb <sub>2</sub> O <sub>9</sub>	C						Dielectric properties [Ve2, Ve3, Ve4]	

in 3.3.4, Tab.

Compound	Sym	a Å	b Å	c Å	angle	Ref.	Remarks	Magnetic Data in 3.3.4, Tab.
A <sub>3</sub> BB <sub>2</sub> X <sub>6</sub> (continued)								
Ba <sub>3</sub> MgRu <sub>2</sub> O <sub>9</sub>	H					Ca2	Hex (6L), magnetic properties 84 < T < 948 °K, Θ <sub>N</sub> = 390 °K [Ca2]	
Ba <sub>3</sub> MgSb <sub>2</sub> O <sub>9</sub>	H	5.83		14.26		Bl8	Hex (6L)	
Ba <sub>3</sub> CaSb <sub>2</sub> O <sub>9</sub>	H	5.99		14.84		Bl8	Hex (6L)	
Ba <sub>3</sub> CoSb <sub>2</sub> O <sub>9</sub>	H	5.84		14.35		Bl8	Hex (6L)	
Ba <sub>3</sub> NiSb <sub>2</sub> O <sub>9</sub>	H	5.82		14.25		Bl8	Hex (6L), optical properties of S.S. with Sr and Nb [Re4a]	
Ba <sub>3</sub> CuSb <sub>2</sub> O <sub>9</sub>	H	5.82		14.22		Bl8	Hex (6L)	
Ba <sub>3</sub> SrSb <sub>2</sub> O <sub>9</sub>	H	6.15		15.6		Bl8	Hex (6L)	
Ba <sub>3</sub> BaSb <sub>2</sub> O <sub>9</sub>	H	6.09		15.9		Bl8	Hex (6L)	
Sr <sub>3</sub> MgSb <sub>2</sub> O <sub>9</sub>	C	7.96				Bl8		
Sr <sub>3</sub> CaSb <sub>2</sub> O <sub>9</sub>	C	8.17				Bl8		
Sr <sub>3</sub> CoSb <sub>2</sub> O <sub>9</sub>	C	7.99				Bl8		
Sr <sub>3</sub> NiSb <sub>2</sub> O <sub>9</sub>	C	3.98				Re4a	Cell probably doubled, optical properties [Re4a]	
Sr <sub>3</sub> CuSb <sub>2</sub> O <sub>9</sub>	C	7.84				Bl8	Optical properties [Re4b]	
Sr <sub>3</sub> SrSb <sub>2</sub> O <sub>9</sub>	T	5.78	5.80	8.19		Bl8		
Sr <sub>3</sub> La <sub>0.5</sub> Li <sub>0.5</sub> Sb <sub>2</sub> O <sub>9</sub>	O	5.62	5.68	8.34		Bl8		
Ba <sub>3</sub> MgTa <sub>2</sub> O <sub>9</sub>	O	5.782		8.00		Bl8		
Ba <sub>3</sub> CaTa <sub>2</sub> O <sub>9</sub>	H	5.895		7.067		Ga10	Crystal growth [Ga7], see Fig. 1 (c)	
Ba <sub>3</sub> MnTa <sub>2</sub> O <sub>9</sub>	H	5.819		7.284		Ga10	P & S [Ga8], crystal growth [Ga7], see Fig. 1 (c)	
Ba <sub>3</sub> FeTa <sub>2</sub> O <sub>9</sub>	H	4.10		7.127		Ga10	See Fig. 1 (c)	
Ba <sub>3</sub> CoTa <sub>2</sub> O <sub>9</sub>	C	5.776				Ga13		
Ba <sub>3</sub> NiTa <sub>2</sub> O <sub>9</sub>	H	5.758		7.082		Ga10	P & S [Ro20], see Fig. 1 (c)	
Ba <sub>3</sub> CuTa <sub>2</sub> O <sub>9</sub>	T	8.132		7.052		Ga10	P & S [Ro20], crystal growth [Ga7], optical properties [Re4a], see Fig. 1 (c)	
Ba <sub>3</sub> ZnTa <sub>2</sub> O <sub>9</sub>	H	5.782		8.432		Ka12	P, S + Prop. [Ve2, Ve3]	
Ba <sub>3</sub> SrTa <sub>2</sub> O <sub>9</sub>	H	5.95		7.097		Ga10	P & S [Ca13], crystal growth [Ga7], see Fig. 1 (c)	
Ba <sub>3</sub> CdTa <sub>2</sub> O <sub>9</sub>	C	4.167		7.47		Ga11	P & S [Ca13], see Fig. 1 (c)	
Ba <sub>3</sub> BaTa <sub>2</sub> O <sub>9</sub>	C	6.10				Ga10	See Fig. 1 (c)	
Ba <sub>3</sub> PbTa <sub>2</sub> O <sub>9</sub>	C	4.250		8.05		Bl8		
Ba <sub>2</sub> Zn <sub>0.5</sub> Ni <sub>0.5</sub> Ta <sub>2</sub> O <sub>9</sub>	C	4.08				Ga10		
Sr <sub>3</sub> MgTa <sub>2</sub> O <sub>9</sub>	C	5.652		6.951		Ga13	P & S [Ro20], see Fig. 1 (c)	
Sr <sub>3</sub> CaTa <sub>2</sub> O <sub>9</sub>	H	5.764		7.096		Ga10	See Fig. 1 (c)	
Sr <sub>3</sub> CoTa <sub>2</sub> O <sub>9</sub>	H	5.630		6.937		Ga10	P & S [Ca13], see Fig. 1 (c)	
Sr <sub>3</sub> NiTa <sub>2</sub> O <sub>9</sub>	H	5.607		6.923		Ga10	P & S [Ca13], see Fig. 1 (c)	
Sr <sub>3</sub> CuTa <sub>2</sub> O <sub>9</sub>	T	7.860		8.248		Ka12	P, S + Prop. [Ve2, Ve3]	
Sr <sub>3</sub> ZnTa <sub>2</sub> O <sub>9</sub>	H	5.664		6.951		Ga10	P & S [Ca13], see Fig. 1 (c)	
Pb <sub>3</sub> MgTa <sub>2</sub> O <sub>9</sub>	C	4.03				Bo5	Prep. [Agf], electrooptic effect [Sm29a]	
Pb <sub>3</sub> CoTa <sub>2</sub> O <sub>9</sub>	C	4.02				Bo5		
Pb <sub>3</sub> NiTa <sub>2</sub> O <sub>9</sub>	C	4.02				Bo5	Prep. [Agf]	

Compound	Sym	a Å	b Å	c Å	angle	Ref.	Remarks	Magnetic Data
La <sub>2</sub> Co <sub>2</sub> B <sup>8+</sup> O <sub>9</sub>	O	5.58	5.58	7.89		Bl8		in 3.3.4, Tab.
La <sub>2</sub> Co <sub>2</sub> NbO <sub>9</sub>	O	5.57	5.57	7.87		Bl8		
La <sub>2</sub> Co <sub>2</sub> SbO <sub>9</sub>	O							
A <sub>3</sub> B <sub>2</sub> B <sup>8+</sup> O <sub>6</sub>								
Ba <sub>3</sub> Cr <sub>2</sub> MoO <sub>9</sub>	H	5.72		14.02		Pa7	Hex (6L)	
Ba <sub>3</sub> Fe <sub>2</sub> MoO <sub>9</sub>	H	5.74		14.08		Bl8	Hex (6L)	
Ba <sub>3</sub> In <sub>2</sub> MoO <sub>9</sub>	C	4.168				Ka12		
Ba <sub>3</sub> Bi <sub>2</sub> MoO <sub>9</sub>	O	6.148	6.184	8.642		Ve2	P & S [Vi3, Ve3], dielectric properties [Vi2b]	
	C	4.37				Vi2b	T > 500 °C	
Ba <sub>3</sub> LiNbMoO <sub>9</sub>	R	4.091				Ka12		
Ba <sub>3</sub> LiTaMoO <sub>9</sub>	C	4.090				Ka12		
Pb <sub>3</sub> Bi <sub>2</sub> MoO <sub>9</sub>	T	11.262		11.452		Vi3	Defect pyrochlore type	
Ba <sub>3</sub> Sc <sub>2</sub> WO <sub>9</sub>	C	8.24			α = 89° 50'	Fv14		
Ba <sub>3</sub> Cr <sub>2</sub> WO <sub>9</sub>	H	5.75		14.35		Pa7	P & S [Ga15], dielectric properties [Ka12]	
Ba <sub>3</sub> Fe <sub>2</sub> WO <sub>9</sub>	H	5.74		14.08		Bl8	Hex (6L)	
Ba <sub>3</sub> Co <sub>2</sub> WO <sub>9</sub>	H	5.74		14.10		Bl8	Hex (6L)	
Ba <sub>3</sub> Y <sub>2</sub> WO <sub>9</sub>	C	8.374				Ga15		
Ba <sub>3</sub> Rh <sub>2</sub> WO <sub>9</sub>	H	5.74		14.15		Bl8	Hex (6L)	
Ba <sub>3</sub> In <sub>2</sub> WO <sub>9</sub>	C	8.321				Ga15	Structure + Prop. [Ka12]	
Ba <sub>3</sub> La <sub>2</sub> WO <sub>9</sub>	C	8.58				Bl8		
Ba <sub>3</sub> Nd <sub>2</sub> WO <sub>9</sub>	C	8.513				Ga15		
Ba <sub>3</sub> Eu <sub>2</sub> WO <sub>9</sub>	C	8.605				Ga15		
Ba <sub>3</sub> Gd <sub>2</sub> WO <sub>9</sub>	C	8.411				Ga15	P & S [Bl8]	
Ba <sub>3</sub> Dy <sub>2</sub> WO <sub>9</sub>	C	8.386				Ga15	Structure + Prop. [Ka12]	
Ba <sub>3</sub> Ho <sub>2</sub> WO <sub>9</sub>	C	4.252				Ka12	Probably ordered	
Ba <sub>3</sub> Er <sub>2</sub> WO <sub>9</sub>	C	8.386				Ga15		
Ba <sub>3</sub> Yb <sub>2</sub> WO <sub>9</sub>						Ga15	No cell dimensions	
Ba <sub>3</sub> Lu <sub>2</sub> WO <sub>9</sub>						Ga15	No cell dimensions	
Ba <sub>3</sub> Bi <sub>2</sub> WO <sub>9</sub>	R	6.131			α = 60° 23'	Ve2	Dielectric properties [Vi3, Ve3, Vi2b]	
Ba <sub>3</sub> LiNbWO <sub>9</sub>	R	4.098			α = 89° 52'	Ka12		
Ba <sub>3</sub> LiTaWO <sub>9</sub>	R	4.095			α = 89° 53'	Ka12		
Sr <sub>3</sub> Fe <sub>2</sub> WO <sub>9</sub>	T	3.945		3.951		Ga15	P & S [Bl8], S.S. with Sr <sub>3</sub> Fe <sub>2</sub> UO <sub>9</sub> [Se6a]	
SrLa <sub>2</sub> Mg <sub>2</sub> WO <sub>9</sub>	C	7.91				Bl8		
SrLa <sub>2</sub> Co <sub>2</sub> WO <sub>9</sub>	C	7.90				Bl8		
Pb <sub>3</sub> Sc <sub>2</sub> WO <sub>9</sub>	C	8.134				Ve3	Dielectric properties [Ve4, Ve2, Ve3, To1]	
Pb <sub>3</sub> Mn <sub>2</sub> WO <sub>9</sub>	C					Ro8	No cell dimensions, Prop. [Ve4, Ro8], S.S. with PbTiO <sub>3</sub> [Di5a]	6
Pb <sub>3</sub> Fe <sub>2</sub> WO <sub>9</sub>	C	4.02				Ro8	Prop. [Ag1, Ro8, Sm10, Sm16, Sm28, To5, To11, Te13, Pl1, Ki6], B site ordering [Yu9]	6
Pb <sub>3</sub> Bi <sub>2</sub> WO <sub>9</sub>	T	10.637		10.799		Vi3	Defect pyrochlore type	

Compound	Sym	a Å	b Å	c Å	angle	Ref.	Remarks	Magnetic Data
A <sub>3</sub> B <sub>2</sub> B <sup>6+</sup> O <sub>9</sub> (continued)								
Pb <sub>3</sub> ScMnWO <sub>9</sub>						<i>Ve4</i>	No cell dimensions	6
Pb <sub>3</sub> CrMnWO <sub>9</sub>						<i>Ve4</i>	No cell dimensions	6
Pb <sub>3</sub> FeMnWO <sub>9</sub>						<i>Ve4</i>	No cell dimensions	6
Pb <sub>3</sub> CdMnWO <sub>9</sub>	O	5.80	5.90	8.138		<i>Ro8</i>	Prop. [ <i>Ve4</i> , <i>Ro8</i> ]	6
Pb <sub>3</sub> CoFeWO <sub>9</sub>						<i>Ve4</i>	No cell dimensions	6
Pb <sub>3</sub> LiNbWO <sub>9</sub>	C	8.090				<i>Vi5</i>	Dielectric properties [ <i>Ve2</i> , <i>Ve4</i> , <i>Vi5</i> ]	
Pb <sub>3</sub> Cd <sub>1/3</sub> Nb <sub>2/3</sub> WO <sub>9</sub>						<i>To1</i>	Dielectric properties [ <i>Ve2</i> , <i>Ve4</i> , <i>Vi5</i> ]	
Ba <sub>3</sub> Cr <sub>2</sub> ReO <sub>9</sub>	O	5.813	5.877	8.178		<i>Sl8</i>	Hex (6L)	
Ba <sub>3</sub> Fe <sub>2</sub> ReO <sub>9</sub>	H	5.70		13.8		<i>Sl8</i>	Hex (6L)	
Ba <sub>3</sub> Cr <sub>2</sub> ReO <sub>9</sub>	C	5.81		14.10		<i>Sl8</i>	Hex (6L)	
Sr <sub>3</sub> Cr <sub>2</sub> ReO <sub>9</sub>	C	8.015				<i>Sl8</i>		
Sr <sub>3</sub> Fe <sub>2</sub> ReO <sub>9</sub>	C	7.890				<i>Sl8</i>		
Sr <sub>3</sub> In <sub>2</sub> ReO <sub>9</sub>	C	8.297				<i>Sl8</i>		
Ba <sub>3</sub> Sc <sub>2</sub> UO <sub>9</sub>	C	8.49				<i>Sl5</i>		
Ba <sub>3</sub> Cr <sub>2</sub> UO <sub>9</sub>	H	5.82		14.6		<i>Sl5</i>	Hex (6L)	
Ba <sub>3</sub> Fe <sub>2</sub> UO <sub>9</sub>	C	8.232				<i>Sl5</i>	P & S [ <i>Ro14</i> ]	
Ba <sub>3</sub> Y <sub>2</sub> UO <sub>9</sub>	C	8.70				<i>Sl5</i>	Slight distortion	
Ba <sub>3</sub> In <sub>2</sub> UO <sub>9</sub>	C	8.512				<i>Sl5</i>		
Sr <sub>3</sub> Cr <sub>2</sub> UO <sub>9</sub>	C	8.00				<i>Sl5</i>		
Sr <sub>3</sub> Fe <sub>2</sub> UO <sub>9</sub>	C	8.066				<i>Ro14</i>	Prop. [ <i>Be51</i> ], S. S. with Sr <sub>3</sub> Fe <sub>2</sub> WO <sub>9</sub> [ <i>Se6a</i> ]	6
Tab. 2d. A <sup>2+</sup> (B <sub>2</sub> B <sub>0</sub> B <sub>2</sub> <sup>1+</sup> )O <sub>3</sub>								
Compound	Sym	a Å	b Å	c Å	angle	Ref.	Remarks	Magnetic Data
Ba[Zn <sub>0.2</sub> Fe <sub>0.2</sub> Nb <sub>0.6</sub> ]O <sub>3</sub>	C	4.08				<i>Ga13</i>		
Ba[Zn <sub>0.2</sub> Fe <sub>0.2</sub> Ta <sub>0.6</sub> ]O <sub>3</sub>	C	4.08				<i>Ga13</i>		
Sr[Zn <sub>0.2</sub> Fe <sub>0.2</sub> Ta <sub>0.6</sub> ]O <sub>3</sub>	C	4.01				<i>Ga13</i>		
Ba[Li <sub>0.25</sub> Nb <sub>0.75</sub> ]O <sub>3</sub>	C	4.095				<i>Ka12</i>		
Ba[Na <sub>0.25</sub> Nb <sub>0.75</sub> ]O <sub>3</sub>	C	4.107				<i>Ka12</i>		
Ba[Na <sub>0.25</sub> Ta <sub>0.75</sub> ]O <sub>3</sub>	C	4.137				<i>Ga6</i>		
Sr[Na <sub>0.25</sub> Ta <sub>0.75</sub> ]O <sub>3</sub>	C	4.055				<i>Ga6</i>		
Ba[Fe <sub>0.75</sub> Nb <sub>0.25</sub> ]O <sub>3</sub>	C	4.07				<i>Ga13</i>		
Ba[Fe <sub>0.75</sub> Ta <sub>0.25</sub> ]O <sub>3</sub>	C	4.07				<i>Ga13</i>		
Sr[Fe <sub>0.75</sub> Nb <sub>0.25</sub> ]O <sub>3</sub>	C	3.96				<i>Ga13</i>		
Ba[Fe <sub>1/7</sub> Fe <sub>4/7</sub> Ta <sub>4/7</sub> ]O <sub>3</sub>	C	4.08				<i>Ga13</i>		
Ba[Co <sub>1/7</sub> Co <sub>4/7</sub> Ta <sub>4/7</sub> ]O <sub>3</sub>	C	4.09				<i>Ga13</i>		
Sr[Co <sub>1/7</sub> Co <sub>4/7</sub> Ta <sub>4/7</sub> ]O <sub>3</sub>	C	4.00				<i>Ga13</i>		
Ba[Na <sub>0.4</sub> W <sub>0.6</sub> ]O <sub>3</sub>	C	4.158				<i>Ka12</i>		

### 3.2 Descriptions of perovskite-related structures

#### 3.2.1 A-cation vacancies

##### 3.2.1.1 No A cations

Because a skeleton of shared-corner octahedra is stable, it is possible to remove all the A cations from the perovskite structure without collapsing the  $BX_3$  subarray. In the case of  $\square \text{ReO}_3$ , for example, the structure remains cubic. However, a partial or a complete collapse of the skeleton is found in many  $\square BX_3$  compounds. The completely collapsed structure has hexagonal-close-packed X layers with one-third of the octahedral sites occupied by B atoms, as indicated in Fig. 19. This results in a simple-cubic array of B cations with corner-shared octahedra having a B-X-B angle of  $132^\circ$ . For comparison, Fig. 19 also shows the corner-shared octahedra across a close-packed  $\square X_3$  plane of the cubic  $\square \text{ReO}_3$  structure, where the B-X-B angle is  $180^\circ$ . It is possible to go from one structure to the other by a simple increase of the B-X-B angle, the B cations forming a simple-cubic array in all structures. In the partially collapsed structure, represented by  $\text{CrF}_3$ , and B-X-B angle is intermediate,  $\approx 150^\circ$ . Trifluorides of the first-row transition metals have the partially collapsed structure, those of the second- and third-row transition metals have the  $\text{ReO}_3$  structure where the number of outer  $d$  electrons per cation is  $\leq 3$ , but the completely collapsed structure where it is  $\geq 6$ . The B cations of the latter group either have no atomic moment ( $\text{Rh}^{\text{III}}$  and  $\text{Ir}^{\text{III}}$  have  $t_{2g}^6 e_g^0$ ) or disproportionate into magnetic and nonmagnetic ions ( $\text{Pd}^{2+}$ ,  $t_{2g}^6 e_g^2$  and  $\text{Pd}^{\text{IV}}$ ,  $t_{2g}^6 e_g^0$ ), so that there are no magnetic interactions between neighboring cations. The other trifluorides, on the other hand, are all antiferromagnetic, and coupling between like atoms of the second and third long periods is stronger than that between like atoms of the first long period. Since the B-X-B superexchange interaction is enhanced by a larger B-X-B angle, it is reasonable to assume that the interactions between neighboring B cations stabilizes the  $\text{ReO}_3$  structure. These interactions may be either weaker interactions between localized electrons, as in the magnetic fluorides, or stronger interactions, as in metallic  $\text{ReO}_3$ . In this connection, stabilization of the cubic structure in the tungsten bronzes  $A_x^m \text{WO}_3$  for  $m x > 0.3$  is significant. The conduction electrons introduce cation-anion-cation interactions while simultaneously reducing the energy gained by a ferroelectric distortion.

Electron-ordering distortions may be superposed on the array of corner-shared octahedra.  $\text{MnF}_3$ , for example, exhibits the Jahn-Teller distortions shown in Fig. 10(a) superposed on the partially collapsed structure.  $\text{WO}_3$ , on the other hand, exhibits several low-temperature phases characteristic of an interplay of antiferroelectric distortions and different degrees of the collapse of the B-X-B angle.

##### 3.2.1.2 The bronze structures

Although  $\square BX_3$  compounds with the  $\text{ReO}_3$  structure and cubic  $\text{ABX}_3$  compounds have the same  $BX_3$  array, complete solid solutions  $\square_x A_{1-x} BX_3$ ,  $0 \leq x \leq 1$ , are not possible. Although there is no ordering of the vacancies for larger  $x$ , except for  $\text{Na}_{0.75} \text{WO}_3$  [A11], for smaller  $x$  there is ordering accompanied by a collapse of the  $BX_3$  array within basal planes perpendicular to a unique axis. Such a collapse creates the tetragonal and hexagonal tunnel structures of Fig. 20. The tetragonal structure contains three types of tunnels, one containing cubic, twelve-coordinated  $A'$  sites, one containing pentagonal-prism, fifteen-coordinated  $A''$  sites, and one small tunnel containing nine-coordinated  $A'''$  sites, which are only occupied by  $\text{Li}^+$  ions. Without  $\text{Li}^+$  ions, all these sites are filled at  $A_{0.2} A_{0.4}' BX_3$ . This phase, which may occur for a

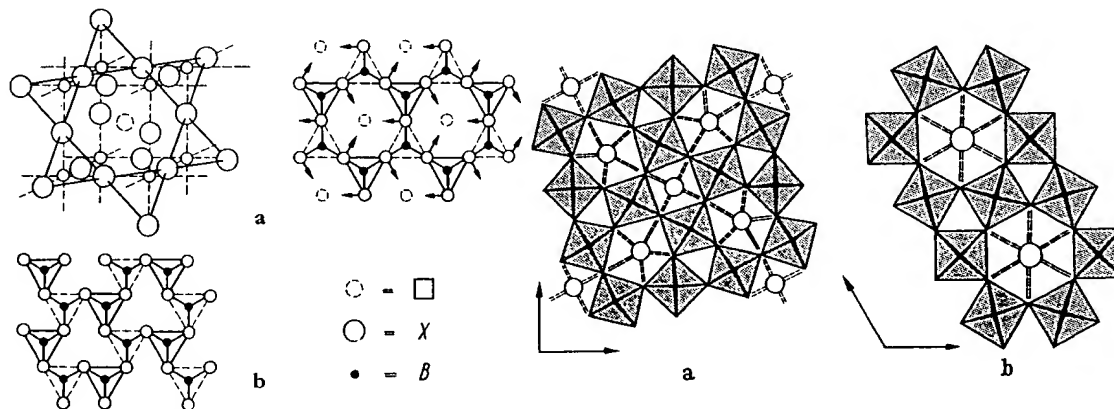


Fig. 19. Projections on B-cation planes of two  $\square BX_3$  structures. Triangles in full and dotted lines represent faces of octahedra below or above the B-cation plane. a) Cubic  $\square \text{ReO}_3$  structure  $\text{DO}_3$ . Arrows indicate cooperative atomic motions that collapse the structure. b) Completely collapsed  $\square \text{RhF}_3$  structure.

Fig. 20. Bronze structures found in  $A_x \square_{1-x} BX_3$  systems. a) Tetragonal (II) structure occurring for  $x \leq 0.6$ . b) Hexagonal structure occurring for  $x \leq 0.33$  [Wal].



range of  $x \leq 0.6$ , is labelled tetragonal (II) in Tab. 3 to distinguish it from the antiferroelectric tetragonal (I) phase of  $\text{WO}_3$ . The hexagonal structure contains hexagonal-prism, eighteen-coordinated  $A$  sites and is restricted to the range of composition  $x \leq 0.33$ . An orthorhombic tunnel structure has also been identified for  $\text{AB}_2\text{O}_6$  compounds [Ga15a].

Tab. 3. Color vs.  $x$  for  $\text{Na}_x\text{WO}_3$  and compositional ranges for the bronze structures in the  $\text{A}_{1-x}^{1+}\text{WO}_3$  perovskites. Adapted from [Di3]

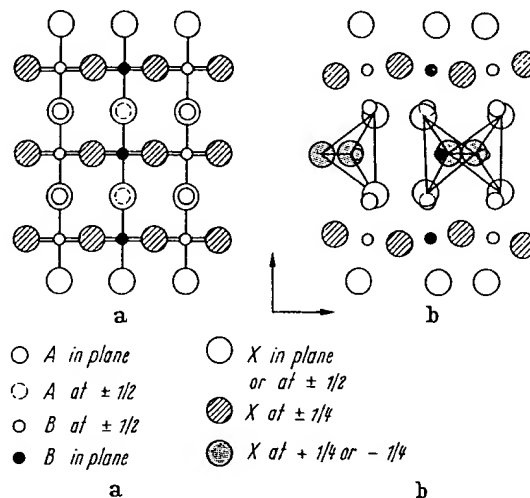
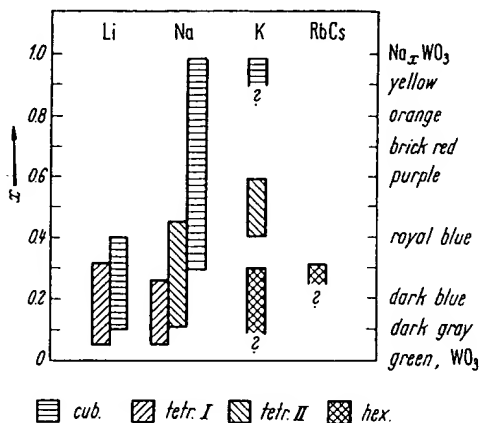


Fig. 21. Projections onto (110) planes of a) cubic perovskite and b) brownmillerite structures. Brownmillerite structure is formed by removing alternate [110] strings of oxygen from central row of a) and regrouping remaining oxygen into the tetrahedra shown in b) [Wat].

### 3.2.2 Anion-deficient compounds

#### 3.2.2.1 Compounds $\text{ABX}_{3-x}$

Several systems  $\text{ABX}_{3-x}$ , where  $0 \leq x \leq 0.5$ , have been reported as anion-deficient perovskites.  $\text{SrTiO}_{2.5}$  and  $\text{SrVO}_{2.5}$ , for example, both give simple x-ray powder patterns in qualitative agreement with the assumption of a perovskite structure having one-sixth of the anions missing at random. Further, the homogeneity range of  $\text{SrTiO}_{3-x}$  is reported [Wat] to extend over  $0 \leq x \leq 0.5$  without any change of lattice parameter. However, if an anion is removed from a close packed structure, the metal atoms to which it was formerly bonded will have highly unsymmetrical coordination, and some local rearrangement of the anion can be expected. The nature of this local rearrangement depends upon the character of the B cation. In order to learn what rearrangements may occur locally, it is necessary to examine those special cases where long-range order occurs, since local changes of cation coordination are difficult to detect by x-ray diffraction and have not been investigated by other methods.

In the system  $\text{SrFe}_{2-x}^{3+}\text{Fe}_{1-x}^{4+}\text{O}_{3-x}$ ,  $0 \leq x \leq 0.5$ , it is known that the  $\text{Fe}^{3+}$  ions are stable in either tetrahedral or octahedral coordination. Therefore, it is reasonable to anticipate the creation of fourfold coordination about half of the  $\text{Fe}^{3+}$  ions in the system. This is possible because the  $d$  electrons of  $\text{Fe}^{3+}$  ions are localized, so that  $\text{Fe}^{3+}$  and  $\text{Fe}^{4+}$  ions are distinguishable, even though the  $d$  electrons of the end member  $\text{SrFe}^{4+}\text{O}_3$  appear to be collective. Support for the creation of tetrahedral sites, as well as a suggestion of how the tetrahedra might be arranged, is given by  $\text{Ca}_2\text{Fe}_2\text{O}_5$ , which has the brownmillerite structure [Be41] of Fig. 21. Within every other (001)  $\text{BX}_2$  plane of the cubic perovskite, alternate [110] rows of anions are removed. The remaining anions in these planes are displaced alternately along  $[\bar{1}\bar{1}0]$  and  $[\bar{1}\bar{1}0]$  directions toward the anion vacancies, the B cations shifting slightly also to maintain equal B-X distances with all four near-neighbor anions. The result is fourfold coordination for all B cations in these (001)  $\text{BX}$  planes, sixfold coordination for all B cations in the alternate (001)  $\text{BX}_2$  planes.

The x-ray pattern of  $\text{K}_2\text{Ti}_2\text{O}_5$  has a strong resemblance to that of perovskite. However,  $\text{KTiO}_{2.5}$  is not an anion-deficient perovskite, but is completely ordered, each  $\text{Ti}^{4+}$  ion having five oxygen near neighbors forming a trigonal bipyramid [An3]. It has little similarity to perovskite.

The oxygen-deficient, tetragonal compounds  $(\text{Ba}_{2x}\text{Bi}_{1-2x})\text{BiO}_{3-x}$ ,  $0.22 < x < 0.5$ , retain an octahedral grouping for Bi in the B sites, but the A positions have only six oxygen near neighbors, two each at 2.7, 3.1 and 3.6 Å [Au1].

These examples indicate that a variety of orderings must occur in anion-deficient perovskites. Further structural work needs to be done.

3.2.2.2 Alloys  $M^cX_{1-x}M^f$ 

Since the alloys  $M^cX_{1-x}M^f$  are generally considered to represent interstitial X atoms in an ordered, face-centered-cubic  $M^cM^f$  alloy, it is not surprising that the phase is stable over a considerable range of anion deficiency. Since these alloys are metallic, it is probable that the X-atom vacancies are randomly distributed.

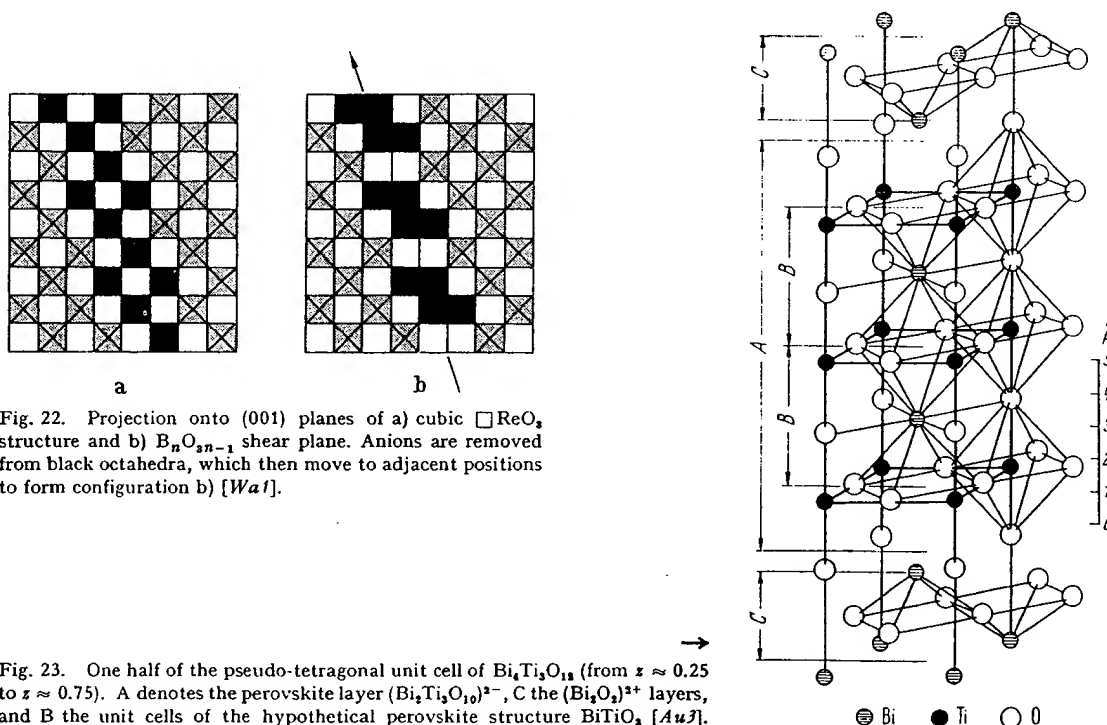
3.2.2.3 Shear structures  $\square BO_{3-x}$ 

Ranges of composition have been reported for  $BO_{3-x}$ , where B = Mo or W. MAGNÉLI [Ma14] has shown that these compositional ranges consist of a series of discrete phases having an x-ray diffraction pattern dominated by a cubic  $\square ReO_3$ -type ( $DO_3$ ) subcell, but exhibiting superlattice lines. The superlattice of any discrete phase is not due to an ordering of anion vacancies within this basic structure, but to a regular interruption of the  $DO_3$  structure by planes of discontinuity across which octahedra share edges rather than corners. In these structures the oxygen vacancies condense into regularly spaced planes and are then eliminated by a shear displacement of the type shown schematically in Fig. 22. These "shear" planes may be constituted in different ways: For the series of phases  $B_nO_{3n-2}$ , six octahedra in a group share edges, and for the phases  $B_nO_{3n-1}$  groups of four octahedra share edges. In both cases the discontinuities continue in two dimensions throughout the structure where they separate  $DO_3$  blocks  $n$  octahedra thick. The  $\beta-WO_{3-x}$  phases,  $0.10 \leq x \leq 0.17$ , belong to the series  $B_nO_{3n-2}$  with  $12 < n \leq 20$ . The observed compositional range  $(W, Mo)O_{3-x}$ ,  $0.07 \leq x \leq 0.12$ , contains six discrete  $B_nO_{3n-1}$  phases corresponding to  $n = 8, 9, 10, 11, 12$ , and  $14$  [Ma17a]. The origin of the shear planes appears to be an interplay between electrostatic and elastic forces: Electrostatic repulsive energies between B cations sharing common octahedral-site edges is minimized by cationic displacements (of ferroelectric type) away from the center of symmetry of the interstice and the shared octahedral edge. These displacements can be cooperative, costing a minimum of elastic energy, if the shared edges are coplanar. The origin of the regular spacing between planes is not established. Presumably it is primarily due to elastic energy, although collective-electron effects [Go11] probably play a contributing role.

## 3.2.3 Structures deficient in B cations

## 3.2.3.1 Bismuth compounds

Bismuth compounds with chemical formula  $(Bi_2A_{m-2})B_{m-1}O_{3m}$  have the structural formula  $(Bi_2O_2)^{2+}(A_{n-1}B_nO_{3n+1})^{2-}$ ,  $n = m - 1$ . These compounds consist of a regular intergrowth of the perovskite structure with  $Bi_2O_2$  sheets consisting of  $BiO_4$  square pyramids sharing edges [Au2], as indicated in Fig. 23. Between the  $Bi_2O_2$  sheets are  $n$  layers of corner-shared octahedra and  $(n - 1)$  layers of perovskite-type A cations in the twelve-coordinated interstices. Where  $n = 1$ , the pyramidal sheets alternate with



single octahedral layers, and no sites are available for A cations. This particular phase has been prepared in a large number of oxides and oxyfluorides, where  $B = \text{Ti, Nb, Ta}$  and the O/F ratio depends upon the valencies of the A and B cations (see Tab. 4).

Many of these compounds are reported to exhibit ferroelectric distortions within the perovskite layers, and they will certainly be important for technical applications in the future.

### 3.2.3.2 Hexagonal $A_nB_{n-1}X_{3n}$ structures

As shown in Fig. 1 (c), the cubic perovskite may be indexed on an hexagonal basis. It consists of cubic stacking of close-packed  $AX_3$  layers with B cations in the all-anion octahedral interstices. Within a (110) plane, B-cation octahedra share common corners as shown schematically in Fig. 3(a). In the  $\text{Ba}_3\text{Ta}_4\text{O}_{15}$  structure [Ga5a], the stacking sequence of the  $AX_3$  layers is  $a-b-c-b-c-a$ , as shown in Fig. 24, and the B-cation vacancies are where the stacking is hexagonal. Thus the structure consists of perovskite blocks  $n$   $AX_3$  layers and  $(n-1)$  B layers thick, separated by a stacking fault at a layer of B-cation vacancies. These hexagonal structures appear to be stabilized where the tolerance factor is  $t > 1$ .

### 3.2.3.3 $AX \cdot (ABX_3)_n$ structures

Materials having compositions intermediate between  $ABX_3$  and  $A_2BX_4$  may have similar diffraction patterns. However, this compositional region contains several phases having the structural formula  $AX \cdot (ABX_3)_n$ . Each phase contains perovskite sheets  $n$  units thick separated by AX (NaCl-type) sheets. The limiting composition  $A_2BX_4$ , corresponding to  $n = 1$ , is shown in Fig. 25. It is important for the theory of magnetism because, if A is nonmagnetic, then by symmetry there is no net molecular field within an antiferromagnetic layer from cations in adjacent antiferromagnetic layers. This permits the study of two-dimensional antiferromagnetism. The  $A_2BX_4$  structure also permits the study of  $B^{2+}$  cations in oxides with a smaller B-X-B separation (hence stronger interaction) than is found in the BO compounds with rocksalt structure. The possible significance of this is illustrated by  $\text{La}_2\text{NiO}_4$ . The  $\text{Ni}^{2+}$  electrons of  $e_g$  symmetry appear to be collective in  $\text{La}_2\text{NiO}_4$ , localized in  $\text{NiO}$ .

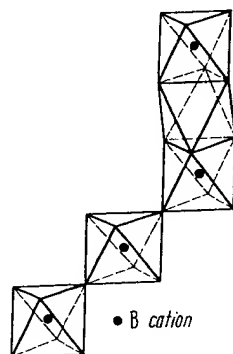


Fig. 24. Schematic (110) projection of the  $\text{Ba}_3\text{Ta}_4\text{O}_{15}$  structure. Horizontal lines refer to  $\text{BaO}_3$  close-packed layers with stacking  $a, b$ , or  $c$ .

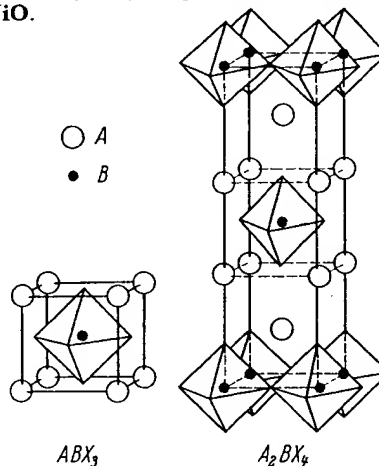


Fig. 25. Comparison of  $ABX_3$  and  $A_2BX_4$  structures [Trf].

### 3.2.4 Data: Crystallographic properties of non- $ABX_3$ compounds of composition $A_xBX_3$ , $\square BX_3$ , $(AX)_n(ABX)_m$ and $\text{Bi}_2\text{O}_2(\text{A}_{n-1}\text{B}_n\text{O}_{3n+1})$ with perovskite-related structure (Tab. 4)

Tab. 4.

See Fig. 20(a) for the tetragonal II bronze structure with  $a \approx 12.5 \text{ \AA}$ ,  $c \approx 4 \text{ \AA}$  and Fig. 20(b) for the hexagonal bronze structure with  $a \approx 7.4 \text{ \AA}$ ,  $c \approx 7.5 \text{ \AA}$ .

Within any section, the compounds are ordered by B-cation atomic number, and the order of the sections is as follows:

Tab. 4a -  $A_xBX_3$

$A_x\text{BO}_3$ ; B = Nb, Mo, Ta, W, Re

$A_x\text{FeF}_3$

Tab. 4b -  $\square BX_3$

Tab. 4c -  $\square BB'X_6$

Tab. 4d -  $(AX)_n(ABX)_m$

X = F<sup>-1</sup>, Cl<sup>-1</sup>; B<sup>2+</sup> = Mg, Cr, Mn, Fe, Co, Ni, Cu, Zn, Cd

X = O<sup>-2</sup>; B = Al, Ti, Cr, Mn, Fe, Co, Ni, Cu, Ga, Ge, Zr, Nb, Mo, Tc, Ru, Rh, Sn, Hf, Ir, Pb, U

Tab. 4e -  $\text{Bi}_2\text{O}_2(\text{A}_{n-1}\text{B}_n\text{O}_{3n+1})$

$n = 1$ ; B = Mo, W       $n = 2$ ; B = Nb, Ta       $n = 3$ ; B = Nb, Ti       $n = 4, 5$  and 8; B = Ti

For abbreviations, see p. 131. Tab. 4a. $A_2BX_3$ compounds							Magnetic Data
Compound	Sym	a Å	b Å	c Å	angle	Ref.	
$A_2NbO_3$	O	12.17	20.5	7.87		<i>Fv1b</i>	Structure and review [ <i>Gal15a</i> ], S.S. with (Pb, Ca, $Sr_{0.5}NbO_3$ [ <i>Su4c</i> , <i>Fv1b</i> , <i>Is3a</i> ], dielectric properties [ <i>Gl0</i> ]  Studied $x = 0.5 \dots 1.0$  Dielectric properties [ <i>Go20</i> , <i>Su4b</i> ], S.S. with (Ba, Sr) $Nb_2O_6$ [ <i>Ba23c</i> , <i>Fv1b</i> , <i>Is2a</i> ], Ti, <i>Kv7</i> , <i>Sm16a</i> , <i>Su4c</i> ], P & S [ <i>Ro16a</i> ], S.S. with Ti, Zr, Sn [ <i>Su1a</i> , <i>Su4b</i> , <i>Su4c</i> ], S.S. with Li, Na, K, Rb, Cs, Y, La, Sm [ <i>Su4b</i> , <i>Su4c</i> ]  Prep. $T < 1250^\circ C$ $T = 570^\circ C$ P & S [ <i>Ke8</i> , <i>Ro13</i> , <i>Sa6a</i> ]; dielectric properties, S.S. with $KSr_2Nb_2O_{15}$ [ <i>Bu5</i> ] P & S [ <i>Ke8</i> , <i>Ro13</i> ]  P & S [ <i>Ke8</i> , <i>Ro13</i> ] P & S [ <i>Ke8</i> , <i>Ro13</i> ] (Ln = Sm $\dots$ Lu) not able to be prepared P & S [ <i>Ko10</i> ], detailed structure [ <i>Tr7</i> ]  P & S [ <i>Ko10</i> ]  $T_{melt} = 1395^\circ C$ Dielectric and optical properties [ <i>Val3</i> , <i>Ge14</i> , <i>Sm6a</i> , <i>Bu5a</i> , <i>Val1a</i> ], Raman effect [ <i>Bu4b</i> ]; S.S. with K [ <i>Bu5a</i> ], Sr [ <i>Val1a</i> ]; elastic proper- ties [ <i>Sp0</i> ], piezoelectric properties [ <i>Wal5a</i> ] Dielectric + optical properties [ <i>Gi1a</i> , <i>Bu5</i> ]
$Ba_{0.5}NbO_{3.5}$						<i>Gal4</i>	
$Sr_{0.95}NbO_3$	T	12.60		3.95		<i>Ri3</i>	
$Sr_{0.7}NbO_3$	C	4.016				<i>Ri3</i>	
$Sr_{0.5}NbO_3$	C	3.981				<i>He12a</i>	
$Sr_{0.3}NbO_3$	O	11.021	7.33	5.604		<i>He12a</i>	
$Ca_{0.5}NbO_3$	O	5.764	15.09	5.232		<i>Fr2a</i>	
$Pb_{0.5}NbO_3$	O	17.51	17.81	7.72			
$La_{0.33}NbO_3$	R	8.664			$\alpha = 88^\circ 30'$	<i>Fv1a</i>	
$Ce_{0.33}NbO_3$	T	12.46		3.907		<i>Fr2a</i>	
$Ce_{0.25}NbO_3$	O	3.911	3.917	7.908		<i>Iy1</i>	
$Pr_{0.33}NbO_3$	O	3.901	3.917	7.886		<i>Iy1</i>	
$Nd_{0.33}NbO_3$	O	3.881	3.897	7.843		<i>Ko10</i>	
$Ln_{0.33}NbO_3$	O	3.891	3.915	7.862		<i>Iy1</i>	
$Th_{0.33}NbO_3$	O	3.878	3.907	7.840		<i>Ro13</i>	
$Pa_{0.25}NbO_3$	T	7.783		7.837		<i>Ke6</i>	
$U_{0.25}NbO_3$	T	7.75		7.81		<i>Ke6</i>	
$Np_{0.25}NbO_3$	T	7.727		7.792		<i>Ke6</i>	
$Pu_{0.25}NbO_3$	T	7.69		7.76		<i>Ke6</i>	
$Am_{0.33}NbO_3$	T	7.67		7.74		<i>Ke6</i>	
$Ba_2KNb_2O_{15}$	T	3.819		7.835		<i>Bu5a</i>	
$Ba_2NaNb_2O_{15}$	T	12.55		4.019		<i>Val3</i>	
$Sr_2KNb_2O_{15}$	O	17.626	17.592	3.995			
$Sr_2KNb_2O_{15}$	T	13.47		3.942		<i>Gi1a</i>	

Compound	Sym	a Å	b Å	c Å	angle	Ref.	Remarks	Magnetic Data in 3.3.4, Tab.
$A_xNbO_3$ (continued)								
$Sr_2NaNb_6O_{15}$	O	17.4	17.4	3.90		<i>Va13</i>	Dielectric + optical properties [ <i>Va11a</i> , <i>Va13</i> ]	
$Na_2LaNb_6O_{15}$	C	3.918				<i>Is5b</i>		
$Na_2BiNb_6O_{15}$	C	3.925				<i>Is5b</i>		
$K_3Li_3Nb_6O_{15}$	T	12.47		4.01		<i>Fu2a</i>	Tetr. W bronze type — dielectric + optical properties [ <i>Va12</i> , <i>Va13</i> , <i>Va11a</i> ] P & S [ <i>Is5b</i> ]	
$K_2LaNb_6O_{15}$	T	12.580		3.930		<i>Sc27</i>		
$K_2CeNb_6O_{15}$	T	12.545		3.913		<i>Sc27</i>		
$K_2PrNb_6O_{15}$	T	12.530		3.918		<i>Sc27</i>		
$K_2NdNb_6O_{15}$	T	12.497		3.924		<i>Sc27</i>		
$K_2SmNb_6O_{15}$	T	12.474		3.917		<i>Sc27</i>		
$K_2EuNb_6O_{15}$	T	12.457		3.914		<i>Sc27</i>		
$K_2GdNb_6O_{15}$	T	12.450		3.912		<i>Sc27</i>		
$K_2TbNb_6O_{15}$	T	12.440		3.910		<i>Sc27</i>		
$K_2DyNb_6O_{15}$	T	12.431		3.903		<i>Sc27</i>		
$K_2HoNb_6O_{15}$	T	12.426		3.899		<i>Sc27</i>		
$K_2YNb_6O_{15}$	T	12.424		3.901		<i>Sc27</i>		
$K_2BiNb_6O_{15}$	O	17.75	17.90	7.84		<i>Is5b</i>	P & S [ <i>Kr2</i> , <i>Kr8</i> ]	
$Rb_2LaNb_6O_{15}$	T	12.633		3.945		<i>Sc27</i>		
$Ba_6(Ti_2Nb_6)O_{30}$	T	12.54		4.01		<i>St23</i>	Tetr. W bronze type, structure determined [ <i>Ja9</i> ]	
$Ba_6(Zr_2Nb_6)O_{30}$	T					<i>Fa1</i>	Tetr. W bronze	
$Ba_6(FeNb_6)O_{30}$	O	17.95	17.95	7.98		<i>Is5b</i>	Prop. [ <i>Fa2</i> , <i>Fa1</i> ] S.S. with Nd, Sm, Eu, Gd [ <i>Fa1</i> , <i>Fa2</i> ]	
$Sr_6(FeNb_6)O_{30}$	O	17.50	17.50	7.72		<i>Is5b</i>		
$A_6(B_xNb_{10-z})O_{30}$	T	≈ 12.5		≈ 3.9		<i>Kr2</i>	Tetr. W bronze type, A = Ba, Sr, Pb, Bi, La, Ce, Nd, Sm, Gd, K; B = Fe, Ni, Mg; dielectric properties [ <i>Kr2</i> ] gives review of the tetr. W bronze structure type	
$Ba_9MgNb_{14}O_{45}$	O	18.00	18.00	8.02		<i>Is5b</i>		
$Sr_9MgNb_{14}O_{45}$	O	17.55	17.55	7.82		<i>Is5b</i>		
$Ba_{0.97}Sr_{0.75}Nb_{2.78}O_{5.78}$	T	12.4032		3.9134		<i>Ja8a</i>	T = 25 °C, complete structure determination	
$K_{0.5}NbO_{2.5}F_{0.5}$	T	12.632		3.950		<i>Ma19a</i>	Tetragonal tungsten bronze	
$A_2MoO_3$								
$Rb_{0.97}MoO_3$	H	7.321		7.683		<i>Bi6</i>	High pressure preparation, metallic conductivity, P & S [ <i>Ch1b</i> ]	
$K_{0.93}MoO_3$	C	3.917				<i>Bi6</i>	High pressure preparation, metallic conductivity, P & S [ <i>Ch1b</i> ]	
$K_{0.89}MoO_3$	C	3.920				<i>Bi6</i>	High pressure preparation, metallic conductivity	
$K_{0.8}MoO_3$	T	12.32		3.859		<i>Bi6</i>	High pressure preparation, metallic conductivity, $\Theta_{cs} = 4.2$ °K [ <i>Sl7a</i> ]	

Compound	Sym	a Å	b Å	c Å	angle	Ref.	Remarks	Magnetic Data
$A_x\text{MoO}_3$ (continued)								in 3.3.4, Tab.
$\text{K}_{0.28}\text{MoO}_3$	M	18.249	7.560	9.855	$\beta = 117^\circ 32'$	Gr2	"Blue Mo bronze"; Prep. [Wo10], metallic conductivity [Bo20], structural discussion [St22], optical properties [Di2a]	
$\text{K}_{0.28}\text{MoO}_3$	M	14.278	7.723	6.387	$\beta = 92^\circ 34'$	St24	"Red Mo bronze"; Prep. [Wo10]. Semiconducting [Bo20], structural discussion [St22]	
$\text{Na}_{0.97}\text{MoO}_3$	C	3.853				Bi6	High pressure preparation, $\Theta_{CS} < 1.3^\circ\text{K}$ [St7a]	
$\text{Na}_{0.90}\text{MoO}_3$	C	3.847				Bi6	Complete structure, random vacancies [St25]; optical properties [Di2a]	
$\text{Na}_{0.15}\text{MoO}_{2.83}$	M	9.57	5.50	12.95		St25		
$\text{A}_x\text{TaO}_3$								
$\text{Ba}_{0.5}\text{TaO}_{3-x}$	T	12.60		3.95		Gal4	( $x = 0 \dots 0.5$ ), P & S [Is2a]	
$\text{Ba}_{0.5}\text{TaO}_3$	H	21.14		3.917		La8	Dielectric properties, P & S [Is2a, Gal4], review [Gal5a]	
$\text{Sr}_{0.5}\text{TaO}_{3-x}$	T	12.41		3.90		Gal4	( $x = 0 \dots 0.5$ ), review [Gal5a]	
$\text{Ca}_{0.5}\text{TaO}_3$	C	3.886				Ja7	Review [Gal5a]	
$\text{Pb}_{0.5}\text{TaO}_3$	O	17.635	17.695	7.757		Is9	Review of literature, P & S [Is2a]	
$\text{Pb}_{0.5}\text{TaO}_3$	T	17.71		7.788		Is9	$T = 300^\circ\text{C}$ , tetr. $T > 270^\circ\text{C}$	
$\text{Cu}_{0.5}\text{TaO}_3$	C	7.522		7.913		Ka16	P & S [Sh12], optical properties [Ka16]	
$\text{La}_{0.33}\text{TaO}_3$	T	3.918		7.878		Iy1	P & S [Ke8, Ro13, Tr8], Prep. [Sa6a]	
$\text{Ce}_{0.33}\text{TaO}_3$	T	3.915		7.836		Iy1	P & S [Ke8, Ro13], Prep. [Sa6a]	
$\text{Pr}_{0.33}\text{TaO}_3$	O	3.895	3.910	7.829		Iy1	P & S [Ke8, Ro13], Prep. [Sa6a]	
$\text{Nd}_{0.33}\text{TaO}_3$	O	3.876	3.916	7.829		Iy1	P & S [Ke8, Ro13], Prep. [Sa6a]	
$\text{Sm}_{0.33}\text{TaO}_3$	O	3.882	3.896	7.785		Iy1	P & S [Ke8, Ro13], Prep. [Sa6a]	
$\text{Eu}_{0.33}\text{TaO}_3$	O	3.871	3.885	7.792		Ke8	P & S [Ke8, Ro13]	
$\text{Gd}_{0.33}\text{TaO}_3$	T	3.874		7.795		Iy1	P & S [Ke8, Ro13]	
$\text{Tb}_{0.33}\text{TaO}_3$	T	3.851		7.780		Ke8	P & S [Ke8, Ro13]	
$\text{Dy}_{0.33}\text{TaO}_3$	T	3.847		7.769		Iy1	P & S [Ke8, Ro13]	
$\text{Ho}_{0.33}\text{TaO}_3$	T	3.841		7.756		Iy1	P & S [Ke8]	
$\text{Er}_{0.33}\text{TaO}_3$	T	3.825		7.754		Iy1	P & S [Ke8]	
$\text{Yb}_{0.33}\text{TaO}_3$	M	3.828	7.749	3.839	$\beta = 90^\circ 54'$	Ro13	P & S [Ke8, Tr8, Ro13, Ly1]	
$\text{Y}_{0.33}\text{TaO}_3$	T	3.824		7.758		Iy1	P & S [Ko10]	
$\text{Th}_{0.25}\text{TaO}_3$	C	7.810		7.78		Ke6	P & S [Ko10]	
$\text{Pa}_{0.25}\text{TaO}_3$	T	7.77		7.773		Ke6		
$\text{U}_{0.25}\text{TaO}_3$	T	7.739		7.75		Ke6		
$\text{NP}_{0.25}\text{TaO}_3$	T	7.70		7.731		Ke6		
$\text{Pu}_{0.25}\text{TaO}_3$	T	7.654		7.820		Ke6		
$\text{Am}_{0.33}\text{TaO}_3$	T	3.889				Ke8		
$\text{K}_{0.5}\text{TaO}_{2.5}\text{F}_{0.5}$	T	12.569		3.961		Ma19a	Tetragonal tungsten bronze	

Compound	Sym	a Å	b Å	c Å	angle	Ref.	Remarks	Magnetic Data in 3.3.4, Tab.
$A_xWO_3$								
$CS_{0.32}WO_3$	H	7.42		7.63		Ma17	Superconducting, $\Theta_{cs} = 1.12^\circ K$ [Sw3]	
$CS_{0.30}WO_3$	H	7.38		7.59		Ma17	Thermal expansion to $720^\circ C$ [We15]	
$Rb_{0.32}WO_3$	H	7.386		7.54		Si7	P & S [Ma17], metallic conduction and magnetic susceptibility [Si7, Si9], optical properties [Doo5]	
$Rb_{0.27}WO_3$	H	7.394		7.516		We15	Superconductivity, $\Theta_{cs} = 1.98^\circ K$ [Sw3], thermal expansion to $970^\circ C$ [We15]	
$(NH_4)_{0.33}WO_3$	H	7.395		7.525		Gi1	Superconductivity $2.2^\circ K \geq \Theta_{cs}$ [Gi1]	
$(NH_4)_{0.08}WO_3$	T	7.60		6.36		Ne8a		
$K_{0.9}WO_3$	C	3.926				Bi6	High pressure preparation (metallic conductivity), P & S [Ch1b]	
$K_{0.58}WO_3$	T	12.326		3.845		We15	Magnetic susceptibility ( $x = 0.53$ ) [Ku5], electric properties ( $x = 0.57$ and $0.63$ ) [Si43], thermal expansion to $750^\circ C$ ( $x = 0.3 \dots 0.55$ ) [We15]	
$K_{0.3}WO_3$	H	7.385		7.513		We15	Electric + magnetic properties [Si48, Si9, Si7], S.S. with Li [Ba11], S.S. with Na [Br8], P & S [Ma12, Ma17, De19], review [Di3, Ma15, Ma18, Si9]	
$K_{0.13}WO_3$	H	7.370		7.515		Ba11	Superconductivity, $\Theta_{cs}$ (Hex) = $0.5^\circ K$ , $\Theta_{cs}$ (Tetr.) = $1.5^\circ K$ [Sw3], magnetic properties [Ku5, Fu1, Gr8, Si43]	
$Na_xWO_3$	C	3.8				Br22	$a = (0.0819 x + 3.7846) \text{ Å}$ [Br22, We2]; cubic, $0.26 < x < 1.0$ ; early preparation [Bo17, Wr1, Ph1, Wo1, Sp1, Sp2, Ka5], P & S [Si37, Si38, Si39, Va5, De6, Ha5, Br8, Ha4, Bi6, Ch16]; neutron diffraction ( $0.56 < x < 0.86$ ) [At1]; electrical properties [Hu8, Hu9, Hu10, Mu3, Mu4, Br21, Fu1, Ga2], reviews [Di3, Ma15, Ma18, Ri1, Si7], optical properties [Di3a]	
	T	12.094		3.748		Ma13	$x = 0.28$ , tetragonal II [Ri1]. Superconductivity, $\Theta_{cs} < 1^\circ K$ [Sw3, Ra12], optical properties [Br22, Da3], NMR [Fr18, Fr19, Na12]	
	T	5.248		3.895		Ma16	$x = 0.10$ , tetragonal I [Ri1]; thermal properties [Sh7, Fu1, Ge11, Ta2, Ve11], Na diffusion [Sm6], electrostatic energy calculated [Sm5]	
$Li_{0.30}WO_3$	H	7.405		7.554		Gi1	Metallic conductivity, superconducting $\Theta_{cs} < 1.3^\circ K$ [Gi1]	
$Li_{0.304}WO_3$	C	3.715				Si10	Magnetic properties, Pauli paramagnetic or diamagnetic [Si10, Co17], metallic conductivity [Co17, Si10, Si7, Sh8], P & S [Ma19, Ma16, Si40]	
$Li_{0.30}WO_3$	C	3.718				Co17	Review [Di3]	

Compound	Sym	a Å	b Å	c Å	angle	Ref.	Remarks	Magnetic Data
$A_xWO_3$ (continued)								in 3.3.4, Tab.
$Li_{0.05}WO_3$	C	3.723				Co17	I. R. spectra [Si7a]	
$H_{0.5}WO_3$	C	3.755		3.88		Gi1	Structure determination by x-ray and neutron dif-	
$H_{0.25}WO_3$	T	5.22				Di2	fraction, I. R. spectra [Si7a]	
$H_{0.1}WO_3$	O	7.247	7.502	3.84		Gi1	I. R. spectra [Si7a]	
$Ba_{0.12}WO_3$	T	12.16		3.843		Co19	$x = 0 \dots 0.13$ ; $x_m = 20 \cdot 10^{-6}$ emu/mole, Novel preparation [Co16]; superconductivity, $x = 0.13$ , $\theta_{cs} = 1.9^\circ K$ [Sw4]	
$Ba_{0.10}Na_{0.33}WO_3$	T	12.12		3.834		Co19	Metallic conductivity	
$Ca_xWO_3$	O	7.340	7.420	3.840		Va2	$x = 0.02$ , $0 < x < 0.01$ (monoclinic); $0.01 < x$ < 0.03 (orthorhombic), studied as function of $T$ [Va2, Va4]	
	T	5.240		3.854		Va2	$x = 0.035$ , $0.03 \leq x < 0.40$ (tetragonal); $0.04 < x < 0.095$ (two phase)	
	T	5.292		3.832		Va2	$x = 0.10$ , $0.095 \leq x < 0.105$ (tetragonal); $0.105 \leq x < 0.125$ (cubic $a = 3.790 \text{ Å}$ ); $x > 0.125$ (two phase)	
$Sn_{0.24}WO_3$	H	7.430		7.581		Gi1	Metallic conductivity, superconducting $\theta_{cs} <$ $1.3^\circ K$ [Gi1]	
$Sn_{0.19}WO_3$	T	12.241		3.774		Gi1	Superconducting $\theta_{cs} < 1.3^\circ K$ [Gi1]	
$Pb_{0.17}WO_3$	T	12.163		3.767		Be30	$x = 0.057 \dots 0.16$ monoclinic, $x = 0.16 \dots 0.35$ tetr.	
$Pb_{0.35}WO_3$	T	12.207		3.782		Be30	Novel preparation [Co16]	
$La_{0.08}WO_3$	C	3.829				Br23	Cubic, ( $x = 0.08 \dots 0.19$ ), metallic conductivity [Sh6]	
$La_{0.02}WO_3$	T	7.52		3.89		Br23		
$Ce_{0.1}WO_3$	C	3.828				Os2	$n_{eff} = 2.5$ , all rare-earth bronzes blue-violet	
$Pr_{0.1}WO_3$	C	3.827				Os2	$n_{eff} = 3.6$	
$Nd_{0.1}WO_3$	C	3.822				Os2	$n_{eff} = 3.8$	
$Sm_{0.1}WO_3$	C	3.817				Os2	$n_{eff} = 1.6$ (temperature dependent), crystal growth [Co14]	
$Eu_{0.16}WO_3$	C	3.828				Os2	$n_{eff} = 3.4$ (temperature dependent), P & S [Sh6]	
$Eu_{0.10}WO_3$	C	3.815				Os2		
$Eu_{0.085}WO_3$	C	3.808				Os2	$n_{eff} = 7.9$ , crystal growth [Co14], P & S [Sh6], relation of $a$ vs. $x$ [We2]	
$Gd_{0.1}WO_3$	C	3.810				Os2	$n_{eff} = 9.6$	
$Tb_{0.1}WO_3$	C	3.808				Os2	$n_{eff} = 10.6$	
$Dy_{0.1}WO_3$	C	3.805				Os2	$n_{eff} = 10.6$ , P & S [Sh6]	
$Ho_{0.1}WO_3$	C	3.801				Os2	$n_{eff} = 9.5$	
$Er_{0.1}WO_3$	C	3.797				Os2	$n_{eff} = 7.5$ , crystal growth [Co14]	
$Tm_{0.1}WO_3$	C	3.794				Os2		

Compound	Sym	a Å	b Å	c Å	angle	Ref.	Remarks	Magnetic Data
----------	-----	--------	--------	--------	-------	------	---------	------------------



Compound	Sym	a Å	b Å	c Å	angle	Ref.	Remarks	Magnetic Data
$A_x\text{WO}_3$ (continued)								in 3.3.4, Tab.
$\text{Yb}_{0.1}\text{WO}_3$	C	3.791				Os2	$n_{\text{eff}} = 4.5$	
$\text{Lu}_{0.1}\text{WO}_3$	C	3.788				Os2	$n_{\text{eff}} = 0$	
$\text{Y}_{0.09}\text{WO}_3$	C	3.800				Br23	Tetr. $x < 0.09$ , metallic conductivity [Sh6]	
$\text{Al}_x\text{WO}_3$	O	7.368	7.476	3.850		Pol0	$x = 0.015, 0.010 < x < 0.030$ orthorhombic; $0.030 < x < 0.105$ , two phase; studied as func- tion of $T$ [Va4]	
$\text{Cu}_{0.77}\text{WO}_3$	O	5.387	5.440	3.784		Pol0	$0.105 < x \leq 0.135$ ; $x > 0.135$ , two phase	
$\text{Cu}_{0.28}\text{WO}_3$	Tr	3.73 5.85	3.88 6.65	7.74 4.88	$\alpha = 134^\circ 45'$ $\beta = 91^\circ 40'$ $\gamma = 93^\circ 37'$	Col8	Semiconducting $\approx 0.15$ eV	
$\text{Ag}_{0.01}\text{WO}_3$	O	3.73	3.85	7.35		Col8	Magnetic susceptibility $\chi_m = 34 \cdot 10^{-6}$ emu/mole	
$\text{Cd}_x\text{WO}_3$	O	7.316	7.532	3.848		Si8	Metallic conductivity, P & S [Po2]	
$\text{In}_{0.05}\text{WO}_3$	T	5.244		3.867		Va3	$x = 0.005, 0.005 \leq x < 0.02$ orthorhombic	
$\text{In}_{0.30}\text{WO}_3$	H	5.233 7.384		3.863 7.508		Bo21	$x = 0.020, 0.02 \leq x < 0.04$ tetragonal	
$\text{In}_{0.33}\text{WO}_3$	H	7.50		7.56		Bo21	$x = 0.01 \dots 0.05$ , P & S ( $x = 0.11$ ) [Bi3]	
$\text{Ti}_{0.38}\text{WO}_3$	T	7.31		12.80		Bo21	$x = 0.2 \dots 0.3$ , metallic conductivity, weak dia- magnetism	
$\text{U}_{0.083}\text{WO}_3$	C	3.812				Sw1	$x = 0.26 \dots 0.33$ ; metallic conductivity	
$\text{U}_{0.125}\text{WO}_3$	C	3.821				Si6	Metallic conductivity, $x = 0.19 \dots 0.36$ ; novel prep- aration [Co16]	
$\text{Cs}_{0.3}(\text{Ta}_{0.3}\text{W}_{0.7})\text{O}_3$	H	7.450		7.821		Ko10	relationship of $a$ vs. $x$ [We2]	
$\text{Rb}_{0.3}(\text{Ta}_{0.3}\text{W}_{0.7})\text{O}_3$	H	7.342		7.715		Ko10	P & S [Sh9]	
$\text{K}_{0.3}(\text{Ta}_{0.3}\text{W}_{0.7})\text{O}_3$	H	7.333		7.685		Ga4	Thermal expansion and resistivity ( $10^8 \Omega \text{cm}$ )	
$\text{K}_{0.5}(\text{Ta}_{0.3}\text{W}_{0.3})\text{O}_3$	T	12.36		3.90		Ga4	Thermal expansion and resistivity ( $10^7 \Omega \text{cm}$ )	
$A_x\text{ReO}_3$						Ga14	Entire range of S. S. with Ta and Nb [De19a]	
$\text{K}_{\approx 0.6}\text{ReO}_3$	C	3.895				Sl2	Metallic conductivity	
$\text{K}_{\approx 0.3}\text{ReO}_3$	H	7.318		7.485		Ch1b	High pressure preparation, $\Theta_{\text{cs}} = 3.6^\circ \text{K}$ [Sl7a]	
$\text{Na}_{\approx 0.6}\text{ReO}_3$	T	3.825		3.841		Sl7a	Metallic, $\Theta_{\text{cs}} < 1.3^\circ \text{K}$ , P & S [Sl2]	
$A_x\text{FeF}_3$								
$\text{Rb}_{0.99}\text{FeF}_3$	H	7.36		7.53		Tr1	Hex ( $x = 0.18 \dots 0.30$ ); P & S [De13a]	
$\text{K}_{0.99}\text{FeF}_3$	C	4.113				De11	( $x = 0.95 \dots 1.0$ ) cubic	
$\text{K}_{0.60}\text{FeF}_3$	T	12.60		3.936		De11	( $x = 0.40 \dots 0.60$ ) tetr	
$\text{K}_{0.25}\text{FeF}_3$	H	7.385		7.510		De11	( $x = 0.18 \dots 0.25$ ) hex	
$\text{Na}_{0.11}\text{FeF}_3$	R	5.37			$\alpha = 59^\circ$	Tr1	$x = 0.0 \dots 0.16$ ; P & S [De13a]	
$\text{Ti}_{0.30}\text{FeF}_3$	H	7.35		7.52		Tr1	Hex ( $x = 0.20 \dots 0.31$ ); P & S [De13a]	

Tab. 4b. □ BX<sub>3</sub> compounds

Compound	Sym	a Å	b Å	c Å	angle	Ref.	Remarks	Magnetic Data
AlF <sub>3</sub>	R	5.029			$\alpha = 58^\circ 31'$	Ke20	P & S [Eh2]	in 3.3.4, Tab.
ScF <sub>3</sub>	R	5.708			$\alpha = 59^\circ 32'$	No10		6
TiF <sub>3</sub>	R	5.519			$\alpha = 58^\circ 53'$	Si2		6
TiOF <sub>2</sub>	C	3.798				Vo3		6
VF <sub>3</sub>	R	5.373			$\alpha = 57^\circ 31'$	Ja2a	Neutron diffraction [Wo13]	
CrF <sub>3</sub>	R	5.2643			$\alpha = 56^\circ 37'$	Kn2	Prop. [Bi7, Ha11, Ha12, Bo33, Ra9], structure [Ja3], neutron diffraction [Wo13] 300 °C	
MnF <sub>3</sub>	R	5.332			$\alpha = 56^\circ 37'$	Kn2	Neutron diffraction [Wo13], Prop. [Bo33, Bo34, Ny1, Kl5, He10, Sm1]	6
	M	8.904	5.037	13.448	$\beta = 92^\circ 44'$	He9		
FeF <sub>3</sub>	R	5.362			$\alpha = 58^\circ 0'$	He11	Neutron diffraction [Wo13], Prop. [Bi7, Shi5, Iw17, Bu1], crystal transformation [Cr5]	6
CoF <sub>3</sub>	R	5.279			$\alpha = 57^\circ 0'$	He11	Neutron diffraction [Wo13], Prop. [He8, Ny1]	6
GaF <sub>3</sub>	R	5.20			$\alpha = 57^\circ 30'$	Br6		
ZrF <sub>3</sub>	C	3.96				Eh3	P & S [Mu1]	6
NbF <sub>3</sub>	C	3.903				Eh4	P & S [Se2], "doubtful"	6
NbO <sub>2</sub> F	C	3.902				Fr15		
MoF <sub>3</sub>	C	3.8985				Gu8	Neutron diffraction [Wi6], P & S [La7]	6
RuF <sub>3</sub>	R	5.408			$\alpha = 54^\circ 90'$	He11	Neutron diffraction [Wi6]	6
RhF <sub>3</sub>	R	5.330			$\alpha = 54^\circ 25'$	He11		6
PdF <sub>3</sub>	R	5.5234			$\alpha = 53^\circ 55'$	He11	Neutron diffraction [Wi6], Prop. [Ba19, Ba20, Ny1, Fi3]	6
InF <sub>3</sub>	R	5.722			$\alpha = 56^\circ 15'$	Mu1		
TeO <sub>3</sub>	R	5.180			$\alpha = 56^\circ 25'$	Du2	Prep. [Lo8]	
TaF <sub>3</sub>	C	3.9012				Gu8	Prop. [Ny1], "doubtful"	
TaO <sub>2</sub> F	C	3.896				Fr15		
WO <sub>3</sub>	M	7.297	7.539	7.688	$\beta = 90^\circ 55'$	Lo6	Structure [Br1, Ta15], neutron diffraction [Lo6], Prop. [Cr7, Cr8, Ta15, Co16, Be22, Iw2, De16, Ke10], optical properties [Di3a], phase trans- formations [Pe3a]	6
Re <sub>0.33</sub> W <sub>0.67</sub> O <sub>3</sub>	C	3.7574				Si2	P & S, [Me11, Bi4, Bi5], crystal growth [Fe21], Prop. [Si2, Fe21, Fe10, Gu6a], structure vs. oxy- gen content [Si2], DeHaas-Van Alphen effect [Ma27a], NMR [Na11a]	
ReO <sub>3</sub>	C	3.7477				Si2		
IrF <sub>3</sub>	R	5.418			$\alpha = 54^\circ 8'$	He11	P & S [Ro2]	
UO <sub>3</sub>	C	4.156				Wa6	P & S [En2]	

Tab. 4c.  $\square$  BB'X<sub>6</sub> compounds

Compound	Sym	a Å	b Å	c Å	angle	Ref.	Remarks	Magnetic Data
BB'X <sub>6</sub>							Structural review [Gi2, Ke11, Co29]	in 3.3.4, Tab.
NaVF <sub>6</sub>	R	5.63			$\alpha = 56^\circ 30'$	Ke11		
LiVF <sub>6</sub>	R	5.30			$\alpha = 56^\circ 18'$	Ke11		
CaMnF <sub>6</sub>	R	5.59			$\alpha = 55^\circ 36'$	Ho14		
MgMnF <sub>6</sub>	R	5.26			$\alpha = 56^\circ 54'$	Ho14		
NaNbF <sub>6</sub>	C	8.26				Ke11	P & S [Co29]	
LiNbF <sub>6</sub>	R	5.47			$\alpha = 58^\circ 6'$	Ke11	Magnetic properties $80 < T < 300^\circ\text{K}$ , $n_{\text{eff}} = 1.66$ , $\Theta_p = -218^\circ\text{K}$ [Ha18]	
NaMoF <sub>6</sub>	C	8.194				Ed3		
LiMoF <sub>6</sub>	R	5.43			$\alpha = 57^\circ 6'$	Bo18		
NaTcF <sub>6</sub>	R	5.77			$\alpha = 55^\circ 48'$	Ed4		
NaRuF <sub>6</sub>	R	5.80			$\alpha = 54^\circ 30'$	Bo18		
LiRuF <sub>6</sub>	R	5.39			$\alpha = 56^\circ 0'$	Bo18		
GePdF <sub>6</sub>	R	5.53			$\alpha = 54^\circ 0'$	Ba21	Magnetic properties, $n_{\text{eff}} = 2.82$ , $\Theta_p = 31^\circ\text{K}$ [Ba21]	
PdPdF <sub>6</sub>	R	5.52			$\alpha = 53^\circ 54'$	Ba21	P & S [He11], see PdF <sub>6</sub>	
SnPdF <sub>6</sub>	R	5.70			$\alpha = 53^\circ 6'$	Ba21	Magnetic properties, $n_{\text{eff}} = 2.98$ , $\Theta_p = 28^\circ\text{K}$ [Ba21]	
PtPdF <sub>6</sub>	R	5.55			$\alpha = 54^\circ 0'$	Ba21	Magnetic properties, $n_{\text{eff}} = 2.72$ , $\Theta_p = 1.2^\circ\text{K}$ [Ba21]	
NaSbF <sub>6</sub>	C	8.184				Te12	P & S [Sc22]	
LiSbF <sub>6</sub>	R	5.44			$\alpha = 57^\circ 0'$	Bu6	Complete structure; P & S [Ke11]	
CaHfF <sub>6</sub>	C	8.462				Ke7		
NaTaF <sub>6</sub>	C	8.28				Ke11		
LiTaF <sub>6</sub>	R	5.48			$\alpha = 58^\circ 0'$	Ke11		
NaWF <sub>6</sub>	C	8.18				Ke11	P & S [Co29]	
LiWF <sub>6</sub>	R	5.45			$\alpha = 57^\circ 24'$	Ke11	Magnetic properties $80 < T < 300^\circ\text{K}$ , $n_{\text{eff}} = 0.5$ , $\Theta_p = -125^\circ\text{K}$ [Ha18]	
NaReF <sub>6</sub>	C	8.18				Ke11		
NaOsF <sub>6</sub>	R	5.80			$\alpha = 55^\circ 12'$	Bo18		
LiOsF <sub>6</sub>	R	5.43			$\alpha = 55^\circ 30'$	Bo18		
NaIrF <sub>6</sub>	R	5.80			$\alpha = 55^\circ 12'$	Bo18		
LiIrF <sub>6</sub>	R	5.41			$\alpha = 56^\circ 0'$	Bo18		
PdPtF <sub>6</sub>	R	5.55			$\alpha = 54^\circ 0'$	Ba21	P & S [Pe11]; magnetic properties $80 < T < 300^\circ\text{K}$ , $n_{\text{eff}} = 1.57$ , $\Theta_p = -100^\circ\text{K}$ [Ha19]	
CaPbF <sub>6</sub>	C	8.476				Ho15		

Tab. 4d. $(AX)_n(ABX_3)_m$ compounds							Magnetic Data
Compound	Sym	a Å	b Å	c Å	angle	Ref.	
Halides							in 3.3.4, Tab.
$Cs_2MgF_4$	T	4.055		13.79		Ba1	No cell dimensions [Be22a]
$Rb_2MgF_4$	T	3.955		13.706		Re6	
$K_2MgF_4$	T	4.07		13.88		Ch8a	
$(NH_4)_2MgF_4$	T	4.007		14.43		Vo1	
$Tl_2MgF_4$	T	3.344	9.533	5.657	$\beta = 87^\circ 12'$	Se2	Not $K_2NiF_4$ type
$Na_2CrF_4$	T	5.215		16.46		Se2	
$Cs_2CrCl_4$	T	5.143		15.73			Possibly distorted $K_2NiF_4$ [Se2]
$Rb_2CrCl_4$	T						
$K_2CrCl_4$	T	4.31		14.63		Co25	$K_2NiF_4$ type
$Cs_2MnF_4$	T					Le7	
$Rb_2MnF_4$	T	4.228		13.89		Co25	P & S [Vo1], Prop. [De20, Br5]
$K_2MnF_4$	T	4.20		13.14		Br5	
$Rb_2FeF_4$	T	4.20		13.38		Tr1	P & S [Vo1, Co25], Prop. [De20, Co15]
$K_2FeF_4$	T	4.140		12.98		De12	
$K_2Fe_2F_7$	T	4.130		21.15		De12	
$Tl_2FeF_4$	T	4.194		13.91		Vo1	
$Rb_2CoF_4$	T	4.135		13.67		Ru6	P & S [Ru3, Ru8]
$K_2CoF_4$	T	4.07		13.08		Ru6	
$Tl_2CoF_4$	T	4.11		14.05		Ru6	Prop. [Ru8, Sr3, Sr2, Va1, Le8], dielectric properties [La1a]
$Rb_2NiF_4$	T	4.087		13.71		Ru8	
$K_2NiF_4$	T	4.006		13.076		Ba10	P & S [Ru3], optical properties [Sc10a]
$(NH_4)_2NiF_4$	T	4.08		13.78		Ru8	Prop. [Ru6, Va1], P & S [Kn1, Gu1a]
$Tl_2NiF_4$	T	4.051		14.22		Ru8	
$Rb_2CuF_4$	T	4.238		13.28		Ru6	P & S [Ru3] — not $K_2NiF_4$ type
$K_2CuF_4$	T	4.145		12.72		Ru6	
$Na_2CuF_4$	M	3.261	9.354	5.601	$\beta = 87^\circ 30'$	Ba3	P & S [Ru3]
$Tl_2CuF_4$	T	4.199		13.66		Ru6	
$(NH_4)_2CuCl_4$	T	7.20	7.20	15.46		Wi9	Prop. [De20, Bo15, Ko8], Prep. [Re7]
$(CH_3NH_3)_2CuCl_4$	O	7.30	7.54	18.55		Gr7	
$(C_2H_5NH_3)_2CuCl_4$	O	7.35	7.47	21.18		Wi9	P & S [Sc10]
$Rb_2ZnF_4$	O	4.125		13.67		Ba1	
$K_2ZnF_4$	T	4.02		13.05		Sc10	
$K_2Zn_2F_7$	T	4.063		21.22		Br12	

Compound	Sym	a Å	b Å	c Å	angle	Ref	Remarks	Magnetic Data
$K_3Zn_2F_7$	T	4.063		21.22		B712		
Halides (continued)								
$(NH_4)_2ZnF_4$	T	4.14		13.97		Cr3		in 3.3.4, Tab.
$Tl_2ZnF_4$	T	4.105		14.10		Vo1		
$Rb_3CdF_4$	T	4.414		13.98		Co27a		
$Rb_3Cd_2F_7$	T	4.403		22.71		Co27a	Prep. [Co26, Co27a] Prep. [Co26, Co27a]	
$K_2CdF_4$								
$K_3Cd_2F_7$	T	5.26		16.88		Si3		
$Ca_3CdCl_4$								
Oxides								
$SrLaAlO_4$	T	3.75		12.5		Ru1	Eu <sup>3+</sup> fluorescence [Ni1]	
$Sr_2TiO_4$	T	3.88		12.58		Ba10	P & S [Ru1, Br11, Lu2, Po9, Ha19a], Eu <sup>3+</sup> fluorescence [Ni1] P & S [Lu2]	
$Sr_2Ti_2O_7$	T	3.90		20.38		Ru2		
$Sr_4Ti_3O_{10}$	T	3.90		28.1		Ru2		
$Ca_3Ti_2O_7$	O	5.412	5.426	19.50		Pe3	P & S [Ro17]	
$Ca_4Ti_3O_{10}$	O	5.404	5.435	27.14		Pe3	P & S [Ro17]	
$NaLaTiO_4$	T	3.76		12.95		Bi12	(Na and Ln ordered). Fluorescence: Eu [Bi12a]	
$NaNdTiO_4$	T	3.76		12.79		Bi12		
$NaSmTiO_4$	T	3.77		12.59		Bi12	Fluorescence: Eu [Bi12a]	
$NaGdTiO_4$	T	3.77		12.46		Bi12		
$NaDyTiO_4$	T	3.77		12.22		Bi12	Fluorescence: Eu [Bi12a]	
$NaTmTiO_4$	T	3.78		12.05		Bi12	P & S [Bi12], fluorescence: Eu [Bi12a]	
$NaLuTiO_4$	T	3.78		11.92		Bi12		
$NaYTiO_4$	T	3.786		12.209		Bi12		
$Na_3Y_2Ti_3O_{14}$	T	3.79		20.2		Re2		
$Na_2Y_2Ti_3O_{10}$	T	3.79		28.2		Re2		
$Eu_2TiO_4$	T	3.89		12.53		Re2		
$Eu_3Ti_2O_7$	T	3.899		20.295		Ro21	P & S [Mc1b]	
$Sr_2CrO_4$	T	3.82		12.4		Ro21	P & S [Mc1b]	
$Sr_2Cr_2O_7$	T	3.82		20.1		Lo1a	Cr <sup>4+</sup> , high pressure preparation	
$SrLaCrO_4$	T	3.84		12.52		Lo1a	Cr <sup>4+</sup> , high pressure preparation	
$Sr_2MnO_4$	T	3.79		12.43		Bi9		
$Ca_2MnO_4$	T	3.667		12.063		Ba10	Substitution of La [Sr2]	
$Ca_3Mn_2O_7$	T	3.709		19.44		Ma6	P & S [Ru1, Br11]	6
$Ca_4Mn_3O_{10}$	T	3.724		26.90		Ma6	97% Mn <sup>4+</sup> ; P & S [Ru1, Br11]	6
$Sr_{1-x}La_xMnO_4$	T					Ma6	97% Mn <sup>4+</sup> ; P & S [Ru1, Br11]	6
$SrLaMnO_4$	T	3.88		12.5		Le7		6
$Sr_2FeO_{4-x}$	T	3.864		12.390		Bi9	$x = 0.3$	
$Sr_3Fe_2O_{7-x}$	T	3.853		20.149		Ga19	$x = 0.1$ , P & S [Br10], Prop. [Ma7]	6

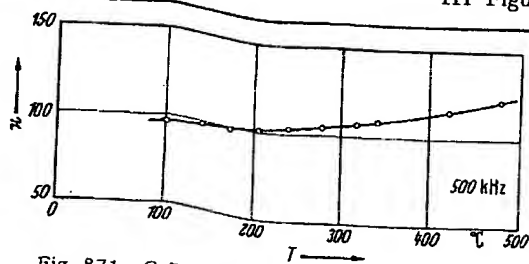
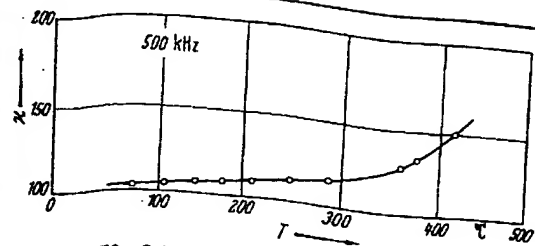
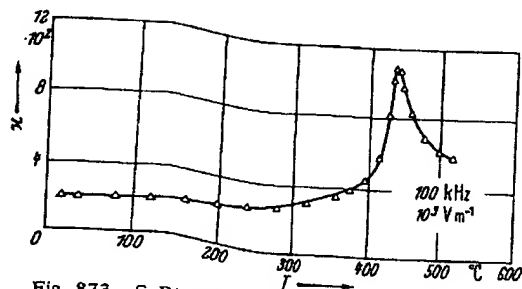
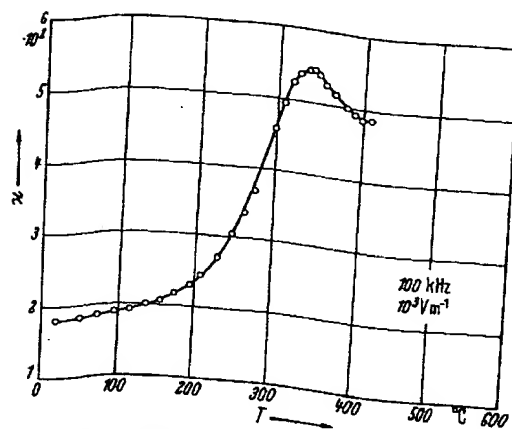
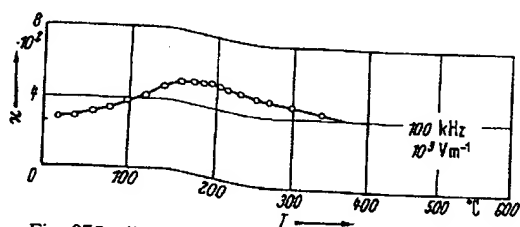
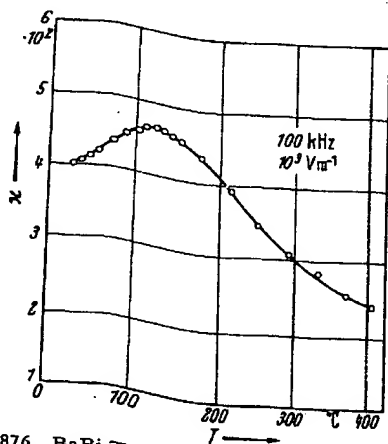
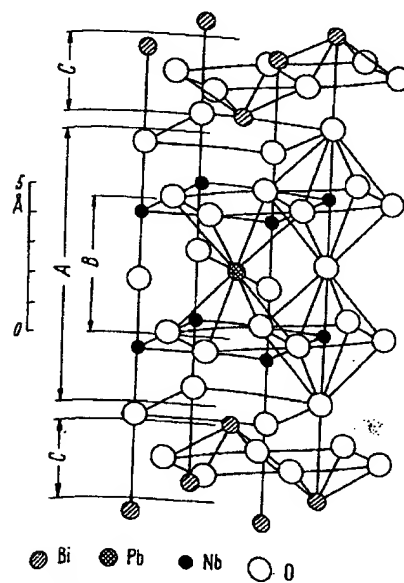
Compound	Sym	a Å	b Å	c Å	angle	Ref.	Remarks	Magnetic Data
Oxides (continued)								in 3.3.4, Tab.
Sr <sub>2</sub> Fe <sub>2</sub> O <sub>7-z</sub> cont.	T	3.892		20.054		Gal19	$x = 1$ , Prop. [Ma7]	
Sr <sub>2</sub> FeO <sub>3</sub> F	T	3.84		12.98		Gal3		
SrLaFeO <sub>4</sub>	T	3.86		12.69		Bl9	Prop. [As6]	6
SrLaCoO <sub>4</sub>	T	3.80		12.50		Bl9		
La <sub>2</sub> CoO <sub>4</sub>	O	5.482	5.539	12.66		Ra2	Prep. [Fo1, Fo3] substitution of Sr [Sr2, Go6]	
La <sub>2</sub> Co <sub>0.5</sub> Li <sub>0.5</sub> O <sub>4</sub>	T	3.77		12.58		Bl9	Prop. [Sr2, Go26]	6
La <sub>1.5</sub> Sr <sub>0.5</sub> CoO <sub>4</sub>	T	3.82		12.58		Bl9		6
La <sub>1.5</sub> Sr <sub>0.5</sub> Co <sub>0.5</sub> Mg <sub>0.5</sub> O <sub>4</sub>	T	3.85		12.62		Bl9		6
Sr <sub>1.5</sub> La <sub>0.5</sub> Co <sub>0.5</sub> Ti <sub>0.5</sub> O <sub>4</sub>	T	3.855		12.652		Ra2	P & S [Fo1, Fo3], Prop. [Sm34, Sm24]	6
La <sub>2</sub> NiO <sub>4</sub>	T						Prop. [Sm34]	6
Pr <sub>2</sub> NiO <sub>4</sub>	T	3.81		12.31		Fo1	Prop. [Sm34, Sm24]	6
Nd <sub>2</sub> NiO <sub>4</sub>	T	3.80		12.51		Bl9		
SrLaNiO <sub>4</sub>	T	3.75		12.89		Bl9		
La <sub>2</sub> Ni <sub>0.5</sub> Li <sub>0.5</sub> O <sub>4</sub>	O	5.36	5.41	13.17		Lo1c		
La <sub>2</sub> CuO <sub>4</sub>	T	3.81		13.24		Lo1c	Prep. [Fr25, Fo1, Fo3] at 420 °C, tetr. T > 250 °C	
Pr <sub>2</sub> CuO <sub>4</sub>	T	3.96		12.23		Fr25		
Nd <sub>2</sub> CuO <sub>4</sub>	T	3.94		12.15		Fo1	P & S [Fr25]	
Sm <sub>2</sub> CuO <sub>4</sub>	T	3.91		11.93		Fo1	P & S [Fr25]	
Eu <sub>2</sub> CuO <sub>4</sub>	T	3.91		11.92		Fr25		
Gd <sub>2</sub> CuO <sub>4</sub>	T	3.89		11.85		Fo1	P & S [Fr25]	
SrLaGaO <sub>4</sub>	T	3.84		12.71		Bl9		
Ca <sub>2</sub> GeO <sub>4</sub>	T	3.70		11.88		Re2	100 kbars, 900 °C required, P & S [Ri86]	
Ba <sub>2</sub> ZrO <sub>4</sub>	T	4.187		13.48		Sc18a		
Sr <sub>2</sub> ZrO <sub>4</sub>	T	5.801		12.445		Pe3	P & S [Sc18a]	
Sr <sub>2</sub> Zr <sub>0.5</sub> O <sub>7</sub>	T	5.798	5.808	20.94		Pe3		
Sr <sub>2</sub> Zr <sub>0.5</sub> O <sub>10</sub>	O	5.795	5.814	29.34		Pe3		
K <sub>2</sub> NbO <sub>3</sub> F	O	3.96		12.67		Ga2		
Sr <sub>2</sub> MoO <sub>4</sub>	T	3.92		12.84		Ba10	P & S [Sc16], Prop. [Ro2a]	6
Ba <sub>2</sub> TcO <sub>4</sub>	T	4.011		13.40		Ke9		
Sr <sub>2</sub> TcO <sub>4</sub>	T	3.902		12.72		Ke9		
Sr <sub>2</sub> RuO <sub>4</sub>	T	3.870		12.74		Ra6	Prop. [Ca2]	6
Sr <sub>2</sub> RhO <sub>4</sub>	T	3.85		12.90		Ra6		
SrLaRhO <sub>4</sub>	T	3.92		12.78		Bl9		
Ba <sub>2</sub> SnO <sub>4</sub>	T	4.130		13.27		We8	P & S [Wa2]	
Sr <sub>2</sub> SnO <sub>4</sub>	T	4.037		12.53		We8	P & S [Wa2]	
Ca <sub>2</sub> SnO <sub>4</sub>	T						Not K <sub>2</sub> NiF <sub>4</sub> type, [We8]	
Ba <sub>2</sub> HfO <sub>4</sub>	T	4.161		13.45		Sc18a		
Sr <sub>2</sub> HfO <sub>4</sub>	T	4.089		12.52		Sc18a		

Compound	Sym	a Å	b Å	c Å	angle	Ref.	Remarks	Magnetic Data
Oxides (continued)								
$\text{Sr}_2\text{IrO}_4$	T	3.89		12.92		Ra7	Prop. [Ro2a]	in 3.3.4, Tab. 6
$\text{Ca}_2\text{IrO}_4$	H	9.423		3.195		Ba5a	Not $\text{K}_2\text{NiF}_4$ type	
$\text{Ba}_2\text{PbO}_4$	T	4.296		13.30		We8	P & S [Wa2]	
$\text{A}_2\text{PbO}_4$						We8	A = Sr + Ca, not $\text{K}_2\text{NiF}_4$ type	
$\text{Cs}_2\text{UO}_4$	T	4.38		14.79		Ko11		
$\text{Rb}_2\text{UO}_4$	T	4.345		13.83		Ko11		
$\text{K}_2\text{UO}_4$	T	4.335		13.10		Ko11		
$\beta\text{-Na}_2\text{UO}_4$	O	5.795	5.97	11.68		Ko11		

Tab. 4e: see next page

Tab. 4e. $\text{Bi}_2\text{O}_2(\text{A}_{n-1}\text{B}_n\text{O}_{3n+1})$ compounds							Magnetic Data
Compound	Sym	a Å	b Å	c Å	angle	Ref.	
$\text{Bi}_2\text{MoO}_6$	O	5.49	5.50	16.24		Bl10	in 3.3.4, Tab.
$\text{Bi}_2\text{WO}_6$	O	5.49	5.50	16.24		Bl10	
$\text{BaBi}_2\text{Nb}_2\text{O}_9$	O	5.533	5.533	25.55		Au2	
$\text{SrBi}_2\text{Nb}_2\text{O}_9$	O	5.504	5.504	25.05		Au2	
$\text{CaBi}_2\text{Nb}_2\text{O}_9$	O	5.435	5.485	24.87		Au2	
$\text{PbBi}_2\text{Nb}_2\text{O}_9$	O	5.492	5.503	25.53		Au2	
$\text{K}_{0.5}\text{Bi}_{1.5}\text{Nb}_2\text{O}_9$	T	5.535		25.72		Is3	
$\text{Na}_{0.5}\text{Bi}_{1.5}\text{Nb}_2\text{O}_9$	O	5.506	5.506	25.26		Au2	
$\text{BaBi}_2\text{Ta}_2\text{O}_9$	O	5.47	5.47	26.94		Au2	
$\text{SrBi}_2\text{Ta}_2\text{O}_9$	O	5.556	5.556	25.60		Su4	
$\text{CaBi}_2\text{Ta}_2\text{O}_9$	O	5.509	5.509	25.06		Au2	
		5.435	5.468	24.97		Is3	
$\text{PbBi}_2\text{Ta}_2\text{O}_9$	T	5.479		25.085		Is3	
$\text{Bi}_3\text{NbTiO}_9$	O	5.496	5.496	25.40		Su4	
$\text{Bi}_3\text{TaTiO}_9$	O	5.405	5.442	25.11		Au2	
$\text{BaBi}_3\text{Ti}_2\text{NbO}_{12}$	O	5.402	5.436	25.15		Au2	
$\text{PbBi}_3\text{Ti}_2\text{NbO}_{12}$	T	3.874		33.70		Su2	
$\text{Bi}_4\text{Ti}_3\text{O}_{12}$	T	3.867		33.55		Su2	
	O	5.410	5.448	32.84		Au3	
$\text{BaBi}_4\text{Ti}_4\text{O}_{15}$	T	5.461		41.85		Su4	
$\text{SrBi}_4\text{Ti}_4\text{O}_{15}$	T	5.428		40.95		Su4	
$\text{CaBi}_4\text{Ti}_4\text{O}_{15}$	T	5.418		40.75		Su4	
$\text{PbBi}_4\text{Ti}_4\text{O}_{15}$	T	5.437		41.35		Su4	
$\text{Bi}_5\text{Ti}_3\text{GaO}_{15}$	T	5.408		41.05		Su4	
$\text{Bi}_5\text{Ti}_3\text{FeO}_{15}$	O	5.445	5.455	41.31		Is12	
$\text{K}_{0.5}\text{Bi}_{1.5}\text{Ti}_4\text{O}_{15}$	T	5.440		41.15		Su4	
$\text{Na}_{0.5}\text{Bi}_{1.5}\text{Ti}_4\text{O}_{15}$	T	5.427		40.65		Su4	
$\text{Ba}_2\text{Bi}_4\text{Ti}_5\text{O}_{18}$	O	5.514	5.526	50.37		Is6	
$\text{Ba}_2\text{Bi}_4\text{Ti}_5\text{Fe}_2\text{O}_{18}$	O	5.490	5.500	50.185		Is12	
$\text{Sr}_2\text{Bi}_4\text{Ti}_5\text{O}_{18}$	T	5.461		48.80		Su4	
$\text{Pb}_2\text{Bi}_4\text{Ti}_5\text{O}_{18}$	T	5.461		49.70		Su4	
$\text{Ba}_3\text{Bi}_4\text{Ti}_5\text{Fe}_3\text{O}_{27}$	O	5.491	5.502	76.20		Is12	




 Fig. 871.  $\text{CaBi}_2\text{Nb}_2\text{O}_9$  (ceramics).  $\kappa$  vs.  $T$  [61S11].

 Fig. 872.  $\text{CaBi}_2\text{Ta}_2\text{O}_9$  (ceramics).  $\kappa$  vs.  $T$  [61S11].

 Fig. 873.  $\text{SrBi}_2\text{Nb}_2\text{O}_9$  (ceramics).  $\kappa$  vs.  $T$  [62S17].

 Fig. 874.  $\text{SrBi}_2\text{Ta}_2\text{O}_9$  (ceramics).  $\kappa$  vs.  $T$  [62S17].

 Fig. 875.  $\text{BaBi}_2\text{Nb}_2\text{O}_9$  (ceramics).  $\kappa$  vs.  $T$  [62S17].

 Fig. 876.  $\text{BaBi}_2\text{Ta}_2\text{O}_9$  (ceramics).  $\kappa$  vs.  $T$  [62S17].

 Fig. 877.  $\text{PbBi}_2\text{Nb}_2\text{O}_9$ . Schematic drawing of crystal structure. One half of the pseudotetragonal unit cell from  $z \approx 0.25$  to  $z \approx 0.75$  is given.  $A$  denotes the perovskite layer  $\text{PbNb}_2\text{O}_7$ ,  $B$  denotes a unit of hypothetical perovskite structure  $\text{PbNb}_2\text{O}_7$ , and  $C$  denotes  $(\text{Bi}_2\text{O}_7)^{2+}$  layers [62S15].

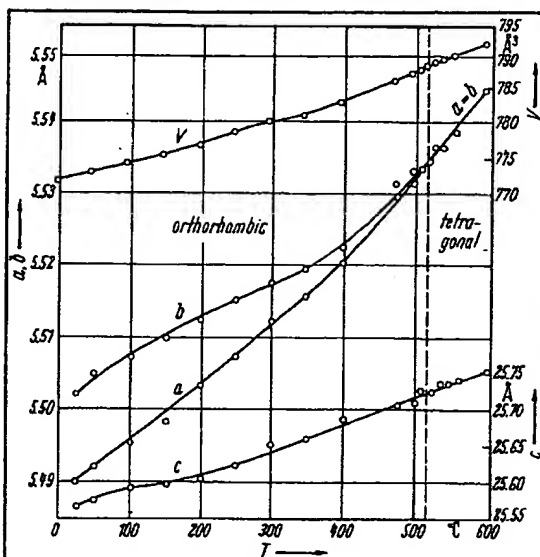


Fig. 878. PbBiNb<sub>2</sub>O<sub>8</sub> (ceramics). Lattice parameters vs. T [6017].

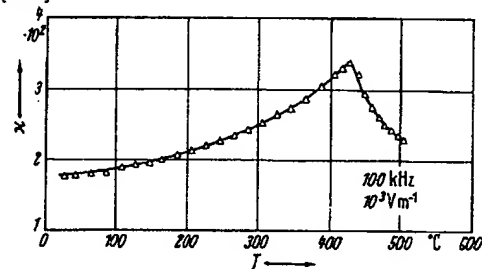


Fig. 880. PbBiTa<sub>2</sub>O<sub>8</sub> (ceramics).  $x$  vs. T [62517].

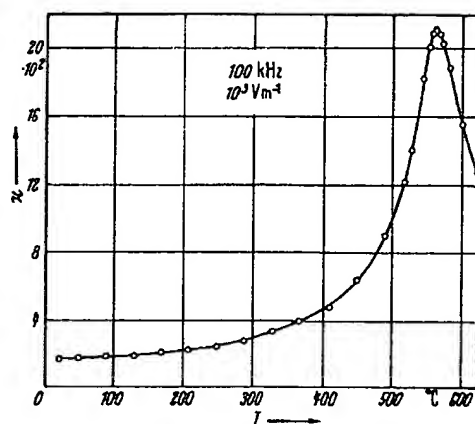


Fig. 879. PbBiNb<sub>2</sub>O<sub>8</sub> (ceramics).  $x$  vs. T [62517].

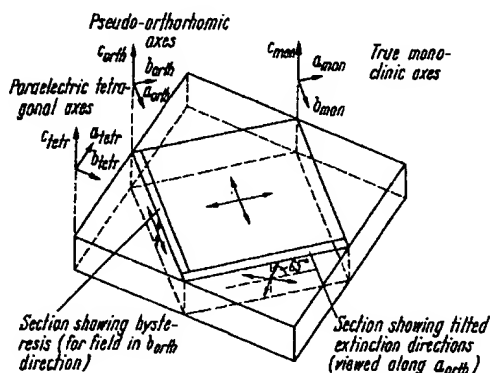


Fig. 881. Bi<sub>4</sub>Ti<sub>3</sub>O<sub>12</sub>. Relationship between the three sets of crystallographic axes [67C6].

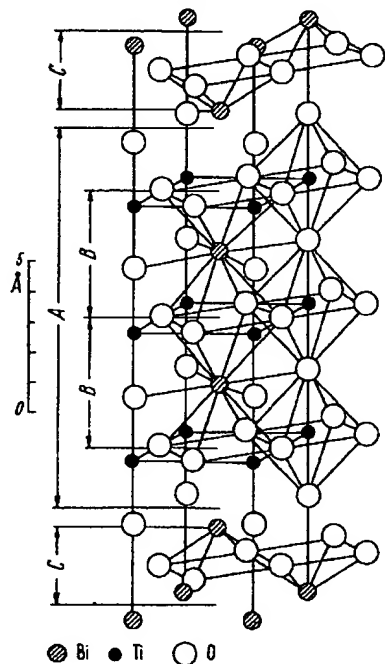


Fig. 882. Bi<sub>4</sub>Ti<sub>3</sub>O<sub>12</sub>. Schematic drawing of crystal structure. One half of the pseudotetragonal unit cell from  $x \approx 0.25$  to  $x \approx 0.75$  is given. A denotes the perovskite layer Bi<sub>2</sub>Ti<sub>3</sub>O<sub>12</sub><sup>2+</sup>, B denotes a unit of hypothetical perovskite structure BiTiO<sub>6</sub>, and C denotes (Bi<sub>4</sub>O<sub>4</sub>)<sup>2+</sup> layers [62515].

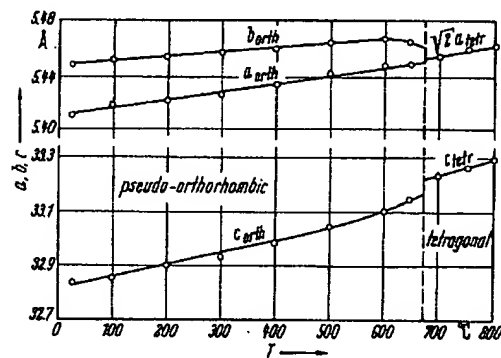


Fig. 883. Bi<sub>4</sub>Ti<sub>3</sub>O<sub>12</sub>. Lattice parameters vs. T [61516].

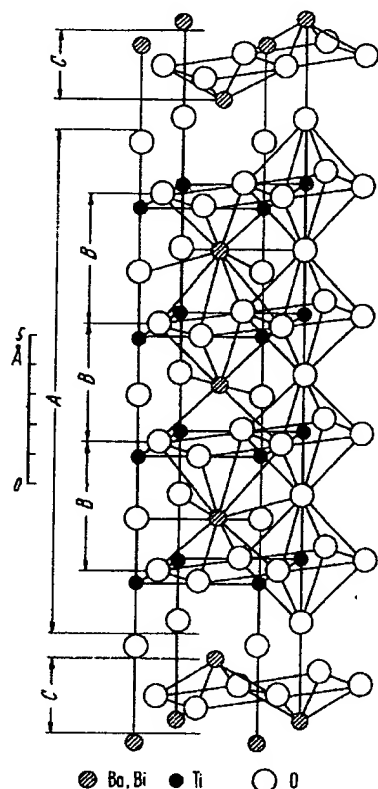


Fig. 890.  $\text{BaBi}_4\text{Ti}_4\text{O}_{13}$ . Schematic drawing of crystal structure. One half of the pseudotetragonal unit cell from  $x \approx 0.25$  to  $x \approx 0.75$  is given.  $A$  denotes the perovskite layer  $\text{BaBi}_4\text{Ti}_4\text{O}_{13}$ ,  $B$  denotes a unit of hypothetical perovskite structure  $(\text{Ba, Bi})\text{TiO}_3$ ,  $C$  denotes  $(\text{Bi}_4\text{O}_3)^{2+}$  layers [62S15].

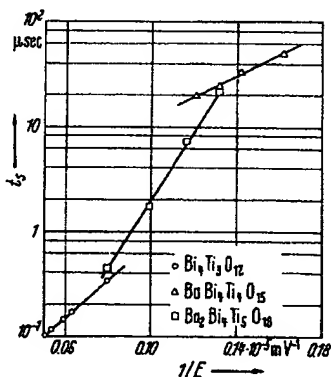


Fig. 892.  $\text{BaBi}_4\text{Ti}_4\text{O}_{13}$ ,  $\text{Ba}_2\text{Bi}_4\text{Ti}_4\text{O}_{13}$ ,  $\text{Bi}_4\text{Ti}_2\text{O}_{11}$ .  $t_s$  vs.  $1/E$ . [62F1].  $t_s$ : switching time.

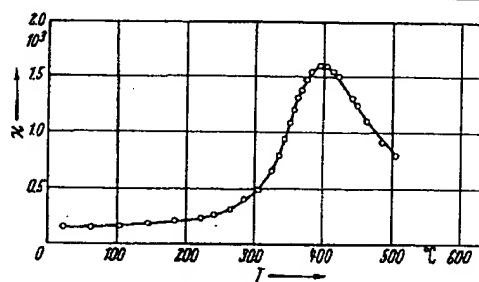


Fig. 891.  $\text{BaBi}_4\text{Ti}_4\text{O}_{13}$  (ceramics).  $\kappa$  vs.  $T$  [61S15].

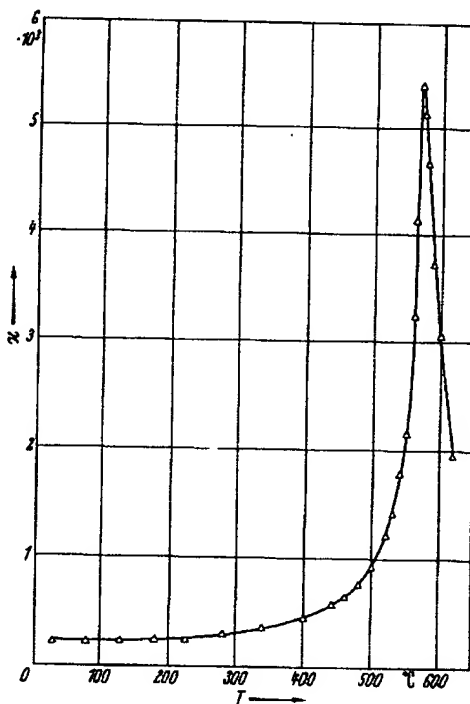


Fig. 893.  $\text{PbBi}_4\text{Ti}_4\text{O}_{13}$  (ceramics).  $\kappa$  vs.  $T$  [61S15].

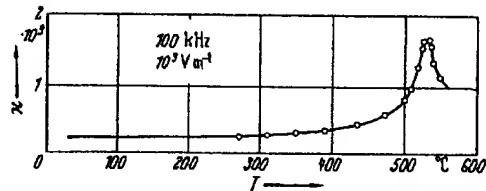


Fig. 894.  $\text{SrBi}_4\text{Ti}_4\text{O}_{13}$  (ceramics).  $\kappa$  vs.  $T$  [62S17].

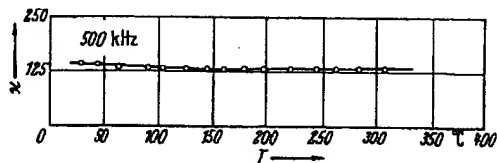


Fig. 895.  $\text{CaBi}_4\text{Ti}_4\text{O}_{13}$  (ceramics).  $\kappa$  vs.  $T$  [61S17].

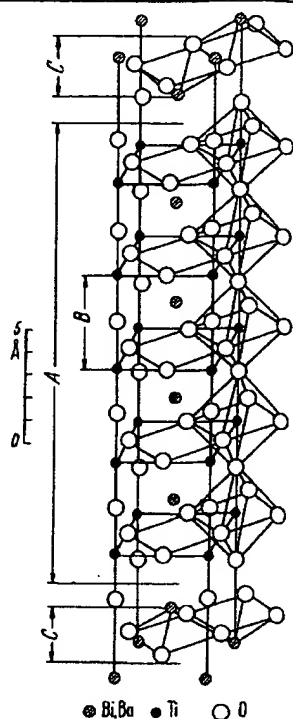


Fig. 896.  $\text{Ba}_2\text{Bi}_4\text{Ti}_5\text{O}_{18}$ . Schematic drawing of the crystal structure. One half of the tetragonal unit cell from  $x = 0.25$  to  $x = 0.75$  is given.  $A$  denotes the perovskitic layer of  $\text{Ba}_2\text{Bi}_2\text{Ti}_4\text{O}_{16}$ ,  $B$  denotes a unit cell of the hypothetical perovskite structure  $(\text{Ba}, \text{Bi})\text{TiO}_3$ , and  $C$  denotes the layers of  $(\text{Bi}_2\text{O}_3)^{2+}$  [6245].

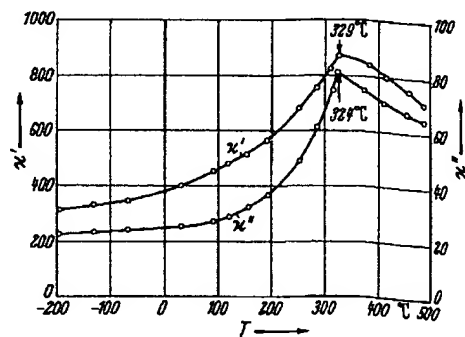


Fig. 898.  $\text{Ba}_2\text{Bi}_4\text{Ti}_5\text{O}_{18}$ .  $\kappa'$  and  $\kappa''$  vs.  $T$  [6245].

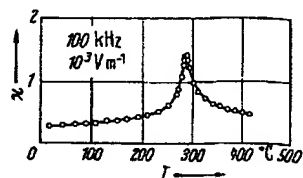


Fig. 900.  $\text{Sr}_2\text{Bi}_4\text{Ti}_5\text{O}_{18}$  (ceramics).  $\kappa$  vs.  $T$  [62517].

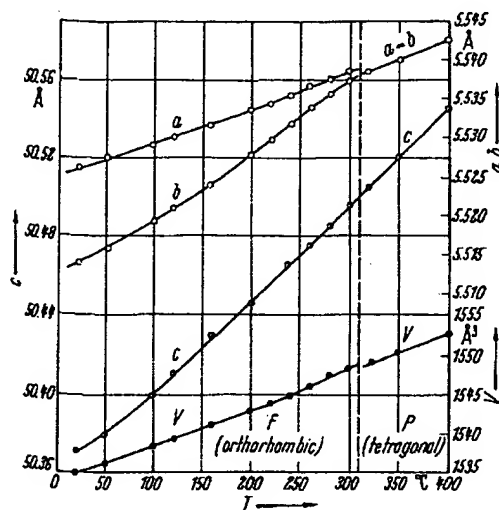


Fig. 897.  $\text{Ba}_2\text{Bi}_4\text{Ti}_5\text{O}_{18}$ . Lattice parameters vs.  $T$  [6315].

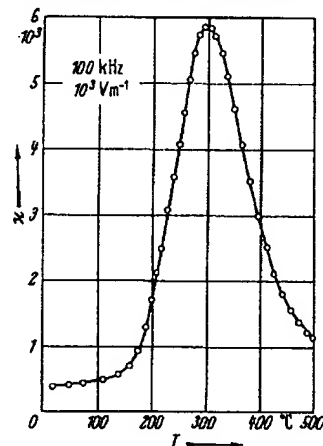


Fig. 899.  $\text{Pb}_2\text{Bi}_4\text{Ti}_5\text{O}_{18}$  (ceramics).  $\kappa$  vs.  $T$  [62517].

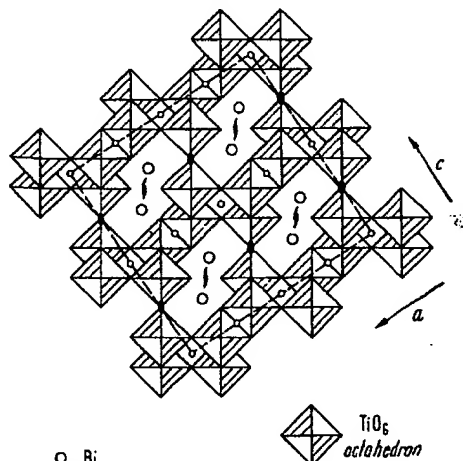


Fig. 901.  $\text{Bi}_4\text{Ti}_4\text{O}_{11}$ . Schematic projection of structure on  $(010)_2[6574]$ .

**This Page is Inserted by IFW Indexing and Scanning  
Operations and is not part of the Official Record**

**BEST AVAILABLE IMAGES**

Defective images within this document are accurate representations of the original documents submitted by the applicant.

Defects in the images include but are not limited to the items checked:

- ☒ BLACK BORDERS
- ☒ IMAGE CUT OFF AT TOP, BOTTOM OR SIDES
- ☐ FADED TEXT OR DRAWING
- ☒ BLURRED OR ILLEGIBLE TEXT OR DRAWING
- ☐ SKEWED/SLANTED IMAGES
- ☒ COLOR OR BLACK AND WHITE PHOTOGRAPHS
- ☐ GRAY SCALE DOCUMENTS
- ☐ LINES OR MARKS ON ORIGINAL DOCUMENT
- ☐ REFERENCE(S) OR EXHIBIT(S) SUBMITTED ARE POOR QUALITY
- ☐ OTHER: \_\_\_\_\_

**IMAGES ARE BEST AVAILABLE COPY.**

**As rescanning these documents will not correct the image problems checked, please do not report these problems to the IFW Image Problem Mailbox.**